UNIVERSITÀ DEGLI STUDI DI PALERMO

Dottorato di ricerca in Scienze Molecolari e Biomolecolari
Curriculum: "Tecnologie delle Sostanze Biologicamente Attive"
Dipartimento Scienze e Tecnologie Biologiche Chimiche e Farmaceutiche (STEBICEF)
SSD CHIM/09

Pulmonary drug delivery systems based on polymeric micro and nanoparticles for the treatment of cystic fibrosis

IL DOTTORE
PORSIO BARBARA

IL COORDINATORE
CH.MA PROF.SSA PATRIZIA DIANA

IL TUTOR
CH.MA PROF.SSA GENNARA CAVALLARO

CICLO XXIX
ANNO CONSEGUIMENTO TITOLO 2017

Table of contents

Chapter 1

Introduction

Living with Cystic Fibrosis…
"One way to gauge how cystic fibrosis lung disease might feel is to breathe for a while through a short length of garden hose. After a short time, you will feel an increasing urgency to breathe more than you are able to – you will probably make increasing efforts to move more air in and out of the hose, but your lungs cannot do that, no matter how much effort is put into it. Now imagine this feeling of "not enough breath", starting off imperceptibly, steadily increasing, never halting or reversing as you grow up through your teenage years. Expecting to enjoy life as it develops you are faced with an increasing amount of mucus and fluid trapping in your lungs that you relentlessly attempt to cough out to be able to breath and survive. The risk of getting a serious CF-specific lung infection from friends with cystic fibrosis means that you cannot even meet in person to gain much needed support. Your condition progressively affects your ability take part in any activities or even to breathe enough to satisfy your most primal biological instinct of humans -to satisfy the hunger for air"- Dr. D. Parsons, Chief Medical Scientist, Respiratory and Sleep Medicine, WCH

1.1 Cystic Fibrosis

Over 70,000 people worldwide have Cystic Fibrosis (CF). It is the most common genetically inherited disease in Caucasian population (1 in 2500 newborns) with fatal outcome.

CF is a multisystemic disease affecting different organs, like lungs, pancreas, liver, kidneys, and intestine. The main organ affected is the lung, where the dysfunction of a channel protein deputate to the hydric-saline balance causes the production of a thick and viscous mucus which leads to airway obstruction, infection, inflammation and end-stage lung disease.

CF-associated pulmonary disease is considered as a primary cause of morbidity and mortality. The outcome for CF patients has improved with introduction of therapies targeted to each step of the disease pathway and careful attention to detail applied by multidisciplinary teams in CF specialized centers. The US CF Foundation's projected that the life expectancy for patients has increased from 14 years in 1969 to 37 years over the past decade, and a UK model predicted that a child born with CF today will typically live to be 50 years of age.

1.1.1 Causes of CF

CF is an autosomal recessive disorder caused by mutations of the gene encoding the CF transmembrane conductance receptor (CFTR) which coding for a cAMP-dependent chloride channel protein [1]. The CFTR gene, found at the q31.2 locus of chromosome 7, is 230,000 base pairs long and creates a protein that is 1,480 amino acids long. More specifically the location is on the long arm of chromosome 7, region 3, band 1, sub-band 2, represented as 7q31.2 [2].

The CFTR channel sits in the epithelial cells of many organs including the lung, liver, pancreas, digestive tract, reproductive and controls the flow of chloride, bicarbonate and carbothiocyanate ions out of the epithelial cells to the covering mucus [3]. Positively charged sodium ions follow passively, increasing the total electrolyte concentration in the mucus, resulting in the movement of water out of the cell via osmosis.

Structurally, CFTR is a member of ATP-binding cassette (ABC) family (figure 1). There are two transmembrane domains (TMDs) with six membrane-spanning domains each, one regulatory (R) domain, located in the center of the protein, and two homologous nucleotide-binding domains (NBDs). The two ATP-hydrolyzing domains allow the protein to use energy in the form of ATP, the two domains comprising 6 alpha helices allow the protein to cross the cell membrane, while the regulatory binding site on the protein allows the activation by phosphorylation, mainly by cAMP-dependent protein kinase [2]. The carboxyl terminal of the protein is anchored to the cytoskeleton by a post synaptic density (PDZ) domain interaction [4].

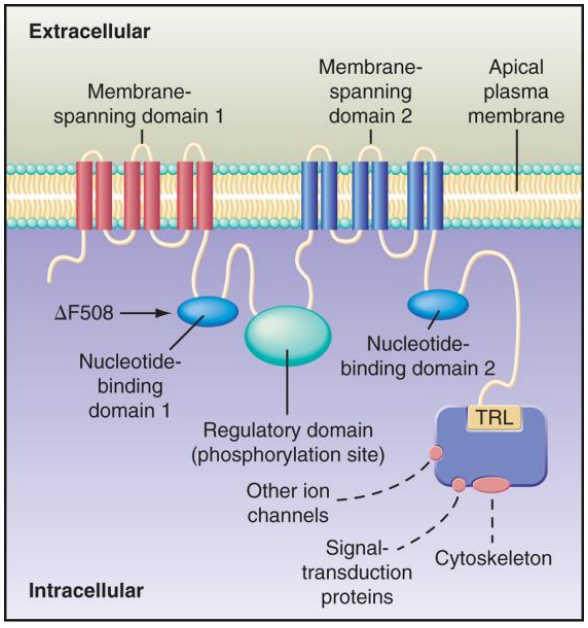

Fig. 1: Structure of CFTR protein

It was found that different genetic modifications in patients with CF will change the severity and frequency of the disease [5].

More than 1500 CFTR mutations have been identified and have different effects on CFTR function, resulting in different phenotypes of the disease and affecting the quantity of CFTR at cell membranes or the function of these channels.

Mutations of CFTR have been divided in six major classes (Table 1 and figure 2) [3]. In patients with class I mutation there is a defective synthesis of full-length CFTR protein, and premature stop codon prevents the full translation of mRNA, resulting in truncated CFTR protein. Consequently few to no mature CFTR proteins are formed. Class II mutations are characterized by defective CFTR protein processing and trafficking thereby defective post-translational processing and transport reduce quantity of CFTR protein delivered to cell surface. Class III mutations cause a defective CFTR channel gating where CFTR is at the cell surface but has reduction in channel-open probability. Class IV mutations has defective CFTR channel conductance in which CFTR is at the cell surface but has impaired movement of ions through channel. Finally, in patients with a class V mutation there is a reduced synthesis of CFTR protein. A splicing defect reduces quantity of properly processed CFTR mRNA transcripts, decreasing quantity of CFTR protein at the cell surface.

The most common mutation is the class II mutation consisting in the deletion of the aminoacid phenylalanine at codon 508 (phe508del or ΔF508), which occurs in about 70 % of CF patients [6].

Table 1: Classification of CFTR mutations.

	Effect on CFTR	**Functional CFTR present**	**Sample mutations**
Class I	Lack of protein production	No	Stop codons (designation ending in X; eg, Trp1282X, Gly542X); splicing defects with no protein production (eg, 711+1G→T, 1717–1G→A)
Class II	Protein trafficking defect with ubiquitination and degradation in endoplasmic reticulum/golgi body	No/substantially reduced	Phe508del, Asn1303Lys, Gly85Glu, Leu1065Pro, Asp1507, Ser549Arg
Class III	Defective regulation; CFTR not activated by ATP or cyclic AMP	No (non-functioning CFTR present in apical membrane)	Gly551Asp, Ser492Phe, Val520Phe, Arg553Gly, Arg560Thr, Arg560Ser
Class IV	Reduced chloride transport through CFTR at the apical membrane	Yes	Ala455Glu, Arg117Cys, Asp1152His, Leu227Arg, Arg334Trp, Arg117His
Class V	Splicing defect with reduced production of normal CFTR	Yes	3849+10kb C→T, 1811+1·6kb A→G, IVS8-5T, 2789+5G→A

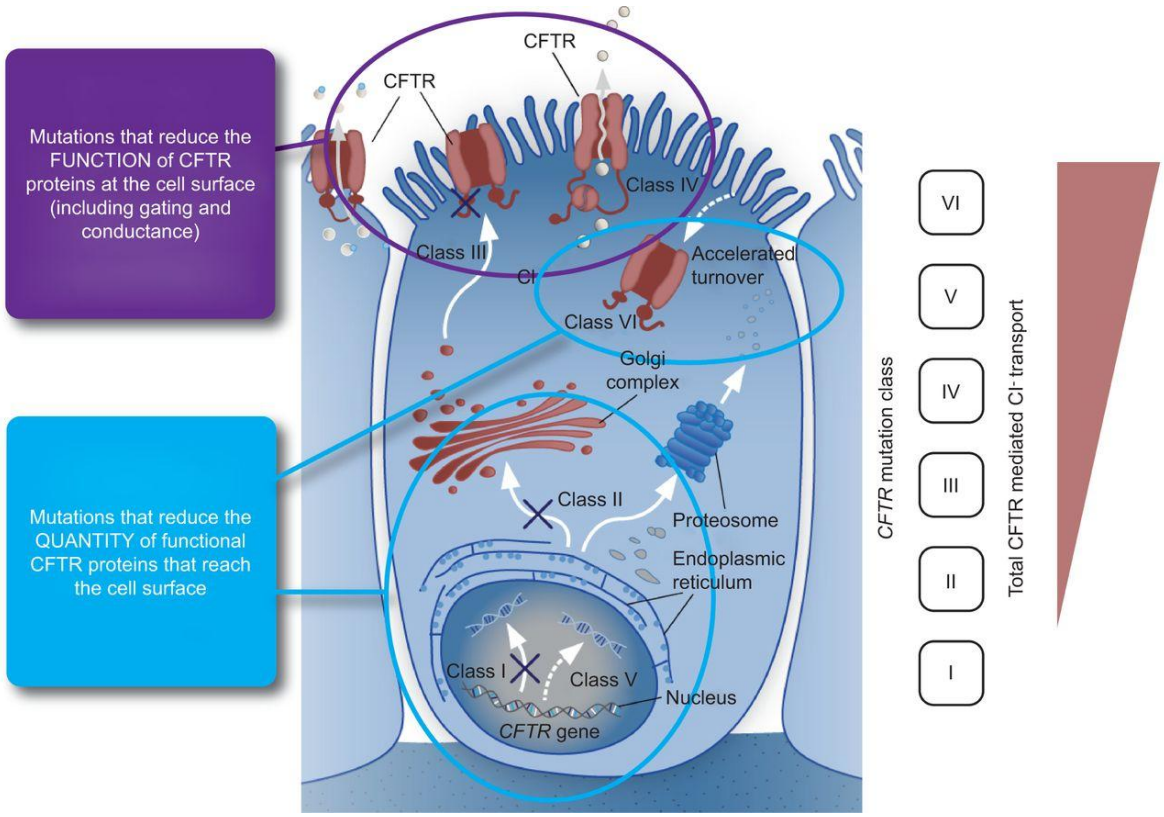

Fig. 2: Classification of CFTR mutations according to their effect on CFTR function.

Several hypothesis regarding how CFTR dysfunction leads to the CF phenotype were outlined in these years, and possibly all of these contribute to the CF pathogenesis.

The commonly accepted explanation for the airway disease in CF is the "low-volume" hypothesis [6], for which the loss of inhibition of epithelial sodium channels, because of CFTR dysfunction, leads to excess sodium and water reabsorption, resulting in dehydration of airway surface materials. The concomitant loss of chloride efflux prevents the epithelium from correcting the low airway surface water volume. The subsequent decrease in periciliary water volume results in a reduction in the lubricating layer between epithelium and mucus, with compression of cilia by mucus causing inhibition of normal ciliary and cough clearance of mucus. According to this hypothesis, mucus on the epithelium forms plaques with hypoxic niches that can harbour bacteria, particularly *Pseudomonas aeruginosa*.

Alternatively, the high-salt hypothesis[3] argues that in the absence of functional CFTR, a sodium and chloride excess is retained in airway surface liquid. The increased concentration of chloride in the periciliary layer disrupts the function of important innate antibiotic molecules (eg, human β-defensin 1), allowing bacteria that are cleared by normal airways to persist in lungs.

Another hypothesis regards the dysregulation of the host inflammatory[3] as the putative basic defect in CF. Support for this hypothesis lies in the fact that abnormally high concentrations of inflammatory mediators are seen in CF cell cultures and uninfected ex-vivo tissue samples. Furthermore, findings from lung lavage studies show that inflammation is present also in children as young as 4 weeks of age who are apparently free of infection, with several imbalance between proinflammatory and anti-inflammatory mediators that favours inflammation.

Finally, the last hypothesis suggests that primary predisposition to infection is a mechanism by which CFTR dysfunction leads to CF-associate lung disease. In CF patients, an increase in asialo-GM1 in apical cell membranes allows increased binding of *P. aeruginosa* and *Staphylococcus aureus* to airway epithelium, without initiation of the CFTR-mediated immune response. The result is that in CF, the rapid and self-limiting response that eliminates *P. aeruginosa* from the airways is lost at the same time as there is enhanced attachment of bacteria to the epithelial surface.

1.1.2 Sign and symptoms

Cystic fibrosis leads to pathological changes in organs that express CFTR, including secretory cells, sinuses, lungs, pancreas, liver, and reproductive tract, as schematized in figure 3.

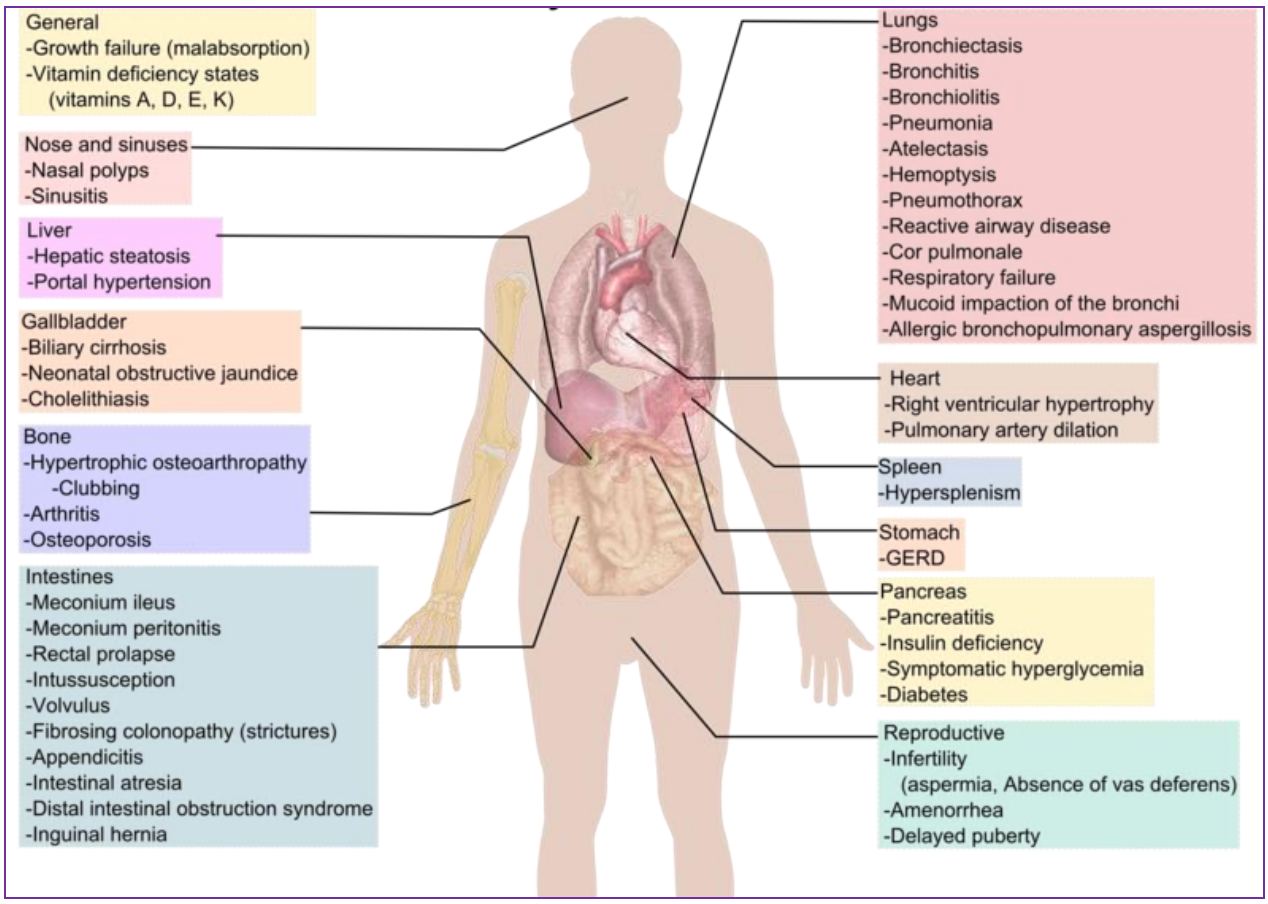

Fig. 3: Clinical manifestation of CF.

1.1.2.1 Pulmonary disease

The lungs of children with CF are normal in appearance at birth, but quickly become infected and inflamed, with polymorphonuclear cells present in bronchoalveolar lavage fluid.

Chronic airway infection, progressing to bronchiectasis, gas trapping, hypoxaemia, and hypercarbia are the hallmark of CF lung disease and pulmonary insufficiency is responsible for at least 80% of CF-related deaths.

Typically, infants with CF are rapidly colonised by *Haemophilus influenzae* or *S. aureus*, or both and within a short time, *P. aeruginosa* becomes the predominant organism found in the airways by 3 years of age. Persistent infection leads to generation and secretion of chemotactic cytokines, which recruit large numbers of polymorphonuclear cells into the airways. *P. aeruginosa* amplifies the cycle of infection and inflammation by releasing toxins and elastases that cleave crucial surface markers on polymorphonuclear cells. These cells then release their own proteases and elastases that exacerbate the injuries to any viable polymorphonuclear cells in the region. Thereafter, bacterial exotoxins and products of the damaged neutrophils spur further polymorphonuclear cell recruitment and increased tissue

damage. Moreover, release of DNA from senescent polymorphonuclear cells leads to increased sputum viscosity.

The airways of CF patients are conducive to the growth of *P. aeruginosa* for several reasons: permissive microenvironments within the hypoxic niches of adherent mucus plaques, an increase of bacterial binding to the epithelium and a decrease in bacterial clearance via innate immune mechanisms[3]. Initially, *P. aeruginosa* grows as a non-mucoid strain that can be cleared by the host, or eradicated with aggressive antibiotic treatment. Over time, *P. aeruginosa* colonies synthesize an alginate coat and form biofilms, that, once established, are difficult if not impossible to clear with standard antibiotic treatment. For this reason, heightened surveillance for *P. aeruginosa* has become of ordinary routine, with strategies to eradicate early infection by use of inhaled antibiotics.

CF airways can be infected with other pathogens, such as *Burkholderia cepacia* (a complex of at least nine different species), *Stenotrophomonas maltophilia*, and *meticillin-resistant S aureus* (MRSA). Many *B. cepacia* species have innate antibiotic resistance, are transmissible from person to person, and are highly virulent. *B. cepacia* complex infections can cause a rapid decline in pulmonary function, and increased mortality in patients with CF.

Occasionally, infection with the complex can cause an invasive, fatal bacteraemia, the so-called “cepacia syndrome”[7], and approximately, the 15–20% of CF patients carry MRSA in their airways.

In addition to bacterial infections, CF patients may develop chronic fungal infection[8] such as Aspergillus fumigatus, Scedosporiumapiospermum, Aspergillus Terreus and /or yeasts (such as Candida Albicans), even if at present, there is no conclusive evidence that fungal organisms cause respiratory decline. The defective mucociliary clearance and the prolonged administration of therapy such as antibiotics and corticosteroid increase the incidence of fungal growth [9].

1.1.2.2 Gastrointestinal sign and symptoms

About the 15 % of newborn infants born with meconium ileus, an obstruction of the terminal ileum caused by the abnormally tenacious meconium and GI secretions extremely viscid and adherent to the intestinal mucosa [3]. Moreover the increase in the fecal volume and increase of intra-abdominal pressure due to coughing causes in about 10 % of CF children rectal prolapses, the protrusion of the rectal intestinal membrane [10].

The second effect of CF on GI is through its effect on pancreas which is involved in digesting of food. The thickened secretions from pancreas blocks the endocrine movement of digestive

enzymes into the duodenum which cause an irreversible damage to pancreas. Eventually, this damage will cause a painful inflammation, known as pancreatitis [11]. In more severe cases, especially in older children and adult, the pancreas duct will be completely closed, which results in atrophy of exocrine gland and progressive fibrosis.

Majority of CF patients (85-90%) have exocrine pancreatic insufficiency. Typical signs of pancreatic insufficiency are greasy stools, flatulence, abdominal bloating, and poor weight gain. Pancreatic insufficiency leads to steatorrhoea, fat-soluble-vitamin deficiency, and malnutrition [12]. At the time CF was first recognized in 1938, the life expectancy of patients was only months; death was caused by malnutrition. With the introduction of pancreatic enzyme replacement therapy, malnutrition became manageable. However, adequate caloric intake and correction of fat-soluble-vitamin deficiencies remain crucial components of disease control.

In addition, malabsorption is a disorder that is common in most CF patients. It is caused by lack of digestive enzymes which lead to difficulty in absorbing nutrients consequently with increase their excretion in feces. Poor absorption of fat soluble vitamins (A, D, E, and K)[12] can lead to dermatitis, anaemia, neuropathy, night blindness, osteoporosis, and bleeding disorders.

Other GI symptoms involve heart burn, constipation, and intestinal blockage by intussusceptions. Furthermore, older patients with CF may have distal intestinal obstruction syndrome due to intestinal blockage by a thickened feces.

Patients with CF are at risk for focal biliary cirrhosis caused by obstruction of intrahepatic bile ducts, but clinically apparent cirrhosis occurs in only about 5% of patients, and usually presents by 15 years of age [13].

1.1.2.3 Endocrine disorders

Pancreatic dysfunction is caused by obstruction of intrapancreatic ducts with thickened secretions. With time, the pancreas undergoes autolysis with replacement of the body of the pancreas with fat. When a certain proportion of islet cells are no longer functional, the patient will develop insulin insufficiency and carbohydrate intolerance, possibly coexisting with insulin resistance.

CF-related diabetes mellitus (CFRD)[3] is not the same as typical type I or type II diabetes mellitus. Several factors unique to CF affect glucose metabolism, including raised energy expenditure, acute and chronic infection, glucagon deficiency, liver dysfunction, decreased intestinal transit time, and increased work of breathing.

Osteoporosis[3] secondary to vitamin D deficiency, chronic systemic inflammation, and intermittent corticosteroid use is increasingly being recognized as a complication of CF. Disturbances in the regulation of calcium and phosphate may result in poor absorption that, in turn, can lead to the development of bone disease and osteoporosis. Bones of patients with osteoporosis are usually weak and easily fracture. In addition, most CF patients show clubbing of their fingers and toes. These symptoms are caused by chronic illness and low oxygen amount in their tissues.

1.1.2.4 Infertility

Studies found that about 97% of CF patients are infertile. Fortunately, they are not sterile and they can get children with help of reproductive techniques [3]. Congenital absence of Vas deferens, which is responsible for connecting the testes to the ejaculatory ducts of the penis, is the main cause of infertility in CF men. Other causes involve azoospermia, teratospermia, and oligoasthenospermia. Some CF women may develop infertility which is resulted either from thickened cervical mucus or malnutrition. In case of malnutrition, it may affect ovulation and cause amenorrhea.

1.1.3 Diagnosis and monitoring

CF may be diagnosed by many different methods including newborn screening, sweat testing, and genetic testing [1, 3]. 10 percent of cases are diagnosed shortly after birth as part of newborn screening programs. The newborn screen initially measures for raised blood concentration of immunoreactive trypsinogen. Infants with an abnormal newborn screen need a sweat test to confirm the CF diagnosis. In many cases, a parent makes the diagnosis because the infant tastes salty. Trypsinogen levels can be increased in individuals who have a single mutated copy of the *CFTR* gene (carriers) or, in rare instances, in individuals with two normal copies of the *CFTR* gene.

Most states and countries do not screen for CF routinely at birth, therefore, most individuals are diagnosed after symptoms (rinopulmonary and GI manifestations), which prompt an evaluation for CF. The most commonly used form of testing is the sweat test, which involves the application of pilocarpine, a substance that stimulates sweating. To deliver the medication through the skin, iontophoresis is used and consists in the placing of one electrode onto the applied pilocarpine and then the passing of an electric current to a separate electrode on the skin. The resultant sweat is then collected on filter paper or in a capillary tube and analyzed for abnormal amounts of sodium and chloride. People with CF have increased amounts of

sodium and chloride in their sweat, and less thiocyanate and hypothiocyanite in their saliva and mucus.

CF can also be diagnosed by identification of mutations in the CFTR gene.

Before pregnancy, measurement of CFTR gene on one or both parents might be used to determine whether newborn child will have CF or not. In case of higher risk of CF in newborn, a test on fetus will be done. The most common commercially available test is looking for 32 or less different mutations. This means that not all mutation types can be determined by this test. Therefore, negatively screen result does not usually mean that the child does not have CF .

In order to diagnose the CF during pregnancy, CF test is usually performed either by amniocentesis (or by chorionic villus sampling done on placenta).

1.1.4 Management and treatment

The best way to manage and treat CF is introducing a multidisciplinary strategy offering protection to airway infection, pulmonary rehabilitation for the entire life, good nutrition, and an active life style. In addition to physician specialized in CF, care is delivered by specialist allied health professionals.

CF dieticians are expert at assessing and monitoring the need for nutritional and pancreatic enzyme supplements in addition to managing enteral feeding. Physiotherapists are integral to the team and offer expert training. Specialist nurses are invaluable in coordinating and managing homecare therapies which allow young people to continue in education and employment. The team should also include social workers, psychologists and pharmacists with expertise in CF. It is recognized that centers providing multidisciplinary care produce better clinical outcomes [1].

Special attention is provided to pharmacological therapy of CF-associated lung disease, being this one the primary cause of death. This pharmacological therapy is targeted at each step in the pathogenesis of disease (figure 4), but the cornerstone in CF is the symptomatic treatment, in order to limit and manage the lung damage caused by the thick and infected mucus, and to improve organ function and quality of life.

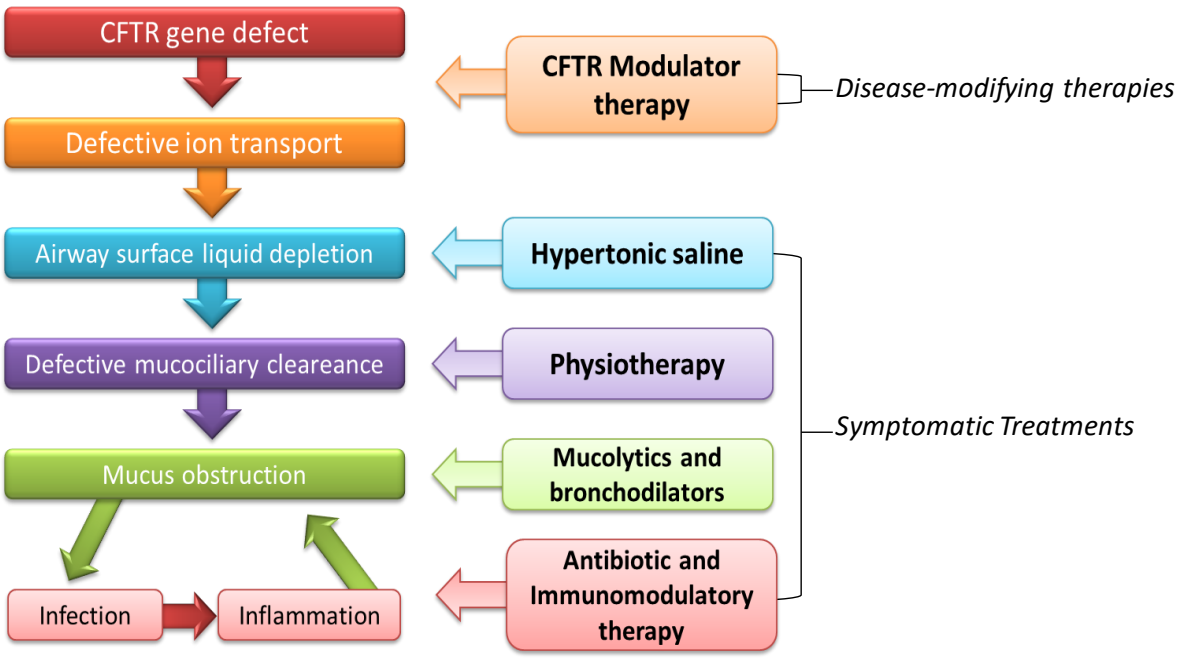

Fig.4: Current therapies for CF and their place in interrupting disease progression.

After many efforts for developing disease-targeted therapies, this decade represents a new era of precision medicine in CF therapeutics thanks to the licensing of small molecules which successfully targets the underlying defect and improves CFTR function in a subgroup of patients in a genotype-specific manner. For the first time, there are now treatments designed to overcome specific mutation abnormalities that restore the function of the defective CFTR protein.

Finally, lung transplantation is an option for selected pediatric and adult patients with advanced or severe lung disease that has failed to respond to standard therapy.

1.1.4.1 Symptomatic treatment of CF-associate lung disease

In CF, lung disease can be treated by different dosage forms and routs of administration such as oral, intravenous (IV), and pulmonary.

In order to clear out the thick mucus or even to alter its characteristics, physiotherapy, mechanical devices and rehabilitation are used. They are extremely consuming time even though there are effective.

An obstacle with CF patient is to find time to respond to treatment while balancing a normal life.

Physiotherapy and airway clearance

Every CF patient must learn an airway clearance technique which enables them to efficiently clear secretions from the airways.

In the past, the primary aim of physiotherapy for CF people was to clear excessive secretions and thus reduce symptoms. The term “physiotherapy” is today used in a much wider sense. In fact, modern physiotherapy in CF is a combination of inhalation therapy, airway clearance techniques, physical education/exercise and ongoing education about the disease and its treatment. Modern physiotherapy is primarily preventative and has to be incorporated into each patient's daily routine in a lifetime perspective,by tailoring a time-efficient treatment that places the least possible burden on the patient or his/her family and makes compliance with the treatment possible.

Daily physiotherapy aimed at ventilating all parts of the lungs and compensating for impaired mucociliary clearance, encourage good posture, avoid musculoskeletal complications, and maintain endurance and allow a good quality of life.

Bronchodilators

Bronchodilators (such as salbutamol, terbutaline, fenoterol, ipatropium bromide, salmeterol etc) are amongst the most frequently used medical therapies in CF patients [14].

CF airway obstruction is the result of different phenomena, like the airways mucosal oedema caused by infection and inflamation, the stimulation of autonomic nerve fibers caused by epithelial damage, the airways smooth muscle contraction by mediators of airway infection, the inflammation and autonomic nerve stimulation, the bronchiectasis and the consequent airway collapse. Thus, the widespread presence of both airways obstruction and hyperresponsiveness in CF has prompted the use of anti-asthma drugs, such as bronchodilators. The use of bronchodilators in CF evidenced improved mucociliary clearance with subsequent improvements in lung function.

Mucolytics and hypersmolar therapy

Giving that dehydration of the airway surface liquid layer has been implicated as the primary initiating event in CF-related lung disease, therapeutic interventions to improve mucus clearance by using mucolytics is a cornerstone of treatment in CF.

The main types of drugs used in CF to improve mucus clearance are mucolytic agents like, N-acetylcysteine, dornase alfa (commonly referred to its FDA-approved medication name known as Pulmozyme®) or aerosolized hypertonic saline (HTS, 3% to 7% NaCl).

HTS is a solution possessing an osmotic pressure greater than that of physiologic isotonic salt solution (0.9% NaCl). Inhalation of HTS has been proposed to significantly improve mucociliary clearance and the popularity of its use has increased on the basis of a number of clinical trials [15]. Several mechanisms have been proposed for the observed effectiveness including changes in the rheological characteristics of the airway mucus, increasing airway surface liquid hydration, inhibition of epithelial sodium channel (ENaC), as well as immunomodulatory effects [15, 16].

Recent studies are revealing that HTS can also function by releasing essential antimicrobial and immune molecules from complexation with ionic matrices thus improving both antimicrobial efficiency and resolution of inflammation (Figure 5) [15].

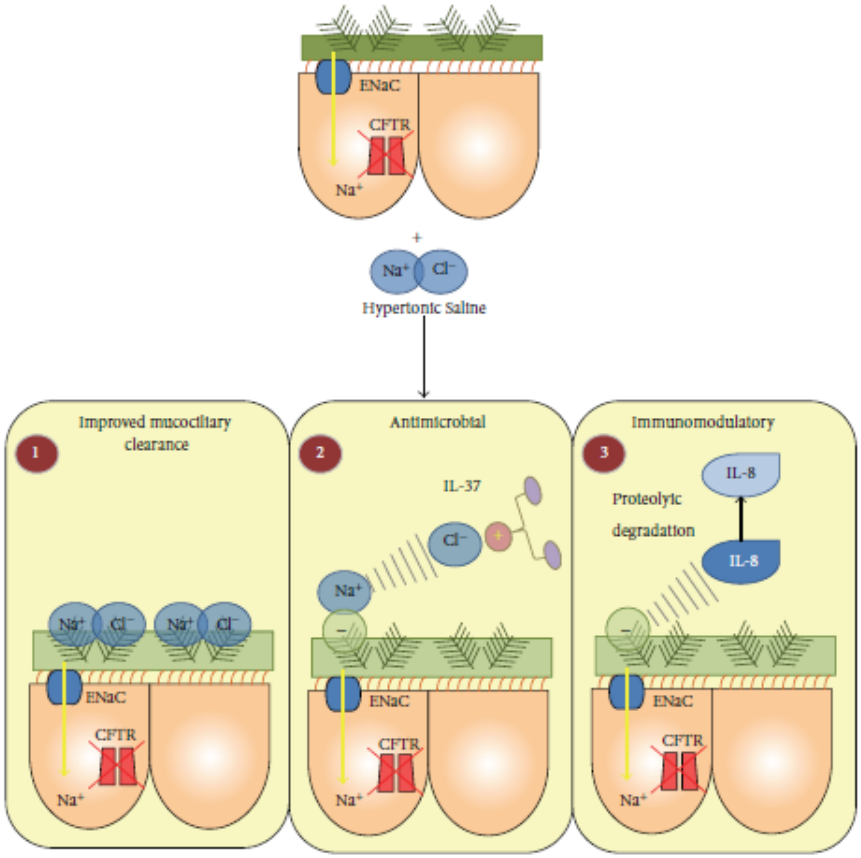

Fig.5: Schematic representation of the antimicrobial, immunomodulatory and mucolytic properties of HTS. (1) HTS draws water into the dehydated CF periciliary layer and improves mucus rheology and enhances mucociliary clearance. (2) LL-37, an antimicrobial protein that is inhibited by anionic glycosaminoglycans (GAGs), is released by HTS via disruption of the electrostatic interaction between LL-37 and GAGs. (3) HTS liberates IL-8 from anionic GAGs rendering the chemokine susceptible to proteolytic degradation by neutrophil elastase, thereby decreasing inflammation.

These observations suggest that HTS has beneficial therapeutic effects other than simply increasing mucociliary clearance, and make this broadly applicable and inexpensive therapy of big value.

One of the most commonly prescribed mucolytic agent is N-acetylcysteine (NAC), which depolymerizes mucus by breaking disulphide bridges between macromolecules and act as an oxygen radical scavenger. NAC can be taken either orally or by inhalation. After oral administration, NAC is reduced to cysteine, a precursor of the antioxidant glutathione, in the liver and intestine. The antioxidant properties could be useful in preventing decline of lung function in CF. Nebulized NAC is commonly prescribed to CF patients, in particular in continental Europe, in order to improve expectoration of sputum by reducing it stenacity.

The nebulization, a time-consuming therapy, of NAC has been associated with bronchospasm in patients with airways hyperresponsiveness, so the routine addition of a bronchodilator to the NAC nebulization fluid has been advocated.

Dornase alfa (Pulmozyme®, Genentech) is a highly purified solution of recombinant human deoxyribonuclease I (rhDNase), an enzyme which selectively cleaves DNA.

Dornase alfa hydrolyzes the DNA present in CF sputum patients and reduces its viscosity, as showed in figure 6, promoting improved clearance of secretions [17].

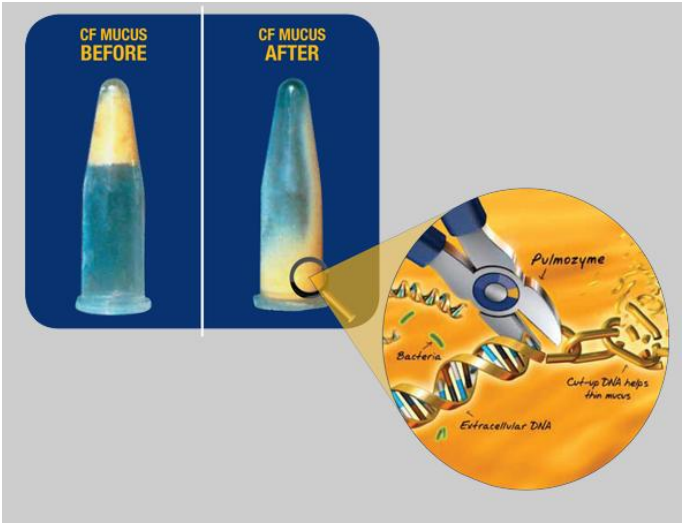

Fig.6: Reduction of sputum viscosity after treatment with Pulmozyme® (www.pulmozyme.com).

In CF patients, dornase alfa is indicated to improve lung function and reduce the risk of pulmonary exacerbations.

Treatment guidelines for chronic respiratory medications in CF patients recommend chronic use of dornase alfa in patients ≥ 6 years old. The use of Pulmozyme® may present side effects that include pharyngitis, conjunctivitis, voice alteration, rash, chest pain and laryngitis.

Antibiotic therapy

CF patients usually used one or more antibiotics depending on the onset stage and the extent of infections, such as prophylaxis, eradication and therapy for chronic infection.

Both sputum results and patient's response are put in consideration to select the type of antibiotics used in routine therapy, used generally for a long period of time.

Antibiotics such as ciprofloxacin and azithromycin [18] are used orally as prophylaxis to prevent infection, while to maintain lung function and decrease the growth of colonized bacteria, inhaled antibiotics, such as tobramycin, colistin and aztreonam are used [19].

Giving that patients who develop chronic infection with *P. aeruginosa* have a faster decline in lung function than non-infected individuals, the first strategy is to postpone the onset of chronic infection by early intervention when *P. aeruginosa* is first isolated, by administering nebulized colomycin for 3 month combined with oral ciprofloxacin for 4 to 6 weeks [1].

Once chronic infection is present, the aim of antibiotic therapy is to reduce the bacteria amount in mucus and thus decrease the important exacerbations, limiting the decline of lung function. Twice daily therapy is therefore recommended with nebulized antibiotics. In Europe, there is a long experience with the use of tobramycin [20].

Infective exacerbations of CF, determined by chest radiography investigation and spirometry, are usually characterized by a change of symptoms, such as new or increased cough with increase of sputum volume and purulence. Oral ciprofloxacin can be used to treat mild exacerbation, while the combination of IV-administered β-lactams and aminoglycosides is generally used as first line approach for moderate and severe exacerbations[1].

Several limitations are associated with the conventional antibiotic therapy, such as the narrow therapeutic index, low sputum concentrations and dose limiting toxicity to different organs, and above all a severe microrganisms resistance to antibiotics [21].

Immunomodulatory and anti-inflammatory therapy

Interrupting the vicious cycle of infection and inflammation is effective in slowing the course of the disease, and antibiotics have long been the staple of pulmonary therapy. Limiting the inflammatory response in the CF lung is effective since inflammation not only damages the lungs directly but impairs local host defences, preventing the clearance of infections.

Traditional anti-inflammatory therapy has been explored in CF: oral steroids have beneficial effect on lung function but this was outweighed by a detrimental effect on growth, on bones, as well as an increased incidence of development of diabetes, generally associated with reduces survival [1]. Among the most frequently administered anti-inflammatory agent we could find triamcinolone, fluticasone, beclomethasone, prednisone, methylprednisone, montelukast and ibuprofen.

Ibuprofen, a non-steroidal anti-inflammatory (NSAID) was first investigated as a CF treatment in 1990 to reduce extreme inflammation [22]. Orally administered high-dose ibuprofen was found to significantly slow the decline in FEV 1 (Forced expiratory volume in the 1st second) over a four-year period [23] and this has been confirmed in subsequent studies that underlined how results obtained from clinical trials were clinically relevant [24–26].

More recently, Carlile and colleagues identified the activity of ibuprofen also as a CFTR corrector, showing as it partially corrects the trafficking of F508del-CFTR (the most common disease-associated mutation), both in vivo and in-vitro [27].

Despite these encouraging results, in clinical the anti-inflammatory approach is rarely practiced because of orally administered NSAID side effects, such as abdominal pain, epitaxis, hemoptosys, and gastrointestinal haemorrhages (Cystic Fibrosis Foundation Patient Registry: Annual Data Report to the Center Directors. Bethesda, Maryland, 2013).

1.1.4.2 CF disease-modifying therapies

Despite the development and implementation of various symptomatic treatments (treatment of obstruction, infection and inflammation) has greatly improved patients survival, many efforts have been made over the past decade for the development of drugs that target defective CFTR proteins caused by specific mutations. These drugs could have a positive impact on the lives of people with CF being disease modifying.

Disease-modifying strategies can be classified into two main categories: small molecules addressing the associated protein defect, named CFTR modulators, and agents that target the genetic mutation, such as gene therapy.

CFTR modulators

In this last decade, many efforts have been done in the research and development of small molecules, named CFTR modulators, focused on targeting certain mutation of CFTR gene, with promising results. These drugs are very specialized and individualized molecules, and

are a typical example of personalized treatment, where only those patients with the specific mutation can be treated with the targeted drug.

CFTR modulators can be classified into three main categories: CFTR read-through agents, CFTR correctors and potentiators.

CFTR read-through agents promote the ribosomal "read-through" of premature termination codons (PTCs) in CFTR mRNA. The first read-through agents examined in CF were the aminoglycoside antibiotics [28, 29], commonly used in CF to combat Gram negative bacteria such as *P. aeruginosa*. Aminoglycoside antibiotics, such as gentamicin, capable of inhibiting ribosomal "proofreading" by binding to the decoding site of rRNA [29], ''force'' read-through of premature stop codons during translation of the CFTR protein. This results in the production of a full-length CFTR protein, which may then be trafficked to the cell surface [28].

Ataluren, formerly known as PTC124, is potentially a more promising read-through agent than gentamicin, inducing functional CFTR production and being well tolerated [28]. The agent is available in an easy-to-use formulation and is currently undergoing clinical trials. Initial clinical studies in healthy adults did not raise any safety concerns and analysis of subjects' peripheral blood mononuclear cells showed no aberrant elongation of CFTR protein [30].

CFTR potentiators increase the open probability of CFTR channels that have gating (Class III) or conductance (Class IV) mutations [31]. People with class III mutations such as G551D have normal amounts of CFTR protein at the cell surface but have primary defects in CFTR channel gating, making them ideal targets for potentiator therapy. Moreover, there is additional evidence from in vitro studies that CFTR potentiators may also enhance the open probability of CFTR channels with Class II mutations, such as F508del [32], even if F508del potentiation could occur if recombinantly expressed channel is already be located on the cell membrane.

Ivacaftor, formerly known as VX-770 (administered orally in tablets or granules under the commercial dosage form called KALYDECO®), is a CFTR potentiator that specifically targets the Class III mutation, G551D, and at 10 μM concentration ivacaftor increased the open probability of G551D-CFTR channels by around 6 fold [28]. Although the precise mechanism of its action remains incompletely understood, evidence suggests that ivacaftor stabilizes the open state of CFTR, thus increasing channel opening time [33]. The discovery of ivacaftor has provided proof of the concept that CFTR related chloride secretion can be potentiated, and other oral compounds such as QBW251 have entered phase II investigation

(NCT02190604; EudraCT 2011-005085-37); several other agents such as GLPG1837 are also in development [29].

Finally, *CFTR correctors* are designed to increase the amount of functional CFTR protein delivered to the cell surface. CFTR correctors repair defective CFTR processing by facilitating proper maturation and delivery of protein to the plasma membrane, and act by interacting directly with CFTR and facilitating its correct folding [29]. Patients with class II mutations, such as F508del mutation which affects the 85-90% of patients, are primary targets for CFTR corrector therapy because the misfolded protein is retained within the endoplasmic reticulum and prematurely degraded.

Lumacaftor (VX-809) is a pharmaceutical drug that acts as a chaperone during protein folding and increases the number of CFTR proteins that are trafficked to the cell surface.

It is available in oral dosage form in combination with ivacaftor, having lumacaftor not enough benefits on its own. This combination, lumacaftor/ ivacaftor with the brand name Orkambi®[34], used to treat people the F508del mutation, was developed by Vertex Pharmaceuticals and the combination was approved by the FDA in 2015.

Gene therapy

In contrast to mutation-specific small-molecule therapy, gene therapy attempts to introduce a normal functioning copy of the CFTR gene into the cells of the conducting airways. If successful, this approach will be available to all patients with CF irrespective of the underlying genetic defect.

CF gene therapy can be achieved by using either viral or non-viral delivery methods[28]. The viral vector binds to the host cell to introduce the coding sequence of wildtype CFTR, which ideally should be persistently transcribed into mRNA, or even be integrated into the cell genome, while non-viral gene therapy involves the delivery of naked DNA or DNA complexes into the cell by vectors other than viruses.

Since the 1990s, research into gene therapy has not provided clear evidence of tangible benefits for clinical practice and currently no gene therapies have been approved for use. In fact, in recent years research into gene therapy has become increasingly limited, largely due to the evidence that gene transfer is more challenging than originally thought; trials in this area are expensive to conduct and research to date suggested limited efficacy of gene transfer vectors.

Nevertheless, the UK CF Gene Therapy Consortium recently embarked on a gene therapy programme. More than a decade of investigation has led to the development of a product that

offers the best currently available gene-transfer potential. A combination of a CFTR-expressing plasmid (pGM169) with a cationic lipid (GL67A) delivered via nebulizer has been assessed in phase I and IIA safety studies (Eudra CT ref 2007-004060-85; NCT 01621867) [35].

1.1.4.3 Lung Transplantation

Lung transplantation is a complex, high-risk, potentially life-saving therapy for the end-stage CF lung disease. The decision to pursue transplantation involves comparing the likelihood of survival with and without transplantation as well as assessing the effect of wait-listing and transplantation on the patient's quality of life [36].

Short-term success with lung transplantation prompted growth in the use of the procedure for CF and fostered hope in children and adults whose CF lung disease had progressed to end stage [36].

Lung transplants do not cure CF patient because the defective gene that causes the disease is found in all the cells of the body, with the exception of the newly transplanted lungs. The median survival for adults after lung transplantation is only 6.4 years [36].

After transplantation, improvements are likely to include standardized care, including induction and maintenance immunosuppression, antimicrobial treatment, patient rehabilitation, and graft surveillance.

Even if lung transplantation remains a high risk procedure, it remains the only treatment option with the potential to ameliorate symptoms, preserve quality of life, and extend life for patients with advanced CF lung disease.

1.2 Pulmonary Therapy

Inhalation has been employed as a method for delivering drugs for more than two thousand years, and benefits have been understood for more than two hundred years. The oldest report came from China and India around 2000 B.C. and are related to the inhalation of smoke from burned herbal preparation based on *Atropa belladonna* and *Datura stramonium* to treat throat and chest disease, like asthma [37]. Through the years, many compounds and mixtures were proposed and used to treat different diseases using various methods of inhalation, from ceramic inhalers to combustible powders and liquid atomizers. The inhalation of vapor from solution of picric acid, iodine or sulfuric acid was very popular in the 20^{th} century to treat tuberculosis and other infections, while the first mentions regarding inhalation of antibiotics to treat pulmonary infections appeared in 40s [38].

Drug delivery to the lungs by inhalation offers a targeted drug therapy for both pulmonary and systemic diseases. The local route of drug administration allows one order of magnitude-lower drug doses to be delivered compared to systemic administration (oral route or parental). The low dosing locally reduces systemic exposure to the drug, systemic side effects, and increases drug therapeutic index. In addition, relatively low enzymatic activity helps maintaining high local drug bioavailability and the non-invasive nature of pulmonary delivery, thanks to the use of portable inhalers, make this route convenient for patients, increasing compliance and adherence to the therapy. Despite inhalation started as a route to treat disease confined to the respiratory tract, in recent years inhalation is used to treat systemic disease as well. The large absorptive surface area of the alveoli, the very thin diffusion path from the airspaces into the blood and the elevated blood flow make the lung a point of entry to the systemic circulation. Drug molecules are absorbed more efficiently from the lung than from any other non-invasive routes of drug administration. As a result, a continuously increasing number of inhaled drugs are becoming available on the market to treat various systemic diseases.

However, pulmonary administration has the difficulty to provide regular and efficient drug deposition at bronchial and alveolar level. In fact, the branched structure of the lungs provides an efficient aerodynamic filter, which hinders the deposition of the drug in depth. Moreover, the pharmacological response of the aerosol depends not only on the amount of deposited particles, but also by the amount retained in the site. In fact, particles deposited on the mucus layer, that covers the conducting airways, may be removed, before being absorbed and exert a biological action, by different mechanisms of elimination, including coughing, dissolution,

mucociliary escalator, translocation from the airways to other sites and phagocytosis by macrophages.

Furthermore, the efficiency of the pulmonary administration depends not only on the innate geometry and physiology of the lungs, but also on different several factors (figure 7).

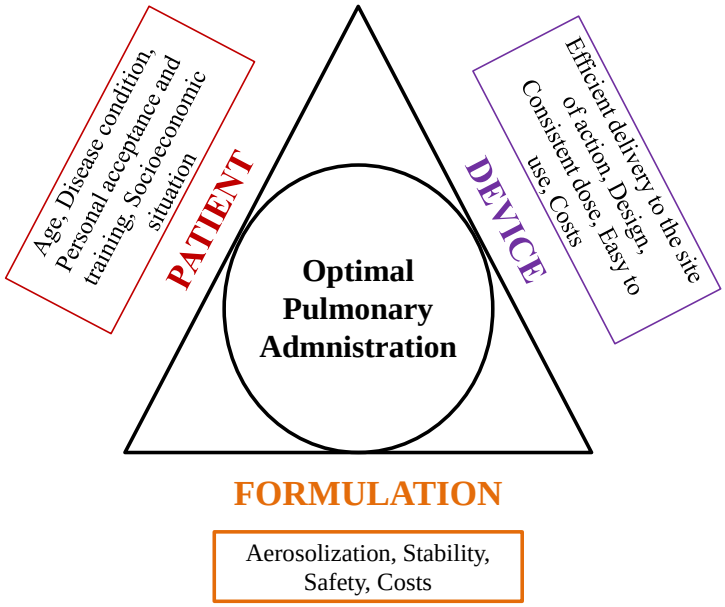

Fig.7: Factors that influence an optimal pulmonary administration.

Indeed, the design of a pulmonary dosage form is a complex task that involves the accurate knowledge of the anatomy and physiology of the respiratory system, the fate of inhaled drugs in order to modify formulation properties, and inhalation devices. Inhalers have to meet the needs of the pulmonary delivery of different formulations for various disease, a sophisticated design for a better aerosol deposition to the lungs but at the same time they have to be simple enough to be adequately used by the patients of different ages, also for special populations, such as pediatric and geriatric patients.

1.2.1 Lungs anatomy and physiology

The respiratory system (figure 8) works with the circulatory system to perform the exchange of oxygen and carbon dioxide with air from the atmosphere [39]. To this end, the lungs exchange respiratory gases across a highly permeable epithelial surface area of about 70-150 m^2, approximately the same area as one side of a tennis court.

Lungs house structures of both the conducting and respiratory zones. Lung conductive zone is composed by trachea, bronchi and bronchioles. Trachea splits into primary right and left

bronchus, and these supply air to the right and left lungs, splitting progressively into the secondary and tertiary bronchi for the lobes of the lungs (two for left lung and three for right lung), and into smaller and smaller bronchioles until they become the respiratory bronchioles. These in turn supply air through alveolar ducts into the alveoli, where the exchange of gases take place. Oxygen diffuses through the walls of the alveoli into the enveloping capillaries.

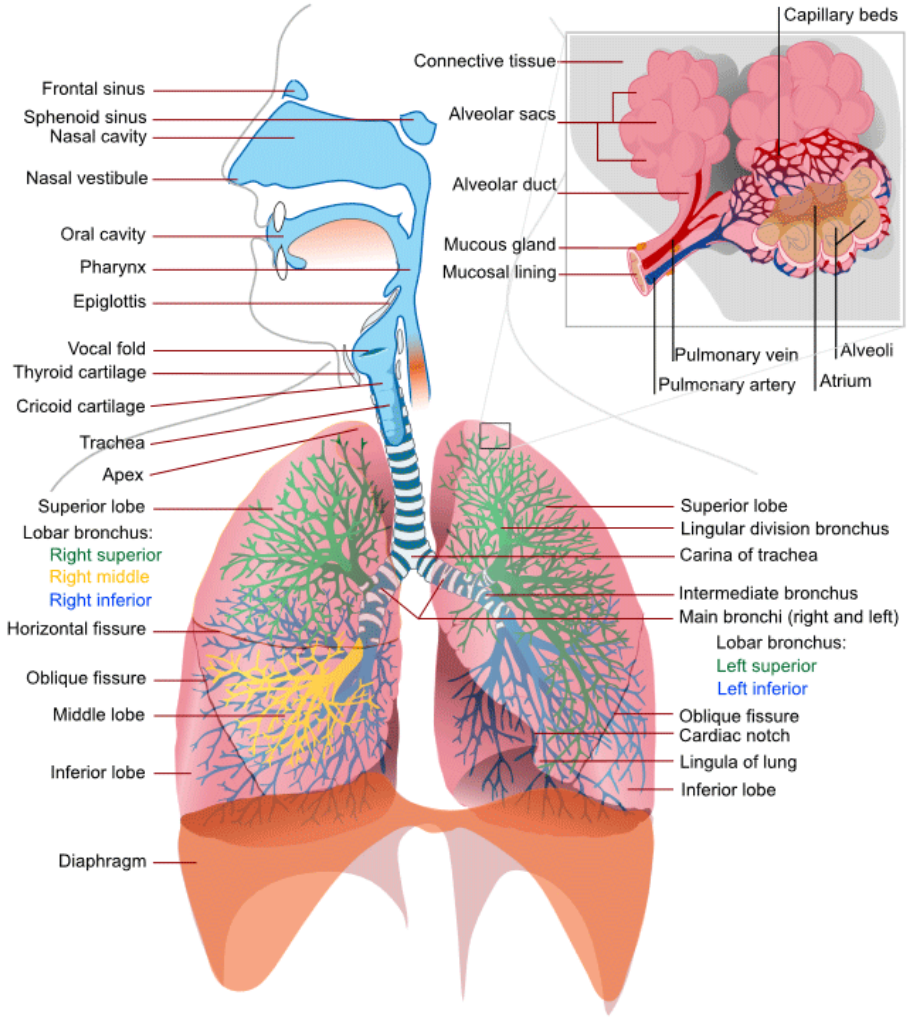

Fig.8: Structures of the pulmonary systems

Air is warmed to 37°C, humidified and cleansed by the conduction zone, particles from the air being removed by the cilia on the respiratory epithelium lining the passageways.

Decrease in airways diameter and the increase in surface area are the two most important factor influencing lung functionality. Trachea diameter is about 1.8 cm, while alveolar ducts diameter is about 0.04 cm, allowing a suitable air penetration into lower airways, necessary to

the lungs expansion. The increase in lung surface area promote exchange of gases from alveolar space and blood of alveolar capillaries.

Another important factor influencing lung functionality is the presence or absence of cartilage in airways [39]. Trachea and bronchi are reinforced with hyaline cartilage in order to hold open the airways, remaining pervious and accessible even when the internal pressure is lower than the outside. The bigger diameter and the rigid structure are responsible of a tiny resistance offered by trachea and bronchi to the airflow. Instead, bronchioles have no cartilage and are surrounded by smooth muscle, that with its contraction influence bronchiole lumen.

The respiratory tract is covered by an epithelium, which varies down the tract (figure 9), and serves to moisten and protect the airways, as a barrier to potential pathogens and foreign particles, and preventing infection and tissue injury by the action of mucociliary clearance [39].

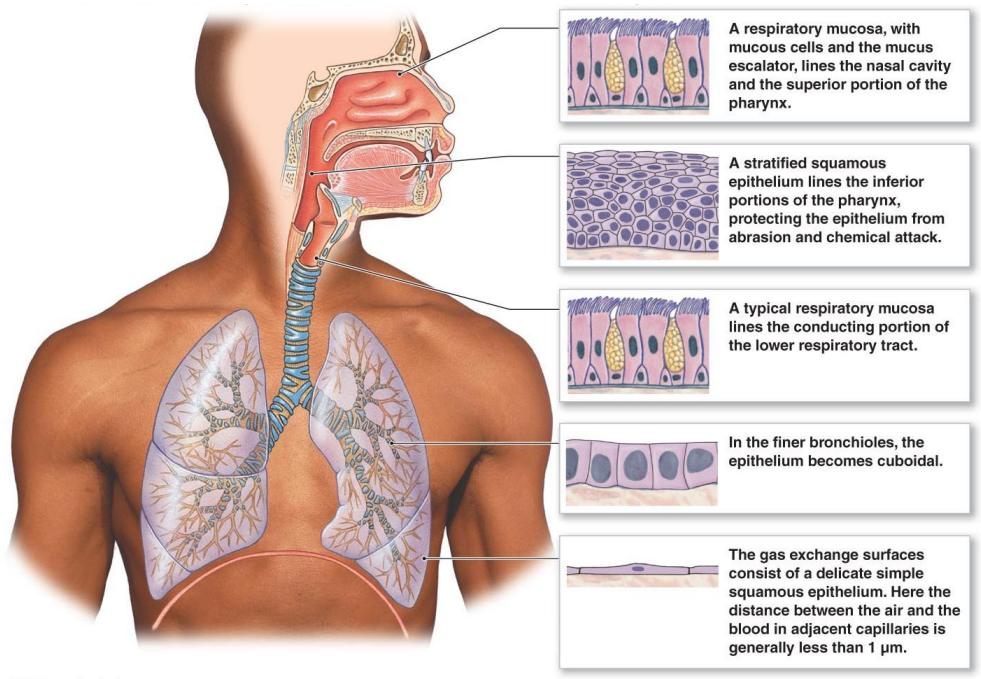

Fig.9: Histology of respiratory system.

The conducting passageways of the respiratory system (nasal cavity, trachea, bronchi and bronchioles) are lined by a ciliated pseudostratified columnar epithelium [39].

The majority of cells composing the ciliated pseudostratified columnar epithelium are ciliated cells, goblet cells and a basement membrane. The ciliated cells are columnar epithelial cells with specialized ciliary modifications. Goblet cells are columnar epithelial cells that contain

membrane-bound mucous granules and secrete mucus and periciliary liquid, which exist in close proximity without getting mixed up.

In healthy individuals, mucus contains 97% water and only 3% solids of which mucins constitute around 30% (the rest is non-mucin proteins, lipids, salts and cellular debris). With this composition, the mucus will have a gel consistency and can easily be cleared from the airways by the ciliary beating. The periciliary liquid layer (PCL) is, instead, occupied by large amounts of mucins and large glycoproteins both of which are tethered to the cilia.

This prevents the entering of larger molecules, such as inhaled particles and mucins of the mucus layer, into the PCL.

This biphasic layer of mucus protects the epithelium from dehydration, helping to humidify the air and providing a protective barrier by trapping inhaled particles.

The basal cells are small, nearly cuboidal cells with the ability to differentiate into other cells types, responding to injury of the airway epithelium.

Down the respiratory tract, in the finer bronchioles the epithelium becomes cuboidal, while alveoli are lined by squamous epithelium, cells sometimes called Type I pneumocytes which facilitate gas exchange. Scattered among the squamous cells are occasional larger cuboidal cells, sometimes called greater alveolar cells or Type II pneumocytes. These cells secrete surfactant, which serves the critical function of reducing surface tension and preventing the collapse of alveoli, and contains 90 % of lipids and 10 % of proteins.

The cell layer thickness of the air-blood barrier gradually decreases from trachea-bronchial region major than 10 µm to the alveolar cells region with a cell layer of 0.3-1 µm.

Alveolar spaces are in communication with the external by the airways, and for this reason, easily accessible by pathogens. The human body is protected by this event thanks to the presence of another cellular type present down the airways and in perialveolar tissue, the lymphocytes and above all macrophages.

1.2.2 Fate of inhaled drugs

Several factors affect the fate of inhaled drugs, and consequently their local availability. These factors include drugs physico-chemical and biological properties, drug deposition into the different regions of the respiratory tract, and above all the clearance mechanisms present in the lung, such as dissolution, mucociliary clearance and macrophage uptake.

1.2.2.1 Deposition in the lungs

The amount and the deposition site in the lungs are strictly depending on the patient characteristics (lungs geometry, sex, age, integrity of pulmonary system or presence of disease) and physical properties of particles, such as particle dimension, density, shape and hygroscopy. The site of deposition of a particle (a drug or a drug delivery system etc.) within the lungs depends on its aerodynamic diameter (d_{aer}) and on the breathing pattern of the patient [40]. The aerodynamic diameter of a particle is equivalent to the diameter of a unit density sphere (ρ_0) that has the same terminal velocity in still air as the particle:

$$d_{aer} = d\sqrt{\frac{\rho}{\rho_0 \chi}}$$

where d is the geometric diameter of the particle, ρ is the particle density and χ is the particle dynamic shape factor denoting deviation of shape from sphericity.

The size of inhaled particles is widely defined by the mass median aerodynamic diameter (MMAD) describing the diameter of a particle of mass equal to the average particle diameter of a population, meaning the diameter of a particle in which the 50 % of the aerosol mass is greater than the other 50 % smaller [41].

Mechanisms of particle deposition include impaction, sedimentation, interception, diffusion and electrostatic deposition [41], as reported in figure 10.

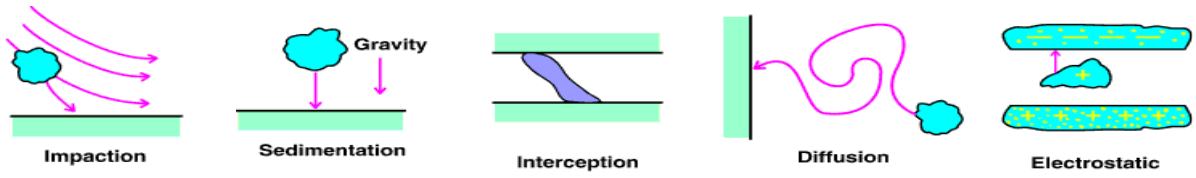

Fig.10: Mechanism of particle deposition into the lungs.

Impaction is the physical phenomenon for which the particle tend to continue on a trajectory through the airway, irrespective of the conformation and curves of the respiratory tract. If particles possess an enough momentum, they will not follow the airflow but at the points where the airflow suddenly changes direction, they collide with the airway wall. This mainly happens in the first 10 bronchial generations, where the air speed is high and the flow is turbulent. This phenomenon mainly affects particles larger than 10 μm, which are mostly retained in the oropharyngeal region.

Sedimentation is a time dependent event for which particles with sufficient mass are deposited due to the force of gravity when they remain in the airway for a sufficient length of time. This

predominates in the last 5 bronchial generations, where the air speed is slow and the residence time is therefore longer.

Interception is mainly the case of fibers or particle with elongated shape that are deposited as soon as they contact the airway wall. This event happens when particle diameter is similar to that of airways, or when they reach points in which the distance between the center of the particle and the surface is lower than the dimension of the same particle.

Diffusion is the phenomenon regarding particles with MMAD smaller than 1 μm that move erratically from one place to another in the airways. This happens as a consequence of the Brownian diffusion, especially at the alveolar spaces, where the air speed is practically zero. These particles are generally not deposited and they are expelled once again upon exhalation.

Electrostatic deposition is the phenomenon for which an electrostatic charged particle, reaching the airways surface, induces a opposite charge on this, which attracts the particle. This attraction could induce the deposition of a particle for electrostatic precipitation.

Filtering of large particles (d_{aer}>5 μm) occurs in the upper airways (mouth, trachea and main bronchi) by inertial impaction; 1 to 5 μm d_{aer} particles deposit by gravitational settling in the central and distal tracts and particles with d_{aer} lower than1 μm are mostly exhaled.

Ultrafine (< 100 nm) particles efficiently deposit by random Brownian motion in the respiratory tract: particles < 100 nm reach the alveolar region while particles < 10 nm already deposit in the tracheo-bronchial region due to their high diffusion coefficients [40], as showed in figure 11.

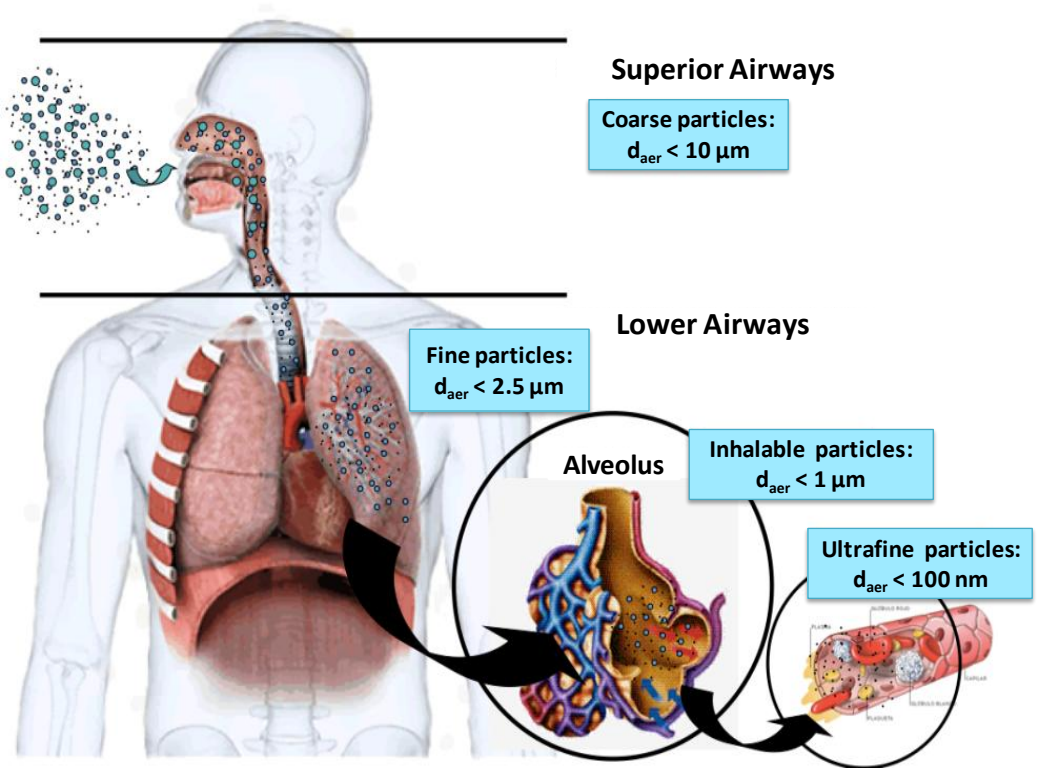

Fig.11: Particle deposition into the lungs depending on their aerodynamic diameter.

Slow inhalation is generally preferred to minimize inertial impaction in upper airways and to increase penetration into the lungs of large particles, whereas small particles are much less sensitive to fast/slow inhalation maneuvers [40]. A breath hold gives time to particles that have penetrated deep into the lungs to sediment on airway surfaces.

As seen from the equation defining d_{aer}, other parameters than the geometric diameter are involved in lung deposition.

Particle density is an important parameter, being d_{aer} function of the square root of particle density. Thus, reducing particle density allow to decrease its d_{aer}. Accordingly, large (> 5 µm) particles can be successfully inhaled deep into the lungs as far as their density is low.

Particle shape can be designed to target different regions of the respiratory tract. For instance, fibers have an aerodynamic diameter few times smaller than their length, which permits deep lung deposition. Unfortunately, a higher lung toxicity has been reported for elongated particles, compared to spherical particles [40].

Charged particles deposit more readily in the lungs than neutral particles. Moisture absorption may increase particle size, which may shift pulmonary deposition upwards.

Hygroscopy is another important factor for particle deposition because the attraction and holding of water molecules from the surrounding affect particle dimension and density and consequently the deposition site. In general, it is considered that hygroscopic growth does not have much of an effect in particles with MMAD less than 0.1μm; meanwhile it is very intense in particles with MMAD larger than 0.5μm [41].

The hygroscopy of molecules can be used to try to favor the deposition of inhaled drugs. Some studies showed that submicrometric or nanometric take the advantage of later growth due to hygroscopy, which enable them to be retained within the lungs [41].

1.2.2.2 Clearance mechanisms in the lungs

Once deposed in the airways, particles could be eliminated by different pathway existing in the lungs, including coughing, dissolution, mucociliary escalator, translocation from the airways to other sites, phagocytosis by macrophages (figure 12).

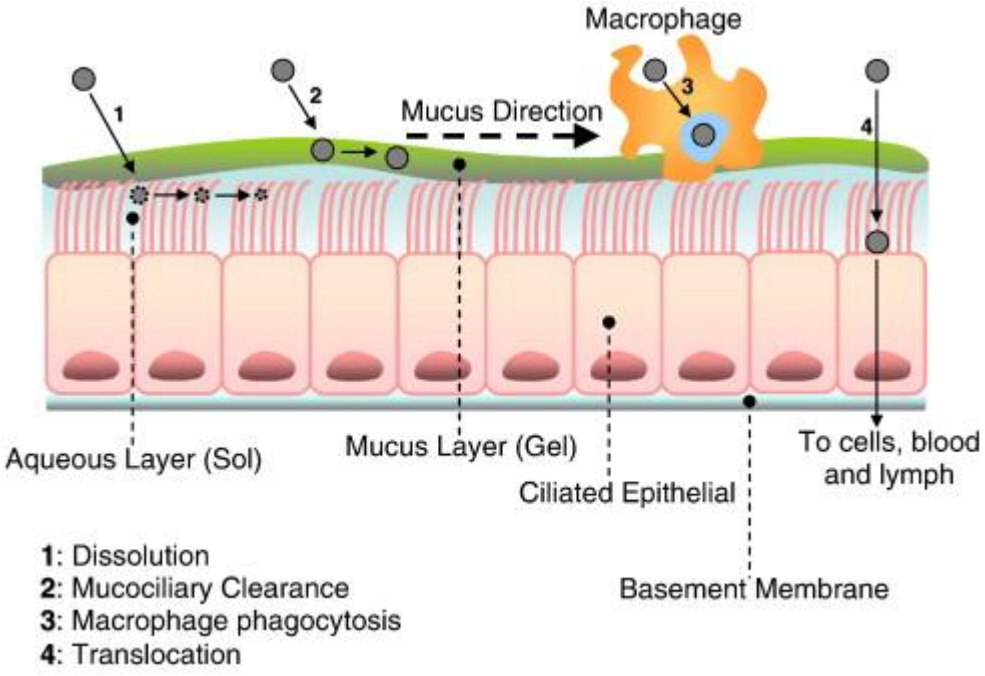

Fig.12: Pathways determining the fate of inhaled particles.

When particles arrive on the airways, they encounter the surfactant on top of the airway lining fluid. The surfactant will enhance the wetting of the particle and help it to sink into the fluid, passing first through the gel phase and then the sol phase [42].

Dissolution

Dissolution depends on the site of deposition, which determines the volume of airway fluids available for dissolution, on drugs solubility and dose [42]. Freely water soluble drugs (organic salts and polar compounds) will dissolve readily in the airway fluid followed by absorption or elimination by the mucociliarly escalator. Sparingly soluble drugs (inhaled corticosteroids, ICS), which have aqueous solubility ranging from 140 to below 0.1 μg/mL need more time to dissolve.

Once dissolved, the drug molecules are diluted in the airway fluid where they can bind to proteins, opsonins, or other constituents and be metabolized and/or absorbed into the blood and lymph. Absorption of the drugs depends on the site such as alveolar or conducting airways (which affects the barrier thickness and surface area) and the drug molecule itself (which impacts on passive diffusion and active uptake by the epithelium).

Mucociliary clearance (MCC)

MCC operates in the ciliated airways where the movement of the cilia transports the mucus carrying the drug or particles on the epithelial surface towards the pharynx-larynx and then to the GI tract [42].

MCC velocities in respiratory airways decrease with airway diameter. The mucus velocity measured in the human trachea is 5.5 mm/min, decreases to 2.4 mm/min in the main bronchi [40]. In reality, dissolution and MCC occur simultaneously and their relative importance would depend on the elimination rate from each of these contributions.

The composition and clearance of respiratory mucus are often altered in patients suffering from respiratory diseases and this may affect the fate of inhaled drug. It has been reported that the thickness of the mucus layer increases from 2 to 30 μm in healthy lungs to more than 250 μm in cases of CF and other obstructive airway diseases [42].

Macrophage uptake

Alveolar macrophages are responsible for clearance of particles deposited in the alveolar region, in which MCC is absent. In response to the deposited particles, alveolar macrophages will migrate to the particles and phagocytise them via chemotaxis involving opsonisation. Macrophage uptake is believed to complete in 6–12 h after deposition of the particles in the alveoli [42]. Once internalized in the macrophages, particles will be either disintegrated by enzymes in lysosomes or accumulated in the lymphatic system draining both airways and alveoli and finally terminating in the mediastinal and hilar lymphonodes. A minor fraction of

the particle-carrying macrophages will migrate to the ciliated airways where they are removed by MCC [42].

Translocation into cells, blood and lymph

This process involves the transcytosis of the particles into the epithelial cells and/or across the epithelia of the respiratory tract into the interstitium and then to blood and lymph. As described earlier, translocation to the lymphatic system can be facilitated by macrophage uptake.

When translocated to the systemic circulation, drug or particles could cause unwanted effects on the blood and other organs in the body. Some biological effects may include inflammation, oxidative stress, cytotoxicity, fibrosis, and immunologic responses [42].

1.2.2.3 Absorption in the lungs

The pulmonary membrane is naturally permeable to small molecule drugs and to many therapeutic peptides and proteins. The epithelium of the lung, the significant barrier to absorption of inhaled drugs, is thick in the trachea (50–60 μm), but diminishes in thickness to an extremely thin in the alveoli (0.2 μm) and change in cell types and morphology going from trachea, bronchi, and bronchioles to alveoli is very dramatic [43]. Lipophilic and non-ionized compounds are transported across respiratory epithelia into the bloodstream more rapidly and in larger amounts than hydrophilic compounds. In general, small hydrophilic compounds (log $P < 0$) have a mean half-life to absorption of around 1 h, whereas lipophilic small molecules (log $P > 0$) are absorbed in approximately 1 min.

The mechanisms of transport across respiratory epithelia depend on the physico-chemical and biological properties of the drug. Lipophilic drugs are mainly absorbed by passive diffusion through the cells whereas hydrophilic drugs are absorbed by diffusion through tight junctions. Some compounds have been shown to use drug transporters as active mechanism of absorption. Furthermore, the rate of macromolecule transport from the airway lumen into the systemic circulation is inversely related to molecular weight. Macromolecules with a molecular weight above 40 kDa are absorbed over several hours, in contrast to peptides or smaller proteins which reach the bloodstream within a few minutes following inhalation. Peptides and small proteins can be subject to local proteolysis and large macromolecules can be cleared by alveolar macrophages. The prolonged presence of macromolecules within the lungs can be utilized to sustain drug presence within the respiratory tract by drug conjugation to macromolecules [40].

The lungs are more permeable to macromolecules than any other portal of entry into the body. Some of the most promising therapeutic agents are peptides and proteins, which could be inhaled instead of injected, thereby improving compliance [43].

The bioavailability of peptides and proteins is 10–200 times greater by pulmonary route as compared with other non-invasive routes [43]. This fact can be attributed to the considerable absorptive surface at the air interface, covered by an extremely small volume of fluid (10–20 ml) and the entire cardiac output rushes through its capillary network, which lies fractions of a micron beneath the absorptive surface [43]. Due to this physiological and anatomical peculiarity, an inhaled aerosol can be widely dispersed and deposited in quite high concentrations in close proximity to the blood stream. Like the interior of the body, the surface fluids of the lung contain also antiproteases that inhibit the enzymatic breakdown of proteins.

1.2.3 Devices for administration of inhaled drugs

A successful pulmonary administration requires the harmonic interaction between the drug formulation and the inhaler device. Since, currently, inhalation therapy is the best option for lung diseases like asthma, CF and chronic obstructive pulmonary disease (COPD), a remarkable scientific interest in the technology for pulmonary delivery was spiked by the fact that the lungs can be used as a portal for systemic drug delivery.

Devices used to deliver therapeutic agents to the lungs are based on one of the three platforms: nebulizers, pressurized metered-dose inhaler (pMDI), and dry powder inhalers (DPIs).

The major problems with the use of inhaler devices are the deposition of aerosolized particles in the oropharyngeal region and upper airways and the lack of coordination between device actuation and patient inhalation, especially difficult in children and the elderly.

1.2.3.1 Nebulizers

There are two types of nebulizers, jet and ultrasonic, that differ in the force used to generate the aerosol from the respective liquid (figure 13). Depending on the model and the manufacturer, nebulizers generate 1–5 μm droplets. Nebulizers do not require patient coordination between inhalation and actuation, thus they are useful for pediatric, elderly, ventilated, non-conscious patients, or those who are unable to use pMDIs or DPIs.

Nebulizers have the capability of delivering larger doses compared to the other aerosol devices even though this will require longer administration times [44].

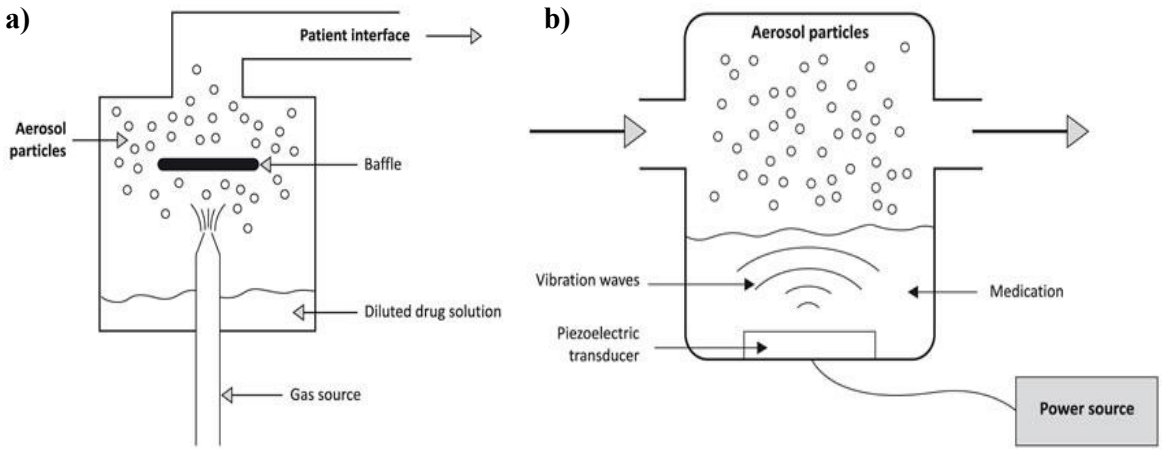

Fig.13: a) Jet and b) ultrasonic nebulizers.

Jet nebulizers are based on the Bernouilli theory, according to which a compressed gas that passes through a narrow orifice creates a low-pressure area upon exiting. The low pressure will cause the aspiration of the liquid formulation, where the drug is dissolved or suspended, and the production of small droplets. Ultrasonic nebulizers use piezoelectric crystals that vibrate at a high frequency within the nebulizing chamber, transmitting the vibratory energy to the liquid that is in contact with it, converting the liquid into an aerosol. Jet nebulizers can generally aerosolize most drug solutions, while ultrasonic nebulizers may not be effective for viscous suspensions or solutions [41].

From the device perspective, the variables that need to be optimized to emit an accurate and consistent dose with the nebulizer are the volume of the drug inhalable solution, the viscosity of the drug solution, the air flow and pressure in case of jet nebulizers and the tubing, mask, or mouthpiece used. A large proportion of the emitted dose from the nebulizers may be lost in the tubing, may remain as “the dead volume”, or be lost in the surrounding area in case of unvented nebulizers, exposing others to the aerosol. The lack of optimization of these variables is the main source of dose variability [44].

A disadvantage for nebulizer users is that they have to be assembled and loaded with the medication before each use. Then they have to be de-assembled and cleaned.

Newest nebulizer models have been put in the market by using novel technology able to circumvent the disadvantages of classic nebulizers. These include breath-enhanced, breath-actuated, and vibrating mesh nebulizers.

Breath-enhanced jet nebulizers are designed to allow air entrainment during inspiration and to vent the expired air outside of the device. The main advantage of this approach is to increase the output rate, which in turn will decrease the administration time.

Breath-actuated nebulizers emit aerosolized droplets only when the patient inhales. No drug is wasted during exhalation as the case of regular jet nebulizers and dissemination of expensive or toxic drugs to the surrounding environment is avoided.

Vibrating mesh nebulizers have a mesh plate that, when it vibrates through the action of the piezoelectric element, breaks the liquid into very fine droplets, which increases the volume of aerosol deposited in the alveoli. A more sophisticate version of a vibrating mesh nebulizer has an electronic indicator that shows when the patient is breathing appropriately, and only then it release the dose, with droplets of MMAD lower than 4 µm and lower drug loss.

1.2.3.2 Pressurized metered-dose inhaler (pMDI)

pMDIs are devices used to administer aerosolized drugs that emit a fixed dose of medication with each pulse [41].

pMDIs are the most popular inhalers to treat local respiratory diseases such as asthma and COPD, and are composed by the canister, metering valve, actuator, and a mouth piece (figure 14).

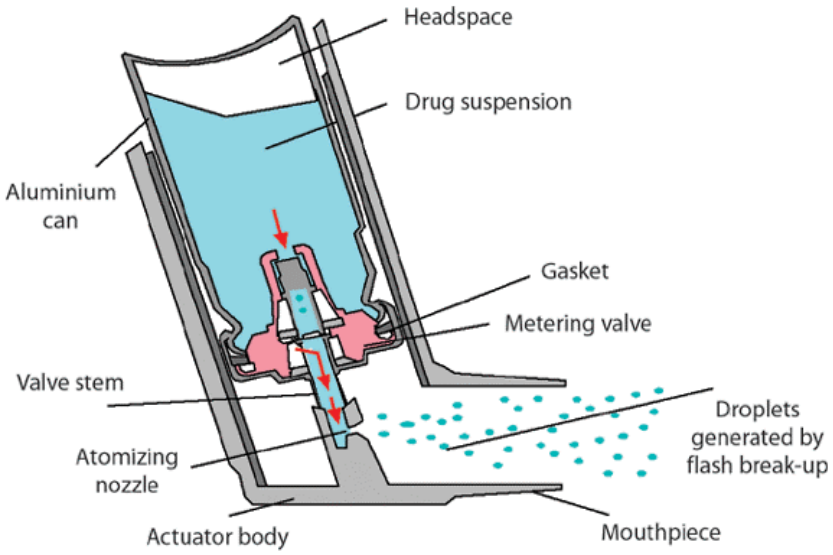

Fig.14: Pressurized metered-dose inhaler (pMDI).

Canisters are made of inert materials, such as plastic, stainless steel, glass, and aluminum. The metering valve is designed to deliver a precise aerosol amount (20–100 µL) each time the

device is actuated. When the inhaler is not used, an inner valve between the canister and the meter chamber is open allowing the chamber to be filled with the propellant–drug mixture in liquid form. At the same time, another outer valve between the meter chamber and the outside air is closed. As the patient presses the canister for dose actuation, the inner valve closes while the outer valve opens releasing the metered drug–propellant mixture retained in the chamber through the actuating orifice in an aerosol form [44]. Internally, the actuator includes the spray nozzle and the expansion chamber in which the released propellant from the metering chamber expands and partially volatizes due to the decrease in pressure.

The design of the actuator significantly influences the performance of pMDIs. Currently actuators are equipped with a dose counter that indicates the number of doses remaining.

pMDIs drug formulations can be solutions or suspensions in a single propellant or propellant mixture and may include excipients such as ethanol or surfactants to solubilize the drug or stabilize a drug suspension. Ideally, propellants should be nontoxic, non-flammable, and compatible with the formulation and provide consistent vapor pressure during the entire life of the product. In the past, the propellant used was chlorofluorocarbons (CFC), but due to their harmful effects on the ozone layer, they have been substituted by hydrofluoroalkanes (HFA). The development of MDI with HFA has also been able to reduce the size of the aerosol droplets and, therefore, improve the lung deposition of the drug [41].

pMDIs can be classified as breath-actuated or coordination devices. Breath-actuated pMDIs are activated when the device senses the patient's breathe and emits the dose in response, solving the problem of poor coordination between inhaler actuation and patient's breathe. Breathe coordinated pMDIs were developed to synchronize the inspiration with the discharge of the dose from inhaler. The inhalation flow rate is coordinated through the actuator and the patient gets time to actuate the pMDI reliably during inhalation.

A novel multidose, propellant-free and hand-held inhaler that represents a new category of inhaler devices is the multidose liquid inhaler named Respimat® Soft Mist™ inhaler [45].

The Respimat® inhaler combines the advantages of pMDIs and nebulizers. It is a small, portable, with no need for power supply (like pMDIs) that slowly aerosolizes propellant free-drug solutions as a soft mist (like nebulizers), thus decreasing the chance for oropharyngeal deposition.

The drug solution for Respimat® is stored in a collapsible bag inside the cartridge which is loaded inside the device. Once the patient presses the dose release button, the energy released from the spring forces the dose into the "uniblock", the unique structural part of this device. The uniblock allows the drug solution to pass through very fine filter channels releasing two

jet streams of drug solution, that converge creating a large fraction of respirable droplets with slow velocity

Spacers and valved holding chambers (VHCs) are used with pMDIs to increase the efficiency of aerosol delivery [44]. A spacer is a tube or extension device that is placed at the interface between the patient and the pMD, while VHC enables the patient to breath from a “standing aerosol cloud” that does not require breath coordination. VHCs have a one-way valve at the mouthpiece end to allow inhalation and prevent exhalation into the chamber.

These inhalation aids reduce the speed of the emitted aerosol and allow the evaporation of propellant from larger droplets reducing oropharyngeal deposition and increasing deep lung deposition. However, they can also reduce the doses delivered from pMDI due to electrostatic precipitation. Newer spacers and VHCs are made of anti-static polymers that minimize adherence of the emitted particles to the inner walls of the spacer. New generations of spacers can indicate whether the patient is inhaling correctly or not, such as those that whistle when the patient is inhaling too quickly [44].

1.2.3.3 Dry powder inhalers (PDI)

DPIs are devices through which a dry powder formulation is delivered by direct delivery of drug into the deep lungs utilizing the patient's respiration. DPIs were designed with the aim to eliminate the inherent coordination difficulties of p-MDI and do not require propellants for their administration, which makes them more respectful of the environment [41].

DPIs formulations have greater chemical stability than liquid formulations, but manufacturing powders with the appropriate characteristics for easy aerosolization and alveolar delivery is more complicated [44]. Performance of DPIs depends on the powder formulation and on inhaler device [46].

Traditional formulation are, generally, micronized drug particles (1–5 μm) blended with an inactive excipient (lactose, mannitol, trehalose, sucrose, sorbitol, glucose) of larger sizes (40 μm). Unoptimized powder blends can exhibit interparticulate cohesive forces (van der Waals forces, mainly), which cause particle aggregates, making powder dispersion very difficult. Drug carrier excipients added in appropriate sizes can reduce such cohesive forces, thus achieving a better flow and more uniform doses.

The design of DPI heavily influences the performance of the device. To aerosolize the drug powder, individual particles are deagglomerated by external forces, which can be airflow shear or particle–particle, particle–device impaction.

The Clickhaler, the Multihaler, and the Diskhaler are designed to feed the powder into a high speed airflow that splits particle agglomerates, thus achieving respirable particles. Other devices like the Spinhaler and Turbohaler (figure 15) depend on the impaction between particles and surfaces of the device to deagglomerate.

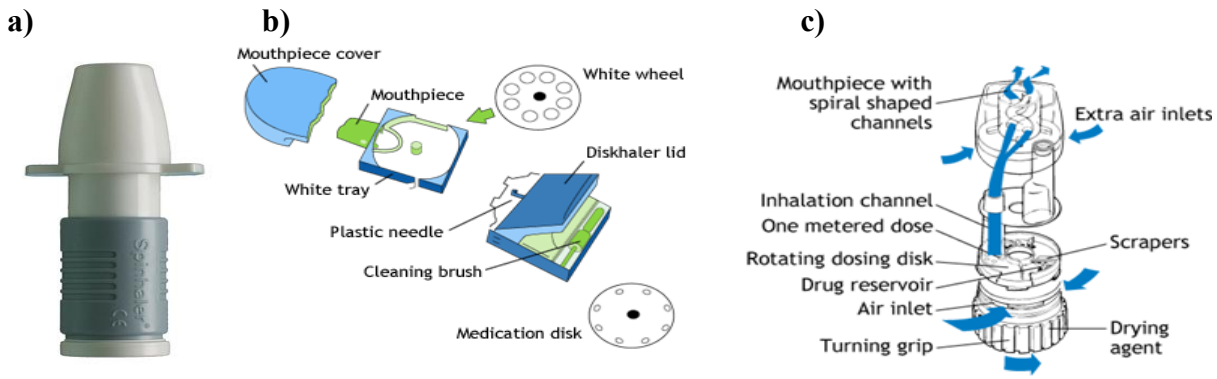

Fig.15: Spinhaler (a), Diskhaler (b) and Turbohaler (c) devices form pulmonary delivery of drugs.

DPIs can be classified by the number of doses the device can carry, the patient contribution to aerosolize the powder, or by the mechanism of powder dispersion.

By the number of doses, DPIs can be classified as single-unit dose, multi-unit dose, and multi-dose reservoirs, and are disposable or reusable. Multi-unit dose DPIs use factory-metered and sealed doses packaged so that the device can hold multiple doses at the same time without having to be reloaded. Multi-dose reservoir DPIs store the powder in bulk and have a built-in mechanism to meter individual doses upon actuation.

An example of multidose dry powder inhaler is ELLIPTA® (by GSK group) which can hold sufficient medication for one month (30 doses) without having to replace cartridges or capsules. This DPI was designed to be easily operated by patients of all ages, including the elderly, and a previous study demonstrated that it can be operated correctly by the majority of volunteers aged 20 years or older without previous experience of inhaler use and without verbal or demonstrative instruction [47]. To prepare the dose, it is necessary to open the cover, sliding the cover down to expose the mouthpiece, and hearing a "click". Before the administration, the patient have to exhale, then put the mouthpiece between their lips, and closing them firmly. Then the patient have only to take a long, steady and deep breath inhaling the medicine (figure 16).

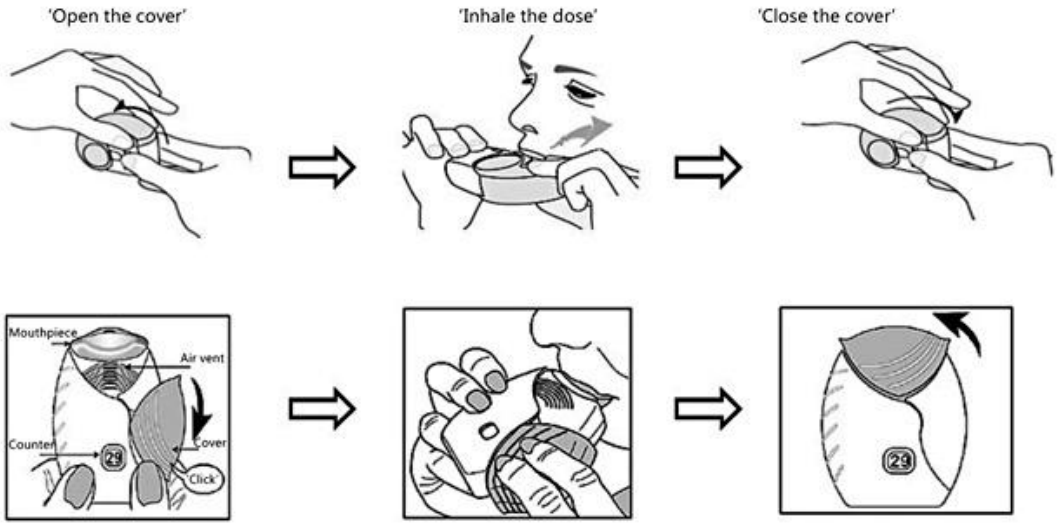

Fig.16: The three-step operation procedure to use the multidose dry powder inhaler ELLIPTA® .

Based on the mechanism for powder aerosolization, DPIs can be classified as passively- or actively-actuated devices. The original passive DPI was a breath-actuated device, relying solely on the patient's inspiration to provide sufficient air flow for entrainment and de-aggregation of the formulation. Device actuation was intrinsically tied to the patient's inhalation, thus avoiding coordination issues associated with p-MDIs.

However, pediatric patients, elderly patients, and those with advanced respiratory diseases are not able to generate enough pressure drop to achieve the optimum flow rate.

To enhance their performance, newer versions of passive DPIs are being developed to solve these issues. Active DPI devices are power assisted and designed with an internal energy source to aerosolize the powder bed in the DPI, so that dose administration is no longer dependent on the patient inspiratory flow rate. This energy source can be a battery, compressed gas, or a spring mechanism.

In active devices, the powder is dispersed by vibration, gas discharge, or an impeller. Some of that have a battery-powered motor that disperses the powder by impaction of a rotating impeller to generate aerosol.

1.3 Pulmonary Therapy in CF

In the last two decades, inhalation of drugs for the treatment of CF related lung disease has been proven to be highly effective. This strategy has circumvent the problem of the poor penetration of intravenously administered drugs into lung parenchymal tissue, and their potential systemic toxicity when given over longer periods of time.

Since inhalation therapy was discussed as part of a European Cystic Fibrosis Society (ECFS) Consensus Conference in 1999 and 2003, several new drug formulations and new inhalation devices have been developed [48]. These concern not only mucolytics and bronchodilators, but also anti-inflammatory drugs and above all antibiotics.

As described before, mucolytics or mucus mobilizers, such as HTS, NAC or Dornase alfa, are routinely used in clinic to improve MCC and consequently lung function. HTS (from 3% to 7% of NaCl), NAC (from 10 to 20 %) and Dornase alfa are administered through inhalation of an aerosol. Currently, the US product information for dornase alfa only recommends jet nebulizer/air compressor combinations for its delivery, but compared with standard jet nebulizer systems, the eRapid system proposed is a more convenient general-purpose electronic nebulizer that is able to deliver dornase alfa with the same efficacy as other devices but with shorter inhalation times[17].

Simultaneously to these commercially available products, different clinical trials have been done to study the effect and safety of other inhaled mucolytics using different mechanism of action, such as denufosol tetrasodium and lancovutide. Denufosol tetrasodium inhalation solution is a selective P2Y2 receptor agonist which activates an alternative chloride channel, which increases the hydration of the respiratory epithelium, improving mucociliary clearance and lung function [49], while lancovutide (Moli1901) inhalation solution is thought to activate intracellular calcium in alternative chloride channels, thereby increasing chloride transport and fluid secretion onto the apical surface of the airway [48].

In 2012 Pharmaxis Pharmaceuticals was authorized to the marketing of Bronchitol®, the first airway-hydrating agent based on mannitol administered as inhalation powder. Mannitol powder, placed in hard capsules, is delivered by using a small DPI device, which is able to perforate the capsules and release the powder when the patient breathe in (figure 17). Lung deposition studies have demonstrated a 24.7% deposition of inhaled mannitol confirming its distribution to the target organ.

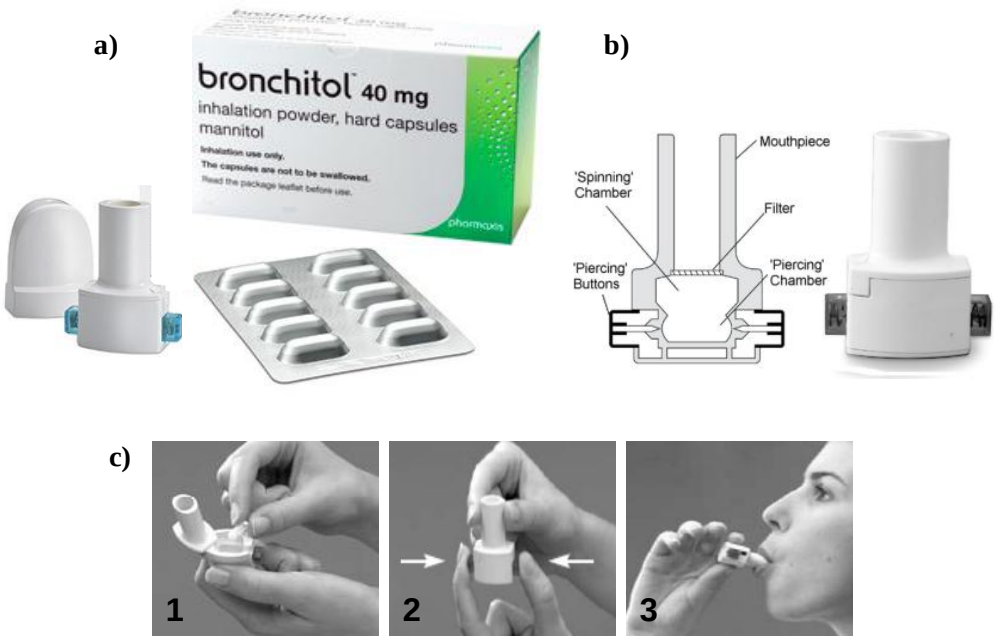

Fig.17: Bronchitol® pack containing the inhalation device and capsules blister (a), diagram of the DPI device (b) and step operation procedure to use Bronchitol® (c).

Mannitol is an osmotic agent, being able to induce influx of water, already used as diuretic and laxative by intravenous and oral admnistration. Even if the mannitol exact mechanism of action in CF is unknown, inhaled mannitol change the viscoelastic properties of mucus, increase the hydration of the periciliary fluid layer and contribute to increase mucus clearance of the retained secretions through mucociliary activity [50].

Short-acting and long-acting inhaled bronchodilators are used to treat of CF pulmonary symptoms, to open the airways, improve airway clearance, and to prevent bronchoconstriction-related symptoms during nebulized therapy with other drugs. Bronchodilators are delivered into the lungs via either a DPI, pMDI or as an aerosol via a nebulizer [51].

Inhaled anti-inflammatory drugs are used to reduce endobronchial inflammation in CF and to minimize systemic adverse effects, experienced with oral corticosteroids.

Inhaled corticosteroid treatment demonstrated significant improvements in daily symptom scores for cough and dyspnoea, is generally well tolerated and the treatment does not affect urine and blood cortisol, or cause any decrease in adrenal reserve or any increase in airway infection [48]. However, a study showed a significant slowing in linear growth in pre-pubertal children receiving dry-powder fluticasone propionate over 12 months [52].

For more than a decade, oral administration at high-dose of ibuprofen NSAID has been studied to slow the deterioration and destruction of the CF lung, but despite the encouraging results, in clinical the anti-inflammatory approach is rarely practiced because of systemic side effects. The recent discover of ibuprofen activity as a CFTR corrector[27] and as an antimicrobial agent itself at high dose with synergic activity with other antimicrobials has rekindled the attention for this drug, and its formulations for pulmonary delivery. Encouraged by this discover, Professor L. Cannon, associate professor of microbial pathogenesis and immunology at Texas A&M Health Science Center, has started a preclinical phase study for ibuprofen nanoparticles administered by pulmonary route for the treatment of inflammation in CF.

However, the main formulation efforts have been made for the production of inhalation dosage forms based on antibiotics. In fact, the diffusion of multi-drug resistant bacteria has focused research attention also on new antibiotic regimens for fighting *P. aeruginosa* chronic infections. Novel lyophilized dry powders for inhalation solutions have been developed for unstable antibiotics, such as aztreonam and colistin. Aztreonam lysine powder for inhalation solution (Cayston®), approved by FDA in February 2010, has been the first new inhaled antibiotic developed for CF in more than a decade[53]. Taking advantage of the different mechanisms of action of antimicrobial peptides, colistimethate sodium (Promixin®) has also been approved for the treatment of colonization and infections of the lung due to susceptible *P. aeruginosa* in CF patients [53].

Tobramycin Solution for Inhalation (TSI) is registered as TOBI® by Novartis (300 mg/5 ml) in combination with a PARI LC PLUS™ reusable jet nebulizer and a suitable compressor. Additionally, tobramycin is present in Bramitob® (300 mg/4 ml) in combination with a PARI LC PLUS™ reusable jet nebulizer and the PARI TURBO BOY™ compressor. Despite tobramycin inactivation in CF airways, caused by the bound between the positively charged antibiotic and the negatively charged DNA fibers and *P. aeruginosa* alginate, intermittent treatment (28-day on/28-day off), using 300 mg of tobramycin twice daily, significantly improved lung function and reduced sputum *P. aeruginosa* density, if compared with placebo in CF patients.

A more sophisticated tobramycin formulation is TOBI® Podhaler® by Novartis [54], a inhalation powder formulation. In this formulation tobramycin is incorporated in microparticles manufactured by an emulsion based spray-drying process [55], designed to create porous particles with a sponge-like morphology, as showed by scanning electron microscope (SEM) in figure 18.

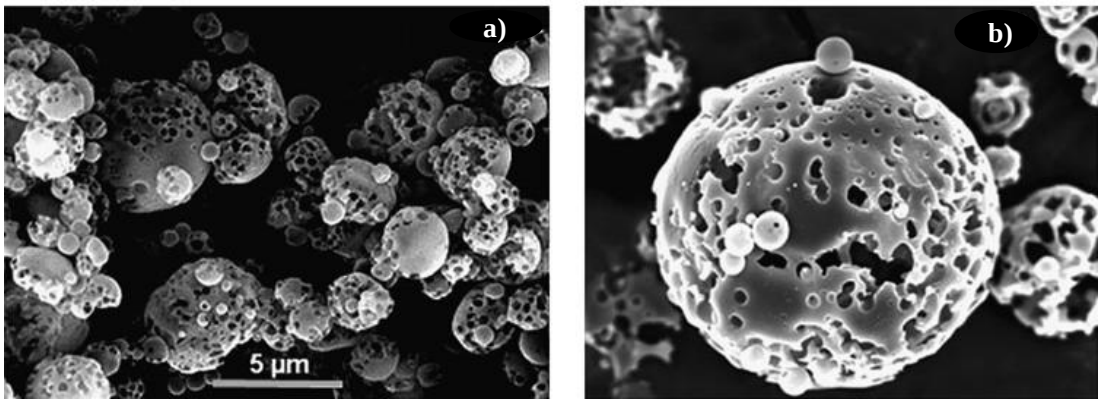

Fig.18: SEM images of TOBI® Podhaler® particles (a), and a particle detail (b) [55].

Trobramycin is delivered by TOBI® Podhaler® via the breath-actuated T-326 Inhaler (Novartis Pharmaceuticals, San Carlos, CA, USA). The T-326 Inhaler is a portable, capsule-based DPI, which is mechanical and does not require an external power source or electronics After inhalation of a 112 mg single dose (4 times, 28 mg capsules) of TOBI® Podhaler® in CF patients, sputum Cmax of tobramycin is about 1.5 times higher than sputum Cmax after inhalation of a single 300 mg dose of TOBI® [54] .

Moreover, the advantages of this formulation include faster delivery, ease of use, portability, reduced need for cleaning (figure 19), and room temperature storage. It is anticipated that the reduced treatment burden and improved dose consistency afforded by TOBI® Podhaler® may translate into improved treatment compliance and better therapeutic outcomes for CF patients with *P. Aeruginosa* airway infections [55].

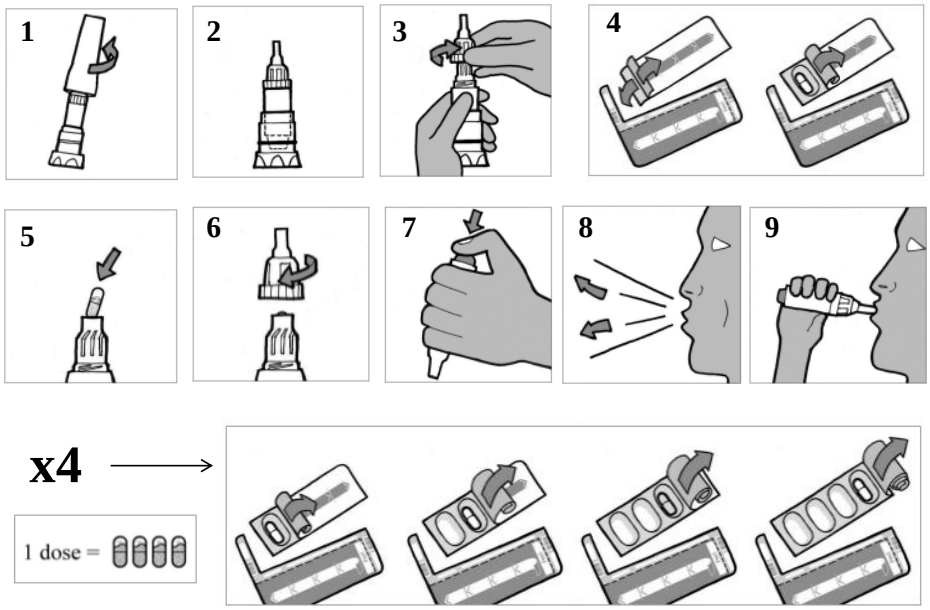

Fig.19: The step operation procedure to use TOBI® Podhaler® DPI.

After TOBI® Podhaler®, two DPI products based on excipient-free spray-dried powders have been also marketed for CF. Colistimethate sodium DPI (Colobreathe®) is approved in Europe for the treatment of chronic *P. Aeruginosa* infections in patients with CF aged ≥ 6years. In a phase III clinical trial in this patient population, colistimethate sodium DPI was effective and generally well tolerated, with similar adverse event profile to that of nebulized tobramycin, except for a numerically higher incidence of cough and abnormal taste [53].

Many efforts have been done in order to produce new inhalable formulations with combinatorial effects, such as oral and inhaled Lynovex® based on cysteamine, in clinical development by NovaBiotics Ltd (Aberdeen, UK), who has demonstrated to have antibacterial, antibiofilm and mucoactive activities. Cysteamine is already established in clinical practice for an unrelated orphan condition, such as cystinosis. For CF therapy, conducted clinical trials demonstrated a mucolytic activity comparable to currently available mucoactive agents, rapid bactericidal action against both metabolically active and persister cells of *P. aeruginosa* and synergistic action with conventional CF antibiotics [56].

The Company is planning to start a US & European registration procedure for Lynovex Oral as well as a phase IIA proof-of-concept clinical study for Lynovex Inhaled later this year.

1.3.1 Barriers in CF lung disease to inhaled therapies

Despite the countless efforts made for the improvement of formulations for the treatment of CF, there are many limitations that prevent important determinants of the clinical outcomes such as drug concentration and permanence at the site of infection as well as the extent of drug penetration through the mucus layer, which are still inadequate.

The success of a CF inhalation therapy is seriously limited by the pathological characteristics of the site of action and administration. Several factor, including extracellular (periciliary layer and mucus barrier) and cellular barrier (bacteria biofilm, airway epithelial cells and phagocytosis) are critical and must be overcome.

1.3.1.1 Extracellular barriers

Mucus barrier

Mucus layer covering respiratory epithelia represents one of the greatest obstacles to overcome, that may strongly affect drug bioavailability and targeting, especially for CF where there is an overproduction of a viscous, highly complex and purulent mucus.

Careful elucidation of mucus chemical composition, of its rheology and thickness is important to the development of inhalable formulation able to overcome this barrier.

Mucus is a viscoelastic gel layer that protects tissues that would otherwise be exposed to the external environment. Mucus is composed primarily of crosslinked, bundled and entangled mucin fibers secreted by goblet cells and submucosal glands of the lamina propria at the apical epithelium. Mucin fibers (figure 20), typically 10–40 MDa in size and 3–10 nm in diameter, are proteins glycosylated via proline, threonine, and/or serine residues by O-linked N-acetyl galactosamine as well as N-linked sulfate-bearing glycans. Glycan coverage of mucins is dense, with 25–30 carbohydrate chains per 100 amino acid residues, and contributes up to 80% of the dry weight of mucus [57].

Most mucin glycoproteins have a high sialic acid and sulfate content, which leads to a strongly negative surface that increases the rigidity of the polymer via charge repulsion. Sialomucin content is suggested to be highly correlated to mucus viscosity and elasticity[57].

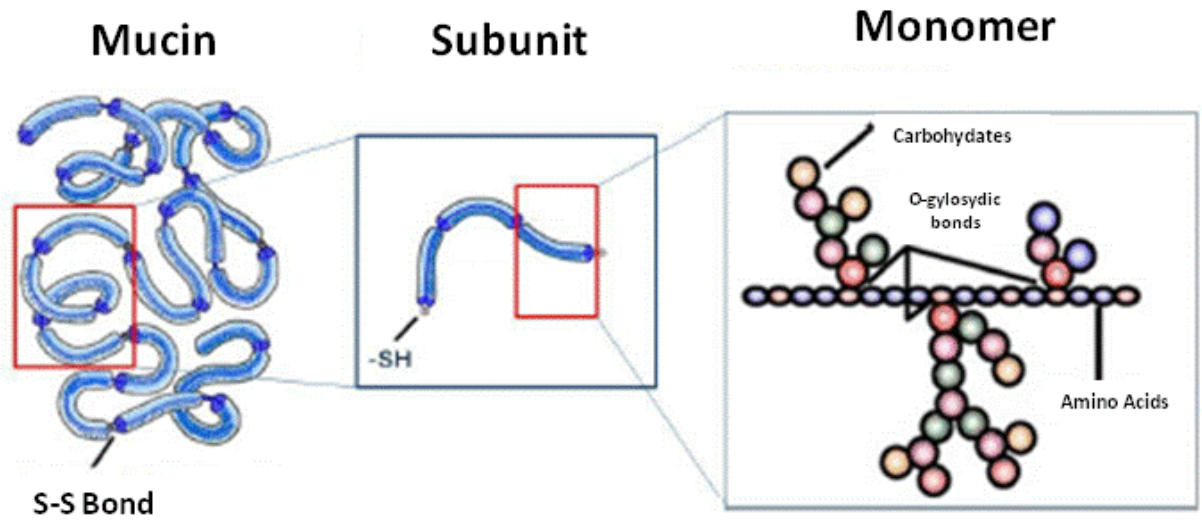

Fig.20: Schematic representation of mucin structure in respiratory mucus.

Mucins can be generally separated into two families: cell-associated mucins ranging between 100 and 500 nm in length that contain a transmembrane domain, and secreted mucins that are up to several microns long [57].

Mucin content, governed by mucin secretion rates as well as the degree of mucus hydration, is a major determinant of mucus rheology. Mucus rheology changes based on the composition of mucins and their glycosylation, both of which vary with age, the host's diet, and the presence of specific disease [57]. In CF, where the mucin to water ratio is significantly increased to ~ 5–10 times greater than normal, mucus viscoelasticity can approach that of rubber, with typical viscosities 10^4–10^5 fold higher than water at low shear rates.

In addition to mucins, mucus contains DNA, lipids, salts, proteins, cells and cellular debris [57].

In healthy subjects, DNA represents approximately the 0.02% of the mucus by mass, with the vast majority originating from debris of shed epithelial cells. Secondary infections in CF cause neutrophil lysis and a further increase of the DNA content to up to 0.5–1.5% of the mucus by weight. This increase is directly responsible for the 10–100 fold further increase in the mucus viscoelasticity associated with the disease.

Lipids, with a mass ratio up to 1–2%, represent a high percentage of the molecules present in mucus and its is associated with hydrophobic domains of mucin glycoproteins. In CF patient, higher total lipid content is correlated with an increased viscoelasticity.

Salts are normally present in mucus secretion, but pathological changes affecting mucus ionic strength, such as in CF, can directly lead to shrinkage or swelling of mucus and, thus, significantly alter mucus viscoelasticity. Also the presence of higher amount of proteins in CF mucus, such as actin, is directly responsible of increased mucus viscosity.

Machrophages, neutrophils, mucoid and non mucoid bacteria are present in CF mucus secretions. However the contribution of cells and their debris to the viscoelasticity of mucus remains unclear. CF mucus is also characterized by a reduced amount of water, around 90 % versus typical 95-97% water present in healthy mucus secretions.

As consequence of this altered composition, CF mucus became an highly complex, viscous secretion, which preclude the diffusion and permeation of drug or particle through it, trapping the adhered particle and eliminating them by the residual MCC.

Mucus is able to trap drugs and particles because it may establish mucoadhesive interactions via hydrophobic, electrostatic and hydrogen-bond interactions.

In addition to its role as barrier that prevents the penetration, mucus may impair the activity and stability of inhaled drugs or particles due to the presence of various soluble macromolecules, proteins, lipids surfactants and ions.

In fact, since mucus in CF patients are mainly composed of negatively charged mucins and DNA, positively charged aminoglycosides, such as tobramycin, may be bound to these compounds, resulting in the inactivation of inhaled antibiotic. Moreover, colloidal stability of cationic polymeric and lipidic gene vectors is altered by their interactions with negatively charged mucus components, resulting in larger aggregates, which can affect and reduce gene transfer efficacy.

Periciliary liquid layer (PCL)

PCL has the length of the outstretched cilia (approximately 7 μm) and provides a low viscosity solution for ciliary beating acting as a lubricant layer for mucus transport.

PCL presents a significant steric barrier to inhaled drugs or particles, beacause the PCL has a fine mesh structure [58]. Moreover, similar to the mucus gel layer, the PCL may also serve as an adhesive barrier since the meshwork is primarily composed of cell-tethered mucins.

In CF lung disease, it appears that the primary pathophysiologic defect is the depletion of PCL volume, resulting in a failure of mucus clearance of bacteria and persistent airways infection.

Infact, the dehydration of the PCL mediated by dysregulation of epithelial sodium channels (ENaC) on the airway epithelium can cause an osmotically-driven collapse of the PCL, which further increases the barrier function to inhaled vectors by making the PCL mesh tighter [59, 60].

1.3.1.2 Cellular barriers

Assuming that the inhaled drugs successfully lands at the lungs and gets away with the extracellular barriers, it has still to be taken up by the target cell, that is the bacteria (for antimicrobials) or airway epithelial cells (for anti-inflammatory agents and disease-modifying agents) to be effective.

Bacteria biofilm

The main challenge of CF chronic infections remains the biofilm-like mode of growth adopted by *P. aeruginosa*, forming complex multicellular mucosa-attached aggregates (biofilm), characterized by massive production of alginates and other extracellular polysaccharides (EPS). Bacteria growing in biofilm display high resistance levels to antimicrobials, due both to reduced penetration of the antibiotic molecules through the EPS layer and to modification in biofilm cell physiology.

The slow penetration and possible entrapment within the biofilm [53], due to electrostatic interactions with the negatively-charged alginate matrix, can strongly reduce the drug availability in proximity of bacteria colonies. In fact, as described before, the efficacy of inhalable tobramycin is to date severely impaired by drug binding in CF airways, likely due to tobramycin/biofilm electrostatic interactions.

Airway epithelial cells

Different categories of CF drugs, such as anti-inflammatory agents or disease-modifying agents (nucleic acid-based therapeutics and CFTR modulators) have to cross the cellular membrane of airway epithelial cells and gain access into the cytoplasm or nucleus, where the final targets are located. The epithelial surface of the airways poses an additional barrier to inhaled drugs that is due to low efficiency of endocytosis across the apical membrane and tight junctions between cells that prevent the access [53]. Moreover, the barrier property of the airway epithelium is altered by obstructive lung diseases, primarily due to structural perturbations of tight junctions. In CF airway epithelial cell, the transepithelial electrical resistance (TEER) is higher and the paracellular permeability is lower compared to the healthy airway epithelium [58].

Moreover, once taken up by target cells, there are several intracellular barriers, including but not limited to acidic vesicles (i.e. endosomes and lysosomes), the molecularly crowded cytoplasm, and the nuclear envelope.

Phagocytosis by macrophage

Resident macrophages can rapidly engulf the foreign drugs or particles as a defense mechanism, representing a critical barrier for the greatest part of inhaled therapies [53, 61].

Particles in the size range of 250 nm to 3 μm are readily phagocytosed by macrophages, with increasing phagocytic uptake with the increase in the particle size within this dimensional range. In contrast, particles smaller than 250 nm are taken up less efficiently by macrophages.

Phagocytosis may pose a more challenging barriers in the lungs of CF patients, where alveolar macrophages are activated [58]. However, there are controversial literature data, highlighting that CF patients have a dysfunctional phagocytosis, ascribed to an inherent defect in both airway neutrophils and macrophages, caused by a reduced expression of cell surface recognition receptors [53].

1.3.2 Polymer-based carriers

Although it can be dated back to the 90s, the concept of using polymer micro- and nanoparticles for pulmonary delivery has evolved during time and is experiencing growing research interest in recent years, in order to overcome the effective barriers and clearance mechanisms present in CF patients. A fundamental feature of polymer systems relies on their ability to exert a prolonged drug release. This is crucial to reduce the number of administrations and increase patient adherence to the complex therapeutic regimen required by chronic lung diseases, such as CF. Micro and nanocarriers composed of polymers with particular physicochemical and biological properties have been identified as attractive candidates, fulfilling the stringent requirements placed on pulmonary delivery devices, such as sufficient association of the therapeutic agent with the carrier particles, co-delivering of different molecules with complementary functionalities, targeting of specific sites or cell populations in the lung, protection of the therapeutic agent against degradation, release of the therapeutic agent at a therapeutically optimal rate, ability to be transferred into an aerosol, stability against forces generated during aerosolization as well as low toxicity and dose frequency, maximized therapeutic efficiency, and minimized adverse side effects.Moreover, various extracellular and cellular barriers maybe successfully circumvented by adequate design of polymer carriers, as schematized in figure 21.

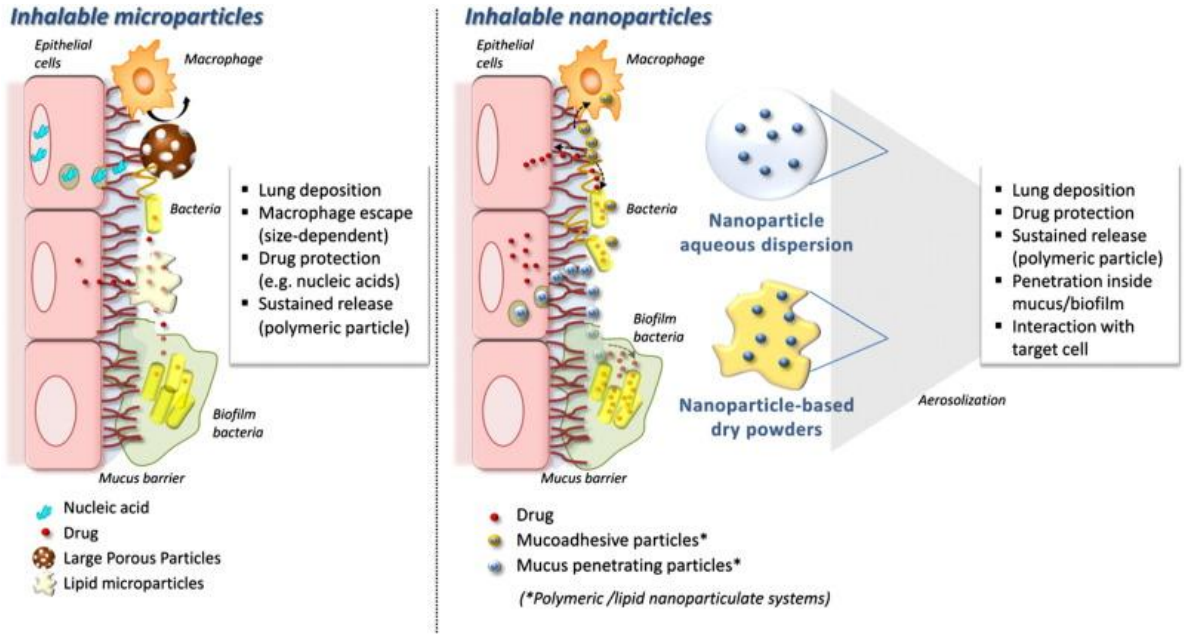

Fig.21: Inhalable drug-loaded particles engineered for overcoming anatomical and biological barriers imposed by CF lung.

The most significant examples of polymer-based carriers tested for CF, along with key in vitro/in vivo findings are reported in Table 2.

Table 2. Examples of polymer-based formulations under development for drug delivery in CF lung.

Polymer	Drug	Formulation	Key findings	Ref.
PLGA microparicles	Plasmid DNA, Reporter gene CAT	Aqueous suspension for nebulization	Sustained in vitro/in vivo PLGA-mediated CAT gene expression (up to 96 h)	[62]
Dextran/PLGA PGA/PLGA microparticles	DNase	Inhalable microparticles (PDI)	Significant reduction in the number of phagocytosed particles by addition of. Enhanced DNase I mucolitic activity on CF sputum.	[63]
PLGA-PEG nanoparticles	PS-341	Aqueous dispersion for nebulization	Efficient lung deposition, followed by biodegradation and release over time demonstrated 2-Fold decrease in proteasomal activity and ability to rescue LPS-induced inflammation as compared to free PS-341	[64]
PVA-Alg/PLGA CS-Alg/PLGA nanoparticles	Tobramycin	Nano-embedded lactose microparticles	In vitro antimicrobial activity against P. aeruginosa NP composition affects transport through artificial CFmucus and in vitro/in vivo deposition pattern of NEM	[65]
Transferrin-gelatin/cloroquine/calcium nanoparticles	Plasmid DNA encoding CFTR	Aqueous dispersion for nebulization	CFTR expression in over 50% of 9HTEo cells IB3-1 complementedwith effective transport activitywhen transfectedwith nanospheres containing the CFTR transgene	[66]
PEI (Linear, 25 kDa)	Plasmid DNA	Nanopolyplexes-embedded mannitol microparticles	Improved transport in CF artificial sputum. Activity loss due to the aggregation of the gene transfer system induced by DNA and mucin	[67]
PEI (Branched, 25 kDa)	Plasmid DNA, CAT and EGFP	Aqueous dispersion for nebulization	No detectable toxicity upon repeated administration. Delivery of plasmid, sustained transgene expression, further boosted at subsequent admnistration	[68]
PEG-PEI (PEG 5 kDa; Branched PEI 25 kDa)	Plasmid DNA encoding CFTR	Aqueous dispersion for nebulization	Rapid penetration of human CF mucus *ex vivo* and mouse airway mucus *ex situ.* Enhanced particle distribution, retention and gene transfer in the mouse lung airways as compared to conventional gene carriers Successful delivery plasmid DNA encoding CFTR in mouse lungs and airways cells, without causing acute inflammation or toxicity	[69]

Abbreviations: CAT = chloramphenicol transferase; CS = chitosan; DPPC = Dipalmitoyl phosphatidylcholine; EGFP = enhanced green fluorescent protein; PEI = poly(ethylenimine); PLGA = poly(lactic-co-glycolic acid); PGA = poly-glutamate; PS-341 = pyrazylcarbonyl-Phe-Leubronate; PVA = poly(vinyl alcohol)

1.3.2.1 Encapsulation and release of the therapeutic agent

A successful drug delivery system should have a high drug-loading capacity, thereby reducing the quantity of polymers composing matrix for administration. Drug loading can be accomplished by two methods. The incorporation method requires the drug to be incorporated at the time of particle formulation. The adsorption/absorption methods calls for absorption of the drug after particle formation; this is achieved by incubating the carrier with a concentrated drug solution.

Drug loading and entrapment efficiency depend on drug solubility in the polymer material, which is related to the matrix composition, molecular weight, drug-polymer interactions, and the presence of end functional groups (ester or carboxyl) in either the drug or matrix [70].

Among various techniques known for the preparation of polymeric particles, precipitation and diffusion methods have the advantage that no additional surfactant is required during particle formation, necessary for emulsion or double emulsion methods [71].

In addition to particle preparation in aqueous media, additional methods have been conceived to prepare micrometric and submicron polymeric particles by spray-drying techniques.

Spray drying allows the continuous conversion of fluids into powders using a one-step process. Moreover, the adjustment of spray drying process parameters enables the manipulation of various particle properties (e.g. size, density and shape). Recent developments in this field rely on improving the fluid breakdown by “electro-spraying” or “vibrating-mesh nozzles”; while electrostatic collectors accomplish high process yields [71].

Release of therapeutic agents from polymeric particles is thought to be controlled by a combination of phenomena, such as drug solubility, desorption of the surface-bound or adsorbed drug, drug diffusion through the nanoparticle matrix, nanoparticle matrix erosion or degradation and the combination of erosion and diffusion processes.

In the case of micro and nanospheres, where the drug is uniformly distributed, drug release occurs by diffusion or erosion of the matrix. If the diffusion of the drug is faster than matrix erosion, then the mechanism of release is largely controlled by a diffusion process. The rapid, initial release, or ‘burst’, is mainly attributed to weakly bound or adsorbed drug to the relatively large surface of particles. It is evident that the method of incorporation has an effect on the release profile.

If the drug is loaded by the incorporation method, then the system has a relatively small burst effect and sustained release characteristics.

If the nanoparticle is coated by polymer, the release is then controlled by diffusion of the drug from the polymeric membrane. Membrane coating acts as a drug release barrier; therefore,

drug solubility and diffusion in or across the polymer membrane becomes a determining factor in drug release. Furthermore, the release rate also can be affected by ionic interactions between the drug and auxiliary ingredients.

Various methods can be used to study the release of drug from the nanoparticle: side-byside diffusion cells with artificial or biological membranes, such as Franz diffusion cells, dialysis bag diffusion, agitation followed by ultracentrifugation/centrifugation or ultra-filtration.

However, the evidence falls by employing simple in vitro release tests. The evaluation of particle behavior in physiologically relevant contexts (*ex vivo* and *in vivo*) should be done to support the claim that polymeric particles may improve pulmonary drug and gene delivery [71].

1.3.2.2 Polymeric materials for pulmonary drug delivery applications

The number of polymers currently available and generally regarded as safe (GRAS) by FDA for improving the technological properties for inhalation is very limited.

Although calling in question safety issues, a number of polymers have been for pulmonary applications and its selection is mainly based on criteria such as its biocompatibility and degradability [71].

Among polymers currently under investigation, synthetic biodegradable polymers represent the most promising class of materials for pulmonary delivery, as evidenced by increasing literature data, fulfilling also important safety concerns. Among them, poly(lactic acid) (PLA) and poly(lactic-coglycolic acid) (PLGA) (chemical structures at figure 22) have generated tremendous research interest due to their excellent biocompatibility as well as their biodegradability [53].

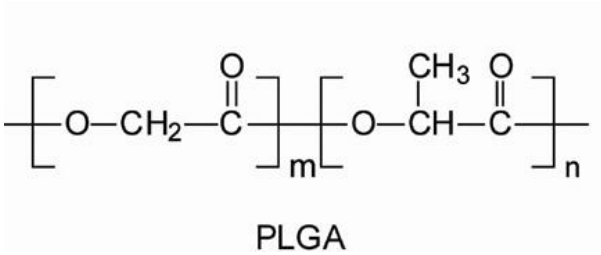

PLGA

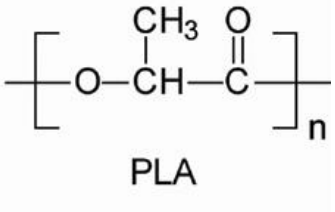

PLA

Fig.22: Chemical structure of PLGA and PLA.

The slow degradation rate (weeks to months), however, would lead to an unwanted accumulation in the respiratory tract, especially when frequent dosing is required [71]. Moreover, for an effective particulate drug delivery system, sufficient drug loading and controlled drug release over a predetermined period of time must be ensured. The low affinity of drugs to the polymeric matrix often leads to relatively fragile interactions between drug and polymer accompanied by fast release rates, especially for hydrophilic drugs, such as some classes of antibiotics.

One way to overcome this problem is to synthesize polymers with particular characteristics, such as faster degradation rates and defined functionality to promote interactions with therapeutic compounds. The functionalization with hydrophilic polymers could confer amphiphilic properties and make them highly suitable for pulmonary formulations.

One of the most used hydrophilic polymer is poly(ethyleneglycol) (PEG, chemical structure in figure 23), a GRAS, uncharged and hydrophilic polymer with several applications.

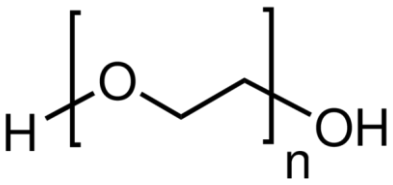

Fig.23: Chemical structure of PEG.

PEG and its derivatives are used commercially in numerous applications, as surfactants, in foods, in cosmetics, in pharmaceutics, in biomedicine, as dispersing agents, as solvents, in ointments, in suppository bases, as tablet excipients, and as laxatives.

PEG is the most used polymer to coat drug carriers based on different nature materials, in order to obtain “stealth” formulations, prolonging the particle permanence in the bloodstream and preventing its eliminarion by reticuloendothelial system (RES) or mononuclear phagocyte system present in various sites of the body [72]. In order to avoid rapid drug absorption, degradation, and evade the pulmonary clearance as well as simultaneously prolong inhalable drug's half-life at the lung, inhaled drugs with “stealth” characteristics are welcome. PEG neutral, flexible, and hydrophilic nature can, in fact, properly produce surface barrier layers that reduce the adhesion of opsonins on the particles making them “invisible” to phagocytic cells. As a natural defensive mechanism, opsonins interact with particles by van der Waals,

electrostatic, ionic, and hydrophobic/hydrophilic forces and especially hydrophobic and charged particles undergo higher opsonisation as compared to hydrophilic and neutrally charged particles [72].

However, if PEG coating on one side reduces the opsonisation process, on the other can induce the complement activation that is involved in the nanoparticle removal. Studies performed with pegylated polymeric nanoparticles confirmed that PEG-coated systems can induce the complement activation, regardless of the PEG chain length and surface density, promoting the clearance by the macrophage uptake of the RES. The complement activation was inversely correlated with the PEG molecular weight suggesting that steric hindrance on the particle surface due to the polymer coating reduces the approach and association of large proteins such as the C3 convertase [72].

Furthermore, 100 nm pegylated liposomes lose their long-circulating characteristic upon repeated injection at certain intervals in the same animal induced by the "accelerated blood clearance (ABC) phenomenon". Anti-PEG IgM selectively bound to the surface of subsequently injected pegylated liposomes, leading to substantial complement activation [73].

Being that it is generally believed that nanocarriers coated with PEG have no immunogenicity, much attention must be paid when carriers are projected and administered *in vivo*, because of this potential unexpected immune responses.

Other polymers used to confer stealth properties to particles have few basic common features: high flexibility and hydrophilicity. Either natural and semisynthetic polysaccharides or synthetic polymers have been used for these purposes. Dextran (Dex), polysialic acid (PSA), hyaluronic acid (HA), chitosan (CS), and heparin are the most used natural polysaccharides. Synthetic polymers include polyvinyl pyrrolidone (PVP), polyvinyl alcohol (PVA), and polyacrylamide (Pam).

An hydrophilic polymer that could be used in order to confer amphiphilic properties to hydrophobic polymers, such as polyesters, is the polyammide α,β-poly(N-2-hydroxyethyl)-D,L-aspartamide (PHEA) [74, 75], which structure is represented in figure 24.

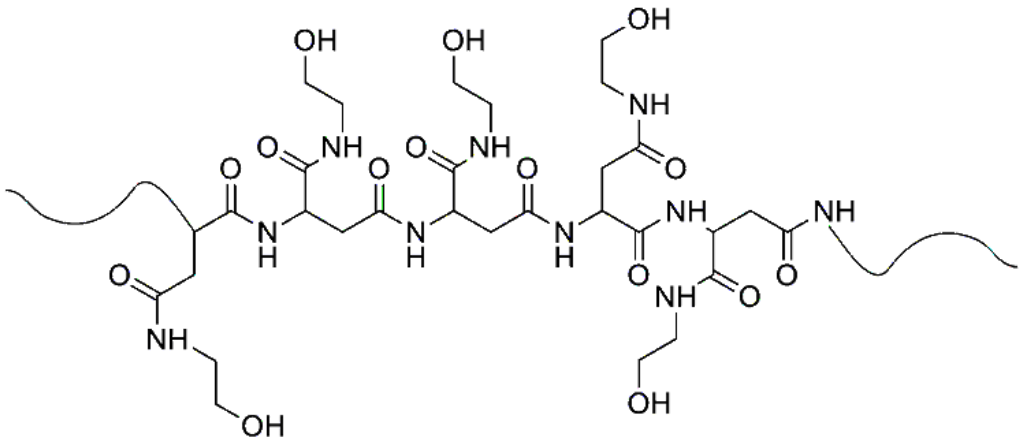

Fig.24: Chemical structure of PHEA.

PHEA is a biocompatible water soluble synthetic polymer, whose derivatives have been largely used for drug and gene delivery applications [76–80], also for the pulmonary administration of anti-inflammatory and antibiotic drugs [81, 82].

Moreover, in the polymer design, the introduction of charged functional groups within the polymer backbone enhances the drug loading and release profile of oppositely-charged therapeutic agents.

Other types of biodegradable polymers suitable for pulmonary application are based on biodegradable poly(anhydride)s, poly(ethers) and poly(ketal)s [83].

1.3.2.3 Polymeric microparticles

Polymeric microparticles (MPs) are spheric particles with size ranged between 1-1000 μm, and are frequently used for pulmonary delivery because they preferentially deposit in the deep lung and do not aggregate under shear force [84].

Novel formulation approaches have involved the creation of polymer-based inhalable MPs to be used in DPIs. Respirable particles have to be small enough for deposition, but also large enough to allow metering of the powder during manufacturing of the dosage form and delivery from the DPI. Among the parameters that can be adjusted to achieve inhalable MPs, mass density and size have drawn researchers' attention to limit loss of drug due to particle aggregation in the inhaler and macrophage-mediated clearance of the particles from the lungs.

Large porous particles (LPPs) with low mass density (<0.4 g/cm^3) and geometric diameter of 1-5 μm can be used to enhance both particle aerosolization behavior and residence time in the lung [53].

Different drugs such as corticosteroids, antibiotics, proteins, and chemotherapeutics have been formulated within polymeric microparticles. Insulin-PLGA MPs for pulmonary delivery have been developed and showed a prolonged residence time extended from 6-48 h compared to free insulin, and docetaxel (DTX)-loaded chitosan microspheres, with a spherical in shape and an optimum drug encapsulation efficiency about 88%, showed that DTX was sustainably released, increasing its bioavailability at the lung, minimizing the systemic toxicity [84].

In order to find a multifunctional therapy for CF, controlling inflammation, infection and mucus secretion, PLGA-PEI LPPs loaded with a decoy oligonucleotide against NF-κB (dec-ODN) were produced and showed dynamic properties optimal for delivery from a breath-actuated DPI, exert a temporal control over dec-ODN released amounts, while preserving its integrity and cause a persistent inhibition of important pro-inflammatory mediator expression (IL-8 and MUC2) as com- pared to naked dec-ODN [85]. Further, LPPs engineering with PEI plays an important role in controlling mucin gene expression and, in turn, may represent a key factor for the *in vivo* improvement of an inhalation therapy based on dec-ODN.

Although current literature data suggest the potential of PLGA MPs for prolonged drug delivery in CF lungs, their use for inhalation is still embryonic and presents some shortcomings. In particular, a huge amount of work has still to be produced on clearance mechanisms and persistence in vivo that may considerably limit the benefit of sustained release inhalation therapy.

Moreover, their influence on the safety is not yet elucidated, and chronic toxicological data are still poor and demand for further studies.

1.3.2.4 Polymeric nanoparticles

Polymeric nanoparticles (NPs) are particles with size ranging from 1-1000 nm, with promising carriers for biological agents to the lung due to advantages including biocompatibility, ease of surface modification, localized action and reduced systemic toxicity [70].

Because of limitations of direct administration of free drugs, nanoparticulate drug delivery systems such as DPI formulations based on NPs have been of interest for pulmonary drug delivery. The prolonged residence of NPs in the lungs due to ability to escape from clearance mechanisms (mucus barriers, mucociliary escalator, macrophage uptake and translocation to the systemic circulation) is amongst the key advantages of NPs. By this approach, the controlled pulmonary delivery of drugs, peptides, proteins, genes, siRNA, and vaccines is possible.

Both natural (albumin, gelatin, sodium alginate (SA), collagen, cyclodextrin, and CS and synthetic (PLA, PLGA, polyacrylates and polyanhydrides) polymers have been used in formulation of pulmonary NPs.

Hydrophilic mucoadhesive polymers, such as CS, SA or hyaluronic acid (HA), have been employed for long time to increase in situ residence of NPs and to allow intimate contact of the delivery system with the mucosa. In a recent work, NPs based on PLGA were produced and the interactions of tobramycin-loaded NPs with the lung environment was investigated. Several helper hydrophilic polymers, that is SA, CS and PVA were used to impart the desired surface, bulk and release properties to PLGA NPs [65].

Biodegradable PLGA-PEG NPs have been recently tested to ameliorate the inflammatory process in CF lung through sustained delivery of PS-341 (pyrazylcarbonyl-Phe-Leuboronate), an extremely potent, stable, reversible and selective inhibitor of chymotryptic threonine protease activity [86]. The efficacy of the developed NPs was evaluated upon intranasal instillation in CF mice, showing a ~2 fold decrease in proteasomal activity as well as the ability to rescue the *P. aeruginosa* LPS-induced inflammation.

More recently, the concept of using hydrophilic mucoadhesive polymers to modulate NP/mucus interactions has been recently called into question [87–89]. In fact, non-adhesive NPs with adequate size, with specific chemical surface properties, called Mucus-Penetrating Particles (MPP), may deeply penetrate a variety of human lung mucus secretions independently on their viscosity, including CF sputum, reaching the surface of epithelium, t allowing a prolonged interaction of the nanocarrier with the targeted substrate. Details on MPP were extensively discussed in the section regarding the strategies to overcome the barriers to inhaled drugs in CF lungs (3.3.1 paragraph).

Due to the small size of NPs, they tend to remain suspended in air, making direct delivery and deposition in the deep lung seriously difficult [90]. Moreover, the use of a pMDI or DPI could result in significant oropharyngeal NP deposition and variation in dosage when the device is not shaken correctly. On the other hand, the use of a nebulizer on the other hand could maintain a relatively constant size of aerosol droplets in the range that easily allows the suspended NPs to reach the distal lung.

1.3.2.5 Polyelectrolyte complexes

Current state of art is witnessing a revolution in new techniques for drug delivery. The use polyelectrolyte complexes (PECs) led to the development of several novel drug delivery

systems capable of controlling the rate of drug delivery, sustaining the duration of therapeutic activity with the possibility of an active targeting to specific tissues [91].

The drug complexation with polymers not only convert the active substances into a non-deleterious form which can be administered, but also have specific effect on the biodistribution, bioavailability or absorption of the active substances.

PECs are the association complexes formed between oppositely charged components (polymer-drug or polymer-drug-polymer), due to electrostatic interaction, exploiting a concept extensively studied in the development of delivery vehicle for gene therapy and oral vaccination. This avoids the use of chemical cross linking agents, thereby reducing the possible toxicity and other undesirable effects of the reagents [91].

Polymers used to prepare PECs are generally soluble in water. Examples of such polymers include DNA, proteins, certain derivatives of cellulose polymers, anionic polysaccharides, and synthetic polymers.

PECs have gained much attention for the pulmonary drug delivery because of their potential in the delivery of drugs susceptible of inactivation or clearance mechanisms in the lungs, which encapsulation and release rate are not acceptable when encapsulated into nano- and microcarriers.

Ionic drugs, such as the antibiotics widely used to treat CF-associated lung infections (tobramycin, ciprofloxacin, ofloxacin, levofloxacin), form complexes with polyelectrolytes and the electrostatically bound drug is released with a rate dependent from the dissociation constant of the PEC. Factors such as pH, viscosity of the polymer solution, ionic nature of disperse drug and ionic strength of the dissolution medium affect drug-polymer interaction.

Being tobramycin inactivated in CF airways because of the bound between the positively charged drug and the negatively charged DNA fibers or *P. aeruginosa* biofilm alginate, a smart strategy was necessary to protect the antibiotic from the inactivation. The encapsulation into nano or micro-particles based on common hydrophobic or amphiphilic polymers was not adequate, as results of the low affinity between the hydrophilic nature of tobramycin and the particle hydrophobic core, with drug loading too low to support their potential use in clinic (drug loading capacity in PLGA-PEG nanoparticles of about 1.9 % wt [65]).

Thus, a more convenient strategy was used by the preparation of tobramycin complex of nanometric size between the drug positive charges and the polyanionic alginate, and with a further PEC stabilization with CS [92]. The prepared nanometric PEC was efficacy against *P. aeruginosa* infections both in vitro and in vivo in a *G. mellonella* model.

Furthermore, a ciprofloxacin complex with the anionic polymer dextran sulfate (DXT) was recently prepared for the treatment of the respiratory pathogen *P. aeruginosa* [93]. In another work, also ofloxacin and levofloxacin antibiotic were complexed with DXT to form ion pair complex of nanometric size by a simple mixing the aqueous solutions of drugs and DXT [94].
The mode of pulmonary delivery plays a crucial role in facilitating PECs deposition and distribution in the lungs. PECs could be administered by nebulization, which could maintain a relatively constant size of aerosol droplets, but a more convenient strategy could be used to delivery PECs as a dry powder to the lungs, with all the advantages of DPI formulations.

1.3.2.6 *Trojan* particles

Each inhaler type has pros and cons that must be considered in the selection of a device, especially for CF patients. If for nebulization there is no special technique requirements, as they are fairly intuitive to use, they can be used at any age and for any disease severity or acuity, it is possible to mix more than one medication and deliver them simultaneously at high dose, nebulizers are more time-consuming than MDI or DPI. Nebulizers require a source of compressed air, an equipment maintenance and cleaning for infection control, and they are also less portable than a MDI or DPI.
DPI devices, easier to use than MDI, do not contain propellants, are very portable and quick to use, providing an higher patient compliance and adherence to the therapy.
As more efficient pulmonary delivery devices, sophisticated dry powder formulations become available, targeting specific cells or regions of the lung, avoiding the lung's clearance mechanisms, being retained within the lung for longer periods.
Moreover, for specific innovative formulations, such as NPs and PECs, the direct pulmonary administration by nebulization is not feasible or convenient. So many efforts have be done to convert them to dry powder formulations, by using smart materials or excipients.
One of the most promising approach to convert these carrier systems to dry powder formulations is the *nano into micro* strategy.
NPs and nanometric PECs could be efficiently encapsulated into "trojan" vehicles, such as nano-embedded microparticles (NEM), which could be realized by spray-drying a dispersion of NPs or PECs in a solution containing sugars or polymers as inert carrier, to obtain a dry systems aerosolizable by using dry powder inhalers (DPI) devices.
NEMs provide an excellent strategy for both stabilization of NPs or PECs and their delivery to the lungs [65, 95–97].

Excipients such as sugars and biocompatible polymers are used to prepare the surrounding stabilizing matrix, generally compatible with a wide range of therapeutic molecules, nanocarriers and applications for different routes of administration.

Materials composing the surrounding stabilizing matrix of NEMs could be inert, only acting as carrier for pulmonary administration (such as lactose), or could possess a specific function.

Other materials that could be used for impairing specific function to NEMs for CF are mucoadhesive materials, such as PVA, CS, HA or DXT etc. Mucoadhesive materials could prolong the residence time of the formulation at the absorption site, allowing intensified contact with the mucus barrier, possibly decreasing the drug administration frequency, increasing the patient compliance and adherence to the therapy.

1.3.2.7 Pulmonary toxicity of polymeric carriers

The same properties that make polymeric carriers attractive as drug delivery systems (size, surface characteristics, chemical composition), also evoke toxicity concerns, particular following pulmonary application.

Safety evaluations of polymeric particles for pulmonary application are currently a subject of intense research, and what it is emerged is that the toxicological potential of particles depends on their degradability, chemical composition, particle size, and concentration at the target site.

For instance, positively-charged carriers showed a higher incidence of pulmonary reactions (cell recruitment, total protein, and lactate dehydrogenase release) than their negatively-charged counterparts, much better tolerated.

These observations point to the fact that material properties play an important role in inducing inflammatory responses in the lung. Thus, for example the slow degradation rate of PLGA is a disadvantage for pulmonary drug delivery, especially when repeated administrations are required. The faster degradation rates of hydrophilic polyesters derivatives make them more suitable for pulmonary formulations.

Especially for NPs it was recently proposed the “nanotoxicological classification system” (NCS), which allows a precise differentiation of toxicological risks for polymeric NPs by a combination of size related effects with risks derived from polymer degradability [98].

Despite many studies focusing on the toxicological responses of polymeric particles administered to the lung, their safety concerns, also at long term period of times, is largely unknown.

1.3.3 Strategies to overcome the barriers to inhaled drugs in CF lung disease

As a result of the strong pulmonary environment, inhaled drugs exhibit low bioavailability at the lungs, a key factor for an optimal therapy especially for CF patients.

To overcome the aforementioned short-comings of "conventional" inhalation therapy, more sophisticated, "intelligent" pulmonary delivery systems are desirable.

Among the large number of potential carrier systems, polymer based micro- and nano-sized vehicles have attracted growing attention due to their controlled release and targeting properties.

Moreover, the design of vehicles with specific physicochemical properties (e.g. size, shape, surface chemistry, and specific surface properties) that bypass the clearance mechanisms of the lung could provide prolonged residence times of the therapeutic agent within the respiratory tract.

Researchers from multidisciplinary fields such as chemistry, biology, toxicology, and biomaterials science heavily studied and investigated these factors in an attempt to identify the optimal parameters for developing an effective particulate-based pulmonary drug delivery system.

1.3.3.1 Overcoming extracellular barriers

As described before, bulk viscosity of healthy human mucus is typically 1000–10,000 times higher than the viscosity of water at low shear rates, and higher viscosity are found for CF mucus [57]. The Stokes–Einstein equation for diffusion in homogeneous fluids predicts that neither viruses nor many hydrophilic macromolecules would be capable of penetrating a fluid layer of this viscosity. Indeed, the diffusion of many macromolecules over extended distances in mucus, or at rates faster than mucociliary clearance, was long assumed to be an improbable event.

That view began to change with increasing evidence that a number of macromolecules rapidly diffuse through mucus. In fact, the main important lesson was provided by nature, and in particular by the transport of viruses through mucus, such as Norwalk (38 nm) and human papilloma virus (HPV, 55 nm) that penetrated the mucus at rates roughly equivalent to those in water [99].

Thus, since mucus affords rapid passage of selected proteins and particles, bulk-fluid macrorheological properties are inadequate for understanding the barrier properties of mucus, especially at length scales relevant to pathogens, toxins, and foreign particles.

The term microrheology has been then used to describe the viscoelasticity at micro- and nanoscale. In contrast to bulk rheology, which provides averaged measurements of physical properties, microrheology can measure heterogeneity and is important for characterizing the local mechanical properties of biological fluids that are overlooked by bulk rheological techniques [57].

As a results of many investigation, the complex structure of human respiratory mucus has been clarified, and it is thought that mucin fibers are interspersed in the aqueous phase to form a mesh with nanopores at low viscosity. If the viscosity of the fluid that fills the pores in mucus is similar to that of water, the diffusion rates of particles significantly smaller than the average mucus mesh pore size, assuming they do not adhere to mucus, are expected to be similar to their rates in water. So, the dynamics of nanoentities diffusing in the nanoscopically heterogeneous mucus are controlled by their local environment rather than the bulk biophysical properties of the mucus gel [57].

It is important to note that this does not reflect a breakdown in the Stokes–Einstein continuum. Instead, for complex biological fluids, the apparent viscosity governing the Stokes–Einstein relation is a function of length scale features reflecting the structural architecture of the medium. The dynamic motions of entities that do not interact with mucus elements and that are small with respect to fluid microdomains remain governed by the Stokes–Einstein relation for diffusion [57].

Mucus-penetrating particles (MPPs)

Understood the enormous potential of complex mucus structure, the attention was then focused on the understanding of the chemical and physical properties that govern the rapid transport of specific viruses in mucus, and thus on the possibility of developing mucus-penetrating particles mimicking the surface properties of viruses.

The penetrating viruses are coated with high-density groups positively and negatively charged, with a dense overall neutral surface charge. This high density surface charge creates an hydrophilic shell that minimizes the hydrophobic entrapment in the mucus layer.

In the light of what is revealed by the penetrating nature of the virus, it is possible to understand what requirements are needed to give to drug delivery systems the mucus-penetrating properties [99].

Considered that the average 3D mesh spacing of CF sputum is in the range between 60 and 300 nm, generally particles with size in this range are able to diffuse through pores generated by the dense fiber mesh of CF mucus.

Moreover, modulating surface chemistry is of considerable importance in order to confer a strongly inert particle surface to the formation of mucoadhesive interactions. Particle surface charge too positive or negative may indicate the formation of attractive or repulsive interactions with mucus components [100], that would prevent the diffusion of particles in mucus [87].

Several studies have suggested that diffusion in the mucus layer could be realized through the particles coating with PEG.

However it was not obvious a priori that PEG could reduce the binding of particles with the mucus components; PEG is in fact widely used as a mucoadhesive agent.

Many evidence have demonstrated that mucus-penetrating properties could generated into particles by selecting PEG molecular weight sufficiently low to avoid mucoadhesive interactions with mucins, and with a suitable PEG coating density to effectively shield or protect the hydrophobic particle core [89, 101]. In fact, a brush-like PEG conformation (figure 25), conferring a corona protection, would facilitate the penetration of pegylated particles through the mucus layer [102]. On the contrary, pegylated NPs with a mushroom-like conformation would increase the time of residence of the adhered fraction of particles on the mucus layer.

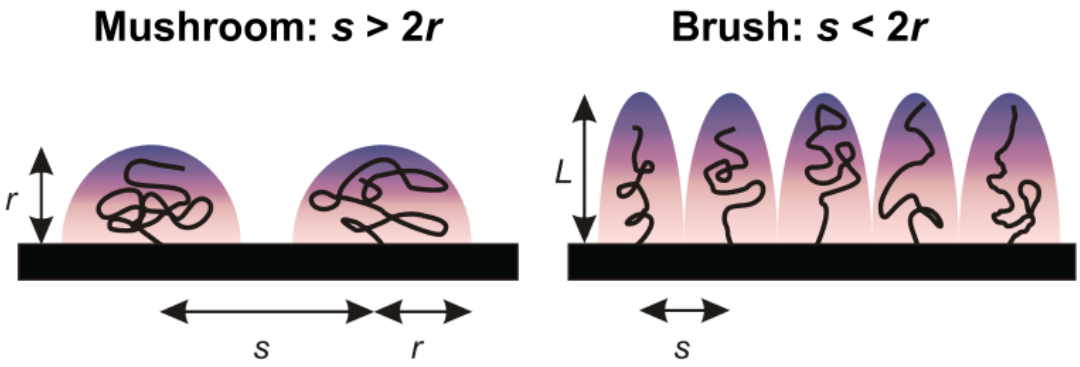

Fig.25: Conformations assumed by polymers at a surface.

The dense surface coating with PEG corona may improve the penetration of inhaled drug carriers through the other mucin-based meshwork barrier found in PCL, if the particle diameters are small enough to fit through the PCL pores.

Therefore, drug carriers that rapidly penetrates the mucus layer and PCL may be retained significantly longer in the lung [58].

Furthermore, pegylation improves colloidal stability of particle in the hostile mucus environment, by minimizing the particle aggregation, thereby providing another means of improving penetration through steric barriers, including mucus layer and PCL. Stability is, in fact, particularly important when particles must diffuse through a thick mucus layer in order to reach underlyng cells [100].

Furthermore, the evidence that larger particles (500 nm) are able to rapidly traverse fresh human cervicovaginal mucus (rheologically and compositionally comparable to healthy respiratory mucus), suggests that it is possible that larger pegylated particles may also transport quickly in mucus through other entry sites [99].

The rapid mucosal transport of large pegylated particles has important implications for the development of therapeutic applications *in vivo*. Larger NPs afford substantially higher drug encapsulation as well as reduced aggregation upon freeze drying.

In addition, as the size of drug-loaded particles increases, the drug-release kinetics are usually greatly improved as well, allowing sustained release of therapeutics over days and even months along with enhanced therapeutic efficacy. In contrast, smaller NPs suffer from large burst release typically within hours upon *in vitro* or *in vivo* application [99].

Although large NPs are preferred for improved drug loading and release kinetics, an optimal size likely exists for mucosal applications. Nanoparticles that are too large, even if they are well-coated so as to avoid mucoadhesion, may not diffuse at rates sufficient for overcoming mucociliary clearance due to the elevated friction forces predicted by the Stokes–Einstein equation. Since mucus layer thickness and mucus clearance time differ among the mucosal tissues, different NP diffusion rates may be required in order to overcome different mucus barriers. Furthermore, for cellular uptake into underlying epithelia, an increase in particle diameter is expected to reduce the rate of endocytosis [99].

The size of MPP must be optimized with all of these considerations in mind, and will likely vary based on the requirements of different mucosal applications.

Another important observation regards the possibility to coat particle or treat mucus with mucolytics agents in order to improve the penetration rates of drug carriers [99].

The use of mucolytics as an adjuvant to particle transport may be particularly important for diseases where mucus is abnormally viscoelastic, such as CF, where water content is reduced and cellular debris is increased, leading to an increase in physical entanglements, a decrease in the average mesh pore spacing, and a pronounced increase in the viscoelastic nature of the sputum.

Consequently, it is thought that disrupting the mucus structure by reducing the number of crosslinks and enlarging the size of pore could be a good strategy to enhance particle transport.

However, it was observed that, Pulmozyme® treatment of undiluted CF sputum reduced its macroviscoelastic properties by up to 50% but does not improve particle diffusion rates. On the contrary the treatment with the DNAase dramatically narrowed the distribution of individual particle diffusion rates in CF sputum, effectively removing the fast-moving "outlier" particle population. This finding suggests that DNAase may reduce, rather than enhance, the efficacy of NP therapeutics such, since the treatment eliminates the fast-moving fraction that may be critical for effective CF therapy [99].

Mucoadhesive approach

Mucoadhesion is commonly defined as the adhesion between two materials, at least one of which is a mucosal surface, and over the past few decades, mucoadhesive drug delivery systems have received a great deal of attention for their positive therapeutic outcomes [103].

The potential use for mucoadhesive systems as drug carriers lies in its prolongation of the residence time at the absorption site, allowing intensified contact with the mucus barrier. Other features associated with the development of controlled drug delivery systems using mucoadhesive molecules include a decrease in drug administration frequency and an increase in patient compliance to the therapy. Therefore, a mucoadhesive system controlling drug release could improve the treatment of diseases, helping to maintain an effective concentration of the drug at the action site.

Various theories exist to explain at least some of the experimental observations made during the mucoadhesion process. Unfortunately, each theoretical model can only explain a limited number of the diverse range of interactions that constitute the mucoadhesive bond [103].

However, the mechanism of mucoadhesion is generally divided in two steps, the contact stage and the consolidation stage, as showed in figure 26.

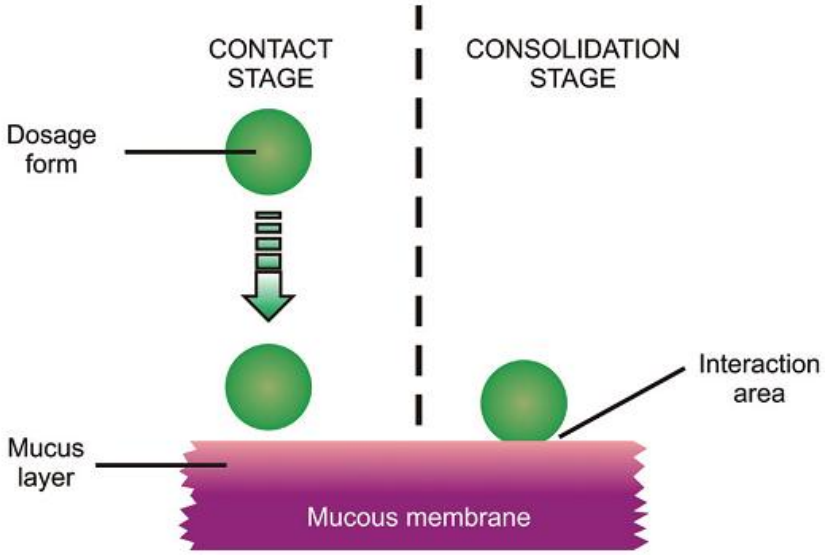

Fig.26: Scheme illustrating the mechanism of mucoadhesion.

The first stage is characterized by the contact between the mucoadhesive particles and mucus with spreading and swelling of the formulation, initiating its deep contact with the mucus layer.

If particle approaches the mucus surface, it will come into contact with repulsive forces (osmotic pressure, electrostatic repulsion, etc.) or attractive forces (van der Waals forces and electrostatic attraction). In the consolidation step the mucoadhesive formulations and the glycoproteins of the mucus mutually interact by means of interpenetration of their chains and the building of secondary bonds. For example, molecules with hydrogen bonds building groups (-OH, -COOH), with an anionic surface charge, high molecular weight, flexible chains and surface-active properties, which induct its spread throughout the mucus layer, can present mucoadhesive properties [104].

Mucoadhesive NPs, coated with mucoadhesive polymers such as poly(acrylic acid) or CS, ones administrated, demonstrated a slower elimination rate, about half that observed with unmodified nanospheres, thanks to its adhesion to the mucus in the lungs as a result of the mucoadhesive interactions [105].

Mucoadhesive MPs of hydroxypropylcellulose (HPC) encapsulating beclomethasone dipropionate (BDP) were administered as powder aerosols, and it was shown that 180 minutes after the administration, more than 95% of BDP were absorbed from the lung following compared to the 86% of pure crystalline BDP, assuring a prolonged lung retention, beneficial

in maximizing the efficacy of BDP and in reducing the side effects caused by its extra lung absorption.

The duration of inhibition of eosinophil infiltration into the airways was maintained for 24 hours following the administration of BDP loaded HPC MPs, while only 1–6 hours for pure crystalline BDP [106], showing a great potential to prolong the therapeutic duration of BDP.

Although mucoadhesion is an experienced approach to increase the bioavailability of drugs delivered via mucosal tissues, important fundamental limitations exist. Since mucoadhesive systems are bound to the mucus layer through interactions with mucin fibers, the transit time of these systems is determined by the physiological turnover time of the mucus layer. Furthermore, as mucoadhesive systems efficiently adhere to mucus, they are largely incapable of penetrating across the mucus layer and entering the underlying epithelia. Thus, mucoadhesive systems are especially unsuitable for delivery of drug and gene molecules that require intracellular delivery.

So, the possibility to engineer MPPs able to cross also the highest viscoelastic mucus layer allowed to overcome the limitations of the mucoadhesive approach (figure 27) [99].

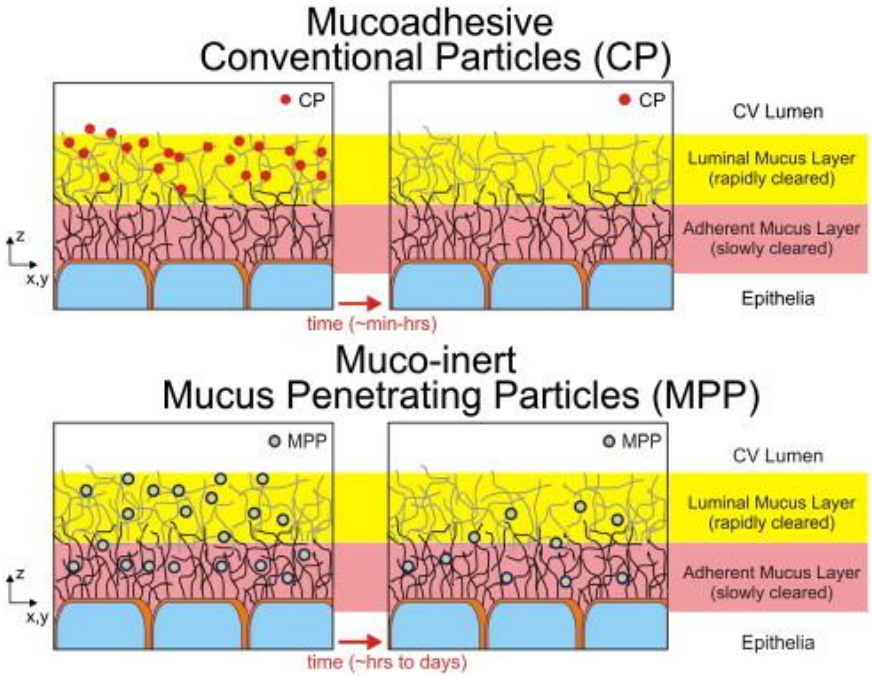

Fig.27: Scheme illustrating the fate of MPPs and CPs administered to a mucosal surface.

These findings were recently questioned by Lehr and coworkers who showed that also mucoinert NPs did not penetrate through native respiratory mucus on physiologically relevant time and length scales, due to highly rigid structures within the mucus [107]. In their work, it

was showed, by *ex vivo* and i*n silico* approaches, the not dependency of muciliary clearance and mucus penetration of micro-, submicrometer and nanoparticles on size, shape, charge and surface chemistry. No significant differences were found between CPs and MPPs.
The fate of inhaled particles after deposition onto the pulmonary mucosa rests, however, unclear and far from being solved, in particular with respect to mucociliary clearance and mucus penetration.

1.3.3.2 Overcoming cellular barriers

Assuming that the strategies adopted to overcome the extracellular barriers to inhaled drugs have worked, they have still to be taken up by the target cell to carry out their pharmacological activity. Antimicrobials have to be uptaked by bacteria, anti-inflammatory agents and disease-modifying agents by airway epithelial cells, avoiding the phagocytosis by alveolar macrophages.

Bacteria biofilm

The careful design of particle carriers with specific size, surface properties, degree of lipophilicity is useful for overcoming also cellular barriers.
Carrier particles can shield their drug cargo from the surrounding medium and protect it from enzymatic inactivation or binding to the biofilm matrix or other components surrounding the biofilm infection site. An axample of that is the binding of aminoglycoside antibiotics to the alginate matrix of mucoid *P. aeruginosa* biofilms, which causes, for example, the inhibition of the activity of tobramycin in CF patients [108].
The longer contact times between the antibiotic and the bacteria biofilm, responsible for the increased antimicrobial effect, could be achieved by using carriers with a surface charge opposite to the surface charge of the bacteria. Charged formulations, especially positive charged particles, allow a complete eradication of the biofilms, attributed to greater binding of the positively charged carriers to the negative bacteria due to electrostatic attractions, possibly inducing fusion with the outer membrane. This approach is called non-specific targeting, and mainly relies on charge based interactions and hydrogen bonding of the carrier with the biofilm [108].
A number of companies are developing liposomal formulations for the treatment of biofilm infections which are currently being evaluated in clinical trials. Using Fluidosomes™, a formulation based on tobramycin containing liposomes, a complete eradication of a chronic pulmonary *P. aeruginosa* infection was obtained in an *in vivo* rat model. The antibiotic was

found to remain mainly in the lungs after liposomal delivery compared to the free drug, which likely reduces systemic side effects and toxicity. Fluidosomes™-tobramycin are currently further developed by Axentis Pharma (Zurich, Switzerland) for the treatment of *B. cepacia* infections in CF patients [108].

Functionalizing drug delivery particles with targeting ligands could be beneficial to achieve accumulation of the particles close to the bacterial cells and to promote close contact of the carrier with the bacteria. Specific targeting is based on targeting ligands that selectively bind to a target molecule inside the biofilm. The use of antibodies on the outer surface of the drug carriers has the advantage of increased specificity and affinity compared to the other targeting strategies [109].

Airway epithelial cells

In order to improve the drug accumulation in airway epithelial cells, carrier surface could be decorated with different functional motifs. Although there is no literature evidence supporting their use in CF, surface exposure of a ligand (proteins, antibodies or immunoglobulin fragments) recognizing a receptor over-expressed in CF airway epithelial cells may further increase carrier selectivity by activating receptor-mediated transport mechanisms [53].

For example, an increased expression of toll-like receptors 2 and 5 has been found at the apical surface of CF lung epithelium, and intercellular adhesion molecule-1 (ICAM-1, CD54) are up-regulated in chronically inflamed airway epithelium [53].

A promising approach that seems to be the solution of overcoming cellular barrier for intracellular drug delivery has emerged over the last decade. Cell-penetrating peptide (CPP) emerged for the enhancement of intracellular delivery of a broad variety of carriers (liposemes, micelles, NPs) and of their incorporated drugs. CPP peptide molecules readily cross the hydrophobic cell membrane with a mechanism not completely elucidated [110].

In the past decade, numerous works have been published on the use of CPPs for successful *in vitro* and *in vivo* intracellular delivery of biologically active macromolecules, enzymes, antibodies, DNA, liposomes, and imaging probes [110].

The most intensively studied CPP is the transactivating transcriptional activator peptide (TATp) derived from the protein transduction domain (PTD) of human immunodeficiency virus type 1 (HIV-1), extending from residues 47 to 57 (YGRKKRRQRRR), and it is rich of positively charged amino acids arginine and lysine.

A self-assembled nanoparticle formulation for protein drug was recently designed with a novel strategy to achieve both excellent mucus permeation and transepithelial absorption

[111]. With insulin as a model drug, NPs possessed a CPP/insulin nanocomplex core and an N-(2-hydroxypropyl) methacrylamide (HPMA) polymer (pHPMA) derivatives coating. Nanoparticles exhibit excellent permeation in mucus due to the mucus-inert pHPMA coating, as well as high epithelial absorption mediated by CPP. The investigation of NP behavior shows that the pHPMA molecules gradually dissociate from the NP surfaces, permeates through mucus, and the CPP-rich core is revealed in time for subsequent transepithelial transport through the secretory endoplasmic reticulum/Golgi pathway and endocytic recycling pathway (figure 28).

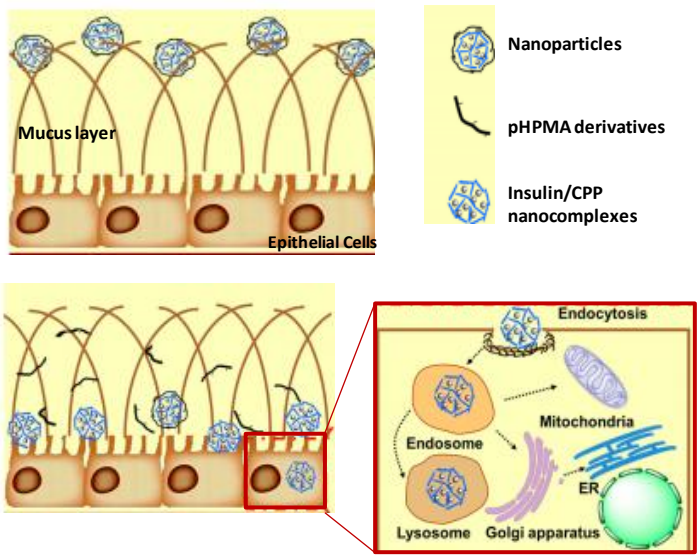

Fig.28: Schematic illustration of the process of the nanoparticle permeation across the mucus layer and the intracellular transport of nanoparticle in the epithelial cells [111].

This formulation exhibit a 20-fold higher absorption than free insulin on mucus-secreting epithelium cells, generating a prominent hypoglycemic response and an increase of the serum insulin concentration in diabetic rats [111].

Avoid or target alveolar macrophage uptake?

Different strategies have been proposed to overcome phagocytosis of inhaled particles by alveolar macrophages present in the deeper lung. The size discriminating particle uptake properties of alveolar macrophages represent a basis for the design of pulmonary controlled release formulations with prolonged residence time. In this regard, large porous particles were developed as controlled pulmonary drug delivery systems, and due to their unique geometry, these particles are not taken up by alveolar macrophages [71].

Dry microparticles display inhalable particle sizes, but once in contact with the moisture of the lung a significant increase in particle size is observed. An approach to delay lung clearance can be achieved by inhalation of submicron particles. Although their small size limits pulmonary deposition, as NPs alone are expected to be exhaled after inhalation (d_{ae}: 0.1–1 μm) researchers are encouraged to develop suitable application forms for inhalation. Aerosol particles suitable for deposition in the deeper lung can be generated by nebulization of polymeric nanosuspensions or aerosolization of NPs-containing MPs by using vibrating-mesh nebulizers [71]. As an alternative to nebulization, polymeric NPs could be encapsulated into composite particles using standard techniques like spray-drying, in "Trojan" particles which, as described before, combine the benefits of both microparticles (aerodynamic behavior) and nanoparticles (avoidance of macrophage clearance) [65].

The decoration of particle surface with high density low molecular weight PEG chains, used to confer mucus-inert properties that prevent the trapping of particles in mucus layer, is an approach used to avoid the endocytosis by macrophages. In fact, thanks to the hydrophilic and electro-neutral surface conferred by PEG coating, particle interactions with cellular membranes are avoided, and consequently their uptake [111].

However many researcher underlined the advantage to target high concentrations of drugs to alveolar macrophages, playing these ones a central role in the progression of infective, inflammatory disease and in immune responses [112].

1.3.4 Assessing the efficacy of inhaled drugs for CF

Comprehensive characterization of toxicity and efficacy of novel inhaled drug products is a complex task involving the determination of deposited, delivered and actual available dose of drug at the lung target [53].

In order to evaluate the deposition of particles in the lungs none of the official pharmacopoeial methods used to assess the quality of an inhalable medicine is fully representative of the complex human lung deposition phase, depending also by the inhalation device, the mode of inhalation or breathing pattern, and even to the human lung anatomy [53]. Furthermore, lung fluid barriers and sophisticated clearance systems are completely neglected by conventional impactors. To fill this gap and look to the formulation in a translation perspective, the evaluation of inhaled drug behavior through the most reliable *in vitro* and eventually *in vivo* experimental models is necessary. Numerous human airway cell culture models, such as bronchial Calu-3 cells or human bronchial epithelial cells (16-HBE) or alveolar A549 cells human lung adenocarcinoma have been used to investigate the safety and

efficacy of inhaled medicines [53]. Moreover, the investigation on CF disease can further benefit from diseased cells, such as immortalized bronchial epithelial cells that exhibit CFTR mutations.

Cell models are also crucial to have key information on drug transport in the mucus layer and establish target formulation parameters (size, surface modification) to attain maximum drug availability to underlining cells. Calu-3 and 16-HBE cells grown on porous supports at an air–liquid interface (ALI) are promising in vitro model of airway epithelia due to its similarity to in vivo physiology [113].

However it is difficult to simulate in vitro the interactions of inhaled drug with lung components. For this reason animal models are still crucial to inhaled drug development. Because of the anatomical complexity and interspecies differences in the lungs, the appropriate choice of animals and drug delivery method is vital during study design. A definitive CF animal model would be a relevant tool not only for a better understanding of CF physiopathology but also for a correct evaluation of the safety and efficacy of inhaled drugs for CF.

Unfortunately, none of the animal models developed fully resemble human CF lung disease [114]. Mice genetically modified for the CFTR gene have been studied for more than fifteen years and are still a key asset in CF research, being a low costs model, possessing a rapid reproduction rate, and an easy maintenance of genetic modification [114, 115]. Nonetheless, CF mice fail to develop CF-like lung disease and do not exhibit the characteristic CF ion transport defects in the lower airways [116, 117]. Thus, the usefulness of these mice for testing the efficacy of anti-pseudomonal or anti-inflammatory agents is questionable [114, 115]. Murine models of acute and chronic lung infection with *P. aeruginosa*, *B. cenocepacia*, *S. aureus*, and *H. influenzae* are still considered valuable resources to mimic the initial and progressive bronchopulmonary infection typical of CF patients[118], possessing similar properties to the human clinical situation, including, at least in part, the resultant airway inflammation.

To overcome intrinsic anatomical limitations of CF mouse models and to better recapitulate the natural progression of CF lung, larger CF animal models, consisting in CFTR-deficient and ΔF508/ΔF508 pig and ferret have been recently generated and begun to demonstrate many phenotypic similarities to the human disease [119]. In the future, these animal models may provide a useful preclinical tool to test emerging inhaled drugs for CF.

Nonetheless, another issue to be addressed is the use of a valid experimental protocol to administer in vivo the formulation under investigation (i.e., drug inhalation through nose or

mouth), that must mimic as closely as possible the intended delivery method of the final product.

In this respect, orotracheal aerosolization or insufflation of either liquid or powder aerosols via mini devices (PennCentury Inc., USA) especially developed for laboratory animals (mice, rats, guinea pigs or larger animals) has become of choice for the assessment of in vivo biodistribution, toxicity and efficacy of inhaled drugs. By this way, only drug formulations with appropriate aerosolization properties can be effectively deposited and distributed along the airways. Furthermore, these devices may ensure accuracy of dosing, which is essential for a dose-related study as well as comparison of different formulations.

Chapter 2

Aim of the thesis

Cystic fibrosis (CF) is an autosomal recessive disorder caused by mutations of the gene encoding the CF transmembrane conductance regulator protein (CFTR). CF affects several organs, including the respiratory tract, exocrine pancreas, intestine, vas deferens, hepatobiliary system and the exocrine sweat gland, but the pathological changes in the lungs are the primary cause of death [120]. In CF, the lack or dysfunction of CFTR in lung airway epithelia ensues in ion transport abnormalities which causes periciliary liquid depletion, dehydration of airway surfaces [121], and production of a sticky mucus layer [59, 122–124]. This results in the failure of mucociliary clearance [125], favoring chronic pulmonary infections by opportunistic bacterial pathogens, and the resulting exhuberant inflammatory response contributes to the dysregulated inflammatory status of CF airways [126, 127].

In the last two decades, the pulmonary therapy, used to treat CF related lung disease, has been frequently used because has the enormous advantage to circumvent the problem of the poor penetration of intravenously administered drugs into lung parenchymal tissue, and to reduce their systemic toxicity when given over longer periods of time.

However, the success of the inhalation therapy is limited by CF pulmonary pathological condition, characterized by the presence of a thick and highly viscoelastic mucus secretions, bacteria biofilm, and the phagocytosis by alveolar macrophages.

Thus, in order to overcome the short-comings of conventional inhalation therapies, more sophisticated pulmonary delivery systems could be designed with the aim to allow the rapid penetration of the drug at the site of disease and, at the same time, to achieve its sustained delivery, reducing the administered dose, the dose frequency, side effects and improving patient compliance.

It is well consolidated that the effectiveness of a pharmacological therapeutic system could be significantly improved by using of new pharmaceutical technologies, able to overcome the existing drawbacks encountered in clinical practice [71].

For this reason, the main purpose of this thesis involve using of micro- and nanotechnologies based on polymeric materials, in order to produce pulmonary drug delivery tools for the treatment of both pulmonary symptoms and the defective ion transport in epithelial cells of CF patients.

The first used approach regards on the preparation of a drug delivery system loaded with tobramycin for the treatment of infections in CF patients. Tobramycin, which structure is reported in figure 29, is an aminoglycoside antibiotic widely used against Gram-negative bacterial infections and particularly useful for the treatment of *Pseudomonas aeruginosa* infections in CF patients.

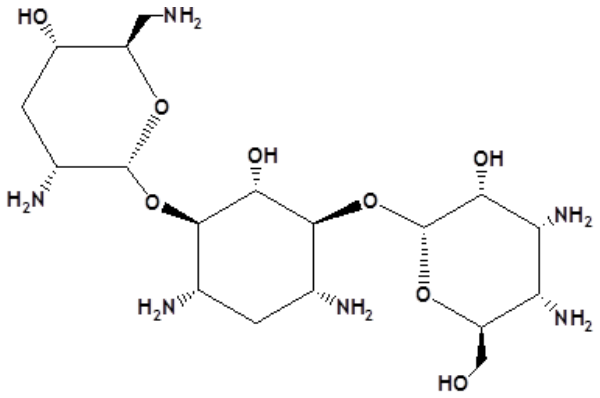

Fig. 29: Chemical structure of tobramycin.

However, important determinants of the clinical outcomes of tobramycin containing commercially available formulations, such as drug concentration and permanence at the site of infection as well as the extent of drug penetration through the mucus layer, are still inadequate. Moreover, since tobramycin is inactivated because of its electrostatic interactions with the negatively charged mucin, DNA fibers and *P. aeruginosa* biofilm alginate in CF airways, a smart strategy was necessary to protect the antibiotic from the inactivation [128].
The tobramycin encapsulation into nano or microparticles based on common amphiphilic polymers is not an adequate strategy, as result of the low affinity between the hydrophilic nature of tobramycin and the particle hydrophobic core, with drug loading too low to support their use in clinic.
Thus, a more convenient strategy was designed and involved the use of a polyelectrolyte complex between tobramycin and a synthetic polyanion based on α,β-poly(N-2-hydroxyethyl)-D,L-aspartamide (PHEA), a biocompatible water-soluble synthetic polymer,

whose derivatives have been largely used for drug and gene delivery applications [76–80], also for the pulmonary administration of drugs [81, 129].

The PHEA-EDA-GlucA polyanion, which chemical structure is reported in figure 30, was synthesized by firstly functionalization of PHEA with ethylenediamine (EDA) chains, and then with glucuronic acid (GlucA)

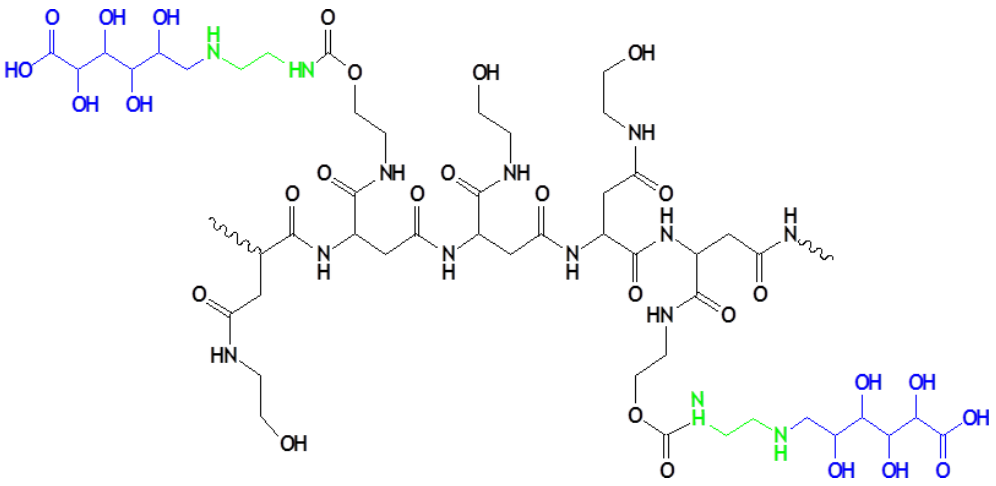

Fig. 30: Chemical structure of PHEA-EDA-GlucA (green: EDA moieties, blue: GlucA residues).

Once synthesized and opportunely characterized, the ion pair complex was obtained by incubating drug and the polymer solution in buffered medium. The interaction between the polymer and tobramycin was evaluated by isothermal titration calorimetry and by determining the antibiotic release profile from the complex.

Then, in order to achieve pulmonary drug delivery system inhalable as dry powder, the polymeric nanocomplex of tobramycin was encapsulated of into “trojan” microparticles (MPs). This “nano into micro” strategy was achieved by spray drying an aqueous solution containing mannitol and tobramycin:PHEA-EDA-GlucA ion pair complex.

Mannitol, which structure is reported in figure 31, is often selected as material to produce inhalable MPs, thanks to its good properties as carrier for pulmonary administration. Furthermore, mannitol was chosen thanks to its osmotic agent nature, being able to induce influx of water from epithelial cell layer to the mucus, with a consequent change of its viscoelastic properties.

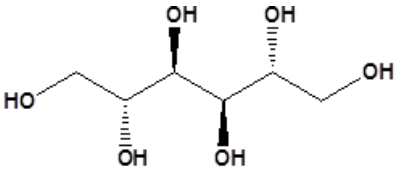

Fig. 31: Chemical structure of mannitol

Produced MPs were characterized in terms of average diameter, drug loading and cell viability towards human bronchial epithelial cells (16-HBE). Tobramycin release profile from MPs and its diffusion in mucus was tested by using a CF artificial mucus (CF-AM) model.

In vitro antipseudomonal activity of tobramycin entrapped into MPs was evaluated by determining the minimum inhibitory concentration (MIC), minimum bactericidal concentration (MBC) and the efficacy in inhibiting *P. aeruginosa* growth in CF-AM.

Finally, in vitro *P. aeruginosa* anti-biofilm properties of produced MPs were evaluated and compared with free tobramycin.

Moreover, since produced MPs containing the tobramycin ion pair complex showed pronounced microbiological activity against *P. aeruginosa*, if compared to free drug, the potential of obtained MPs was enhanced by adding special materials.

Materials used together with mannitol were N-acetylcysteine, L-arginine or cysteamine, having each one a specific action in the improvement of pulmonary function in CF patients.

N-acetylcysteine is commonly prescribed to CF patients, depolymerizing mucus by breaking disulphide bridges between macromolecules, consequently improving expectoration of sputum and lung function. Arginine nebulization has the potential to improve CF lung function by increasing the airway NO production, while cysteamine possesses a combinatorial action, being a mucoactive agent with a mucolytic activity comparable to currently available mucolytics, having a rapid bactericidal action against *P. aeruginosa*, and a synergistic action with conventional CF antibiotics.

Moreover, in order to evaluate if the mucoadhesive approach was a better strategy in order to enhance the antibiotic activity of tobramycin, improving its residence time on mucus, polyvinilalchol (PVA, structure in figure 32) was used as polymeric MP matrix for the encapsulation of tobramycin:PHEA-EDA-GlucA ion pair complex.

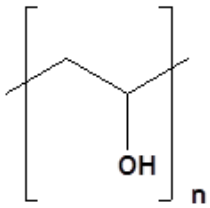

Fig. 32: Chemical structure of PVA.

Thanks to its biocompatibility, mucoadhesive properties and its ability to achieve a sustained delivery of several bioactive agents, PVA meets the requirements need for the design of a pulmonary drug delivery systems [130, 131].

Potentially muoadhesive MPs were then produced by spray drying an aqueous solution containing the tobramycin:PHEA-EDA-GlucA ion pair complex and PVA, alone or mixed with N-acetylcysteine, L-arginine or cysteamine.

Both mannitol and PVA based MPs were characterized in terms of average diameters, drug loading and cell viability towards 16-HBE cells. MPs effect on CF-AM, tobramycin release and diffusion profile in CF-AM was evaluated and compared to the unique commercially available dry powder MP formulation containing tobramycin, TOBI® Podhaler® by Novartis.

In vitro antipseudomonal activity of produced MPs was evaluated and compared with TOBI® Podhaler®.

The second aim of this thesis was the design of mucus-penetrating nanoparticles (NPs) for the treatment of lung inflammation and the defective ion transport in epithelial cells of CF patients.

Mucus-penetrating NPs may deeply penetrate a variety of human lung mucus secretions independently on their viscosity, achieving a sustained delivery of hydrophobic drug.

Fluorescent polymeric NPs with mucus-penetrating properties were realized starting from a synthetic amphiphilic copolymer, named PHEA-RhB-PLA-PEG, which structure is reported in figure 33.

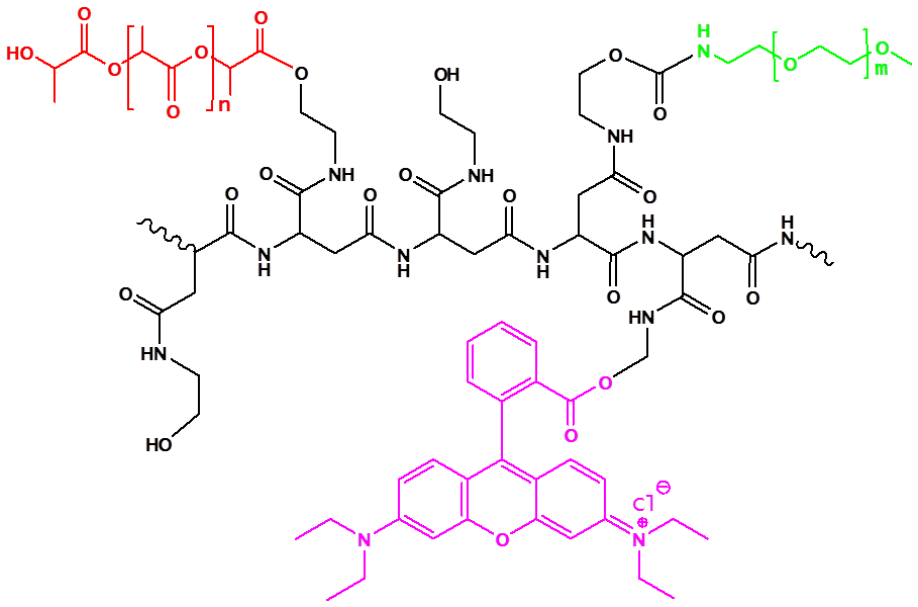

Fig. 33: Chemical structure of PHEA-RhB-PLA-PEG graft copolymer (n = 194, m = 44), (pink: RhB moieties, red: PLA chains, green: PEG chains).

PHEA was covalently linked with rhodamine B (RhB) moieties, polylactide (PLA) and poly(ethyleneglycol) (PEG). The derivatization of PHEA with these three functionalities has different aims. First, the functionalization of PHEA with RhB is a valid approach to introduce a fluorescent probe, with high absorption coefficient and photostability. The chemical and enzymatic stability in physiological conditions of the ester binding between RhB and PHEA was evaluated, being this one an important factor because allow the efficient tracking of PHEA-RhB derivatives-based NPs through the mucus layer.

Second, the grafting of PHEA-RhB with different amount of PLA allowed to introduce biodegradable hydrophobic chains, giving amphiphilic properties to the resulting copolymers and making them suitable for the preparation of fluorescent NPs (FNPs).

Third, the derivatization of PHEA-RhB-PLA copolymers with different amount of PEG, allows to obtain particles with different hydrophilic surfaces, that potentially shield and protect their hydrophobic core minimizing mucoadhesive interactions with mucins in mucus layer.

Once obtained and properly characterized, FNPs were easily obtained without the use of surfactants or stabilizing agents, and then characterized in terms of mean size, zeta potential, morphology, and fluorescence properties.

Moreover, being the slow degradation rate of PLA and PLA derivatives a disadvantage for pulmonary drug delivery, especially when repeated administrations are required, the

biodegradability of produced NPs was evaluated in isotonic media mimicking the physiological environment.

In particular, an equivalent non-rhodaminated NP formulation was incubated at 37 °C for 21 days, and pH, ^{1}H-NMR, FT-IR, PCS and SEC analyses were carried out in order to obtain qualitative and quantitative informations on the hydrolysis process undergone by NPs.

Once evaluated all requirements for NP based pulmonary delivery systems, NPs based on PHEA-RhB-PLA and PHEA-RhB-PLA-PEG with two different PEG content were used to assess requirements for the mucus-penetrating ability, evaluating them in terms of suitable morphology, mean size, surface charge, surface PEG density, and conformation of PEG chains on the NPs surface.

Moreover, their cytocompatibility towards 16-HBE cells, the ability to elude steric interactions with mucin fibers and to diffuse through CF-AM was evaluated as function of surface PEG coverage.

Then, ibuprofen was chosen as drug to be administrated by pulmonary delivery, since limiting the inflammatory response in the CF lung could be effective, not only because inflammation damages the lungs directly but also because impairs local host defences, preventing the clearance of infections.

Ibuprofen, which structure is reported in figure 34, is a hydrophobic non-steroidal anti-inflammatory (NSAID), first investigated as a CF treatment in 1990 and currently studied in CF patients to reduce extreme inflammation in the lungs.

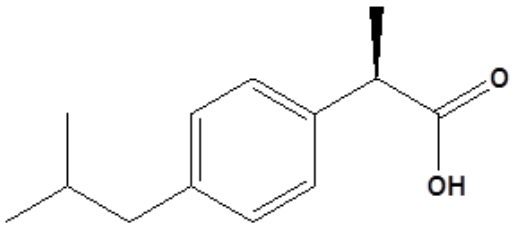

Fig. 34: Chemical structure of ibuprofen.

Despite encouraging results obtained, in clinical the anti-inflammatory approach is rarely practiced because of systemic side effects. However, the recent discover of ibuprofen activity as a CFTR corrector [27] and as an antimicrobial agent itself [22] at high dose with synergic activity with other antimicrobials has rekindled the attention for this drug, and its formulations for pulmonary delivery, that could allow to obtain higher local drug concentrations and minimize side effects if compared to the oral route of administration.

Thus, in order to overcome the limitations caused by the poor penetration through the CF high dense and viscoelastic mucus barrier, ibuprofen was loaded in mucus-penetrating FNPs.
After having determinated the ibuprofen content into FNPs, ibuprofen release profile and uptake capacity within the lung epithelial cells in presence of CF-AM was tested and compared to free ibuprofen.

Finally, mucus penetrating NPs were also loaded with the CFTR potentiator ivacaftor (structure in figure 35), in order to correct the defective ion transport caused by the impaired CFTR function.
On April 2015, the Italian Medicines Agency (AIFA) concluded the negotiation phase for Kalydeco®, the orally dosage form containing ivacaftor, for CF patients with class III mutations (G551D, G1244E, G1349D, G178R, G551S, S1251N, S1255P, S549N o S549).

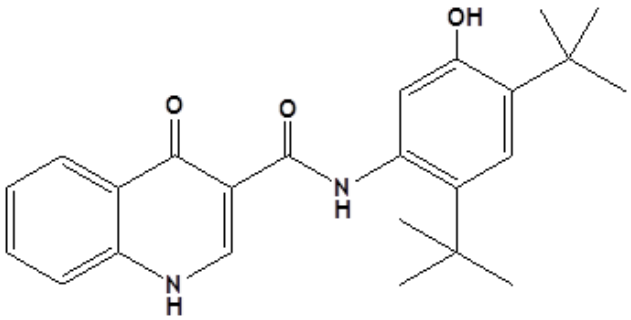

Fig. 35: Chemical structure of ivacaftor.

Even if the discovery of ivacaftor has provided a proof of concept that CFTR related chloride secretion can be potentiated, an enhanced activity could be shown if this drug was administered by pulmonary route, increasing the drug concentration at the site of disease and reducing systemic side effects.
For this reason, ivacaftor was loaded in mucus-penetrating NPs based on a mixture of PHEA-RhB-PLA-PEG, at the highest PEG content, and another derivative of PHEA-PLA, named PHEA-PLA-Tat (figure 36).

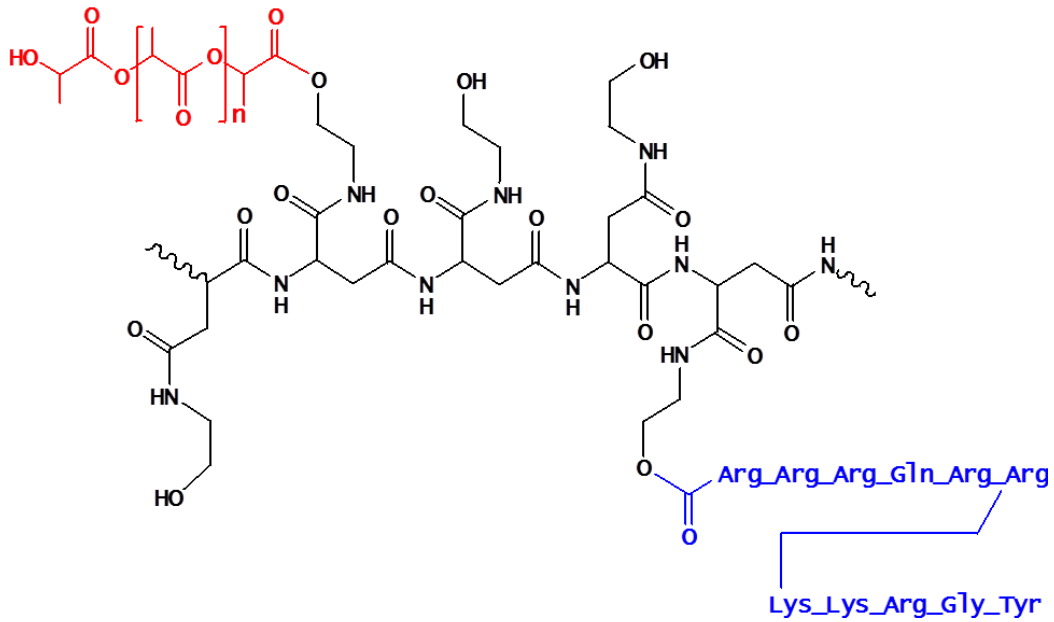

Fig. 36: Chemical structure of PHA-PLA-Tat (n=194).

Tat is the most intensively studied amongst the cell penetrating peptides, widely used for the successful intracellular delivery of biologically active substances.

In this case, PHEA-PLA was derivatized with Tat in order to improve the intracellular uptake of ivacaftor containing NPs, generally limited by the high density PEG on NP surface.

FNPs, based on an equal mixture of PHEA-RhB-PLA-PEG and PHEA-PLA-Tat or PHA-PLA were produced by using a nanoprecipitation method and properly characterized. Cell viability of produced FNPs towards 16-HBE cells, their requirements for the mucus-penetrating properties, their ability to elude steric interactions with mucin fibers and to diffuse through CF-AM, was evaluated in presence or in absence of the Tat ligand.

Chapter 3

Results and discussion

3.1 *Nano Into Micro* strategy: polyanion-tobramycin nanocomplexes into microparticles for the treatment of infection in cystic fibrosis (CF)

In order to obtain an inhalable drug delivery system able to overcome the CF mucus barrier and at the same time to achieve a sustained delivery of tobramycin, a *nano into micro* strategy was used. For this reason, the potential of a mannitol microparticle-based formulation (MPs) containing a polymeric polyelectrolyte complex of tobramycin, was realized for the treatment of pulmonary infections of *Pseudomonas aeruginosa* in CF.

A nanometric ion pair complex between tobramycin and an anionic derivative of α,β-poly(N-2-hydroxyethyl)-D,L-aspartamide (PHEA), PHEA-EDA-GlucA, was realized in order to modulate tobramycin release from obtained MPs, while mannitol was chosen as MPs surrounding matrix because, as osmotic agent, it induce the influx of water in the mucus layer from the underlying epithelial cells, diluting it and thus facilitating the drug diffusion.

This *nano into micro* formulation was realized by optimizing the spray-drying process and the composition of an aqueous solution containing mannitol and the ion pair complex between tobramycin and PHEA-EDA-GlucA.

3.1.1 Synthesis and characterization of PHEA-EDA-GlucA

To obtain an anionic derivative of PHEA which contains pendant carboxylic groups able to interact with tobramycin, PHEA was first functionalized with a proper amount of ethylenediamine (EDA) moieties to obtain PHEA-EDA [132, 133].

The reaction was conducted by first activating the hydroxyl groups present on PHEA backbone with bis(4-nitrophenyl) carbonate, and then followed by the reaction with EDA.

The chemical structure of PHEA-EDA copolymer is reported in the figure 37.

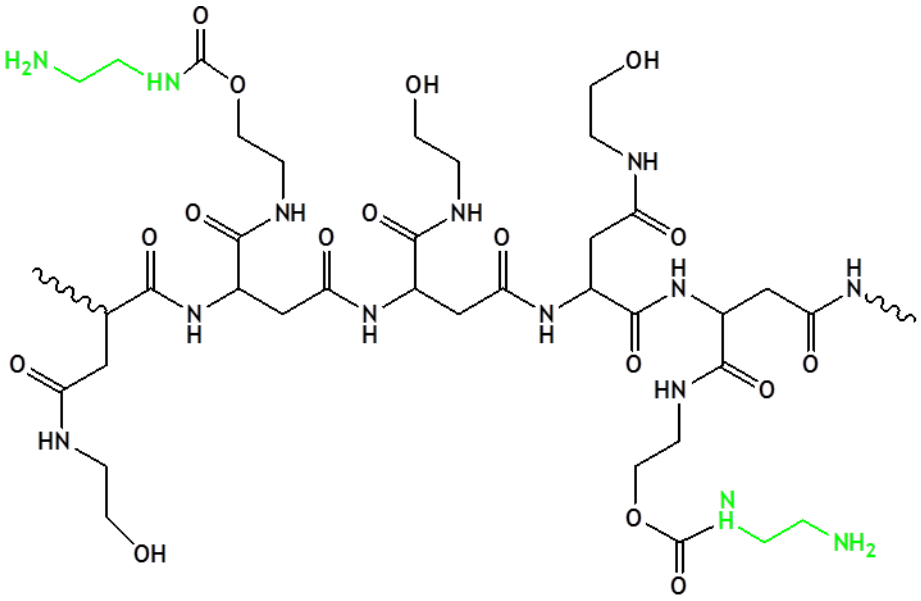

Fig. 37: Chemical structure of PHEA-EDA (green: EDA moieties).

PHEA–EDA copolymer was purified and then characterized through ^{1}H-NMR analysis (figure 38), which confirmed the introduction of EDA groups in PHEA backbone.

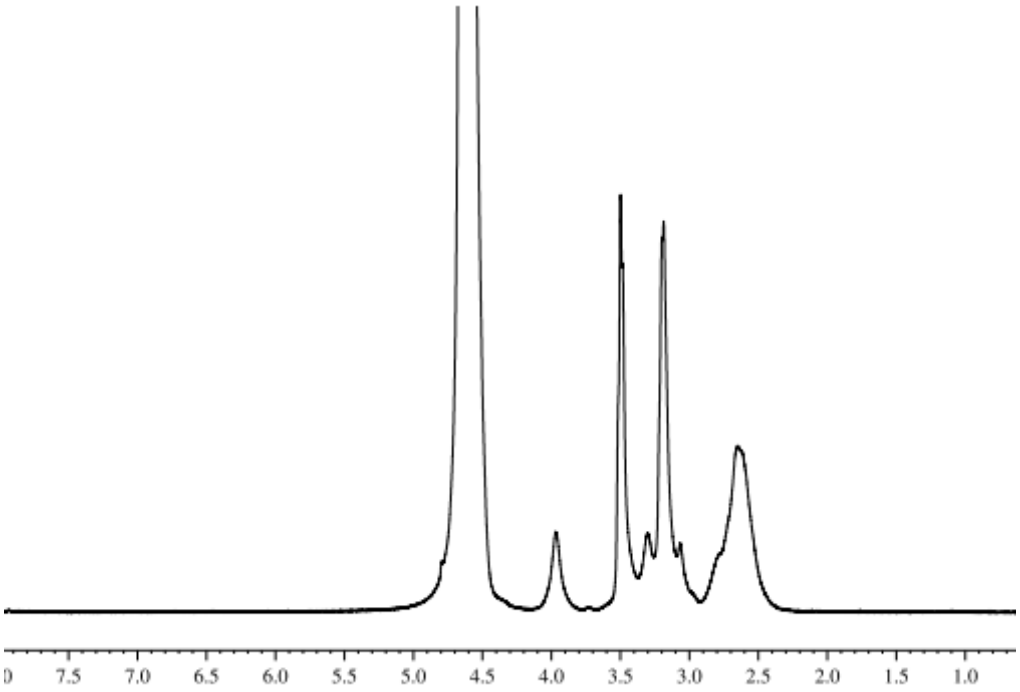

Fig. 38: ^{1}H-NMR spectrum of PHEA-EDA.

In particular, ^{1}H-NMR spectra allowed the quantification of pendant amine groups in the polymer chain by comparing the integral of the peak related to EDA-derivatized hydroxyethyl

groups of PHEA at δ 3.97, with the integral of the peak related to protons assignable to methylenes of polymer backbone at δ 2.64.

The degree of derivatization of PHEA-EDA with EDA molecules (DD_{EDA}) was find to be equal to 50 mol % on PHEA-EDA repeating units.

SEC analysis was used to confirm the occurrence of derivatization and study the molecular weight and polydispersity indexes of the obtained copolymer. As already known [78, 133], after the reaction with EDA chains, PHEA-EDA copolymer resulted to have a $\overline{M}_w$ almost 1.5 times lower than PHEA (table 3), being the $\overline{M}_w$ of PHEA-EDA and PHEA 26.3 and 38.4 kDa, respectively. This reduction is probably ascribable to the degradation of the polyammidic backbone of PHEA caused by EDA molecules in the used experimental conditions, and/or to a conformational change caused by the introduction of EDA chains to the PHEA backbone.

Table 3. Chemical composition (DD_{EDA}, DD_{GlucA} mol %), weight-average molecular weight ($\overline{M}_w$) and polydispersity index ($\overline{M}_w/\overline{M}_n$) of synthesized copolymers.

Copolymers	**Derivatization Degree (mol %)**		**Molecular Weight**	
	DD_{EDA}	DD_{GlucA}	$\overline{M}_w$ (kDa)	$\overline{M}_w/\overline{M}_n$
PHEA	-	-	38.4	1.62
PHEA-EDA	50 ± 0.2		26.3	1.57
PHEA-EDA-GlucA	50 ± 0.2	49.5±0.1	27.8	1.44

The glucuronidated copolymer PHEA-EDA-GlucA was then synthesized by a reductive amination reaction in aqueous medium at pH 9 between D-(+)-Glucuronic acid γ-lactone (GlucA) and primary amine functions of PHEA-EDA, in the presence of sodium cyanoborohydride, as reported in the scheme 1.

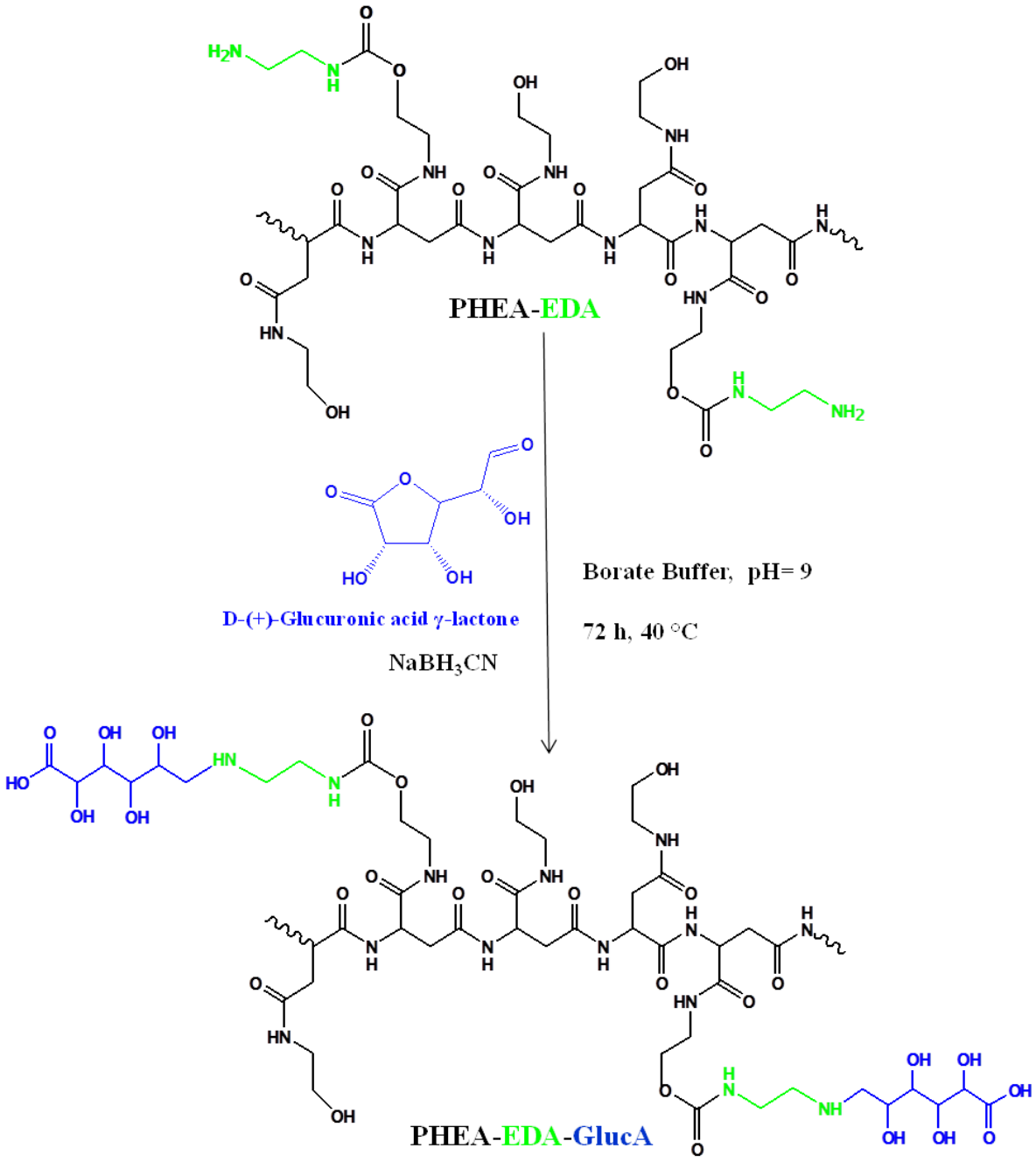

Scheme 1: Synthesis of PHEA-EDA-GlucA copolymer (green: EDA moieties, blue: GlucA residues).

DD_{GlucA} of PHEA-EDA-GlucA was calculated indirectly by determining the amount of residual EDA molecules on PHEA-EDA and on PHEA-EDA-GlucA by using the 2,4,6-Trinitrobenzene sulfonic Acid (TNBS) colorimetric assay [78, 134]. Being the starting DD_{EDA} equal to 50 mol % on PHEA-EDA repeating units and the residual EDA moles after derivatization about 0.5 ± 0.1 mol%, it can be assumed that DD_{GlucA} is equal to 49.5 mol %.

The reductive amination reaction efficiency between EDA moieties on PHEA-EDA and GlucA was determined to be 97.6 ± 1.3 % using the acid-base titration method, confirming that almost all amino groups on PHEA-EDA are derivatized with GlucA.

SEC analysis confirmed the occurrence of derivatization, being $\overline{M}_w$ of PHEA-EDA-GlucA increased if compared to the starting PHEA-EDA and in accordance with the theoretical value considering the starting PHEA-EDA and the resulting DD_{GlucA} (table 3).

3.1.2 Preparation and characterization of tobramycin:PHEA-EDA-GlucA ion pair complex

On the basis of obtained data, it can be assumed that about all EDA residues on PHEA-EDA are derivatized with GlucA and that each PHEA-EDA-GlucA chain possess about 50 free pendant carboxylic groups.

On the other hand, given that each tobramycin molecule has five protonable amino groups (figure 39a), a ion pair complexation was obtained between tobramycin and PHEA-EDA-GlucA in aqueous medium at pH 6 (Trizma buffer, 0.05M), schematized in figure 39 b.

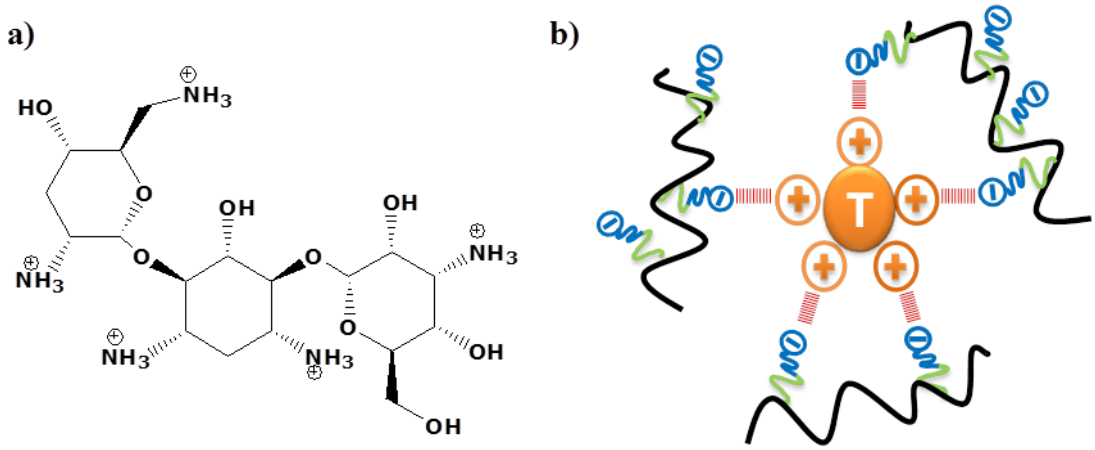

Fig. 39: a) Chemical structure of tobramycin; b) schematic representation of tobramycin:PHEA-EDA-GlucA ion pair complex structure.

Main size values of obtained ion pair complex (table 4) resulted to be about 90 nm, ranging between 90.4 and 90.7 nm if determined in isotonic phosphate buffer (PBS pH 7.4) or Trizma buffer (pH 6). Moreover, being ζ potential values of PHEA-EDA-GlucA –14.8 ± 0.9 and –16.5 ± 1.1 mV in PBS (pH 7.4) and Trizma buffer (pH 6) respectively, the lower values detected for the ion pair complex (table 4) in both media is ascribable to the complexation with the positive net charges of tobramycin.

Table 4: Mean size, polydispersity index (PDI) and ζ potential of tobramycin:PHEA-EDA-GlucA ion pair complex in PBS (pH 7.4) and Trizma buffer (pH 6).

Tobramycin:PHEA-EDA-GlucA ion pair complex			
Medium	**Mean Size (nm)**	**PDI**	**ζ Potential (mV)**
Trizma buffer (pH 6)	90.4 ± 6.2	0.298 ± 0.04	- 7.7 ± 0.3
PBS (pH 7.4)	90.7 ± 5.8	0.306 ± 0.02	- 9.1 ± 0.7

The effective spontaneous formation of the ion pair complex and the interaction capacity between drug and copolymer were investigated through isothermal titration calorimetry (ITC) by injecting tobramycin aqueous solution to a PHEA-EDA-GlucA aqueous solution and by carrying out three experiments where the molar concentrations of amino groups (belonging to tobramycin) or carboxylic groups (belonging to PHEA-EDA-GlucA) were varied. In particular, the experiment A was performed by using a polymer solution containing 141 mM of carboxilic groups and a drug solution containing 1337 mM of amino groups, the experiment B 141 mM of carboxylic groups and 321 mM of amino groups, and the experiment C 282 mM of carboxylic groups and 321 mM of amino groups, respectively.

A very good reproducibility of the binding experiments was obtained for all the three experiments (data not shown), probing all the ratios of the binding curve.

In figure 40, binding isotherm and heat rate flow resulted from the experiment C are reported as an example. An exothermic reaction was observed, indicating that an interaction occurs between the antibiotic and the synthesized copolymer.

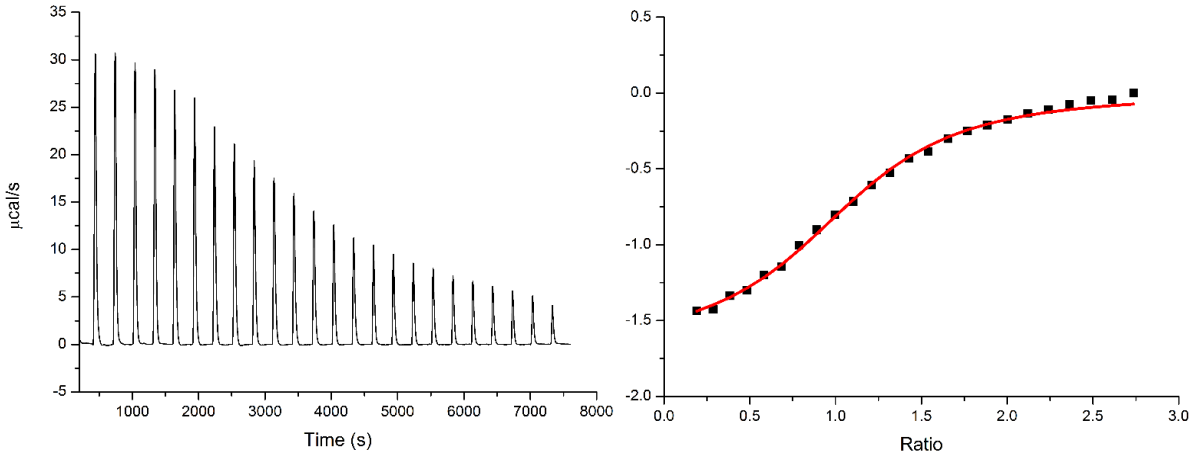

Fig. 40: Isothermal titration calorimetry (experiment C). On the left, binding isotherm obtained using Incremental Injection ITC, by titrating tobramycin (321 mM) into a PHEA-EDA-GlucA solution (282 mM of carboxylic groups). On the right, the heat rate flow of the same titration.

In order to obtain all binding parameters for tobramycin:PHEA-EDA-GlucA ion pair complex formation, the independent one-site binding model was used, where the analytical solution for the normalized heat associated with each injection is determined by the formula:

$$Q_i = \frac{V_0 \Delta H}{v_{inj} L_{syr}} \left([PL]_i - [PL]_{i-1} \left(1 - \frac{v_{inj}}{V_0} \right) \right) + q_d$$

where V_0 is the reaction volume, ΔH is the enthalpy of binding, $[PL]$ is the concentration of polymer-ligand complex, L_{syr} is the ligand concentration in the syringe, and q_d is the background injection heat effect. The concentration of polymer-ligand complex after any injection is calculated by solving and applying the following equations:

$$[P]_t \frac{K[L]}{1 + K[L]} + [L] - [L]_t = 0$$

$$[PL] = [P]_t \frac{K[L]}{1 + K[L]}$$

where K is the equilibrium binding constant, and $[P]_t$ and $[L]_t$ are the bulk concentration of polymer and ligand in the calorimetric cell, while [L] is the free concentration of ligand.

The analysis, performed in terms of the ratio NH_2/COOH, gave the apparent stoichiometry of the interaction. This value was used to scale the concentration ratio data to an effective concentration of interacting carboxylic groups.

By using this model, the following binding parameters were obtained: the binding constant K=1.86E+02 M^{-1}, a stoichiometry n=1.098, an exothermic enthalpy change ΔH=-1.66 kcal/mol, a dissociation constant Kd=5.37E-03 M. Moreover, the free energy, ΔG, was determined from the binding constant ($\Delta G = -RTlnK$), and entropy, ΔS, from the definition of the Gibbs energy ($\Delta G = \Delta H - T\Delta S$). Respectively, a negative ΔG of -3.1 kcal/mol and a positive entropy change ΔS of 4.75 cal/mol·K were found, indicating that the process was enthalpically driven.

From a proper calculation, it was determined that the obtained molar 1:1 stoichiometry of interaction between NH_2 and COOH corresponds to a weight ratio between tobramycin and PHEA-EDA-GlucA equal to 1:5.

In order to evaluate the stability of the obtained tobramycin:PHEA-EDA-GlucA ion pair complex, a release study was performed in sink conditions by using the dialysis method [81]. In particular, tobramycin:PHEA-EDA-GlucA ion pair complex was prepared by mixing two aqueous solutions at pH 6 containing tobramycin and PHEA-EDA-GlucA at a final weight ratio of 1:5 (corresponding to 1:1 NH_2:COOH molar ratio) and left stirring overnight at room temperature. Moreover, in order to evaluate if a twice amount of COOH could increase the stability of the ion pair complex, modulating thus the drug release, the stability study was also carried out by using a weight ratio between tobramycin and PHEA-EDA-GlucA of 1:10 (corresponding to 1:2 NH_2:COOH molar ratio).

In figure 41, the percentage of released tobramycin from the ion pair complex (at the drug:copolymer weight ratio of 1:5 and 1:10), and the diffusion profile of the drug through the dialysis membrane are reported.

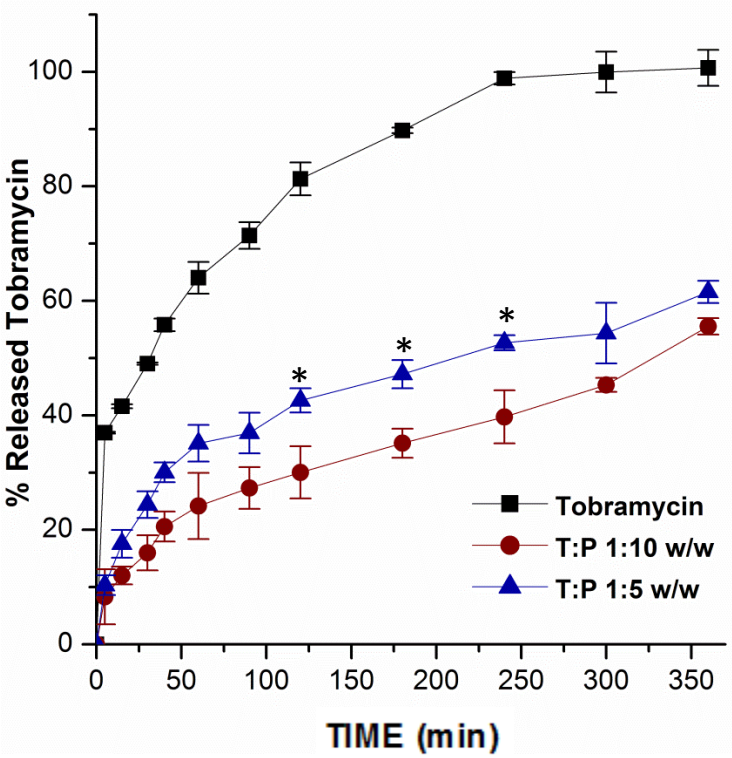

Fig. 41: Release profile of tobramycin from tobramycin:PHEA-EDA-GlucA ion pair complex at the weight ratio 1:10 (T : P 1:10 w/w) and 1:5 (T : P 1:5 w/w) as a function of incubation time at 37 °C (* $p < 0.05$) compared to the diffusion of tobramycin trough dialysis membrane in phosphate buffer medium at pH 7.4.

Results showed that when tobramycin is involved in the formation of the ion pair complex with PHEA-EDA-GlucA, it is slowly released in the aqueous medium and that the presence of an higher amount of anionic copolymer did not increase the stability of the complex. In particular, the lower amount of tobramycin released from the ion pair complex at a drug:copolymer ratio of 1:10 w/w is not statistically significant from that released from the complex at 1:5 w/w, except for the points from 2 to 3 h, demonstrating that the drug release is not affected by an increased amount of copolymer in the ion pair complex.

Moreover, after 6 h of incubation, the amount of tobramycin released from the ion pair complex at the drug:copolymer ratio of 1:5 reached the 50 wt% of the total amount, while at the same incubation time the diffusion through dialysis membrane reached about the 100 wt%.

These results demonstrate that the interaction of tobramycin with the anionic copolymer PHEA-EDA-GlucA is effectively able to retard the drug release in an aqueous medium; thus the ion pair complex obtained at a tobramycin:PHEA-EDA-GlucA weight ratio of 1:5 was chosen for carrying out further experiments.

3.1.3 Preparation of mannitol-spray dried microparticles (MPs)

With the aim to realize a formulation for pulmonary administration of tobramycin, mannitol MPs were obtained by following a spray drying process and by using the Nano Spray Dryer B-90, a widely known technology to produce particles for drug delivery, especially for the pulmonary route of administration [135].

The Büchi Nano Spray Dryer B-90 offers a new, simple and alternative approach for the production of particles if compared to the classical spray drying process. The strength of the Büchi Nano Spray Dryer B-90 lies in its vibration mesh spray technology, creating, before evaporation, tiny droplets in a size range of a smaller order of magnitude than in classical spray dryers. This is a revolution in spray drying technology, making it possible to produce powders from submicron to few microns size range with very narrow distributions [135].

In order to optimize the formulation, solutions at different compositions in terms of weight of mannitol and tobramycin:PHEA-EDA-GlucA ion pair complex were spray dried and results in terms of average diameter, recovery yield and entrapped amount of tobramycin (expressed as Drug Loading, DL, and Entrapment Efficiency, EE) are reported in table 5.

Table 5. Composition for 100 mL of spray dried solution, recovery yield (wt %), average diameter (μm), drug loading (DL, wt %), and entrapment efficiency (EE, wt %) of obtained formulations.

Sample	Mannitol:PHEA-EDA-GlucA:tobramycin weight ratio (g)	Recovery Yield (wt %)	Average diameter (μm)	DL (wt %)	EE (wt %)
MPs-A	2:0:0	48.8 ± 2.3	5.9 ± 0.8	-	-
MPs-B	1.5:0:0	54.0 ± 3.8	4.7 ± 0.6	-	-
MPs-C	**1:0:0**	**76.3 ± 3.1**	**2.5 ± 0.9**	**-**	**-**
MPs-D	1:0.8:0.16	ND	ND	ND	ND
MPs-E	**1:0.4:0.08**	**68.5 ± 1.7**	**2.2 ± 0.7**	**5.3 ± 0.7**	**98.1 ± 0.01**
MPs-F	1:0.3:0.06	71.1 ± 3.6	2.1 ± 0.5	4.3 ± 0.2	97.7 ± 0.04
MPs-G	1:0.4:0	73.4 ± 1.2	2.2 ± 0.8	-	-

N.D.: Not Definable; Formulation selected for further analysis highlighted in bold text.

When mannitol was spray dried alone, the best characteristics in terms of recovery yield and average diameter were obtained at an aqueous concentration of mannitol of 1g/100 mL (sample MPs-C). In particular, as evident from the table 3, for empty mannitol MPs (MPs-A,

MPs-B and MPs-C samples), the average diameter decreased as the mannitol amount in the aqueous solution spray dried decreased from 2 to 1 g, allowing to obtain particles with suitable average diameter for a proper administration to the lungs. Moreover, the recovery yield for sample MPs-C raised about the 76 wt%, resulting in an optimal recovery yield percentage, nullifying the most critical limitation of the spray-drying technique.

Tobramycin-loaded MPs with suitable characteristics in terms of average diameter, DL and EE were obtained when a weight ratio between mannitol, tobramycin and PHEA-EDA-GlucA equal to 1:0.4:0.08 was chosen (sample MPs-E). In particular, as evident from the table 3, decreased amounts of ion pair complex into the mannitol solution allowed to improve the characteristics of obtained formulations. In fact, for the sample MPs-D, with a 1:0.8:0.16 mannitol:PHEA-EDA-GlucA:tobramycin weight ratio, it was impossible to recover the MPs due to the formation of a sticky film for the high concentration of the polymer, while for the MPs-E and MPs-F samples it was possible obtaining MPs with the desired characteristics in terms of recovery and average diameter. In particular, both MPs-E and MPs-F samples showed a good DL, being 5.3 and 4.3 wt % respectively, which correspond to an EE respectively of 98.1 and 97.7 wt%.

On the basis of these data, sample MPs-E was chosen for the further characterization, while MPs-C was used as control.

Morphological characterization was carried out on both MPs-C and MPs-E by scanning Electron Microscopy (SEM). SEM images, shown in figure 42, highlighted the spherical shape and micron-sized particles. Moreover, the absence of difference in the surface characteristics of both empty and drug-loaded MPs suggests that tobramycin:PHEA-EDA-GlucA ion pair complex is entrapped inside the MPs. Comparing size distribution profiles of both MPs-C and MPs-E, no significant differences are evident, suggesting that the presence of tobramycin: PHEA-EDA-GlucA ion pair complex in MPs-E does not influence in a significant manner the technological properties of obtained spray-dried MPs.

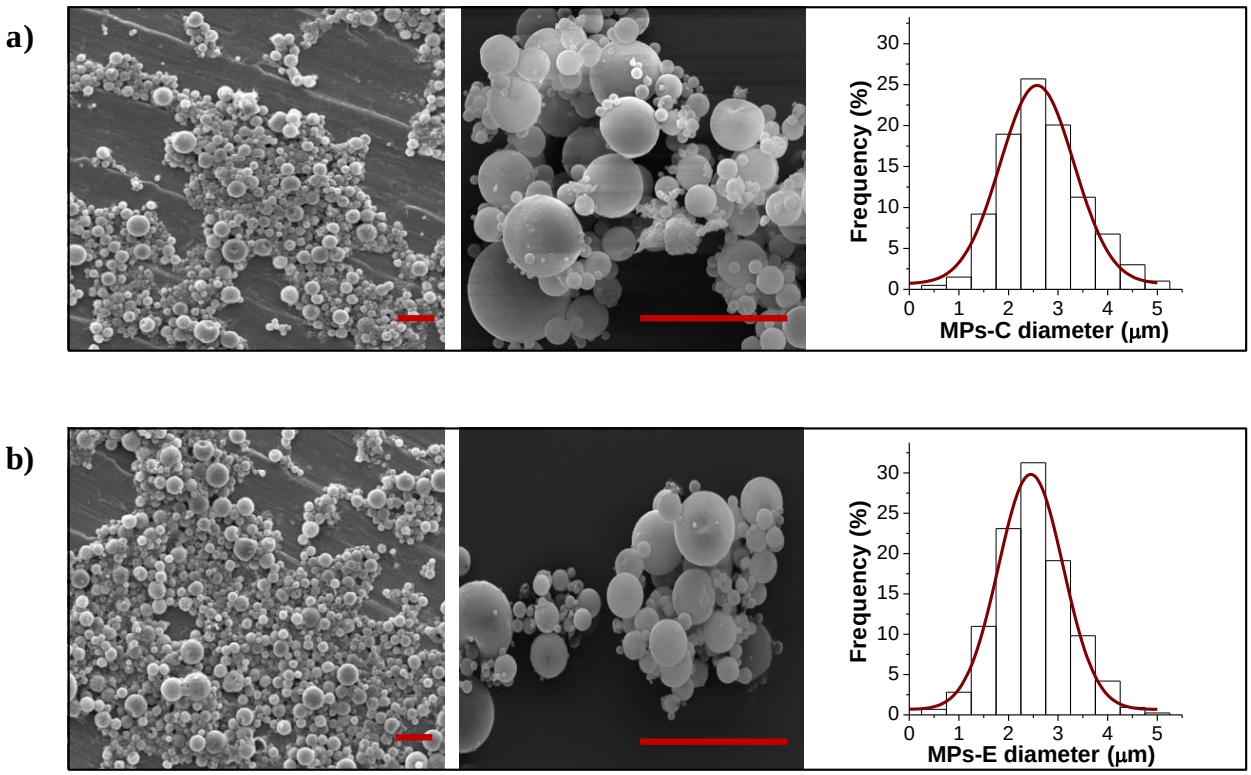

Fig. 42: SEM micrographs and size distribution of samples MPs-C (a) and MPs-E (b), (scale bar represents 10 μm).

3.1.4 Effect of MPs on rheological properties of CF artificial mucus (CF-AM)

To evaluate as the presence of MPs could modify the viscoelastic properties of CF-AM, a rheological study was carried out.

CF-AM was prepared following a previously described method [65, 136, 137]. Mucins, DNA, surfactant, salts and amino acids were added taking in account the physical-chemical composition, biochemical properties and the rheological behavior of CF sputum. In particular, mucins and DNA were added being the main biopolymers that constitute the sputum network, while amino acids were included because they are actually present in high amounts in lungs with disease [137].

As already known, obtained CF-AM showed a rheological behavior typical of pseudo-plastic fluids, with a viscosity reduction after shear stress increase similar to that observed for whole sputum of patients affected by CF [136].

CF-AM was incubated alone or in the presence of increasing amounts of MPs-E as dry powder (0.5, 2 and 3.5 mg) for 1h at 37°C and then analyzed with a rheometer. Storage modulus (G'), loss modulus (G'') and complex viscosity (η*) obtained for CF-AM treated

with MPs-E were compared to the untreated CF-AM and reported in figures 43 a, b and c, respectively.

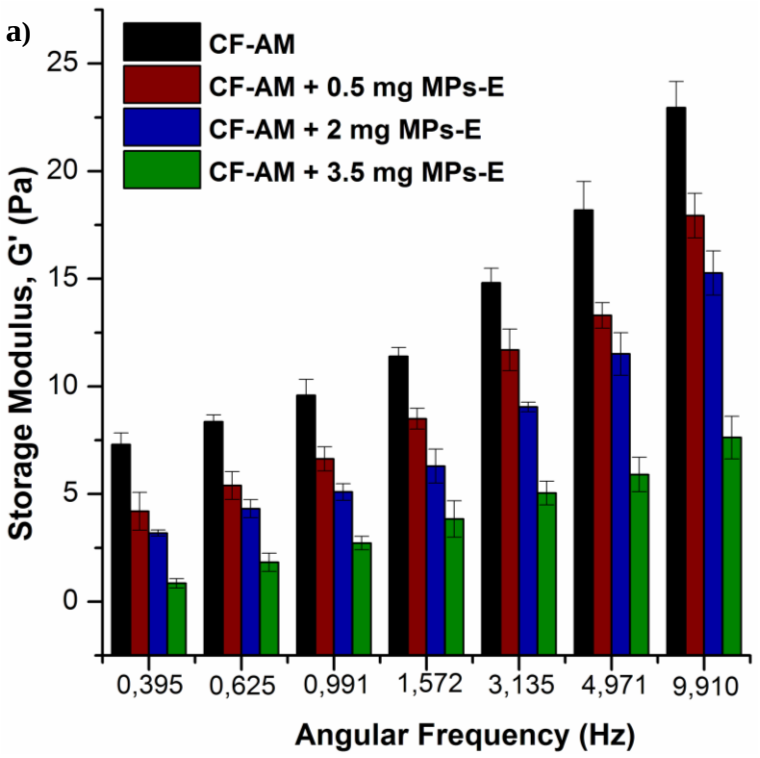

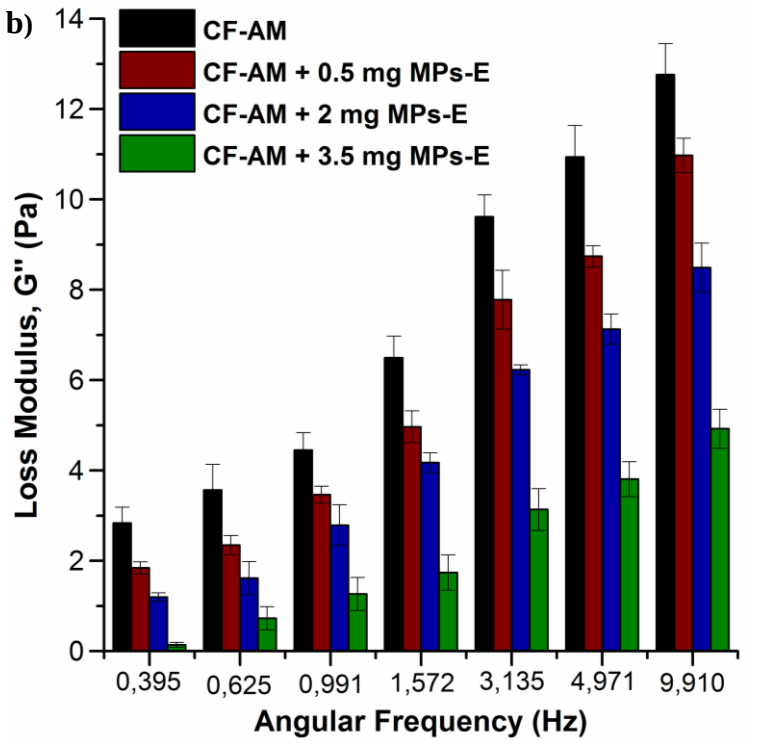

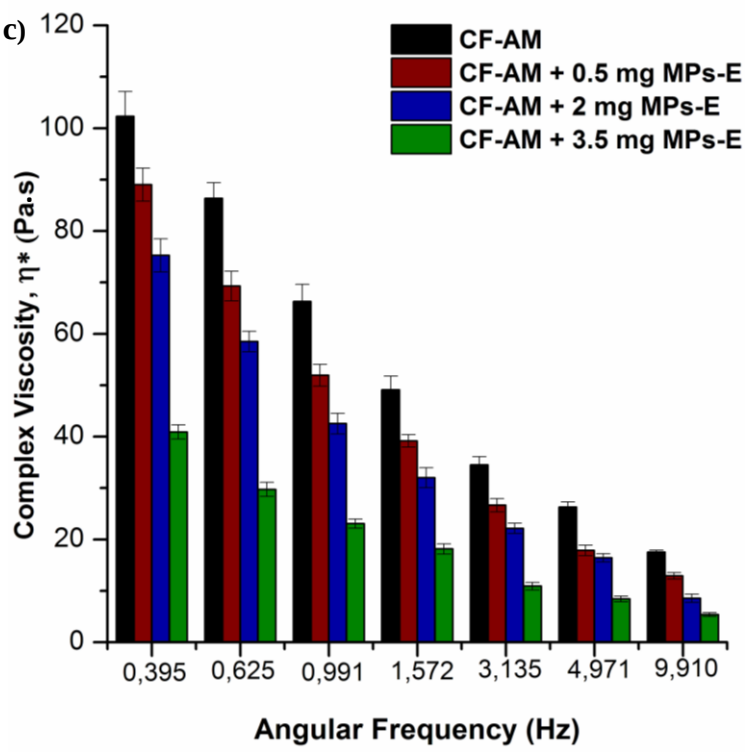

Fig. 43: (a) Storage modulus (G'), (b) loss modulus (G''), and (c) complex viscosity (η*) of CF-AM after 1h of incubation alone or in the presence of 0.5, 2 and 3.5 mg of MPs-E.

As evident from these graphics, MPs are able to alterate the voscoelastic properties of the mucus layer, being able to reduce G', G'', and η* and to reduce these parameters as amount of MPs deposed on CF-AM increases. In particular, when CF-AM is treated with 0.5 mg (* <0.05), 2 mg and with 3.5 mg (** $p<0.01$) of MPs, G', G'', and η* values of CF-AM are significantly lower than that obtained with CF-AM alone. The same values are significantly lower for CF-AM treated with 3.5 mg compared to that obtained after the treatment with 2 and 0.5 mg (** $p<0.01$), while no significant differences exist between G' and G'' values obtained for CF-AM treated with 2 or 0.5 mg of MPs.

This reduction of rheological parameters seems to support the hypothesis that the osmotic agent mannitol, once deposed on mucus layer in lung airways, is able to increase the influx of water from neighboring regions, such as the epithelium cell layer. This local hydration effect results in an increase of the macroporosity of the polymer network constituting the mucus and consequently to a reduction of the macrorheology of the mucus, facilitating thus the transport of drugs through it [136].

However, under used experimental conditions, the hydratation effect couldn't be explained because of the absence of cells from which the water could be drawn. So, the observed

reduction of G', G'', and η* seems to be ascribable only to a deconstruction of the polymer network constituting the mucus. Therefore, the presence of epithelial cells could induce in vivo an influx of water that probably increases the positive effects of prepared systems.

3.1.5 Evaluation of tobramycin diffusion profile from MPs in CF-AM

On the basis of the obtained results in terms of impact of MPs-E on CF-AM and in order to know the ability of obtained MPs-E to retain the antibiotic and to ensure a sustained release at the site of action by diffusing through the CF-AM layer, a tobramycin release study from MPs-E and its diffusion in CF-AM was performed by using a vertical Franz-type diffusion cell.

The tobramycin release and diffusion profile from MPs-E in CF-AM were reported in figure 44 as a function of incubation time.

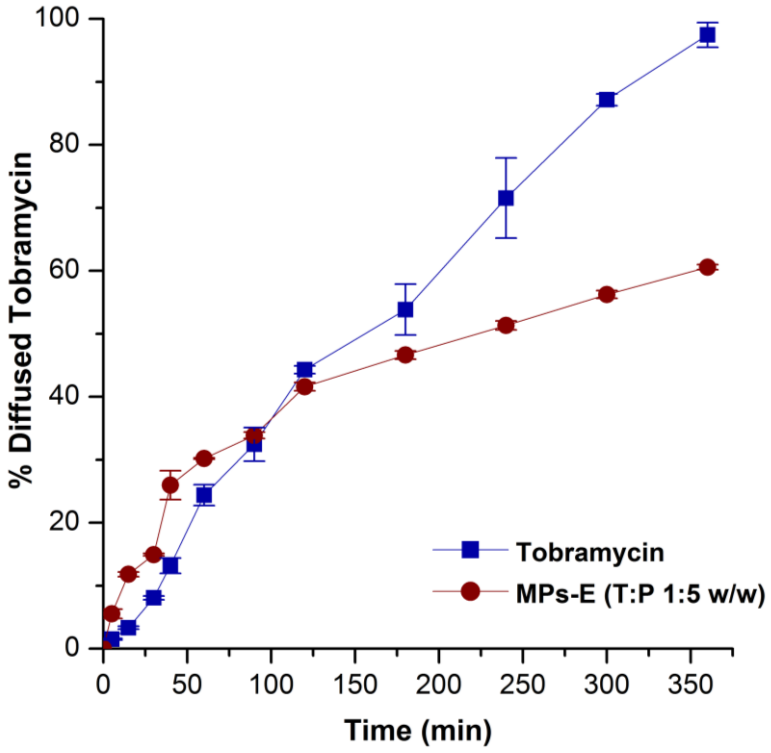

Fig. 44: Diffusion of tobramycin from MPs-E through CF-AM layer in Franz-cells as a function of incubation time at 37°C.

Results showed that the entrapment into MPs is able to influence the diffusion kinetics of tobramycin in CF-AM. In particular, the amount of tobramycin diffused until the first hour is significantly higher than the diffused free drug. After this time, the trend is inverted, and the

amount of tobramycin released from MPs and diffused through CF-AM resulted to be lower than the free drug.

This behavior could be explained considering the ability of mannitol to modify the rheological properties of CF-AM, as described above. So, until the first hour, MPs could facilitate the transport of the antibiotic to the acceptor chamber, while free tobramycin diffuses slower due to the high viscous CF-AM layer and probably to binding interactions with mucus components in this environment [128, 138]. Then, a sustained release of tobramycin from MPs is obtained thanks to its participation in the ion pair complex with PHEA-EDA-GlucA, that, as showed above, allowed to release an amount of tobramycin that doesn't exceed the 60 wt% of the total entrapped drug after 6 h incubation.

These results showed the unique properties of this MPs formulation, able to deliver the antibiotic by an initial effect on rheological modification of the the CF-AM layer, allowing a rapid transport of the drug through CF-AM layer and reaching the receptor chamber, and by offering then a sustained delivery thanks to its interaction with PHEA-EDA-GlucA.

3.1.6 In vitro cytocompatibility on human bronchial epithelial cells (16-HBE)

To evaluate the potential in vivo use of these MPs for trating CF patients, cytocompatibility of MPs-C (empty) and MPs-E (loaded with the ion pair complex) was evaluated by the MTS assay on 16-HBE cells at different MPs concentrations after 4 h incubation (fig. 45a). Moreover, cell viability was also evaluated in the presence of free tobramycin and PHEA-EDA-GlucA, in a wider range of concentrations (fig. 45b).

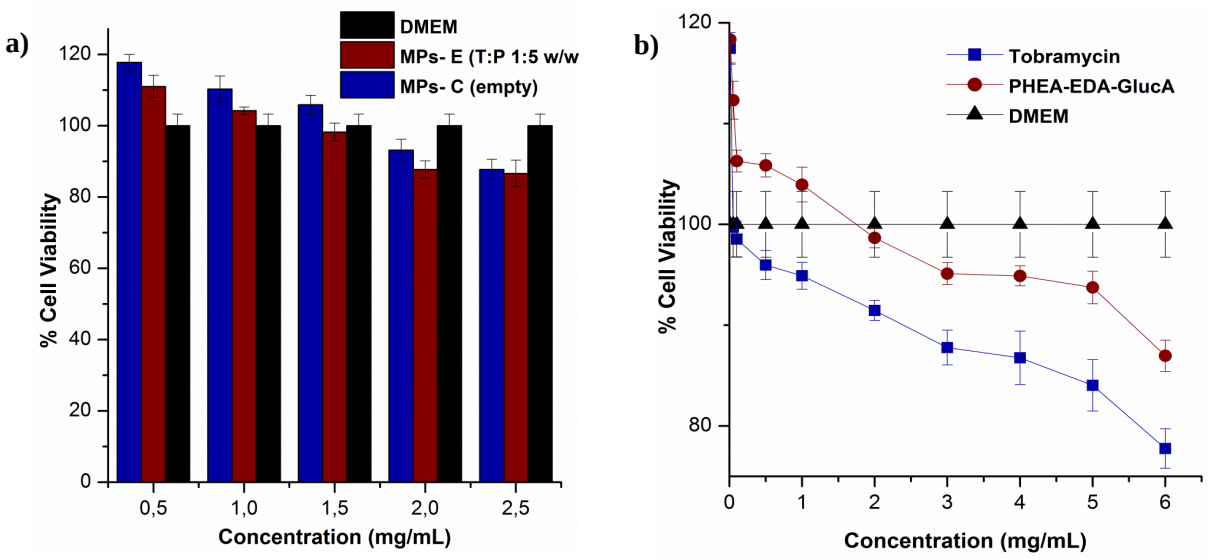

Fig. 45: Cell viability % on 16-HBE cells after 4 h incubation with (a) MPs-C (empty) and MPs-E (loaded with the ion pair complex) and with (b) PHEA-EDA-GlucA and tobramycin.

As can be seen in figure 45a, all MPs samples showed an excellent cytocompatibility at all tested concentrations. In fact, all samples showed a cell viability higher than 80 % compared to the control and the cell viability increased at lower concentration of the samples incubated (fig. 45a). Further, no significant differences exist between empty and drug-loaded MPs at all tested concentrations.

As evident in figure 45a, at lowest concentrations of MPs-C and MPs-E exert a proliferative effect on cellular growth, thanks to the presence of mannitol sugar.

Figure 45b showed the cell viability of 16-HBE in the presence of tobramycin or PHEA-EDA-GlucA in concentrations ranging from 0.01 to 6 mg/mL. At all tested concentration both the copolymer and the antibiotic showed excellent cytocompatibility, being cell viability of PHEA-EDA-GlucA, significantly higher than that of tobramycin (* $p<0.05$).

3.1.6 In vitro antipseudomonal activity

In vitro antipseudomonal activity was determined as minimum inhibitory concentration (MIC) against *P. aeruginosa*. MIC of tobramicyn:PHEA-EDA-GlucA ion pair complex at a weight ratio of 1:5 and MPs-E were determined and compared to that of free tobramycin. Moreover, MIC values of PHEA-EDA-GlucA copolymer, MPs-C (empty) and MPs-G (loaded with only PHEA-EDA-GlucA copolymer) were determined and used to understand if the components of the formulation, such as mannitol or copolymer, possessed intrinsic antibacterial properties.

Minimum Bactericidal Concentration (MBC) values of tobramicyn:PHEA-EDA-GlucA ion pair complex at a weight ratio of 1:5 and MPs-E were also determined and compared to tobramycin MBC. MIC and MBC values are reported in table 6.

Table 6. In vitro antipseudomonal activity expressed as MIC and MBC values as concentration of tobramycin (µg/mL).

Sample	MIC (µg/mL)	MBC (µg/mL)
Tobramycin	32	32
Tobramycin:PHEA-EDA-GlucA 1:5 w/w	16	32
MPs-E	8	16

Tobramycin:PHEA-EDA-GlucA ion pair complex and MPs-E have been found to interfere with microbial growth of *P.aeruginosa*. In particular, MPs-E showed the best activity, with MIC values, expressed as concentration of tobramycin, equal to 8 µg/mL, a value lower than that of free tobramycin.

Concerning the MBC values, *P.aeruginosa* showed susceptibility to the antibacterial action of tobramycin:PHEA-EDA-GlucA ion pair complex and MPs-E. Also in this case, MPs-E resulted the most active with a MBC, expressed as concentration of tobramycin, equal to 16 µg/mL.

On the contrary, we did not find any antibacterial activity for MPs-C, MPs-G and the polymer at the maximum tested concentration equal to 128 µg/mL.

Moreover, the antipseudomonal activity of tobramicyn:PHEA-EDA-GlucA ion pair complex and MPs-E was compared to that of free tobramycin in a experimental model mimicking CF mucus environment [136]. In particular, it was determined after 90 min incubation with P.aeruginosa laden CF-AM and evaluated in terms of log reduction of viable bacterial count (CFU/mL), as reported in figure 46.

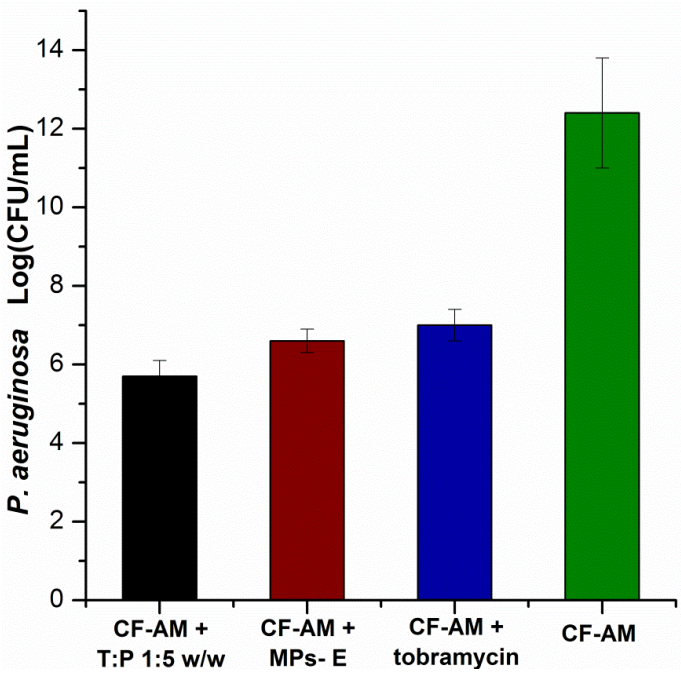

Fig. 46: *P. aeruginosa* laden CF-AM bacterial growth in the presence of tobramycin, tobramycin:PHEA-EDA-GlucA ion pair complex and MPs-E.

As can be seen from the graphic in figure 46, there is a significant reduction in *P.aeruginosa* growth when CF-AM is treated with the ion pair complex and MPs-E. However, as expected, after the incubation time, there is no significant difference between the log reductions of CFU/mL obtained for tobramycin:PHEA-EDA-GlucA ion pair complex MPs-E compared to that of free tobramycin.

The permissive microenvironments within the hypoxic niches of adherent mucus plaques, present in mucus secretion of CF patients airways, increased bacterial binding to the epithelium and decreased bacterial clearance via innate immune mechanisms.

Over time, *P. aeruginosa* colonies synthesize an alginate coat and form biofilms, that, once established, are difficult to clear with standard antibiotic treatment.

For this reason, a preliminary evaluation of *P.aeruginosa* antibiofilm properties of MPs-E were realized and compared to free tobramycin.

In this preliminary screening of *in vitro* anti-biofilm properties we found a very interesting activity of MPs-E to prevent *P.aeruginosa* biofilm formation, more pronounced than free tobramycin (figure 47).

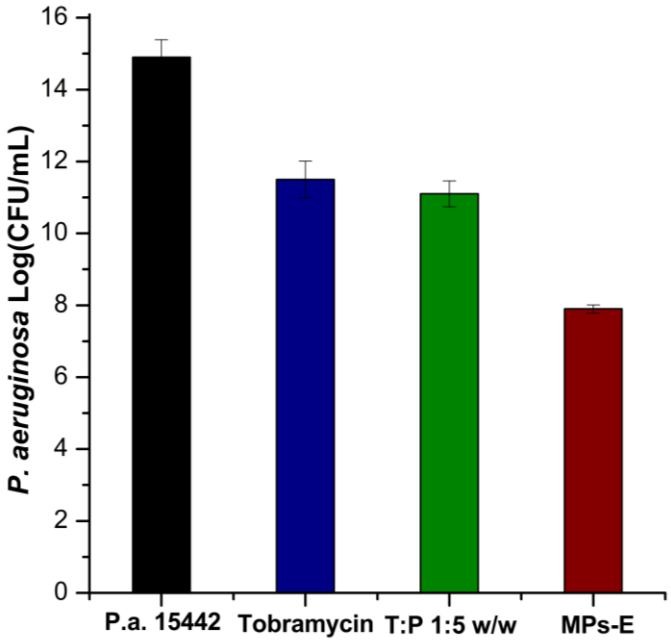

Fig. 47: Inhibition of *P.aeruginosa* biofilm formation in the presence of tobramycin, tobramycin:PHEA-EDA-GlucA ion pair complex and MPs-E.

In fact, the values of log reduction of viable bacterial counts (CFU/mL) were respectively 3.8 and 7 respectively for tobramycin and MP-E, while no differences exist between tobramycin and tobramycin:PHEA-EDA-GlucA ion pair complex.

The improvement of inhibition activity of *P.aeruginosa* biofilm formation for MPs-E is ascribable to the presence of mannitol, which improves microorganism aminoglycoside sensivity at sub-MIC concentration by changing the osmolarity of the broth that create a less favorable growth environment. Moreover, other authors [139] reported mannitol ability to create a proton-motive force (PMF) and exert a metabolic effect responsible of an enhancement of microorganism susceptibility to antibiotics.

Finally, a comparable activity against a pre-formed 24 hours old biofilm was observed with similar values of log reductions between free tobramycin (8.8), tobramycin:PHEA-EDA-GlucA ion pair complex (8.9) and MPs-E (8.7), as reported in figure 48.

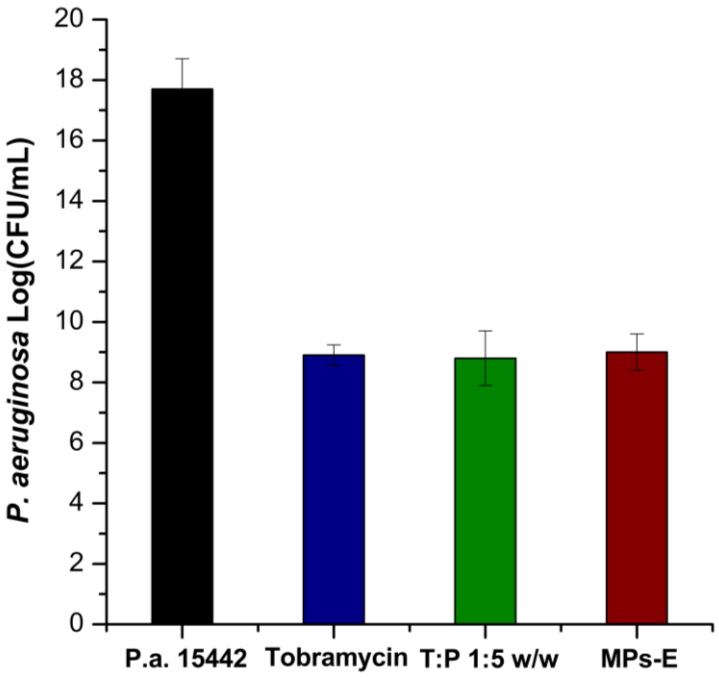

Fig. 48: Inhibition of *P.aeruginosa* 24h old biofilm in the presence of tobramycin, tobramycin:PHEA-EDA-GlucA ion pair complex and MPs-E.

3.1.7 Conclusion

A new "*nano into micro*" approach was realized as potential pulmonary delivery system for tobramycin in the treatment of *P. aeruginosa* infections in CF.

In particular, mannitol MPs, with adequate characteristics for pulmonary administration (spherical shape and micrometer size), were produced by spray drying and loaded with a tobramycin:PHEA-EDA-GlucA ion pair complex-loaded of nanometric size.

The mannitol micrometric matrix of this *nano into micro* formulation is able to modify the rheological properties of CF-AM, facilitating the drug diffusion, but at the same time, thanks to the participation of tobramycin to the ion pair complex with PHEA-EDA-GlucA, MPs are able to achieve a sustained tobramycin delivery at the site of disease, potentially resulting in higher efficacy, lower required dose and side effects.

At the same time, MPs loaded with the nanometric ion pair complex showed pronounced microbiological activity against *P.aeruginosa* pathogens and their biofilm, showing an interesting activity in inhibiting biofilm formation.

These results demonstrate the potential of obtained MPs as drug delivery systems for the treatment of pulmonary infections in CF patients and encourage further investigation.

3.2 Optimization of smart pulmonary drug delivery systems of tobramycin for the treatment of *P. aeruginosa* infections in CF

Since produced MPs containing the Polyanion:Tobramycin ion pair Complex (PTC) showed pronounced microbiological activity against *P. aeruginosa* pathogens and on their biofilm, the potential of obtained MPs was enhanced by adding helping materials with specific functions.
Materials used together with mannitol to the MP matrix were N-acetylcysteine (NAC), L-Arginine (Arg) and cysteamine (Cyst).
NAC is commonly prescribed to CF patients, depolymerizing mucus by breaking disulphide bridges between macromolecules, consequently improving expectoration of sputum and lung function. Arg nebulization has the potential to improve CF lung function by increasing the airway NO production, while Cyst mucolytic activity is comparable to currently available mucoactive agents, having also a rapid bactericidal action against both metabolically active and persister cells of *P. aeruginosa*, and synergistic action with conventional CF antibiotics.
Moreover, in order to evaluate if the mucoadhesive approach was a better strategy in order to enhance the antibiotic activity of tobramycin, PVA was used as polymeric MP matrix for the encapsulation of PTC
Optimized MPs were then produced by spray drying an aqueous solution containing the PTC and mannitol or PVA, alone or mixed with NAC, Arg or Cyst.
Tobramycin release from obtained MPs and its diffusion profile in CF-AM was evaluated and compared to the unique commercially available dry powder formulation containing tobramycin, TOBI® Podhaler® (Novartis).
Finally, in vitro cell viability of obtained MPs towards 16-HBE cells was evaluated and compared to TOBI® Podhaler® .

3.2.1 Optimization of tobramycin:PHEA-EDA-GlucA ion pair complex-containing MPs

All MPs formulations were produced by following the spray drying process, using the same experimental conditions employed for the production of MPs-C and MPs-E (paragraph 3.1), which showed the best characteristics in terms of recovery yield and suitable dimensions for the pulmonary administration.
For empty MPs, aqueous mannitol or PVA solutions at the concentration of 1 g/100 mL were used to obtain Man or PVA MPs. To each Man or PVA MP composition, NAC, Arg or Cyst helping materials were added at the weight ratio of 1:0.1, to produce Man-NAC, Man-Arg,

Man-Cyst, PVA-NAC, PVA-Arg and PVA-Cyst respectively. Results in terms of recovery yield and average diameter are reported in table 7.

Table 7. Composition for 100 mL of spray dried solution, recovery yield (wt %) and average diameter (μm) of obtained empty MP formulations.

Sample	**Mannitol or PVA: helping material weight ratio (g)**	**Recovery Yield (wt %)**	**Average diameter (μm)**
Man	1:0	76.3 ± 3.1	2.5 ± 0.9
Man-NAC	1:0.1	72.6 ± 4.0	2.3 ± 1.1
Man-Arg	1:0.1	69.3 ± 2.2	2.4 ± 0.8
Man-Cyst	1:0.1	75.9 ± 2.6	2.2 ± 0.9
PVA	1:0	78.5 ± 1.6	2.6 ± 0.8
PVA-NAC	1:0.1	78.3 ± 2.9	2.8 ± 1.2
PVA-Arg	1:0.1	74.7 ± 3.2	2.7 ± 0.9
PVA-Cyst	1:0.1	78.9 ± 2.1	2.5 ± 0.6

Excellent characteristics in terms of recovery yield and average diameter were obtained.
In particular, as evident from the table 7, the recovery yield was always higher or equal to the 70 wt%, nullifying the most critical limitation of the spray-drying technique.
Moreover the average diameter of obtained MPs is ~2.5 μm, suitable for the pulmonary deposition.
PTC loaded MPs with adequate characteristics in terms of average diameter, DL and EE were obtained when a weight ratio between mannitol or PVA, helping material and PTC equal to 1:0.1:0.48 was chosen (table 8).

Table 8. Composition (for 100 mL of spray dried solution), recovery yield (wt %), average diameter (μm), DL, (wt %), and EE (wt %) of PTC loaded MP formulations.

Sample	PTC: Mannitol or PVA: helping material weight ratio (g)	Recovery Yield (wt %)	Average diameter (μm)	DL (wt %)	EE (wt %)
PTC_Man	0.48:1:0	68.5 ± 1.8	2.2 ± 0.7	5.3 ± 0.7	98.1 ± 0.01
PTC_Man-NAC	0.48:1:0.1	66.9 ± 3.2	2.4 ± 0.9	5.2 ± 0.8	96.3 ± 0.02
PTC_Man-Arg	0.48:1:0.1	60.1 ± 1.9	2.3 ± 0.6	5.1 ± 0.6	94.4 ± 0.01
PTC_Man-Cyst	0.48:1:0.1	64.1 ± 2.8	2.2 ± 1.3	5.2 ± 0.6	96.3 ± 0.02
PTC_PVA	0.48:1:0	69.2 ± 2.6	2.5 ± 0.5	5.3 ± 0.8	98.1 ± 0.02
PTC_PVA-NAC	0.48:1:0.1	64.6 ± 3.5	2.4 ± 0.6	5.3 ± 0.7	98.1 ± 0.01
PTC_PVA-Arg	0.48:1:0.1	62.8 ± 1.4	2.8 ± 0.7	5.2 ± 0.6	96.3 ± 0.02
PTC_PVA-Cyst	0.48:1:0.1	79.9 ± 2.5	2.6 ± 0.9	5.2 ± 0.8	96.3 ± 0.02

The presence of PTC in mannitol or PVA aqueous solution to spray-drying caused a slightly reduction of recovery yield, caused by the tendency of PHEA-EDA-GlucA to form thin and sticky film in the collecting cylinder, more difficult to recover.

At the same time, for PTC loaded MPs no significant differences were observed in terms of average diameter if compared to empty MPs.

Further, no significant differences were observed between mannitol and PVA based MPs, and the presence of helping materials did not influence MPs technological properties, being recovery yield, average diameter, DL and EE similar for all formulations.

DL values between 5.1 and 5.3 wt % were obtained, reflecting optimal respectively EE values from 97.3 to 98.1 wt%.

Morphological characterization was carried out on all MP formulations by SEM.

SEM images, shown in figure 49, highlighted the spherical shape and micron-sized particles.

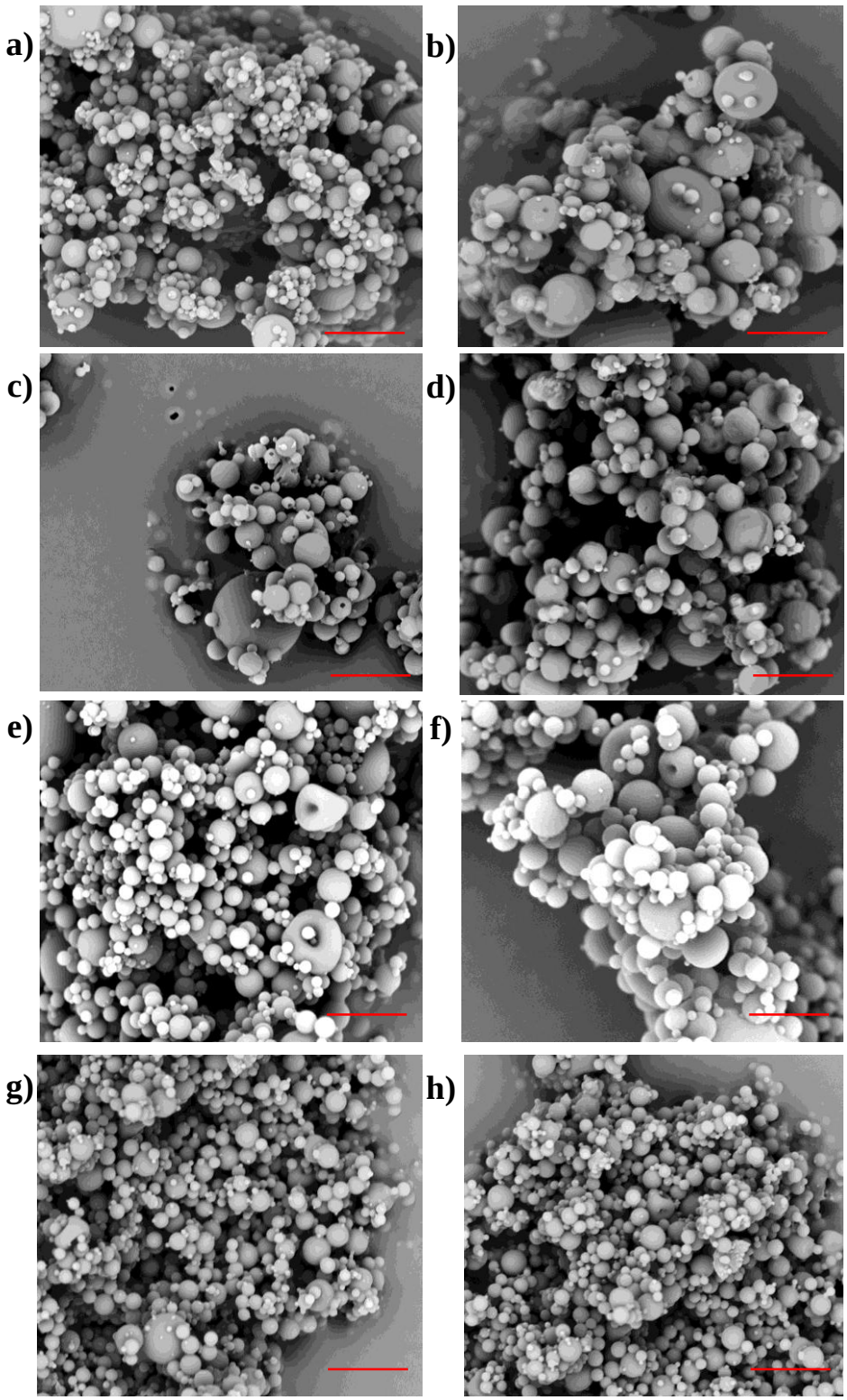

Fig. 49: SEM micrographs of a) PTC_Man, b) PTC_Man-NAC, c) PTC_Man-Arg, d) PTC_Man-Cyst, e) PTC_PVA, f) PTC_PVA-NAC, g) PTC_PVA-Arg and h) PTC_PVA-Cyst.

SEM images evidenced the further absence of difference between various MP matrix composition, confirming that the presence of helping materials did not influence MPs technological properties.

3.2.2 Effect of MPs in CF-AM

To evaluate if the presence of MPs could influence the CF-AM properties, an evaluation of MPs interactions with CF-AM components and a rheological study was carried out.

Interactions between MPs and CF-AM components

Interactions between MPs and CF-AM were evaluated by turbidimetric measurement [65].

In particular, the absorbance at the λ of 650 nm of MPs CF-AM dispersions (2 mg/mL) was measured at 0, 15, 30, 45, 60, 90, 120, 180, 240, 300, 360 and 480 min after incubation at 37°C and compared to the absorbance obtained for untreated CF-AM, and treated with TOBI® Podhaler® MPs at the same concentration at each time point.

Obtained data are reported in figure 50 as function of incubation time.

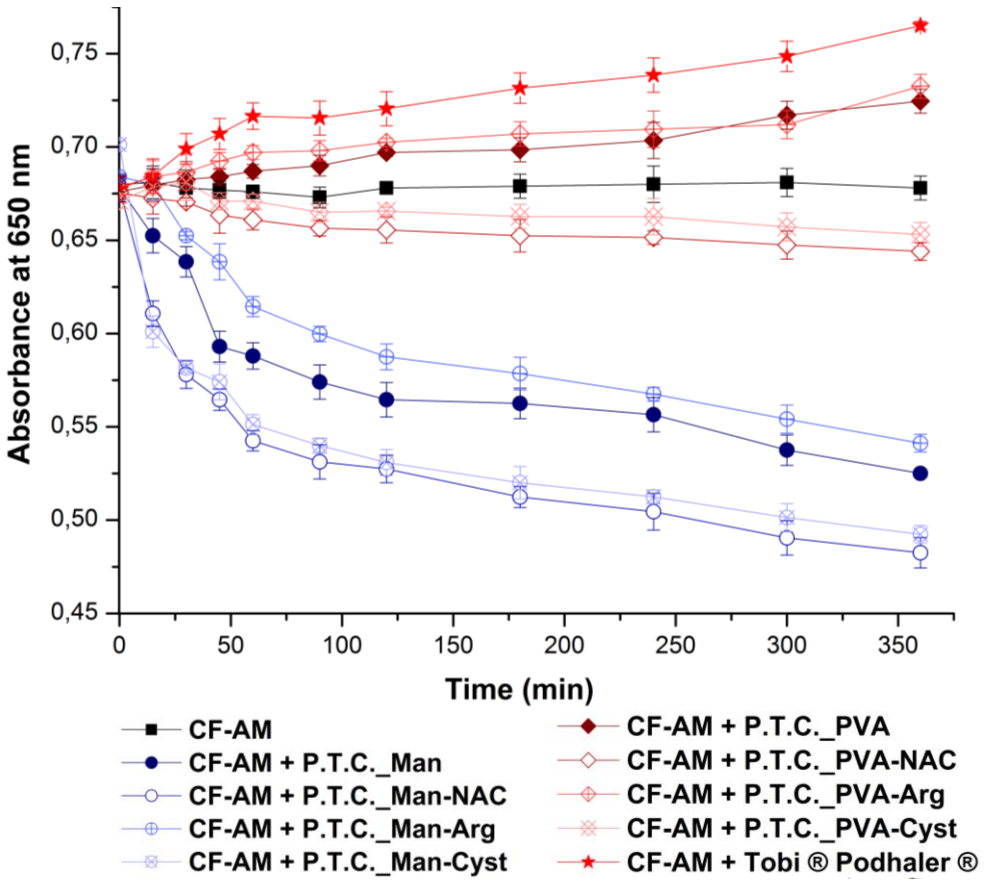

Fig. 50: Turbidity of CF-AM dispersions of PTC_Man-NAC, PTC_Man-Arg, PTC_Man-Cyst, PTC_PVA-NAC, PTC_PVA-Arg and PTC_PVA-Cyst, after incubation at 37 °C as

function of incubation time. The turbidity of untreated CF-AM and treated with f TOBI® Podhaler® MPs is used as control.

Since absorbance at λ 650 nm of CF-AM treated with all MP formulations is almost the same at time zero, values of turbidity obtained when the MPs are incubated with CF-AM for longer period of time evidenced an immediate difference in the interaction behavior of MPs with mucus components depending on MP chemical compositions.

An evident difference is visible between the turbidity of CF-AM treated with PTC loaded MPs based on mannitol and those based on PVA. In fact, starting from 15 min incubation at 37 °C, the turbidity of CF-AM is significantly lower when it is treated with PTC loaded mannitol-based MPs than untreated CF-AM or treated with PTC loaded PVA-based MPs.

Further, the turbidity of CF-AM treated with TOBI® Podhaler® MPs is significant higher if compared to that obtained from PTC loaded PVA-based MPs and above all from mannitol-based MPs CF-AM dispersions.

A difference exists even amongst MPs based on the same main component but which differs for the helping material. In fact, the turbidity of CF-AM treated with PTC_Man-Arg is significantly higher than that obtained for CF-AM treated with PTC_Man-NAC and PTC_Man-Cyst (**$p<0.01$). In addition, the turbidity of CF-AM treated with PTC_Man-NAC and PTC_Man-Cyst is significantly lower than that obtained for CF-AM treated with PTC_Man (**$p< 0.01$), while no significant differences exist between the turbidity of CF-AM treated with PTC_Man-NAC and PTC_Man-Cyst.

Also for PTC loaded PVA based MPs it is possible to observe the influence exerted by the helping material on interacting behavior with CF-AM components. In fact, the turbidity of CF-AM treated with PTC_PVA and PTC_PVA-Arg is significantly higher than that obtained for CF-AM treated with PTC_PVA-NAC and PTC_PVA-Cyst (**$p< 0.01$). Moreover, no significant differences exist between the turbidity of CF-AM treated with PTC_PVA and PTC_PVA-Arg and between the turbidity of CF-AM treated with PTC_PVA-NAC and PTC_PVA-Cyst.

The influence exerted by the helping materials on CF-AM turbidity is ascribable with their interaction nature with CF-AM components. In fact, the presence of Arg to mannitol MPs is able to invert their turbidimetric behavior, being Arg a zwitterion, able to interact with mucus components via electrostatic interactions and hydrogen bonds.

The opposite influence was observed, instead, when NAC and Cyst were used as helping materials in MPs formulations. In fact, NAC and Cyst exert their well-known mucolytic

action on CF-AM, whose deconstruction is observed with a decrease of the absorbance values at 650 nm if compared to only Man or PVS MPs, respectively.

From figures 50 it could be also visible the difference in the interaction behavior of MPs with mucus components in relation with the incubation time. In fact, the turbidity of CF-AM significantly decreased over the incubation time when it is treated with all PTC loaded mannitol-based MPs (**p< 0.01). On the contrary a significant increase is visible for the turbidity of CF-AM when it is treated with PTC_PVA, PTC_PVA(Arg) (*p< 0.05) and TOBI® Podhaler® MPs (**p< 0.01) over the incubation time.

These results suggested the occurring of interactions of different nature between PTC loaded mannitol or PVA based MPs and CF-AM components. In fact, since mannitol is able to alter the CF-AM mesh structure, the resulting increasing in the macroporosity of the mucus polymer network is observed in this study with a significant reduction of the turbidity that, from the beginning, progressively decreases over the incubation time. On the contrary, interactions of mucoadhesive nature are established from the beginning between PTC_PVA, PTC_PVA(Arg), TOBI® Podhaler® MPs and mucus components, as underlined by the observed higher turbidity, that further increases over the incubation time.

CF-AM rheology

To evaluate as the presence of MPs could modify the viscoelastic properties of CF-AM, a rheological study was carried out.

CF-AM was incubated alone or in the presence of both PTC loaded mannitol and PVA-based MPs (2 mg/mL) for 1h at 37°C and then analyzed with a rheometer. Storage modulus (G'), loss modulus (G'') and complex viscosity (η*) obtained for CF-AM treated with all produced formulations were compared to untreated CF-AM and treated with the same amount of TOBI® Podhaler® MPs.

Obtained data were reported in figures 51, 52 and 53.

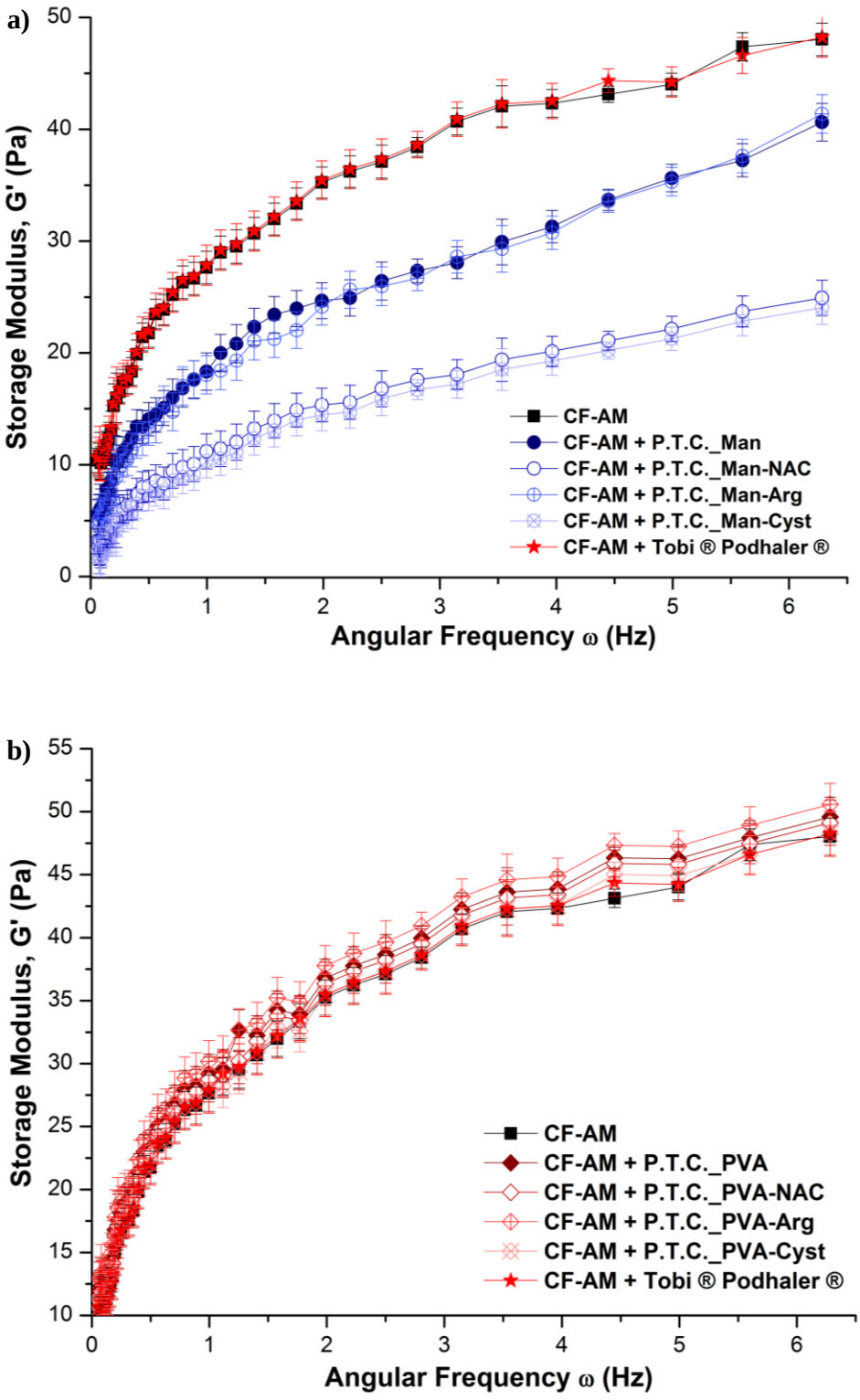

Fig. 51: Storage modulus (G') for PTC loaded MPs based on: a) mannitol (PTC_Man-NAC, PTC_Man-Arg, PTC_Man-Cyst); b) PVA (PTC_PVA-NAC, PTC_PVA-Arg, PTC_PVA-Cyst).

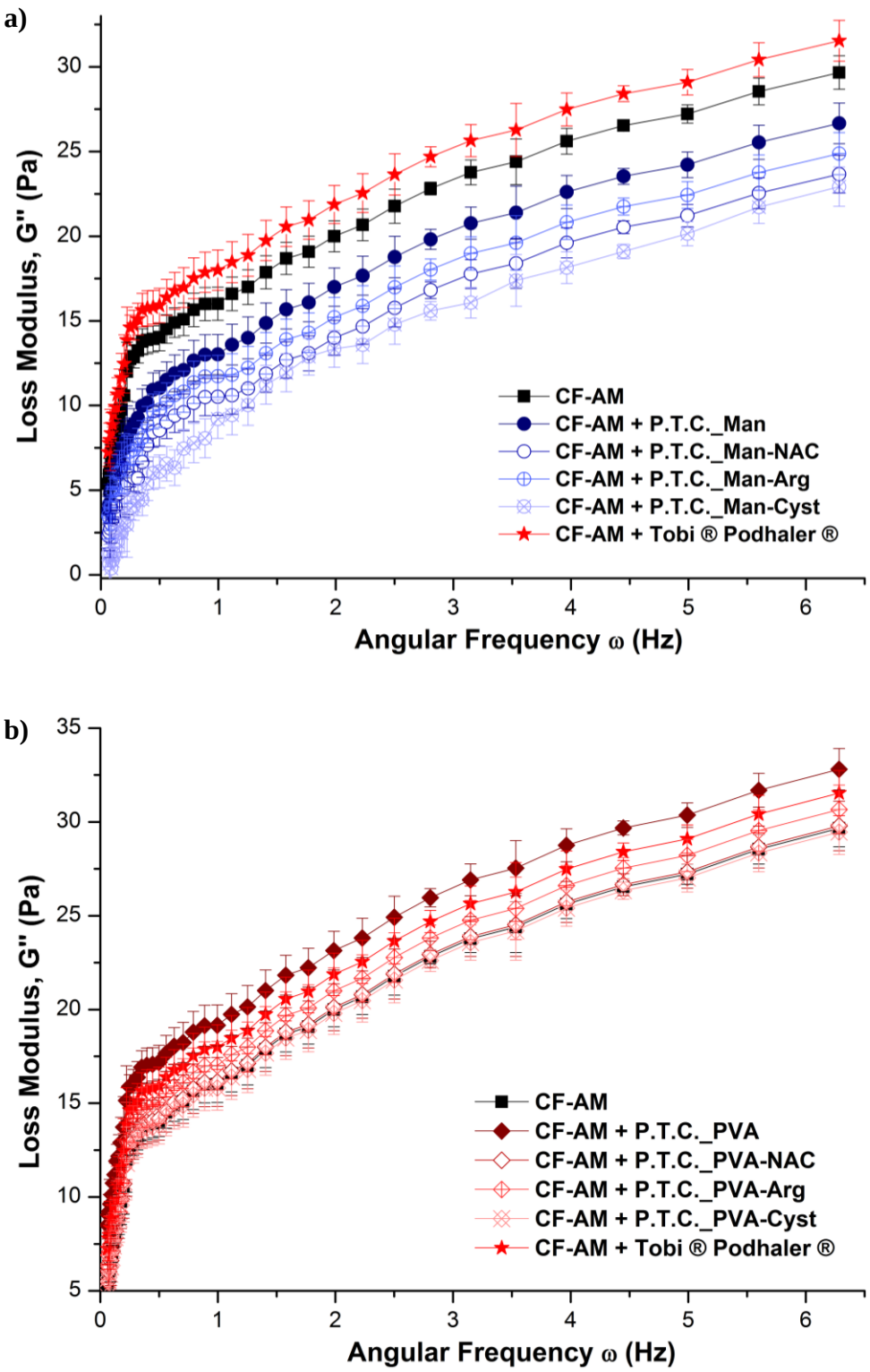

Fig. 52: Loss modulus (G'') for PTC loaded MPs based on: a) mannitol (PTC_Man-NAC, PTC_Man-Arg, PTC_Man-Cyst); b) PVA (PTC_PVA-NAC, PTC_PVA-Arg, PTC_PVA-Cyst).

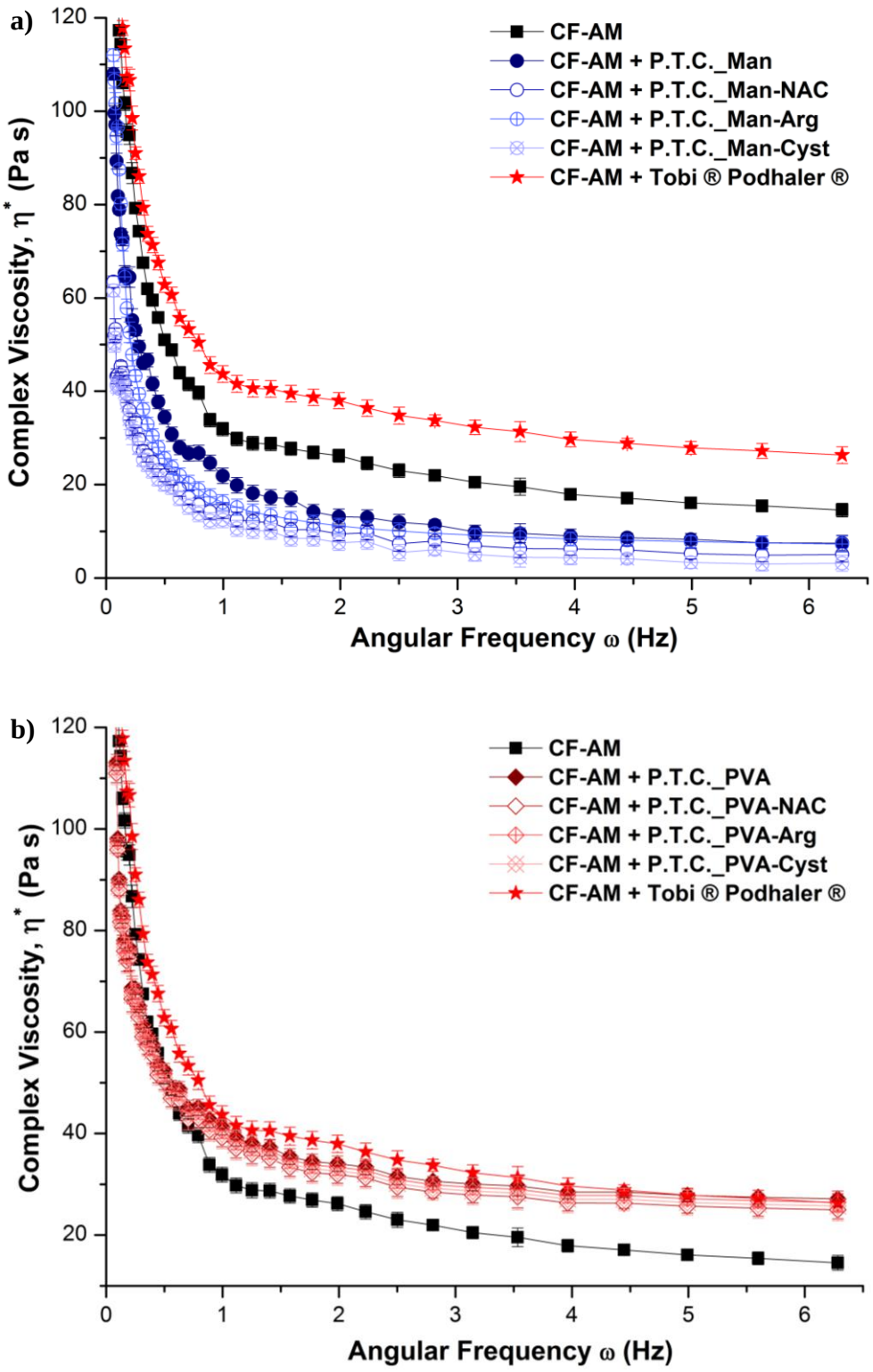

Fig. 53: Complex viscosity (η*) for PTC loaded MPs based on: a) mannitol (PTC_Man-NAC, PTC_Man-Arg, PTC_Man-Cyst); b) PVA (PTC_PVA-NAC, PTC_PVA-Arg, PTC_PVA-Cyst).

As evident from these graphics, PTC loaded MPs are able to alter the viscoelastic properties of the mucus layer, being able to change G', G'' and η* of CF-AM.

An immediate difference is visible between G', G'' and η* of CF-AM treated with PTC loaded MPs based on mannitol and PVA. In fact, rheological parameters of CF-AM treated with PTC loaded mannitol-based MPs are significantly lower if compared to those obtained for untreated CF-AM or treated with PTC loaded PVA-based MPs.

Moreover, rheological parameters of CF-AM treated with PTC loaded mannitol-based MPs are significantly lower if compared to those obtained for CF-AM treated with TOBI® Podhaler® MPs. Further, even if G' and G'' values of CF-AM treated with TOBI® Podhaler® MPs are comparable to those obtained for untreated CF-AM, η* values of CF-AM treated with TOBI® Podhaler® MPs are significantly higher than that obtained for untreated CF-AM.

Moreover, a difference exists also for rheological parameters even amongst MPs based on the same main component but which differ for the helping material. In fact, G', G'' and η* values of CF-AM treated with PTC_Man-NAC and PTC_Man-Cyst is significantly lower that obtained for CF-AM treated with PTC_Man-Arg and PTC_Man (** $p < 0.01$), while no significant differences exist between rheological parameters of CF-AM treated with PTC_Man-NAC and PTC_Man-Cyst and between G', G'' and η* values of CF-AM treated with PTC_Man-Arg and PTC_Man.

Contrariwise, the influence exerted by the helping material was not evident for rheological parameters of CF-AM treated with PTC loaded MPs based on PVA.

The reduction of rheological parameters observed in 3.1.4. paragraph for PTC loaded mannitol MPs (named MPs-E) was observed also for PTC_Man-Arg, and especially for PTC_Man-NAC and PTC_Man-Cyst, having NAC and Cyst a consolidate mucolytic action on CF-AM, whose deconstruction caused the reduction of viscoelastic properties of CF-AM.

Results obtained from the rheological evaluation are in agreement with data obtained from the turbidimetric study, underling the potential of helping materials in the enhancement of PTC loaded mannitol-based MPs properties.

3.2.3 Evaluation of tobramycin diffusion profile from MPs in CF-AM

On the basis of the obtained results in terms of impact of MPs on CF-AM and in order to know the ability of obtained MPs, at different chemical composition, to retain the antibiotic and to ensure a sustained release at the site of action by diffusing through the CF-AM layer, a tobramycin release and diffusion profile in CF-AM was performed by using a vertical Franz-type diffusion cell.

Results were reported in figure 54 as a function of incubation time.

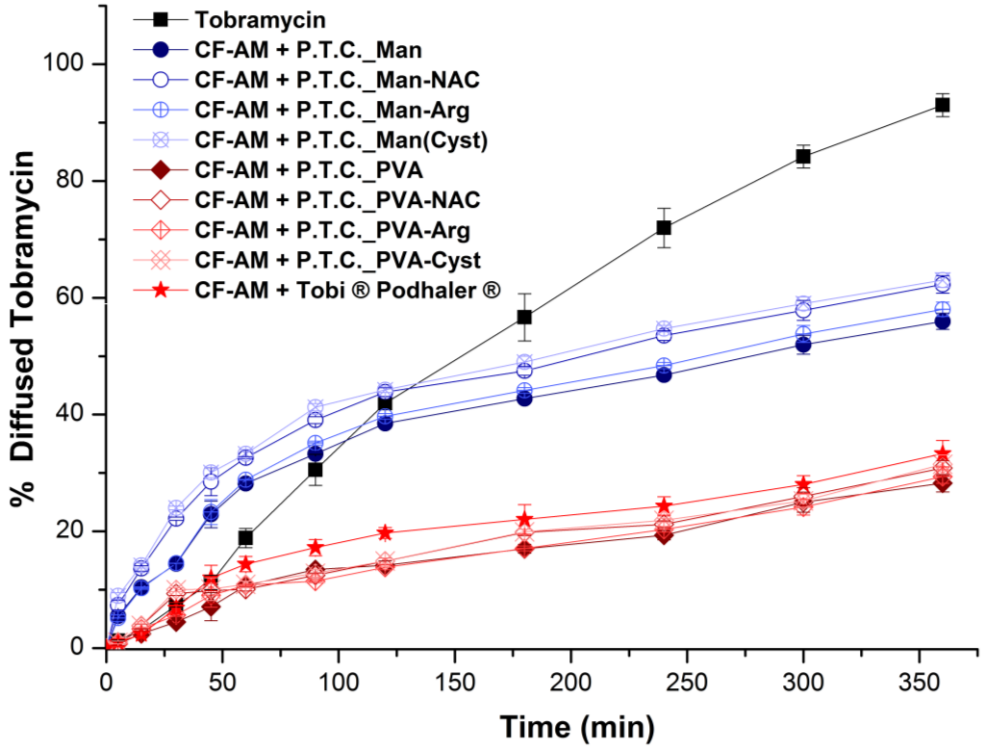

Fig. 54: Diffusion of tobramycin from prepared MPs through CF-AM layer in Franz-cells as a function of incubation time at 37°C.

Results showed that the entrapment into MPs is able to influence the diffusion kinetics of tobramycin in CF-AM, in a manner that is dependent on the chemical composition of MPs.
In particular, the amount of tobramycin that reach the acceptor chamber until the second hour from the PTC loaded mannitol-based MPs is significantly higher than that of diffused free drug. After this time, the trend is inverted and the amount of tobramycin released from MPs resulted to be lower, achieving a sustained delivery for a longer period of time. This behavior could be explained considering the ability of mannitol to modify the rheological properties of CF-AM, as described in 3.1.5 paragraph. So, until the second hour, MPs could facilitate the transport of the antibiotic to the acceptor chamber, while free tobramycin diffuses slower due to the high viscous CF-AM layer and probably to binding interactions with mucus components in this environment [128, 138]. Then, a sustained release of tobramycin from MPs is obtained thanks to its participation to the ion pair complex with PHEA-EDA-GlucA, that, as showed above, allowed to release an amount of tobramycin that doesn't exceed the 60 wt% of the total entrapped drug after 6 h incubation.

The influence exerted by the helping materials to the formulations observed by turbidimetry and rheological studies, are visible also for the tobramycin diffusion profile from PTC loaded mannitol-based MPs. In fact, tobramycin released from PTC_Man-NAC and PTC_Man-Cyst and diffused through CF-AM layer is significantly higher (* $p < 0.05$) than that observed for PTC_Man and PTC_Man-Arg, thanks to the NAC and Cyst mucolytic action, adjuvant to the mannitol ability as rheological modifier.

On the other hand, the amount of tobramycin that reach the acceptor chamber from the PTC loaded PVA-based MPs, until the first hour, is almost the same respect to the diffusion of free drug, ì after this time PTC loaded PVA-based MPs achieved a sustained delivery that doesn't exceed the 30 wt% of the total entrapped drug after 6 h incubation.

This behavior is ascribable since PTC loaded PVA based MPs, interacting with mucus components, are retained in the CF-AM layer where particles are hindered in their diffusion. As results of the mucoadhesion, tobramycin sustained delivery is not imputable only to the tobramycin participation in the ion pair complex with PHEA-EDA-GlucA, but above all to the dissolution of PVA MP matrix, slower than that of mannitol MPs, that immediately dissolve. In fact, PVA dissolution in aqueous solution depends on its $\overline{M}_w$ and on its degree of hydrolysis. PVA polymer used in this study, with a $\overline{M}_w$ in the range from 31 to 50 kDa and hydrolyzed at the 98-99 %, dissolved slowly in aqueous media.

The influence exerted by the helping materials to the formulations was not observed for PTC loaded PVA based MPs, as already observed for the absence of changes in rheological parameters between CF-AM treated with PTC_PVA, PTC_PVA-NAC, PTC_PVA-Arg or PTC_Man-Cyst.

Finally, the amount of tobramycin released from TOBI® Podhaler® MPs and diffused through CF-AM layer is comparable to that obtained for PTC loaded PVA-based MPs, as result, also in this case, of the establishment of interactions between MPs and mucus components, with a consequent mucoadhesion. The tobramycin sustained release offered by TOBI® Podhaler® MPs is ascribable, as also showed for PVA MPs, to a slower dissolution of the water-insoluble TOBI® Podhaler® MP matrix based on the phospholipid 1,2-distearoyl-sn-glycero-3,phosphocholine.

These obtained results highlighted the unique properties of mannitol based MPs formulation, especially those containing NAC and Cyst mucolytics, able to deliver the antibiotic by an initial effect on rheological modification of mucus, allowing a rapid transport of the drug

through CF-AM layer and reaching the receptor chamber, and by offering then a sustained delivery thanks to its interaction with PHEA-EDA-GlucA.

3.2.4 In vitro cytocompatibility on human bronchial epithelial cells (16-HBE)

To evaluate the potential in vivo use of produced MPs, cytocompatibility was evaluated by the MTS assay on 16-HBE cells at different MPs concentrations after 4 h incubation (fig. 55).

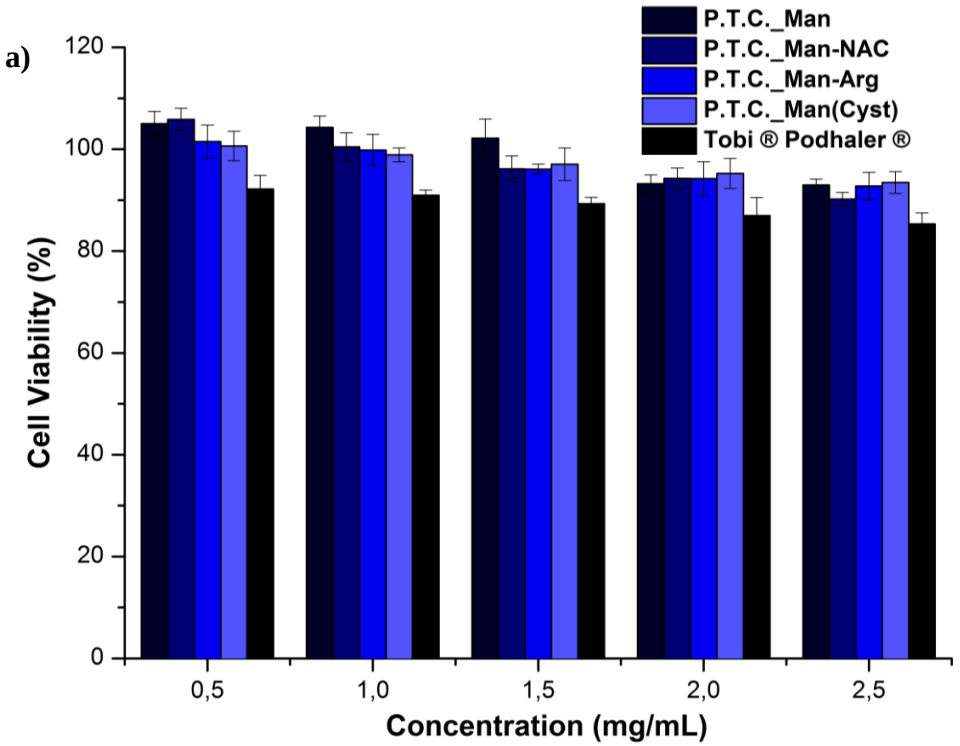

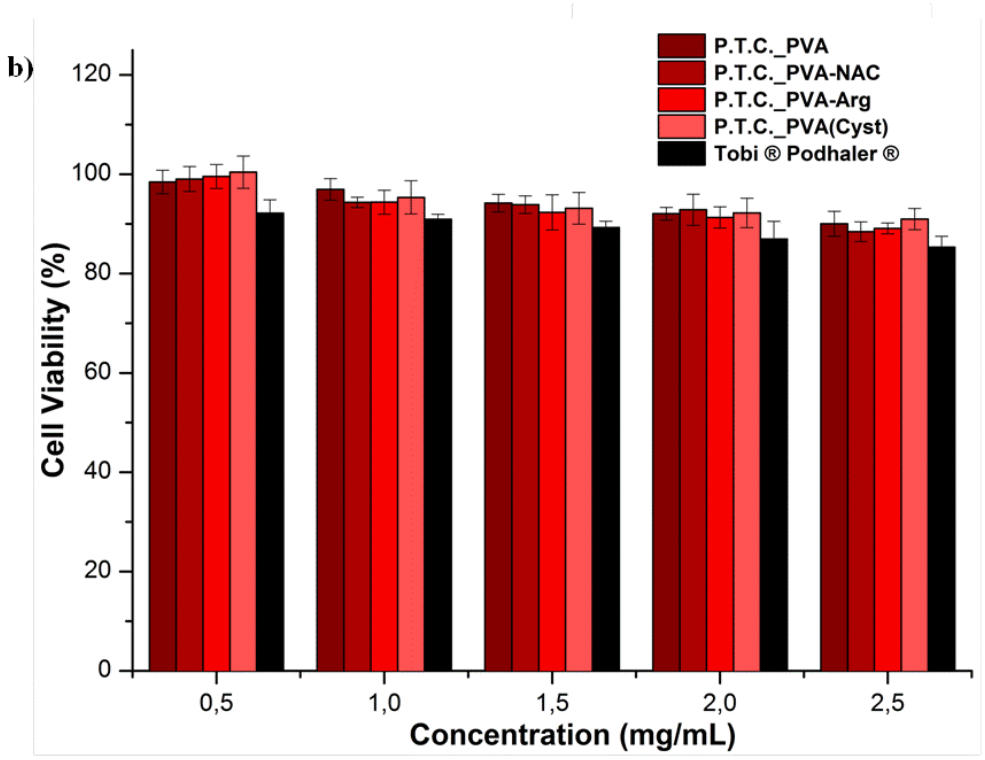

Fig. 55: Cell viability % on 16-HBE cells after 4 h incubation with PTC loaded MPs based on: a) mannitol (PTC_Man-NAC, PTC_Man-Arg, PTC_Man-Cyst) and b) PVA (PTC_PVA-NAC, PTC_PVA-Arg, PTC_PVA-Cyst).

As can be seen in figure 55, all MPs samples showed an excellent cytocompatibility at all tested concentrations after 4 h incubation. In fact, all samples showed a cell viability higher than 80 % compared to the control and the cell viability increased at lower concentration of the samples incubated.

3.2.5 Conclusions

In this paragraph, the pronounced microbiological activity against *P. aeruginosa* infections of *nano into micro* formulation developed in the precedent paragraph was enhanced by adding helping materials with specific functions.

Materials used together with mannitol to the MP matrix were N-acetylcysteine (NAC), L-Arginine (Arg) and cysteamine (Cyst). Moreover, PVA was used as polymeric MP matrix for the encapsulation of the polyanion–tobramycin complex (PTC), in order to evaluate if the mucoadhesive approach was a better strategy.

Optimized MPs were then produced by spray drying an aqueous solution containing the PTC and mannitol or PVA, alone or mixed with NAC, Arg or Cyst. The produced formulations were then compared with the only one commercially available dry powder inhalatory formulation based on MPs loaded with tobramycin, named Tobi® Podhaler®, by Novartis.

All produced MPs showed adequate characteristics for pulmonary administration, as spherical shape, micrometric size and high cytocompatibility towards human bronchial epithelial cells.

All produced MPs are able to modify rheological properties of CF-AM. In particular, PTC loaded mannitol-based MPs, and specifically those containing NAC and Cyst as helping material, are able to reduce the viscosity of mucus secretions. Contrariwise, PTC loaded PVA-based MPs seem to interact with CF-AM components via mucoadhesive interactions, which further increases over the incubation time.

Moreover, PTC mannitol-based MPs, and in particular those containing NAC and Cyst as helping material, are able to facilitate the drug diffusion, and at the same time to achieve a sustained tobramycin delivery, thanks to its participation to PTC, while PTC PVA-based MPs are not able to increase the drug diffusion, caused by the establishment of mucoadhesive interactions between MPs and mucus components, but are able to achieve a more sustained tobramycin release, thanks to the slower dissolution of PVA MP matrix.

Futher, as result of conducted studies in presence of CF-AM, it was possible to show how Tobi® Podhaler® MPs formulation interacted with CF-AM components via mucoadhesive interactions and consequently was not able to increase the drug diffusion, but was able to achieve a more sustained tobramycin release, thanks to the slower dissolution of its water insoluble phospholipidic MP matrix.

Results obtained showed as produced MPs potentially could result in formulations of higher efficacy, for which it could be possible reducing the administered dose, the frequency of administrations, side effects and consequently antibiotic resistance problems.

3.3 Preparation and characterization of biodegradable fluorescent particles based on pegylated polyaspartamide–polylactide copolymers as delivery systems for hydrophobic drugs

In this paragraph, the synthesis and the characterization of novel amphiphilic graft copolymers with tunable properties, useful to obtain polymeric fluorescent nanoparticles (FNPs) by following easily scaling up processes and by using starting materials with suitable structural and functional properties, is reported.

The starting copolymers are obtained by chemical conjugation of rhodamine (RhB) moieties, polylactic acid (PLA), and the O-(2-aminoethyl)-O'-methyl poly(ethylene glycol) (H_2N-PEG-OCH_3) on the PHEA. In particular, PHEA is firstly functionalised with RhB to obtain PHEA-RhB, then with different amount of PLA to obtain PHEA-RhB-PLA, and finally, PEG chains are grafted on PHEA-RhB-PLA derivatives to obtain PHEA-RhB-PLA-PEG graft copolymers.

The preparation and characterization of polymeric FNPs with tunable properties and spherical shape was realized by using the emulsion-high pressure homogenization (HPH)-solvent evaporation techniques.

Being the slow degradation rate of PLA and PLA derivatives a disadvantage for pulmonary drug delivery, especially when repeated administrations are required, the biodegradability of produced NPs was evaluated in isotonic media mimicking the physiological environment.

3.3.1 Synthesis and characterization of PHEA-RhB-PLA-PEG graft copolymer

The first synthetic step was the covalent linkage of RhB on PHEA. RhB was chosen as fluorescent probe because of high absorption coefficient, photostability and other properties of rhodamine dyes so that many strategies were recently developed in order to covalently link them to biomolecules, polymers and surfaces [90, 140].

To obtain the fluorescent derivative of PHEA, the first reaction step was the derivatization of PHEA with RhB to obtain PHEA-RhB, by using carbonyldiimidazole (CDI) as coupling agent.

The synthetic procedure and chemical structure of PHEA-RhB copolymer is reported in the Scheme 2.

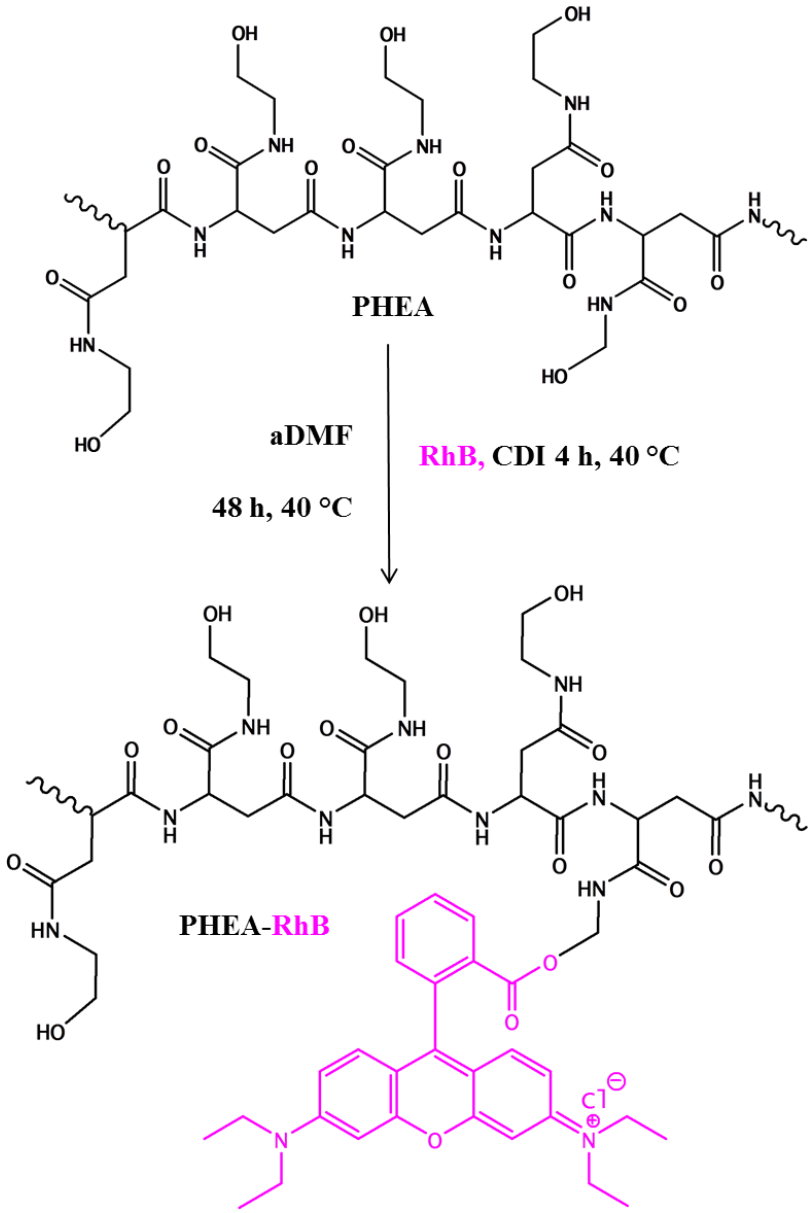

Scheme 2: Synthesis of PHEA-RhB (pink: RhB moieties).

The obtained product was soluble in water, dimethylsulfoxide, dimethylformamide, such as starting PHEA.

DD_{RhB} was calculated from the ^{1}H-NMR spectrum in D_2O (figure 60) by comparing the integral of the peaks related to protons between δ 7.90-8.60 (H= 10), attributed to protons of RhB aromatic rings to the integral related to protons at δ 3.32 attributed to –NH-**CH_2**-CH_2-O- (belonging to PHEA).

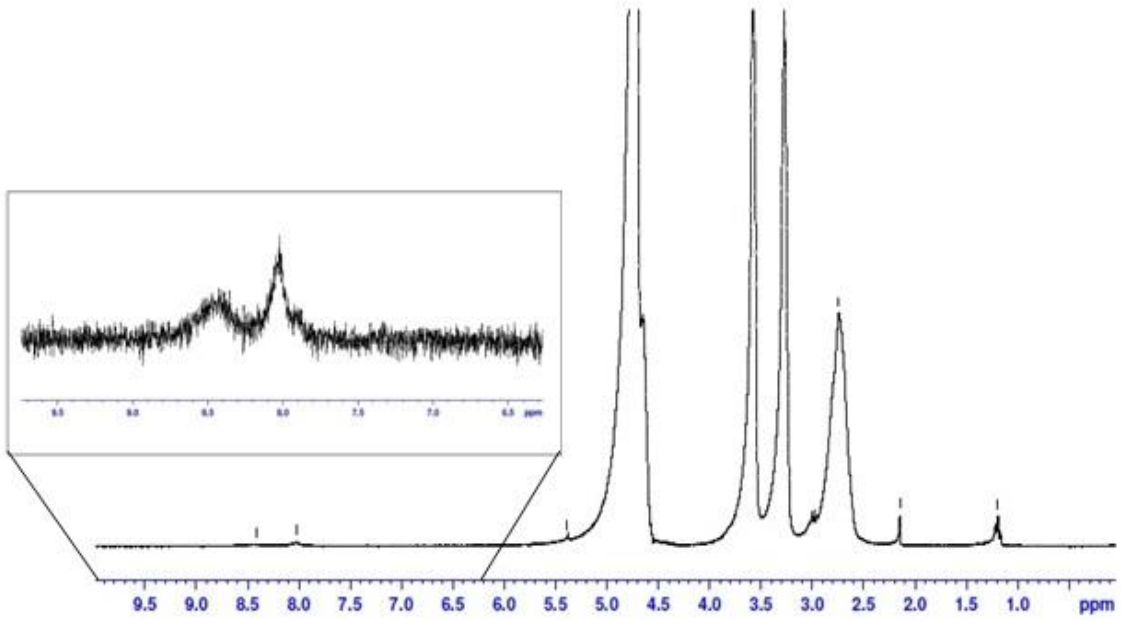

Fig. 60: ^{1}H-NMR spectrum of PHEA-RhB.

The DD_{RhB} was expressed as mean values of three determinations and resulted to be 0.55 ± 0.05 mol% of repeating units. By proper calculation it is possible to determine that DD_{RhB} corresponds to about 1-2 RhB molecules for each PHEA chain.

The confirmation that the RhB molecules were chemically linked to the polymer was obtained by HPLC analysis that revealed the absence of free RhB in the isolated product.

The $\overline{M}_w$ of PHEA-RhB copolymer results to be equal to 35 kDa with a $\overline{M}_w/\overline{M}_n$ of 1.41.

The apparently reduction of PHEA-RhB $\overline{M}_w$ value compared to that of PHEA (38 kDa)could be attributed to a modification of the PHEA conformation due to the linkage of RhB.

Being well known from the literature that the conjugation of RhB to molecules or polymers could cause the shift of the maxima absorption wavelength, the reduction of molar extinction coefficient (ε) of PHEA-RhB were determined and compared to that of RhB aqueous solutions by recording UV-Vis spectra. It was found that the maxima absorption wavelength was shift from 554 nm (RhB) to 561 (PHEA-RhB) nm, and ε resulted to be 117000 $M^{-1}cm^{-1}$ for RhB and 53200 $M^{-1}cm^{-1}$for PHEA-RhB.

However, although this latter is halved than that of RhB, ε of PHEA-RhB is still high to plane the synthesis of a further copolymer starting from PHEA-RhB to use for fluorescence experiments.

Then, in order to obtain fluorescent polymeric derivatives of PHEA with amphiphilic nature, hydrophobic PLA chains with a $\overline{M}_w$ of 14.0 kDa were grafted on PHEA-RhB backbone allowing obtaining a resulting copolymer suitable for preparing polymeric particles. To do this, different amounts of PLA chains were grafted onto PHEA-RhB copolymer.

In particular, the free carboxyl groups of PLA were activated for 4 h by using CDI as coupling agent and diethyleamine (DEA) as catalyst, and left to react with hydroxyl side groups on PHEA for 72 h, in organic environment at 40°C.

The used amounts of CDI and DEA were calculated according to $R_4 = 2$ and $R_5 = 8.5$, where R_4 is the molar ratio between CDI and PLA, and R_5 is the molar ratio between DEA and PLA, as described in the experimental part.

In order to obtain three different hydrophobization degrees, molar ratio between PLA and hydroxyl-carrying PHEA-RhB repeating units were chosen equal to $R_6 = 0.06$, 0.08, or 0.1, and obtained derivatives were indicated in the text as PHEA-RhB-$PLA_{(A)}$, PHEA-RhB-$PLA_{(B)}$ and PHEA-RhB-$PLA_{(C)}$ graft copolymers, respectively.

The synthetic procedure and chemical structure of PHEA-RhB-PLA copolymer is reported in the Scheme 3.

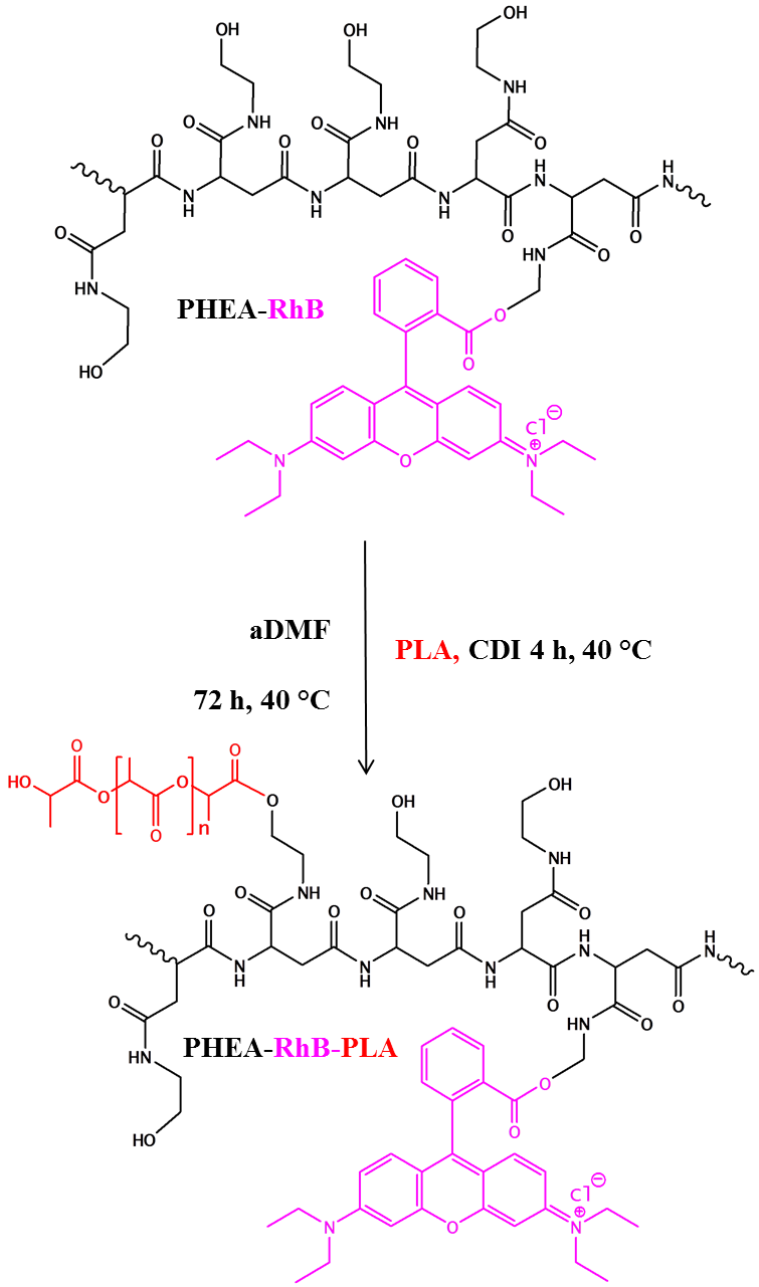

Scheme 3: Synthesis of PHEA-RhB-PLA graft copolymer (n = 194), (pink: RhB moieties, red: PLA chains).

Thanks to the introduction of hydrophobic PLA chains to the water soluble PHEA-RhB copolymer, all the obtained copolymers were insoluble in water, but soluble in dimethylsulfoxide, dimethylformamide and dichloromethane.

DD_{PLA} of PHEA-RhB-$PLA_{(A)}$, PHEA-RhB-$PLA_{(B)}$ and PHEA-RhB-$PLA_{(C)}$ was calculated by comparing the integral of the peaks related to protons between δ 1.40-1.80 (H= 582) as well as to protons (H= 194) between δ 4.20-4.60 and δ 5.20-5.90 (assigned to –O-CO-CH(**CH_3**)-

O- and -O-CO-**CH**(CH_3)- (belonging to linked PLA chains), respectively, to the integral related to protons at δ 4.89 attributed to -NH-**CH**(CO)CH_2- (attributed to PHEA backbone).
The typical ^{1}H-NMR spectrum in DMF-d_7 of PHEA-RhB-PLA graft copolymers is reported in figure 61.

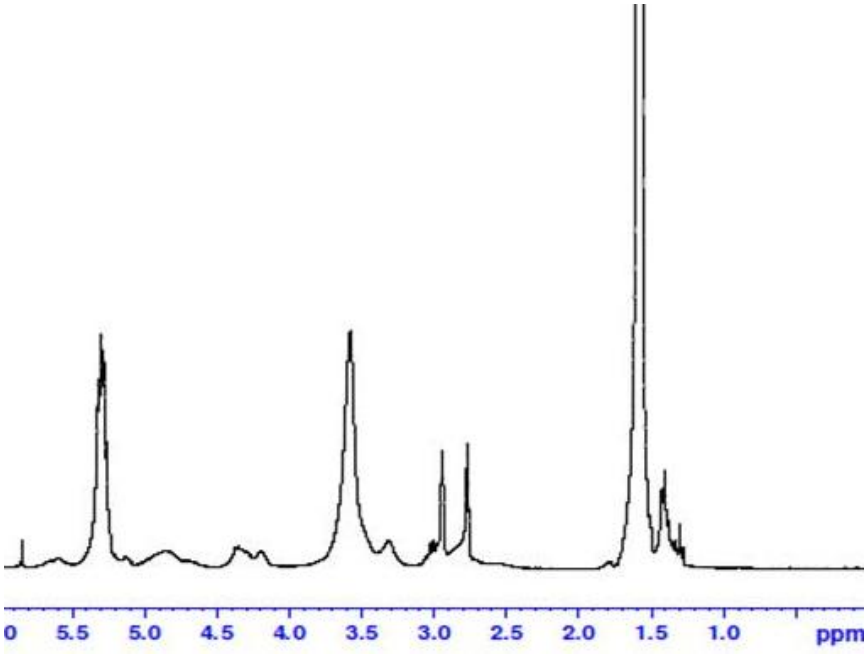

Fig. 61: ^{1}H-NMR spectrum of PHEA-RhB-PLA (PHEA-RhB-$PLA_{(A)}$ sample as an example).

The DD_{PLA} were expressed as mean value of three determinations and resulted to be 1.9 ± 0.2, 4.0 ± 0.2, and 6.2 ± 0.3 mol% for PHEA-RhB-$PLA_{(A)}$, PHEA-RhB-$PLA_{(B)}$ and PHEA-RhB-$PLA_{(C)}$ graft copolymers, respectively. By proper calculation it is possible to determine that 5, 10 and 15 PLA chains are present for each PHEA-RhB-$PLA_{(A)}$, PHEA-RhB-$PLA_{(B)}$ and PHEA-RhB-$PLA_{(C)}$ chain, respectively. Thus, with a simple synthetic strategy, it is possible to obtain fluorescent copolymers with different hydrophilic/hydrophobic ratios.
The functionalization by PLA chains was confirmed by SEC analysis, where the $\overline{M}_w$ of PHEA-RhB-$PLA_{(A)}$, PHEA-RhB-$PLA_{(B)}$ and PHEA-RhB-$PLA_{(C)}$ graft copolymers resulted to be equal to 86.9, 185.0 and 230.0 kDa, respectively (see table 10).

Table 10. Chemical composition, weight-average molecular weight ($\overline{M}_w$) and polydispersity index ($\overline{M}_w/\overline{M}_n$) of obtained copolymers.

	Chemical composition (mol %)			Molecular weight	
Copolymers	**DD_{RhB}**	**DD_{PLA}**	**DD_{PEG}**	$\overline{M}_w$ (kDa)	$\overline{M}_w/\overline{M}_n$
PHEA	---	---	---	38.7	1.62
PHEA-RhB	0.55 ± 0.05	---	---	35.0	1.41
PHEA-RhB-$PLA_{(A)}$	0.55 ± 0.05	1.9 ± 0.2	---	86.9	1.45
PHEA-RhB-$PLA_{(B)}$	0.55 ± 0.05	4.0 ± 0.2	---	185.0	1.58
PHEA-RhB-$PLA_{(C)}$	0.55 ± 0.05	6.2 ± 0.3	---	230.0	1.62
PHEA-RhB-PLA-$PEG_{(A)}$	0.55 ± 0.05	1.9 ± 0.2	5.9 ± 0.3	101.4	1.41
PHEA-RhB-PLA-$PEG_{(B)}$	0.55 ± 0.05	4.0 ± 0.2	4.9 ± 0.4	225.0	1.51
PHEA-RhB-PLA-$PEG_{(C)}$	0.55 ± 0.05	6.2 ± 0.3	4.2 ± 0.3	246.0	1.68
PHEA-RhB-PLA-$PEG_{(D)}$	0.55 ± 0.05	4.0 ± 0.2	2.0 ± 0.3	220.0	1.38
PHEA-RhB-PLA-$PEG_{(E)}$	0.55 ± 0.05	4.0 ± 0.2	8.5 ± 0.5	238.0	1.31
PHEA-RhB-PLA-$PEG_{(F)}$	0.55 ± 0.05	4.0 ± 0.2	12.1 ± 0.4	254.2	1.40

These values are quite in accordance with the theoretical values calculated for PHEA-RhB-$PLA_{(A)}$, PHEA-RhB-$PLA_{(B)}$ and PHEA-RhB-$PLA_{(C)}$ graft copolymers, considering the starting PHEA $\overline{M}_w$ and the resulting DD values in RhB and PLA, respectively (see Table 1).
Moreover, this value also demonstrated that no degradation phenomena occurred in PHEA-RhB copolymer due to the reaction conditions chosen for obtaining PHEA-RhB-PLA graft copolymers.

Once obtained, PHEA-RhB-$PLA_{(A)}$, PHEA-RhB-$PLA_{(B)}$ and PHEA-RhB-$PLA_{(C)}$ graft copolymers were functionalized with H_2N-PEG-OCH_3 to obtain PHEA-RhB-PLA-$PEG_{(A)}$, PHEA-RhB-PLA-$PEG_{(B)}$ and PHEA-RhB-PLA-$PEG_{(C)}$ graft copolymers.
PHEA-RhB-$PLA_{(B)}$ was used instead to obtain pegylated copolymers with the same DD_{PLA} but different PEG content. For this reason, starting from PHEA-RhB-$PLA_{(C)}$ three different amount of H_2N-PEG-OCH_3 were added to produce PHEA-RhB-PLA-$PEG_{(D)}$, PHEA-RhB-PLA-$PEG_{(E)}$ and PHEA-RhB-PLA-$PEG_{(F)}$ graft copolymers.
This functionalization was carried out by activating the free -OH on each PHEA-RhB-PLA derivative via disuccynimidyl carbonate (DSC) and by using triethylamine (TEA) as catalyst, in organic environment.

In particular, for PHEA-RhB-PLA-$PEG_{(A)}$, PHEA-RhB-PLA-$PEG_{(B)}$ and PHEA-RhB-PLA-$PEG_{(C)}$ copolymers, a theoretical molar ratio between the free amine-terminated H_2N-PEG chains and the free -OH on PHEA-RhB-PLA (R_7) equal to 0.075 was fixed, while the amount of DSC and TEA were defined according to R_8 equal to 0.1 and R_9 equal to 1.0, where R_8 is the molar ratio between DSC and the hydroxyl-carrying PHEA-RhB-PLA repeating units and R_9 is the molar ratio between TEA and DSC.

For PHEA-RhB-PLA-$PEG_{(D)}$, PHEA-RhB-PLA-$PEG_{(E)}$ and PHEA-RhB-PLA-$PEG_{(F)}$ copolymers, R_7 was equal to 0.04, 0.16 and 0.22, respectively; R_8 was fixed to 1.0, while R_9 was equal to 0.03, 0.12 and 0.18, respectively.

The synthetic procedure, reaction conditions and general chemical structure of PHEA-RhB-PLA-PEG graft copolymers are reported in the scheme 4.

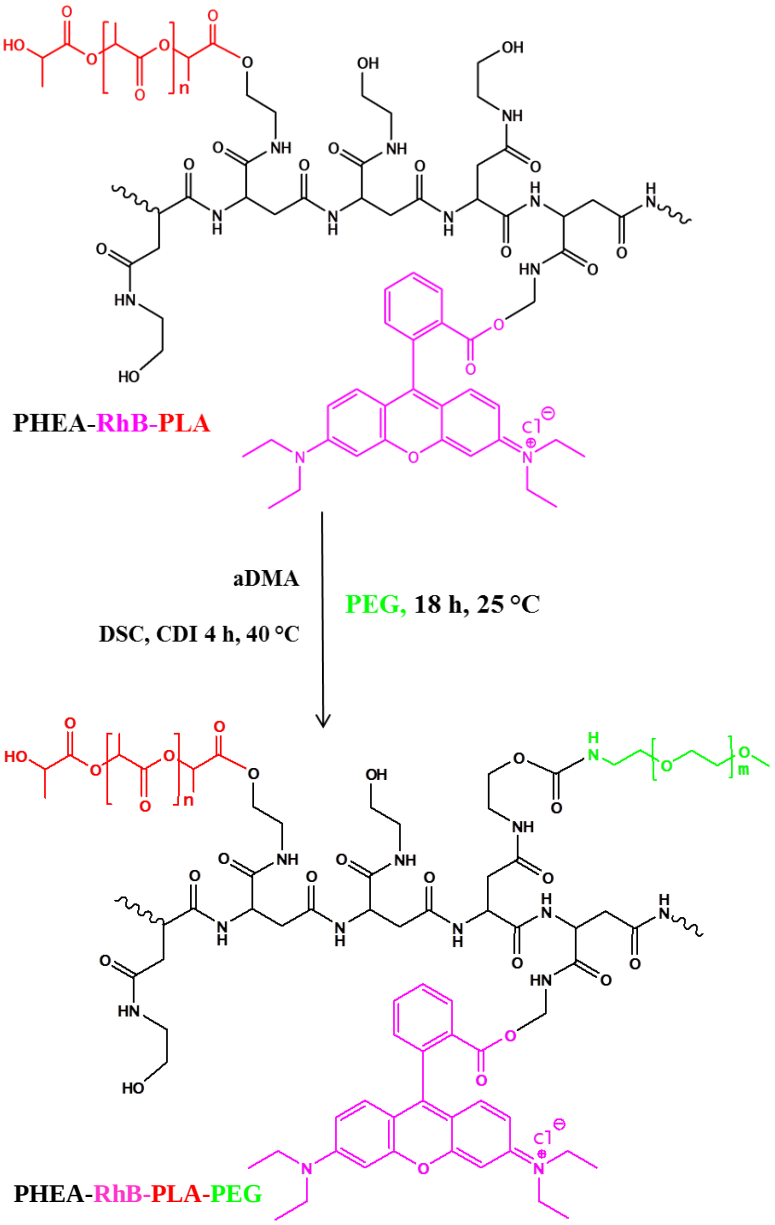

Scheme 4: Synthesis of PHEA-RhB-PLA-PEG graft copolymer (n =194, m = 44), (pink: RhB moieties, red: PLA chains, green: PEG chains).

All the obtained copolymers were soluble in acetone, dimethylsulfoxide, dimethylformamide and dichloromethane and insoluble in water.

DD_{PEG} of obtained PHEA-RhB-PLA-$PEG_{(A)}$, PHEA-RhB-PLA-$PEG_{(B)}$, PHEA-RhB-PLA-$PEG_{(C)}$, PHEA-RhB-PLA-$PEG_{(D)}$, PHEA-RhB-PLA-$PEG_{(E)}$ and PHEA-RhB-PLA-$PEG_{(F)}$ copolymers was calculated by comparing the integral of the peak related to protons (H=176) at δ 3.77 attributed to -$\mathbf{CH_2}$-$\mathbf{CH_2}$-O- (belonging to PEG_{2000}) with the integral related to protons (H=2) a δ 3.50 attributed to -NH-$\mathbf{CH_2}$-CH_2-O- (belonging to PHEA).

The typical ^{1}H-NMR spectrum in DMF-d_7 of PHEA-RhB-PLA-PEG graft copolymers is reported in figure 62.

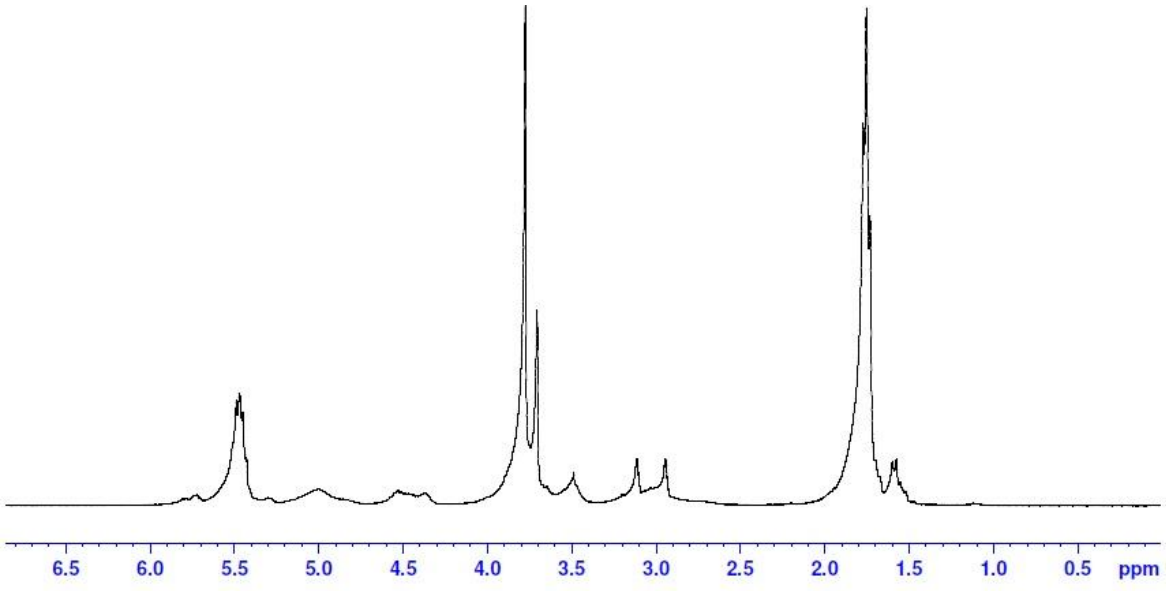

Fig. 62: ^{1}H-NMR spectrum of PHEA-RhB-PLA-PEG (PHEA-RhB-PLA-PEG$_{(B)}$ sample as an example).

The DD_{PEG} were expressed as mean value of three determinations and resulted to be 5.9 ± 0.3, 4.9 ± 0.4, 4.2 ± 0.3, 2.0 ± 0.3, 8.5 ± 0.5, and 12.1 ± 0.4 mol% for PHEA-RhB-PLA-PEG$_{(A)}$, PHEA-RhB-PLA-PEG$_{(B)}$, PHEA-RhB-PLA-PEG$_{(C)}$, PHEA-RhB-PLA-PEG$_{(D)}$, PHEA-RhB-PLA-PEG$_{(E)}$ and PHEA-RhB-PLA-PEG$_{(F)}$, respectively.

Also on these pegylated derivatives, the $\overline{M}_w$ and the $\overline{M}_w/\overline{M}_n$ values were determined by SEC analysis (table 10). These values are in accordance with the theoretical values calculated considering each starting PHEA-RhB-PLA $\overline{M}_w$ and the resulting DD values in PEG derivatization.

Moreover, these values also demonstrated that no degradation phenomena occurred in each PHEA-RhB-PLA copolymer backbone due to the reaction conditions chosen for obtaining the corresponding PHEA-RhB-PLA-PEG graft copolymers.

3.3.2 Preparation and characterization of FNPs

In order to evaluate the capability of obtained copolymers to act as nanoparticle-forming material and simultaneously as emulsion-stabilizing agent thanks to its amphiphilic properties, PHEA-RhB-PLA-PEG graft copolymers were chosen to obtain NPs.

The followed procedure was the emulsion-high pressure homogenization (HPH)-solvent evaporation method (scheme 5).

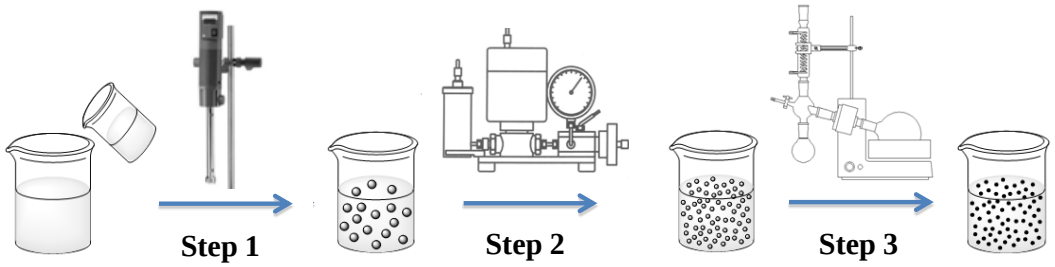

Scheme 5: Schematic representation of the polymeric nanoparticle preparation by emulsion-high pressure homogenization (HPH)-solvent evaporation method.

Polymeric FNPs with small size and low width of distribution were easily obtained by the high pressure homogenization (HPH)-solvent evaporation method. In particular, a primary o/w emulsion was obtained by addition of the copolymer organic solution to an aqueous phase (*step* 1 of scheme 5), which was diluted and subjected to HPH (*step 2*). Then, the extraction of the organic solvent under reduced pressure allows the polymer precipitation and the formation of FNPs (*step 3*), that were freeze-dried in the presence of a cryoprotectant.

FNPs prepared starting from PHEA-RhB-PLA-PEG$_{(A)}$, PHEA-RhB-PLA-PEG$_{(B)}$, PHEA-RhB-PLA-PEG$_{(C)}$, PHEA-RhB-PLA-PEG$_{(D)}$, PHEA-RhB-PLA-PEG$_{(E)}$ and PHEA-RhB-PLA-PEG$_{(F)}$ copolymers were respectively called FNPs $_{(A)}$, FNPs $_{(B)}$, FNPs $_{(C)}$, FNPs $_{(D)}$, FNPs $_{(E)}$ and FNPs $_{(F)}$.

The use of surfactants or other stabilizing agents, normally request for particle production, was avoided thanks to the amphiphilic properties of the starting polymeric material.

After preparation, FNPs were characterized in terms of mean size, polydispersity index (PDI), and ζ potential in PBS at pH 7.4 by using Photon Correlation Spectroscopy (PCS). Analytical data are reported in Table 11.

Table 11: Mean size, PDI and ζ potential in PBS at pH 7.4.

FNPs	Mean Size (nm)	PDI	ζ Potential (mV)
$FNPs_{(A)}$	161.2 ± 3.4	0.164 ± 0.015	-6.8 ± 0.46
$FNPs_{(B)}$	155.6 ± 6.9	0.206 ± 0.022	-7.1 ± 0.31
$FNPs_{(C)}$	152.5 ± 4.4	0.189 ± 0.032	-7.2 ± 0.54
$FNPs_{(D)}$	141.2 ± 2.3	0.226 ± 0.015	-7.5 ± 0.39
$FNPs_{(E)}$	185.4 ± 9.7	0.158 ± 0.020	-5.5 ± 0.44
$FNPs_{(F)}$	188.6 ± 10.1	0.101 ± 0.032	-3.0 ± 0.52

All produced FNPs show nanoscaled mean size (~140-180 nm) and low values in surface charge (from -3 to -6.8 mV), that could be attributed to the presence of linked PEG chains onto the NP surface that gives a more shielded surface.

These values were significantly higher when NPs were obtained by using non-pegylated copolymers. In fact, FNPs, prepared starting from PHEA-RhB-$PLA_{(B)}$ by using the high pressure homogenization (HPH)-solvent evaporation method, showed lower dimensions (139.4 ± 3.6) and higher ζ potential values (-9.00 ± 0.16).

SEM image (figure 63) and preliminary fluorescence investigation (figure 64) of $FNPs_{(B)}$ were reported and are representative of the other produced FNPs.

SEM images revealed spherical shape and confirms mean size obtained by DLS measurements.

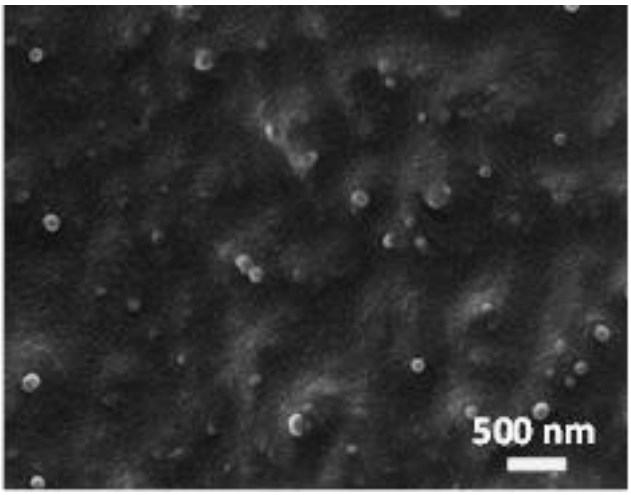

Fig. 63: SEM image of FNPs ($sample_{(B)}$ as an example) .

The fluorescence investigation revealed that all samples possess high fluorescent properties. These properties give to these polymeric fluorescent particles great potential for in vitro and in vivo fluorescence imaging application.

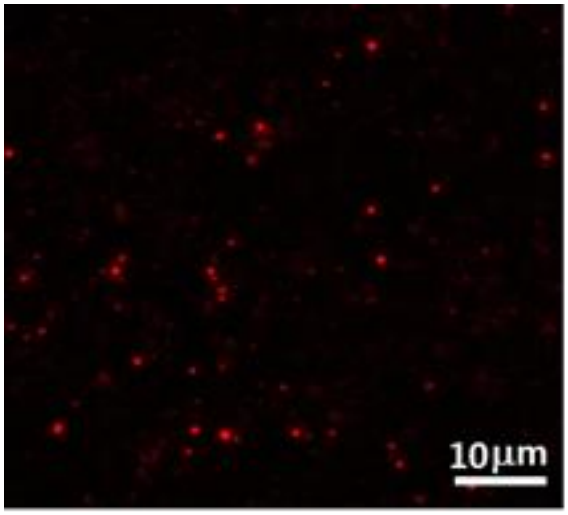

Fig. 63: Fluorescence microcopy image of FNP water dispersion (sample$_{(B)}$ as an example).

Being buffer at pH 7.4 the preferred medium for dispersing particles for most biological experiments, the physical stability of FNP aqueous PBS dispersions was evaluated by monitoring mean size and width of distribution as a function of incubation time until 24 h.
Results, reported in Table 12 a and b, showed that for no significant changes in the initial mean size and ζ potential were observed after 24 h of incubation, indicating their high stability.

Table 12: Mean size (a), and ζ potential values (b) of FNPs in PBS at different incubation time.

a)	**Mean Size (nm)**	
Sample	**t_0**	**$t_{24\ h}$**
FNPs $_{(A)}$	161.2 ± 3.4	153.8 ± 10.1
FNPs $_{(B)}$	155.6 ± 6.9	148.2 ± 17.2
FNPs $_{(C)}$	152.5 ± 4.4	140.9 ± 14.3
FNPs $_{(D)}$	141.2 ± 2.3	135.5 ± 18.9
FNPs $_{(E)}$	185.4 ± 9.7	165.8 ± 17.1
FNPs $_{(F)}$	188.6 ± 10.1	174.2 ± 10.8

b)	ζ Potential (mV)	
Sample	**t_0**	**$t_{24\ h}$**
FNPs $_{(A)}$	- 4.2 ± 0.8	- 3.8 ± 0.9
FNPs $_{(B)}$	- 6.8 ± 0.5	- 5.1 ± 1.9
FNPs $_{(C)}$	- 7.1 ± 0.3	- 6.4 ± 0.8
FNPs $_{(D)}$	- 7.2 ± 0.5	- 6.9 ± 1.5
FNPs $_{(E)}$	- 7.5 ± 0.4	- 6.6 ± 1.7
FNPs $_{(F)}$	- 5.5 ± 0.6	- 4.4 ± 2.0

For the use of FNPs in fluorescent imaging, it is very important that the fluorescent probe is stably linked to the systems. For this reason, the chemical and enzymatic stability of fluorescent dye covalently linked to the copolymer backbone by ester linkage was investigated in mimicking physiological conditions.

FNPs $_{(B)}$ were chosen because possess a chemical composition, in terms of DD_{PLA} and DD_{PEG} that is intermediate of all produced FNPs.

FNPs $_{(B)}$ were incubated until 4 days of incubation at 37°C in PBS at pH 7.4 and at pH 5.5 to mimic the different physiological compartments. The stability of covalent linkage was determined by evaluating the amount of released RhB from FNPs $_{(B)}$ at prefixed time intervals across a dialysis tube. For comparison, this experiment was also carried out on PHEA-RhB, to evaluate if the great accessibility of ester linkage between RhB and PHEA in the water-soluble starting copolymer could modify the degradation profile of the covalently linked dye. Moreover, the RhB diffusion profile alone was investigated in each medium in order to determine the diffusion rate of the free fluorescent probe across the dialysis membrane. The diffusion rate resulted to be very fast and the amount of RhB detected in the external compartment reached the 100 wt % since the first hour, being the free RhB freely soluble in aqueous media. The amount of released RhB was expressed as percentage ratio between the weight of released RhB at the prefixed time and the total amount of RhB linked to $FNPs_{(B)}$ or PHEA-RhB copolymer and expressed as function of incubation time (figure 64).

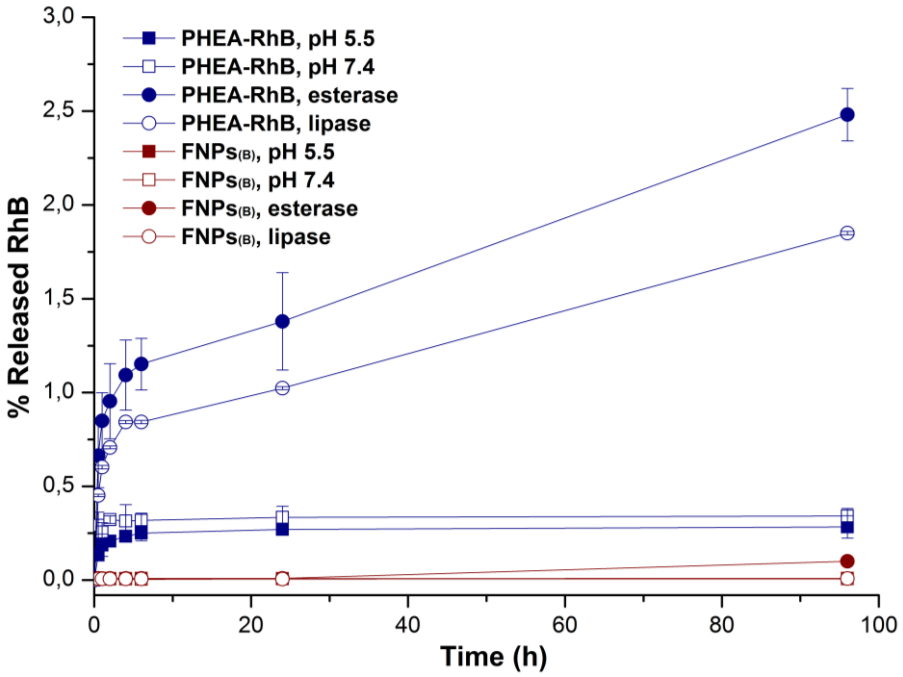

Fig. 64: RhB release profiles from FNPs and PHEA-RhB polymer incubated in PBS at pH 5.5 and at 7.4, in presence or not of lipase and esterase enzyme dispersion.

As can be seen, the percentage of RhB released from FNPs $_{(B)}$ in all investigated media, is almost null until 4 days incubation. For PHEA-RhB, the percentage of degradation was below 0.4 wt% on the total linked amount to the PHEA backbone; although this value is higher than that found for FNPs, is still very low if compared to the total linked amount to the PHEA backbone.

Enzymatic stability was carried out in presence of esterase or lipase enzyme by following the experimental protocol described for the chemical stability (figure 64). Also in this case, RhB release from FNPs $_{(B)}$ is negligible, while the amount that is released from PHEA-RhB was equal to about 2.5 and 1.8 wt % after 4 days incubation, in presence of esterase and lipase, respectively.

Results of chemical and enzymatic stability could be explained considering that being PHEA-RhB soluble in aqueous media, ester linkage between RhB and PHEA backbone is more accessible by the enzyme than the same linkage when entrapped into the FNPs.

3.3.2 Evaluation of biodegradability of produced NPs

The biodegradability of pegylated polyaspartamide–polylactide copolymers based NPs was evaluated on NPs prepared starting from a non-rhodaminated polymer, with a chemical compostition and molecular weight similar to that of PHEA-RhB-PLA-PEG$_{(B)}$, chosen

because possess an intermediate chemical composition amongst all synthesized copolymers, and compared with NPs composed by only PLA.

Synthesis and characterization of PHEA-PLA-PEG graft copolymer

In order to allow the grafting of PLA onto PHEA, the free carboxyl groups of PLA were activated for 4 h by using CDI as coupling agent, and then the activated PLA derivative was left to react with hydroxyl side groups on PHEA for 72 h, as described before for PHEA-RhB-PLA.

DD_{PLA} of PHEA-PLA graft copolymer in PLA chains was calculated by ^{1}H-NMR spectrum (figure 65), comparing the integral of the peaks related to protons between δ 1.3-1.7 (H= 582) as well as to protons (H= 194) between δ 4.2-4.5 and δ 5.1-5.5 (assigned to –O-CO-CH(C**H**$_3$)-O- and -O-CO-C**H**(CH_3)- (belonging to linked PLA chains), respectively, to the integral related to protons at δ 4.8 attributed to -NH-C**H**(CO)CH_2-, belonging to PHEA.

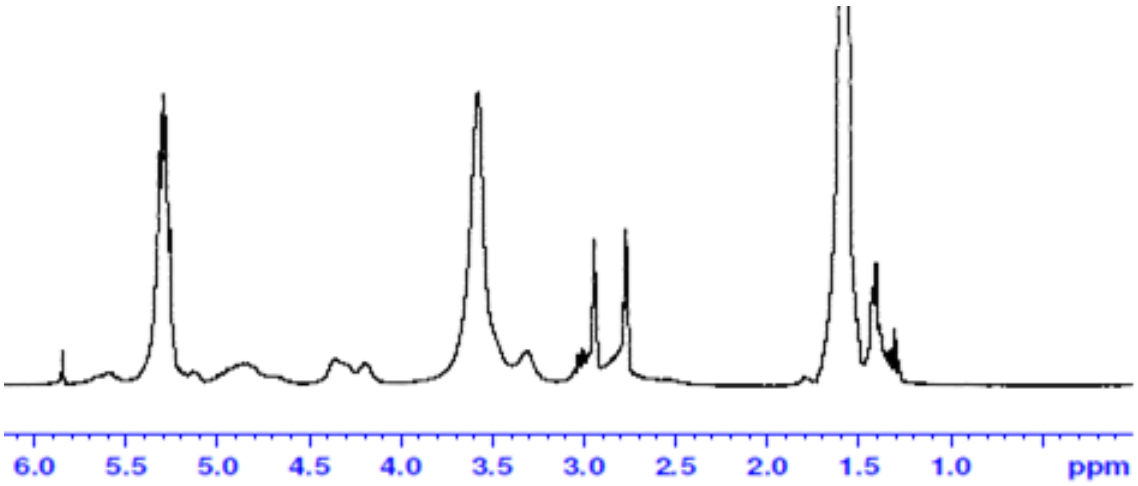

Fig. 65: ^{1}H-NMR spectrum of PHEA-PLA graft copolymer.

The DD_{PLA}, was expressed as mean value of three determinations and resulted to be 2.4 ± 0.3 mol% of repeating units.

PHEA-PLA graft copolymer was then functionalised with PEG chains, by activating the free -OH on PHEA-PLA via DSC and by using TEA as catalyst, in organic environment.

Chemical structure of PHEA-PLA-PEG graft copolymer is reported in figure 66.

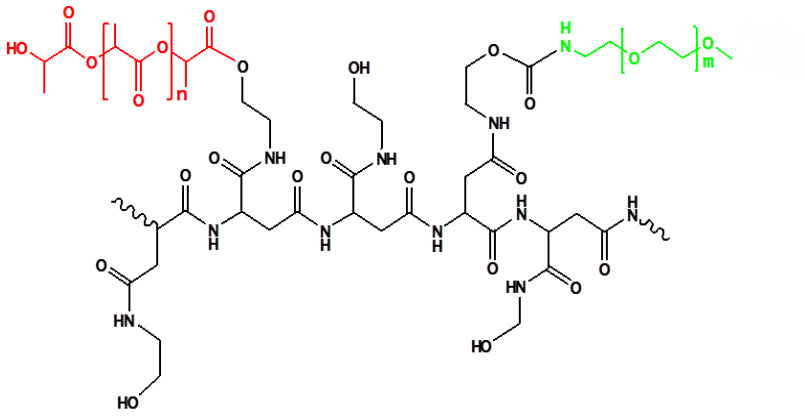

Fig. 66: Chemical structure of PHEA-PLA-PEG graft copolymer (n =194, m = 44), (red: PLA chains, green: PEG chains).

DD_{PEG} was calculated by ^{1}H-NMR spectrum (figure 67), comparing the integral of the peak related to protons (H=176) at δ 3.7 attributed to -**CH_2-CH_2**-O- (belonging to PEG_{2000}) with the integral related to protons (H=2) a δ 3.5 attributed to -NH-**CH_2**-CH_2-O- (belonging to PHEA).

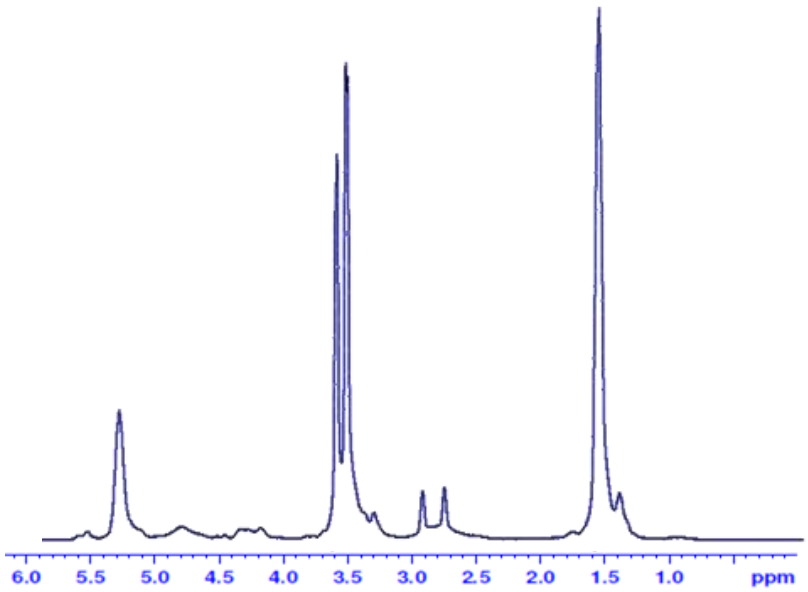

Fig. 67: Chemical structure of PHEA-PLA-PEG graft copolymer (n =194, m = 44), (red: PLA chains, green: PEG chains).

The DD_{PEG} of PHEA-PLA-PEG resulted to be 5.0 ± 0.2 mol%. To properly characterize the obtained PHEA-PLA-PEG copolymers from the molecular point of view, $\overline{M}_w$ values were

determined by SEC analysis. These values result to be equal to 209.0 kDa and are in accordance with the theoretical values calculated for PHEA-PLA-PEG copolymer.

Preparation and characterization of PHEA-PLA-PEG NPs

As already done for FNPs produced starting from PHE-RhB-PLA-PEG, non fluorescent polymeric NPs, based on PHEA-PLA-PEG graft copolymer, were successfully obtained by the high pressure homogenization (HPH)-solvent evaporation method.

In detail, a primary o/w emulsion was obtained by vigorously mixing the organic polymeric solution with twice-distilled water, that was diluted with twice-distilled water and subjected to HPH. Then, the extraction of organic solvent under reduced pressure allowed the formation of NPs, that were freeze-dried in the presence of a cryoprotectant.

After redispersion in a proper medium, PHEA-PLA-PEG NPs were characterized in terms of mean size, width of distribution and ζ potential in two neutral media, PBS at pH 7.4 and NaCl 0.9 wt% by using PCS. Analytical data are reported in table 13.

Table 13: Mean size, PDI and ζ potential of NPs in PBS at pH 7.4 and NaCl 0.9 wt%

FNPs	Mean Size (nm)	PDI	ζ Potential (mV)
PBS at pH 7.4	130.7 ± 26.9	0.205 ± 0.09	-5.2 ± 0.7
NaCl 0.9 wt%	109.7 ± 21.1	0.194 ± 0.04	-4.4 ± 0.9

Obtained NPs show nanoscaled size and slightly negative zeta potential in isotonic media, and spherical shape as showed by SEM images reported in Fig. 68.

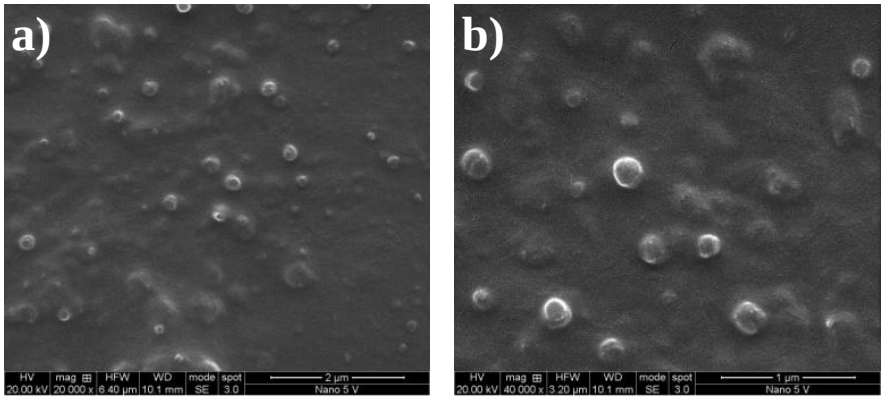

Fig. 68: SEM images of PHEA-PLA-PEG NPs at two magnifications: a) 20000 x; b) 40000 x.

Chemical degradation studies

Being biodegradability and biocompatibility fundamental requirements for the potential use of NPs as drug delivery systems in vivo, a chemical degradation study in media mimicking physiological compartments was carried out on PHEA-PLA-PEG NPs.

In effect, PLA, that is a basic component of both synthesized graft copolymers used to realize NPs, could undergo chemical hydrolysis of ester linkages. In particular, PLA chains, that are insoluble in water at high molecular weights, could be transformed by degradative processes in shorter chains until water soluble low molecular weight-oligomers or/and lactic acid (LA) monomers.

In general, the degradation mechanism of PLA-based systems depends on size and, in particular, it is homogeneous (bulk degradation) in the matrix of nanometric systems, due to the possibility of free diffusion of the degradation products out of the systems. Moreover, another key factor that could influences either the degradation mechanism or the rate is the chemical composition of the PLA-based material that forms NP matrix.

It is well known that NP systems based on PLA homopolymers release entrapped drugs through a diffusion mechanism due to the crystallinity and slow biodegradation rate of PLA copolymer. On the other hand, amphiphilic PLA copolymers based systems show a degradation rate depending on polymeric chemical composition and ratio between hydrophilic and hydrophobic portions. Thus, by varying the material composition, drug delivery systems could be obtained with adequate degradation that could strongly influence the drug release rate.

For this reason, degradation studies were carried out on PHEA-PLA-PEG NPs in two different buffered aqueous solutions at pH 5.5 and at pH 7.4, to mimic physiological compartments, and compared to PLA NPs, produced by using the same preparation process and which shows comparable size and surface charge.

In particular, the degradation process was carefully investigated by following the time-depending changes of different parameters, such as the pH of incubation medium, which reduction is indicative of the polymeric matrix degradation. Moreover, the weight of recovered nanoparticles and mean size were monitored as a function of incubation time, as well as their chemical composition.

In Scheme 6, the experiment steps are depicted.

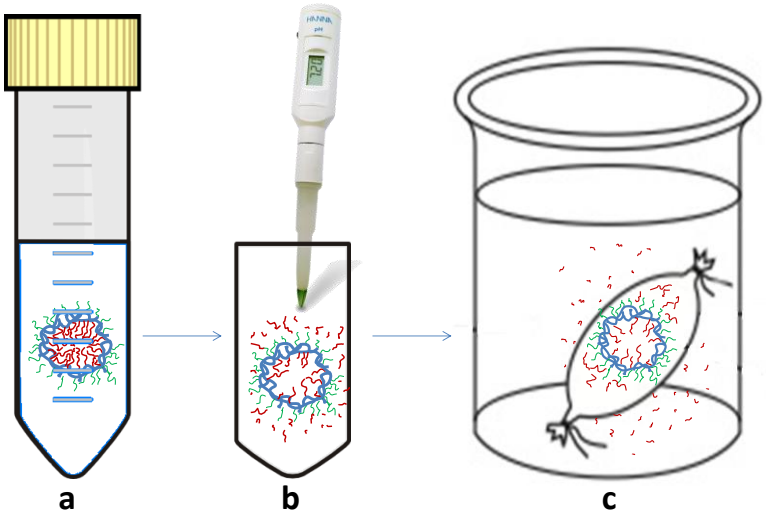

Scheme 6: The experiment steps of chemical hydrolysis study: (a) incubation of NPs samples at pH 5.5 or 7.4 buffer solutions; (b) evaluation of pH at prefixed time intervals; (c) purification of degraded NP samples by dialysis before characterization.

In particular, exactly weighted NPs were incubated for 21 days at 37°C at pH 5.5 and at pH 7.4 (step a). Before incubation, the initial pH value of each obtained dispersion was measured. At pre-set time intervals (3, 7, 14 and 21 days), the pH value of the dispersing medium was evaluated (step b) and then the NP dispersions were purified by exhaustive dialysis against bidistilled water (step c) in order to remove the formed water soluble hydrolysis products (mainly LA oligomers or monomers); each purified residual sample was then lyophilized to estimate the NP yield after degradation, and characterized by mean size measurements, ^{1}H-NMR, FT-IR and SEC analyses.

In figure 69, the variations of pH of each sample after incubation in media at pH 5.5 and 7.4 as a function of incubation time, respectively, are reported.

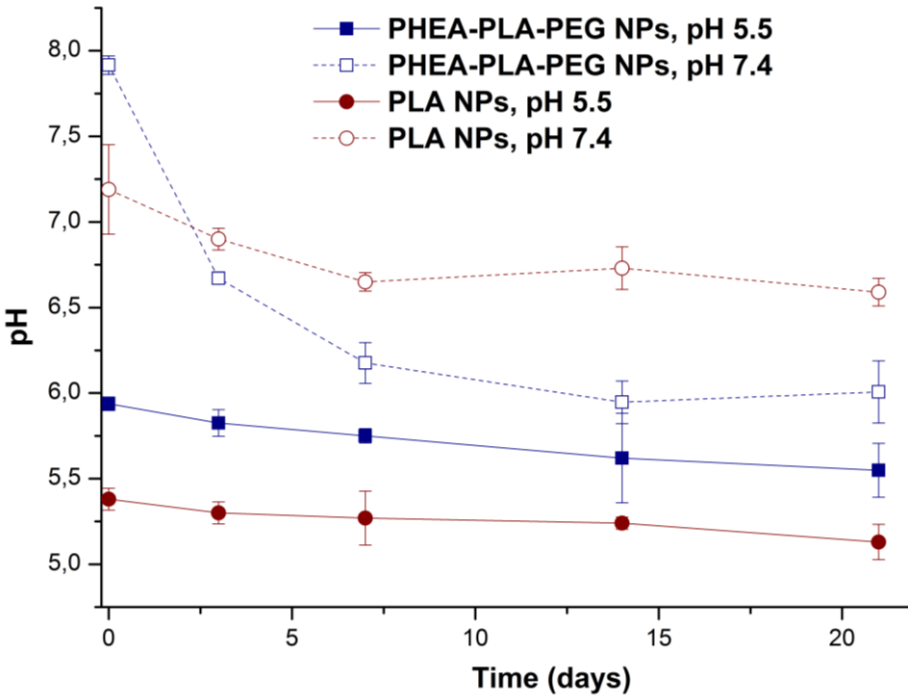

Fig. 69: Variations of pH of the incubation media at initial pH 5.5 and pH 7.4 as afunction of incubation time.

It is evident from the graphics that in both media a reduction of initial pH value of the dispersion occurred as a function of incubation time, which could be ascribed to the release of LA molecules and/or oligomers from NPs. In particular, for PHEA-PLA-PEG NPs, initial pH of the incubation medium decreases of about 0.39 in pH units after 21 days incubation at pH 5.5; while this variation was about 1.92 after 21 days incubation at pH 7.4.
In the same figure the variations in pH values of the media where NPs based on PLA were incubated, are also reported. In this case, the pH changes are equal to 0.25 and 0.60 after 21 days incubation at pH 5.5 and 7.4, respectively. This result could suggest the hypothesis that degradation of PLA NPs is slower than that showed by PHEA-PLA-PEG NPs.

Being the pH variations sign of effective degradation of PHEA-PLA-PEG NPs, weight reduction of recovered samples was determined as a function of incubation time, after purification by dialysis (step c in scheme 5), that is after removal of water soluble hydrolysis products.
In particular, oligomers with a molecular weight until 830 Da, corresponding to about 9-10 repeating units of LA, are soluble in aqueous solutions with neutral pH, so it could be removed by dialysis [33].

In figure 70, the yields of recovered samples at pH 5.5 and pH 7.4, expressed as residual on initial weight percent ratio, are reported as a function of incubation time.

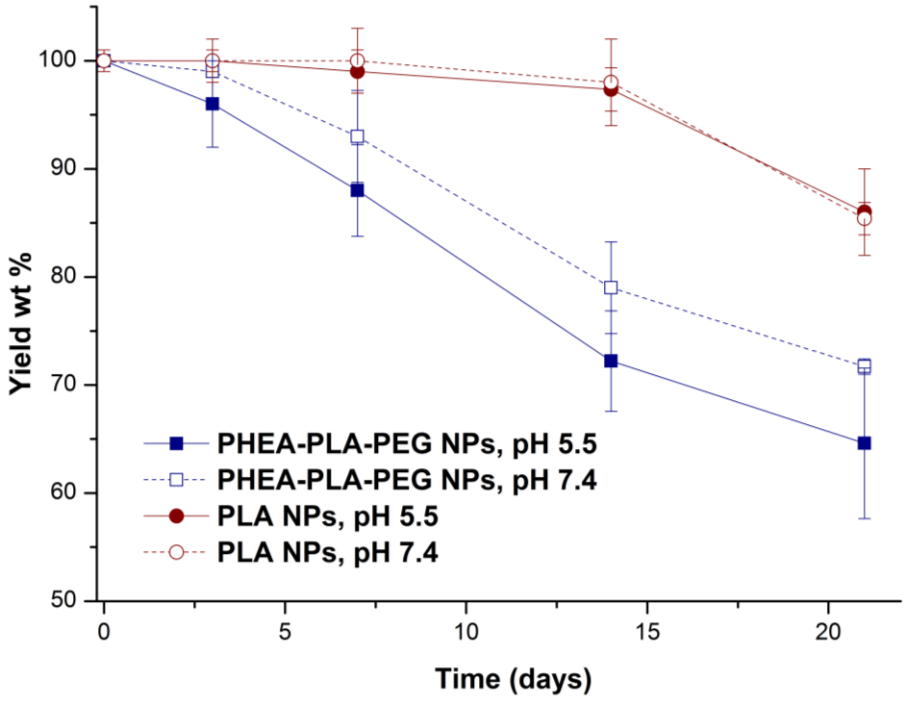

Fig. 70: Variations of yields wt% of recovered samples after 21 days incubation in isotonic media at pH 5.5 and pH 7.4 as a function of incubation time.

As can be seen, a gradual decrease of recovered sample weights is evidenced by increasing the incubation time, which seems to have a rate faster until 14 days and become slower from 14 to 21 days of incubation. This yield reduction could be mainly attributed to the loss of water soluble PLA portions of copolymers, removed by dialysis as described in scheme 5 (step c).

Moreover, the degradation seems to be greater at pH 5.5 than at pH 7.4, although this difference is not significant. In particular, after 14 days incubation at pH 5.5, the percentage of recovered sample is 72.2 wt %, while at pH 7.4 about 79.0 wt%, respectively.

In the same figure, the variation of recovered sample weight of PLA NPs as a function of incubation time in the same media is reported for comparison. The degradation of these NPs is significantly slower than that showed by PHEA-PLA-PEG NPs in both media (*$p<0.01$), especially after 14 and 21 days of incubation.

This result confirms data obtained by monitoring the pH change of incubation media reported in figure 69. In effect, after 14 days of incubation of PLA NPs, the degradation is lesser than 3 wt% in both media.

Since the degradation process causes the loss of polymeric portions, on recovered NPs a study was carried out to evaluate the change in mean size, as a function of incubation time in each medium.

In figure 71, the mean size of recovered samples after incubation at pH 5.5 and 7.4, determined in NaCl 0.9 wt% saline solution is reported.

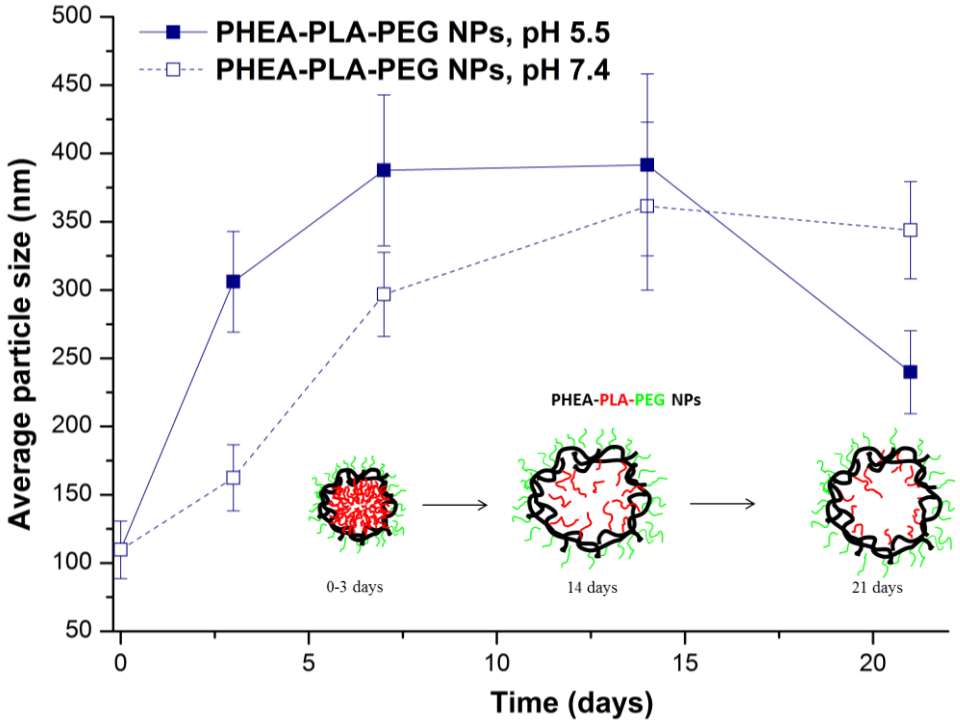

Fig. 71: Variations of average particle size of recovered samples after 21 days incubation in isotonic media at pH 5.5 and pH 7.4 as a function of incubation time.

As can be seen, in both incubation media an increase of both mean size is evidenced compared to initial values. This result could be explained considering that the degradation of PLA in copolymers constituting NP samples and responsible of the NP core formation, implies a reduction of both extent and ability of auto-aggregation behaviour of PLA-containing copolymer. As a consequence, a gradual disaggregation of NP core occurs as a function of incubation time. Therefore, the dimensional analysis shows the presence of bigger particles, which at pH 5.5 appears since early incubation days. Moreover, at the same pH, an apparent reduction of mean size occurs with the increase of incubation time from 14 to 21 days of incubation, probably due to the loss of more significant polymeric portions from NP samples.

Since the yield decrease and the size variation could be attributed mainly to the PLA hydrolysis in PHEA-PLA-PEG copolymer, a ^{1}H-NMR investigation on all recovered samples was carried out in order to determine the residual PLA amount in these sample.

In each ^{1}H-NMR spectrum, the moles of LA repeating units linked to the copolymer were determined before and after incubation at different times. In the latter case, also PLA oligomers still not linked to PHEA backbone but so big to be still insoluble in water will be inevitably included.

In figure 72, the degradation % of NP samples, expressed as percentage of PLA repeating units lost due to the hydrolysis process respect to those initially linked to PHEA backbone, is reported as a function of incubation time.

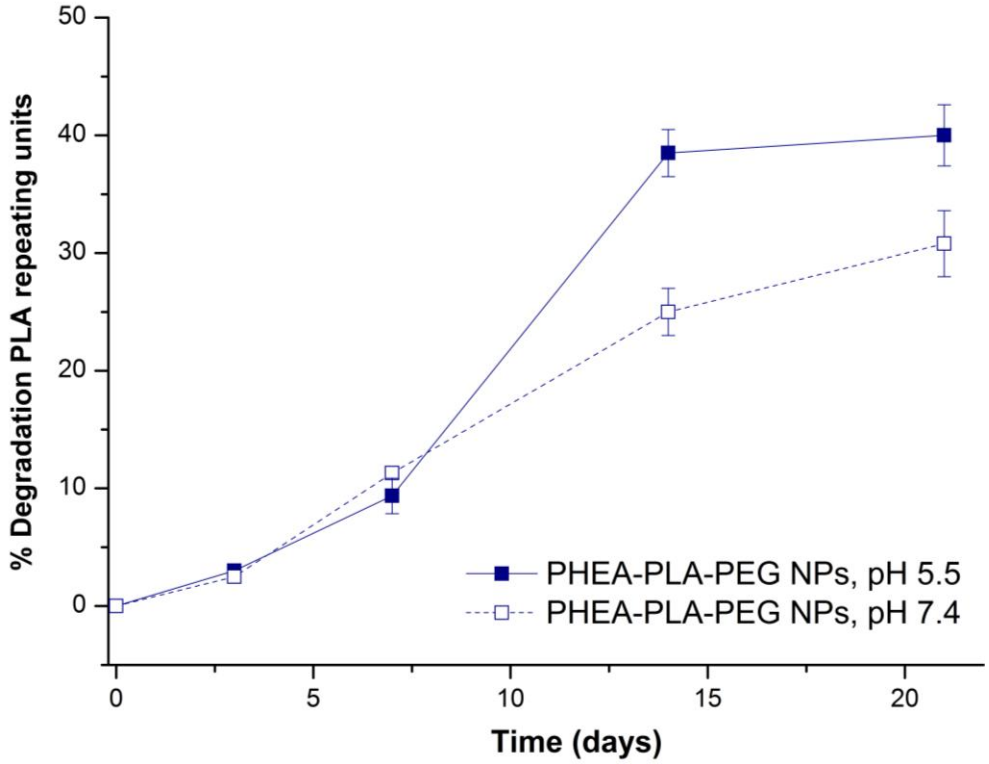

Fig. 72: NP degradation as a function of incubation time at pH 5.5 and pH 7.4.

As shown in the graphic in figure 72, in all cases, the degradation process progresses with a higher speed until 14 days incubation and show a slowdown from 14 to 21 day. Moreover, after 14 days of incubation at pH 5.5, the degradation % of NPs is significantly higher (*$p<0.01$) than that resulted after incubation at pH 7.4. However, the percentage of lost lactic acid units was not higher than 40 wt% after 21 days of incubation in both samples.

Data are in agreement with the reduction in the percentage yield of each recovered as a function of incubation time and indicate that the greater loss in weight of the sample is determined by the degradation of the PLA, as water-soluble PLA polymeric portions such as LA unimers and/or oligomers.

From the ^{1}H-NMR spectra analysis a slightly reduction of DD_{PEG} is evidenced after 14 and 21 days of incubation, that could be attributed to the concomitant loss from the samples of water-soluble copolymer portions different from PLA.

The FT-IR analysis of recovered samples further confirmed that degradation occurs mainly on PLA copolymer portions.

In Fig. 73, the FT-IR spectrum of NPs, incubated for 14 days at pH 5.5 and 7.4 is reported.

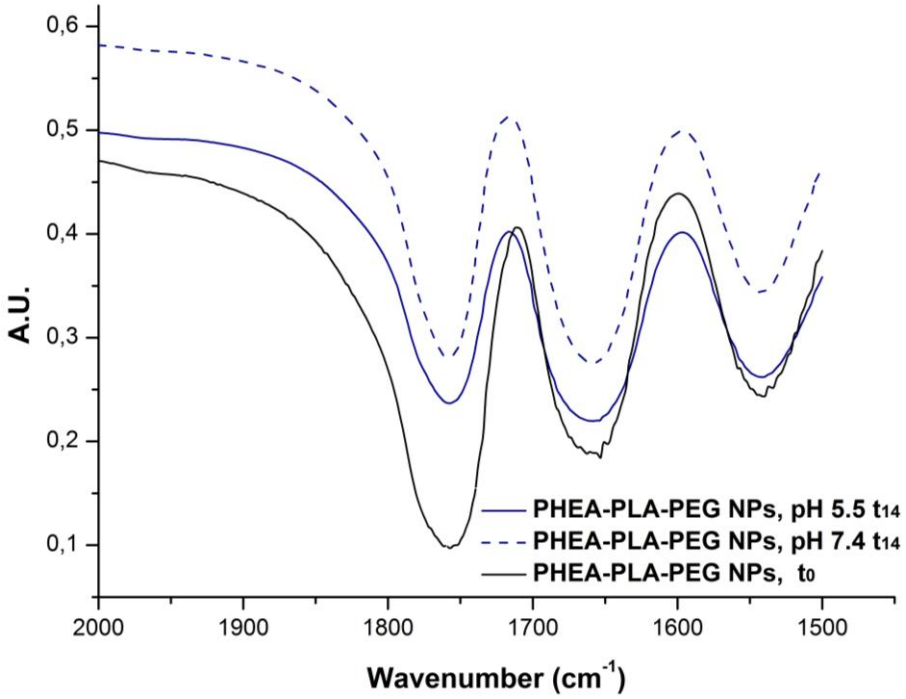

Fig. 73: FT-IR overlay spectra of recovered PHEA-PLA-PEG NP sample as a function of incubation time at (a) pH 5.5 and (b) pH 7.4.

As can be seen, in FT-IR spectrum of PHEA-PLA-PEG NP sample, that shows a relative ratio between peaks at 1757 cm^{-1} and at 1654 cm^{-1}, attributable respectively to the asymmetric stretching of PLA ester carbonyl and PHEA amidic carbonyl groups, it is highlighted a greater degradation at pH 5.5 than at pH 7.4.

Since from described analyses it is not possible to distinguish if in the recovered NPs the water insoluble PLA fractions linked or not to PHEA backbone are still present (because it is not possible to separate them by dialysis), SEC analysis of recovered products was carried out in order to confirm the presence of free and water-insoluble PLA chains still present in the recovered NP samples.

In Fig. 74, SEC profile overlay of recovered PHEA-PLA-PEG NP sample is reported, after 14 days incubation.

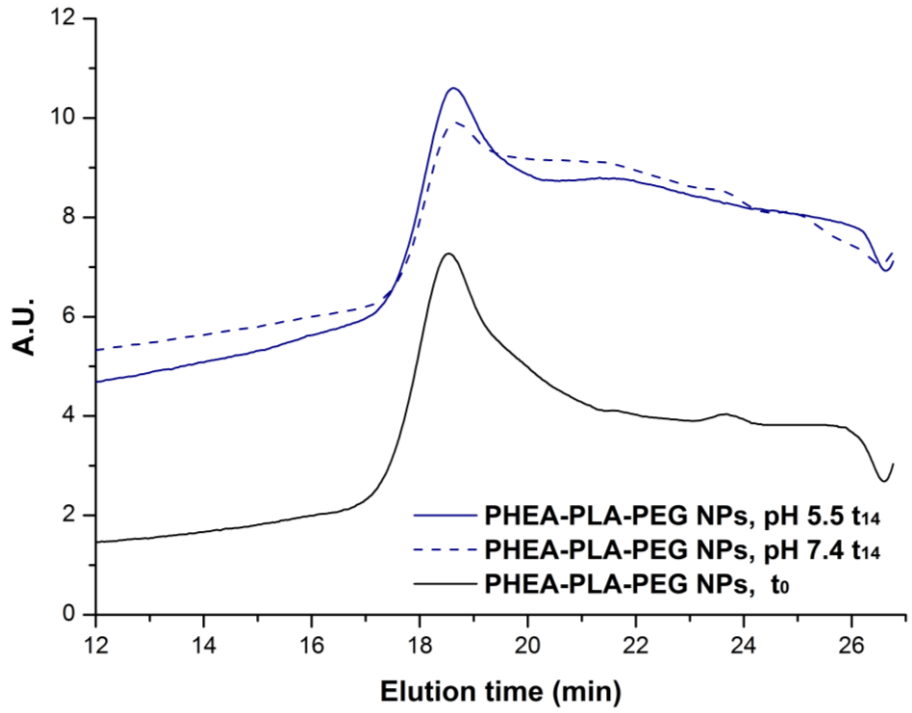

Fig. 74: SEC profile of recovered PHEA-PLA-PEG NP sample after 14 days incubation at (a) pH 5.5 and (b) pH 7.4.

From SEC profile, it can be seen a peak corresponding to the starting copolymer and the formation of a peak forming of a bimodal curve, that is attributed to the partially degraded polymer.

3.3.3 Conclusions

In this paragraph, the synthesis and characterization of novel amphiphilic graft copolymers bearing rhodamine RhB moieties, different amount of PLA and PEG chains, and their use for the preparation of polymeric FNPs without the use of stabilizing agents, are described.

To do this, the fluorescent derivatives of PHEA were obtained by chemical reaction of PHEA with RhB. Then, fluorescent polylactide-polyaminoacid conjugates with different amounts of grafted PLA were obtained by chemical reaction of PHEA-RhB with increasing amount of polylactic acid PLA, and subsequent reaction with different amount of CH_3O-PEG-NH_2, obtaining PHEA-RhB-PLA-PEG graft copolymers.

Starting from the PHEA-RhB-PLA-PEG derivative different DD_{PLA} and DD_{PEG}, fluorescent particles with different shape were successfully prepared by high pressure homogenization (HPH)-solvent evaporation method or emulsion-solvent evaporation method. Obtained fluorescent particles have nanometre size, slightly negative zeta potential and spherical shape as showed by SEM images.

Moreover, chemical and enzymatic stability of the ester linkage between the fluorescent dye and copolymer, essential for imaging application, was demonstrated until 4 days of incubation. Thus, fluorescence and technological properties revealed that these particles possess a great potential for in vitro and in vivo imaging applications.

Finally, the biodegradability of these particles was demonstrated by carrying out a chemical stability study until 21 days by incubating NPs based on non-rhodaminated similar copolymer in two media mimicking physiological compartments.

The degradation seems to be dependent from the matrix chemical composition, involve mainly PLA and is more evident at pH 5.5 than at pH 7.4. Results demonstrate that obtained pegylated systems degrade faster than PLA NPs and the degradation rate could be tuned by varying the chemical composition of the matrix; so these systems can potentially be used as biodegradable carriers of drugs, avoiding critical bioaccumulation phenomena.

3.4 Ibuprofen containing pegylated polyaspartamide–polylactide mucus-penetrating based nanoparticles for the treatment of lung inflammation in CF

In this paragraph, the preparation of mucus-penetrating NPs for pulmonary administration of ibuprofen in patients with CF is described.

FNPs based on PHEA-RhB-PLA-$PEG_{(D)}$ and PHEA-RhB-PLA-$PEG_{(E)}$ graft copolymer, whose synthesis and characterization is described in 3.3.1 paragraph, were chosen to study the mucus-penetrating ability in terms of surface PEG density and conformation of PEG chains on the NP surface. For this reason PHEA-RhB-$PLA_{(B)}$, the starting polymer used for the further pegylation reaction that lead to PHEA-RhB-PLA-$PEG_{(D)}$ and PHEA-RhB-PLA-$PEG_{(E)}$, was used to produce unpegylated FNPs used as control.

FNPs obtained from PHEA-RhB-$PLA_{(B)}$, PHEA-RhB-PLA-$PEG_{(D)}$ and PHEA-RhB-PLA-$PEG_{(E)}$ copolymers were named $PEG_{0\%}$-FNPs, $PEG_{2\%}$-FNPs and $PEG_{8.5\%}$-FNPs, respectively.

Once prepared, requirements for the mucus-penetrating ability of NPs were assessed in terms of suitable morphology, mean size, surface charge, surface PEG density, and conformation of PEG chains on the NP surface. Moreover, their cytocompatibility on human bronchial epithelial cells (16-HBE), the ability to elude steric interactions with mucin fibers and to diffuse through CF-AM was evaluated as function of surface PEG coverage.

Then, ibuprofen was chosen as drug to be administrated by pulmonary delivery, by using mucus-penetrating NPs as tool to overcome the limitations caused by the poor penetration of drugs through the CF high dense and viscoelastic mucus barrier.

Ibuprofen, a non-steroidal anti-inflammatory (NSAID), reduces the extreme inflammation in CF lungs and, a recently discovered, possesses a CFTR corrector [27] and antimicrobial activity.

Thus, ibuprofen loaded mucus-penetrating NPs were prepared and characterized. After having determinated the ibuprofen content into NPs, ibuprofen release profile and uptake capacity within the lung epithelial cells in presence of CF-AM was tested and compared to free drug.

3.4.1 Assessment of requirements for mucus penetration ability

Three fundamental requirements are needed to give to drug delivery systems the mucus-penetrating properties: size and morphology, surface charge and chemical surface property of NPs [99].

Considered that the average 3D mesh spacing of CF sputum is in the range between 60 and 300 nm, generally particles with size in this range are able to diffuse through pores generated by the dense fiber mesh of CF mucus. Moreover, modulating surface chemistry is of considerable importance in order to confer a strongly inert particle surface to the formation of mucoadhesive interactions. Particle surface charge too positive or negative may indicate the formation of attractive or repulsive interactions with mucus components [100], that would prevent the diffusion of particles in mucus [87]. Many evidence have demonstrated that mucus-penetrating properties could generated into particles by pegylation, selecting PEG molecular weight sufficiently low to avoid mucoadhesive interactions with mucins, and with a suitable PEG coating density to effectively shield or protect the hydrophobic particle core [89, 101]. In fact, a brush-like PEG conformation would facilitate the penetration of pegylated particles through the mucus layer [102].

For this reason, size, morphology, ζ potential and surface PEG density were evaluated to understand if prepared $PEG_{0\%}$-FNPs, $PEG_{2\%}$-FNPs and $PEG_{8.5\%}$-FNPs possessed the requirements necessary to the mucus-penetrating ability.

Size morphology and ζ potential

$PEG_{0\%}$-FNPs, $PEG_{2\%}$-FNPs and $PEG_{8.5\%}$-FNPs were produced by using the high pressure homogenization (HPH)-solvent evaporation method described in 3.3.2 paragraph and were characterized in terms of mean size, PDI and ζ potential in aqueous PBS solution, and data are reported in table 14.

Table 14: Mean size, PDI and ζ potential of FNPs in PBS before and after freeze-drying.

Before freeze-drying			
FNPs	**Mean Size (nm)**	**PDI**	**ζ Potential (mV)**
$PEG_{0\%}$-FNPs	167.8 ± 6.8	0.262 ± 0.026	-6.86 ± 0.76
$PEG_{2\%}$-FNPs	182.6 ± 7.1	0.225 ± 0.015	-5.72 ± 0.25
$PEG_{8.5\%}$-FNPs	191.8 ± 2.2	0.198 ± 0.017	-3.88 ± 0.32
After freeze-drying			
$PEG_{0\%}$-FNPs	139.4 ± 3.6	0.208 ± 0.018	-8.00 ± 0.16
$PEG_{2\%}$-FNPs	141.2 ± 2.3	0.226 ± 0.015	-7.45 ± 0.39
$PEG_{8.5\%}$-FNPs	185.4 ± 9.7	0.158 ± 0.020	-5.50 ± 0.44

As can be seen, main size values of obtained FNPs are quite similar, ranging between 167.8 and 191.8 nm. In order to evaluate how the freeze drying process could affect mean sizes, PCS analysis was repeated after the freeze-drying in the presence of a cryoprotectant. As shown also in table 14, mean size and PDI values of $PEG_{0\%}$-FNPs, $PEG_{2\%}$-FNPs and $PEG_{8.5\%}$-FNPs are not significantly different from those obtained before the freeze-drying process, showing how the presence of trehalose as cryoprotectant has been useful in order to maintain the technological properties of FNPs.

All NP populations seem to be quite mono-dispersed being PDI around 0.2, as attended from the use of the HPH-solvent evaporation method.

In table 14, ζ potential values in a PBS aqueous solution, before and after freeze-drying, are reported. $PEG_{0\%}$-FNPs, $PEG_{2\%}$-FNPs and $PEG_{8.5\%}$-FNPs showed a slightly negative ζ potential values and, also in this case, no significant differences are evidenced between ζ potential values before (-6.86, -5.72 and -3.88 mV, respectively) and after (-8.00, -7.45, -5.50 mV, respectively) the freeze-drying process, confirming the absence of aggregation due to the freeze-drying process.

Images of $PEG_{0\%}$-FNPs, $PEG_{2\%}$-FNPs and $PEG_{8.5\%}$-FNPs, obtained by using an inverted epifluorescence microscope after the freeze drying process, are shown in figure 75.

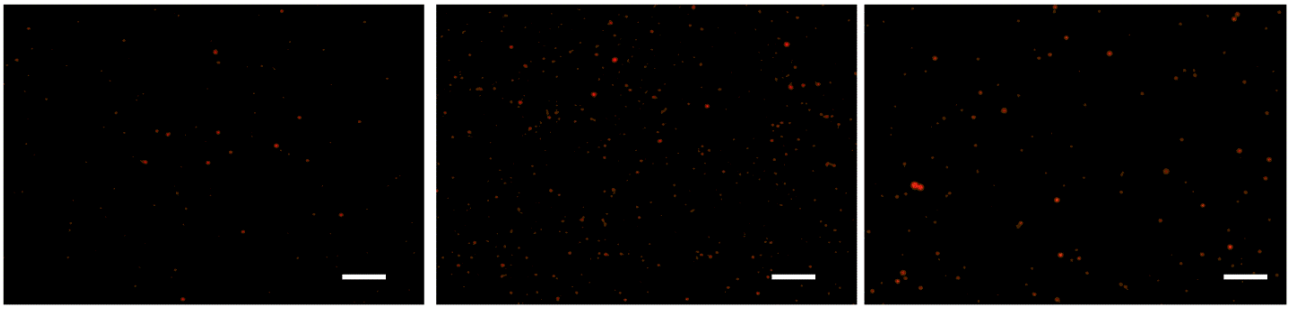

Fig.75: Fluorescence images of $PEG_{0\%}$-FNPs, $PEG_{2\%}$-FNPs and $PEG_{8.5\%}$-FNPs aqueous dispersions (bar represents 20 μm).

All samples possess high fluorescent properties, giving to these FNPs the necessary fluorescence for in vitro imaging application, allowing their tracking in further experiments useful to evaluate their mucus-penetrating properties.

Atomic force microscopy (AFM) measurements obtained for $PEG_{2\%}$-FNPs and $PEG_{8.5\%}$-FNPs are shown in figure 76. AFM, used to study the detailed morphology of the NPs, gave clear 3D morphological images, highlighting a spherical nanoparticle shape and homogenous size.

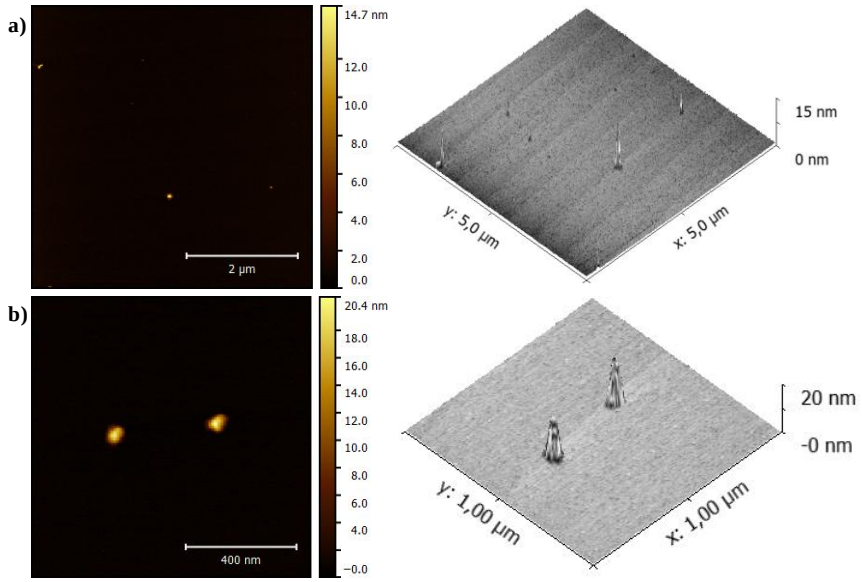

Fig.76: AFM images of $PEG_{2\%}$-FNPs (a) and $PEG_{8.5\%}$-FNPs (b).

Surface PEG density

In order to evaluate the effective amount of PEG moieties on the surface of $PEG_{2\%}$-FNPs and $PEG_{8.5\%}$-FNPs, a ^1H NMR study was carried out [141–143].

Firstly, a calibration curve was carried out with PEG solutions in D_2O, in concentration ranging between 10^{-7} and 10^{-5} M by measuring the signal at 3.6 ppm and by using RhB as internal standard.

By comparing the integrals of the PEG peak in the spectra of $PEG_{2\%}$-FNPs and $PEG_{8.5\%}$-FNPs dispersions in D_2O to the calibration curve, the quantity of PEG on the FNPs surface was found to be equal to respectively 0.00162 and 0.00432 mmol of PEG, increasing as DD_{PEG} of starting copolymers increases from 2 to 8.5 mol%. These amounts corresponds to about the 61 and 56 mol % of the total amounts of PEG embedded into $PEG_{2\%}$-FNPs and $PEG_{8.5\%}$-FNPs, demonstrating as the highest part of PEG molecules are on the FNPs surfaces.

By assuming all surface PEG chains were full length of 2 kDa PEG, the surface PEG density [Γ] was calculated as the number of PEG molecules per 100 nm^2 NP surface area.

PEG density can be calculated [88] by dividing the total PEG content (M PEG, mol) detected by ^1H NMR, by the total surface area of all FNPs as in the following equation:

$$[\Gamma] = [\frac{M_{PEG} \times 6.02 \times 10^{23}}{\frac{W_{NP}}{d_{NP}} / \frac{4}{3}\pi(D/2)^3} / 4\pi(D/2)^2] \times 100$$

where W_{NP} is the total mass of NPs, d_{NP} is the density of NP (here it is assumed that the density of NPs is equal to the density of polymer, 1.21 g/mL for PLA), D is the particle diameter as measured by the dynamic light scattering.
By using this formula [Γ] was calculated and reported in the table 15.

Table 15: Amount of PEG moieties on the NP surface, surface PEG density [Γ] and ratios of PEG density to full surface coverage [Γ/Γ*] of $PEG_{2\%}$-FNPs and $PEG_{8.5\%}$-FNPs.

FNPs	Amount of PEG on NP surface (mmol)	[Γ] (#PEG/100 nm^2)	[Γ/Γ*] ratio
$PEG_{2\%}$-FNPs	0.00162 ± 0.00021	30 ± 3.8	2.7 ± 0.3
$PEG_{8.5\%}$-FNPs	0.00432 ± 0.00013	100 ± 2.9	9.1 ± 0.4

The [Γ] obtained values for $PEG_{2\%}$-FNPs and $PEG_{8.5\%}$-FNPs demonstrated their high surface PEG density: 30 and 100 molecules of PEG per 100 nm^2 are located on the NPs surface, which correspond to about 18,000 and 108,000 molecules respectively of PEG.
In order to assess the entity of the surface PEG density and the PEG chains conformation on the NP surface, [Γ*], which represent the number of unconstrained PEG molecules that occupy 100 nm^2 of particle surface area was calculated. In order to determine [Γ*], the surface area occupied by a single PEG chain could be calculated considering that a single PEG chain occupies an area at the interface given by a sphere of diameter ξ, as elsewhere reported [88]:

$$\xi\ (\mathrm{nm}) = 0.076\ \sqrt{\mathrm{m}_{\mathrm{PEG}}}$$

where m_{PEG} is the molecular weight of the PEG chain. The surface area occupied by one PEG molecule can be determined from $\pi(\xi/2)^2$. ξ for PEG 2 kDa was calculated and resulted to be 3.4 nm and occupies an area that is 9.07 nm^2. Then, the number of PEG molecules to fully cover 100 nm^2 surface area, [Γ*], is 11.025.
[Γ/Γ*] resulted to be 2.7 and 9.1 for $PEG_{2\%}$-FNPs and $PEG_{8.5\%}$-FNPs respectively (table 15). Both these values are higher than 1, indicating an high surface PEG density in produced NPs, where PEG molecules are in a brush-like conformation.
The brush-like conformation assumed by PEG chains on the FNP surfaces was further confirmed by comparing the surface PEG density to the Flory Radius (F) [144] which

represents the end-end distance from one end of a polymer to the other end, that resulted to be about 9.5 nm for 2 KDa PEG [145].

Since $PEG_{2\%}$-FNPs and $PEG_{8.5\%}$-FNPs have an high surface PEG density (30 and 100 chain of PEG per 100 nm^2 respectively) the distance between the attachment points of PEG molecules on the FNP surfaces is smaller than the PEG end-end distance (9.5 nm), avoiding the possibility to create a loop on the FNPs surface. So, in both FNPs, PEG chains will acquire a brush regime, with long, thin bristles of PEG extending from the NP surface. This brush like conformation is a need for imparting mucus penetration properties to NPs. In fact, as reported elsewhere [102] the traditional 'brush' PEG corona would facilitate the penetration of the pegylated particles through the mucus layer and the subsequent interaction with the mucosa, which would promote their absorption by mucosal cells. On the contrary, pegylated NPs with a loop conformation (mushroom) would increase the time of residence of the adhered fraction of particles on the mucus layer.

Others polymeric NP systems [88, 101]'[146],with similar characteristics in terms of size, zeta potential, surface PEG density and PEG chains conformation, demonstrated a strong ability to rapidly penetrate the human mucus.

If compared to them, produced dense brush-like PEG coated NPs ($PEG_{2\%}$-FNPs and $PEG_{8.5\%}$-FNPs) could strongly possess the ability to diffuse through mucus layers, without undergoing significant steric obstruction in pores generated by mucin fibers meshes and without establishing attractive or repulsive mucoadhesive interactions with the mucin fibers.

3.4.2 Evaluation of FNPs penetration through CF-AM

The obtained pegylated FNPs seemed to possess all requirements necessary for mucus penetrating properties. So, in order to investigate their mucus-penetrating ability, the CF-AM mucus model was used.

Firstly, the interactions between FNPs and CF-AM were evaluated by turbidimetric measurements [65]. In particular, CF-AM dispersions of $PEG_{0\%}$-FNPs, $PEG_{2\%}$-FNPs and $PEG_{8.5\%}$-FNPs were prepared and the absorbance at the λ of 650 nm was measured during 24 h incubation at 37°C.

Obtained data are reported in figure 77 as function of incubation time.

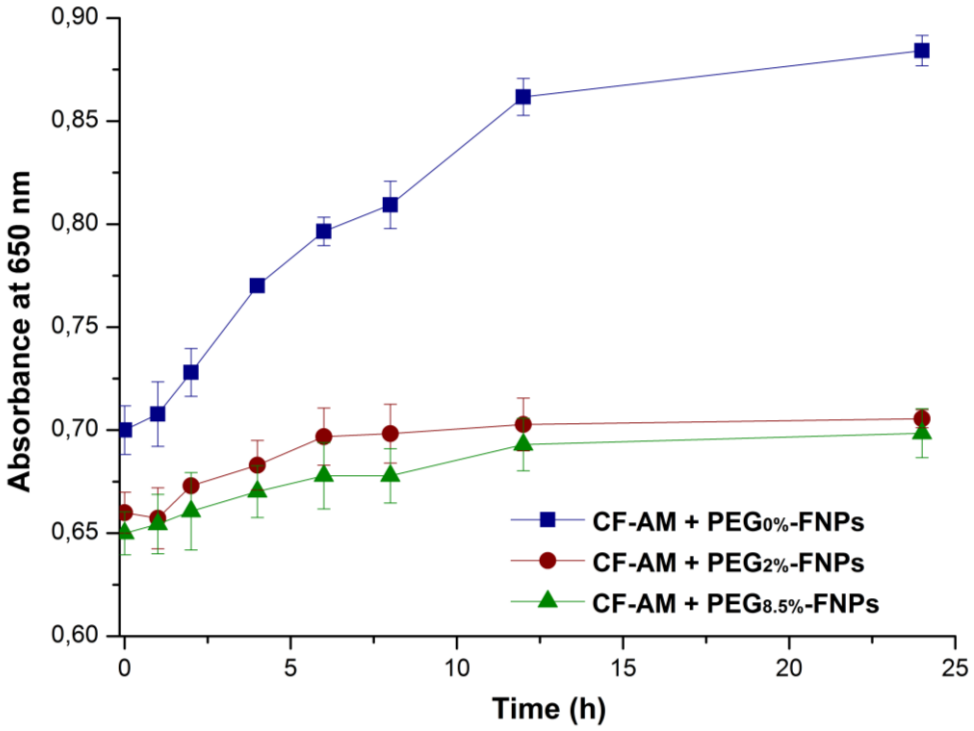

Fig.77: Turbidity of $PEG_{0\%}$-FNPs, $PEG_{2\%}$-FNPs and $PEG_{8.5\%}$-FNPs dispersions in CF-AM, after incubation at 37 ° C as function of incubation time.

Since absorbance at λ 650 nm of $PEG_{0\%}$-FNPs, $PEG_{2\%}$-FNPs and $PEG_{8.5\%}$-FNPs water dispersions is almost the same, the different values of turbidity obtained at time 0, when the FNPs are dispersed in CF-AM, evidenced an immediate difference in the interaction behavior of FNPs with mucus components, such as DNA or mucin fibers.

As evident from the graph, the absorbance of $PEG_{0\%}$-FNPs sample at time 0 is significantly higher than that of pegylated samples (** $p < 0.01$), indicating that interactions with mucin fibers are established from the beginning. Moreover, the absorbance at 650 nm for $PEG_{0\%}$-FNPs sample increased significantly until 24 h (** $p < 0.01$), indicating that these interactions progressively increased over time.

Contrariwise, $PEG_{2\%}$-FNPs and $PEG_{8.5\%}$-FNPs did not show a similar behavior, being absorbance at 650 nm not significantly different at 0 and 24 h. These results, suggesting the not occurring of interactions between pegylated FNPs and CF-AM components, indicate the potentiality of these FNPs to penetrate through the mucus layer.

Measurements of interactions between FNPs and CF-AM was also assessed by evaluation of the ζ potential of FNPs dispersions in CF-AM [65] during 24 h incubation at 37 ° C (figure 78).

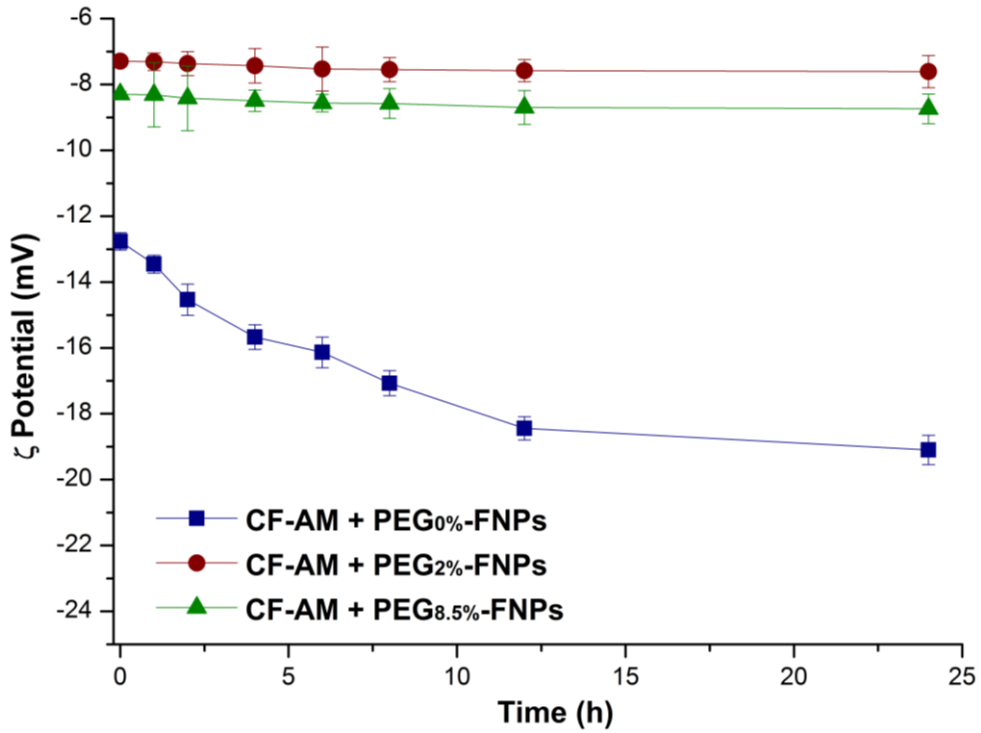

Fig.78: ζ potential values of $PEG_{0\%}$-FNPs, $PEG_{2\%}$-FNPs and $PEG_{8.5\%}$-FNPs dispersions in CF-AM as function of incubation time at 37°C.

Data confirmed the development of interactions between $PEG_{0\%}$-FNPs and mucin fibers interspersed in the mucus layer having ζ potential values increasing significantly over 24 h (** $p<0.01$), while demonstrated that $PEG_{2\%}$-FNPs and $PEG_{8.5\%}$-FNPs do not interact with mucins in CF-AM, being values constant over 24 h.

These results showed how surface pegylation has allowed FNPs to avoid the mucoadhesive interactions within mucin fibers, conferring to both $PEG_{2\%}$-FNPs and $PEG_{8.5\%}$-FNPs an high potential of mucus penetration.

In the light of the encouraging results so far obtained, CF-AM was also used to study the mucus-penetrating ability of FNPs by using a penetration test as reported elsewhere [65, 136]. This test allows to exploit the presence of RhB covalently linked to all copolymer based FNPs, with an effective tracking of FNPs through the mucus layer by using the commonly used detection technique, as UV spectrophotometry.

In particular, $PEG_{0\%}$-FNPs, $PEG_{2\%}$-FNPs and $PEG_{8.5\%}$-FNPs CF-AM dispersions were placed each one in a vial over a CF-AM layer. Below the AM layer, an agarose gel was present with the function to capture FNPs which could diffuse through the CF-AM layer. Each vial was then incubated at 37°C and at regular time frames all the CF-AM were withdrawn.

Finally, agarose gels were rinsed with distilled water, melted at 60°C, placed in quarts cuvettes and analysed by UV spectrophotometry. This procedure is schematized in Scheme 8, reported in the experimental part of this thesis.

The absorbance at the λ of 561 nm (given by RhB linked to FNPs) was recorded and reported in figure 79, as function of incubation time for each sample.

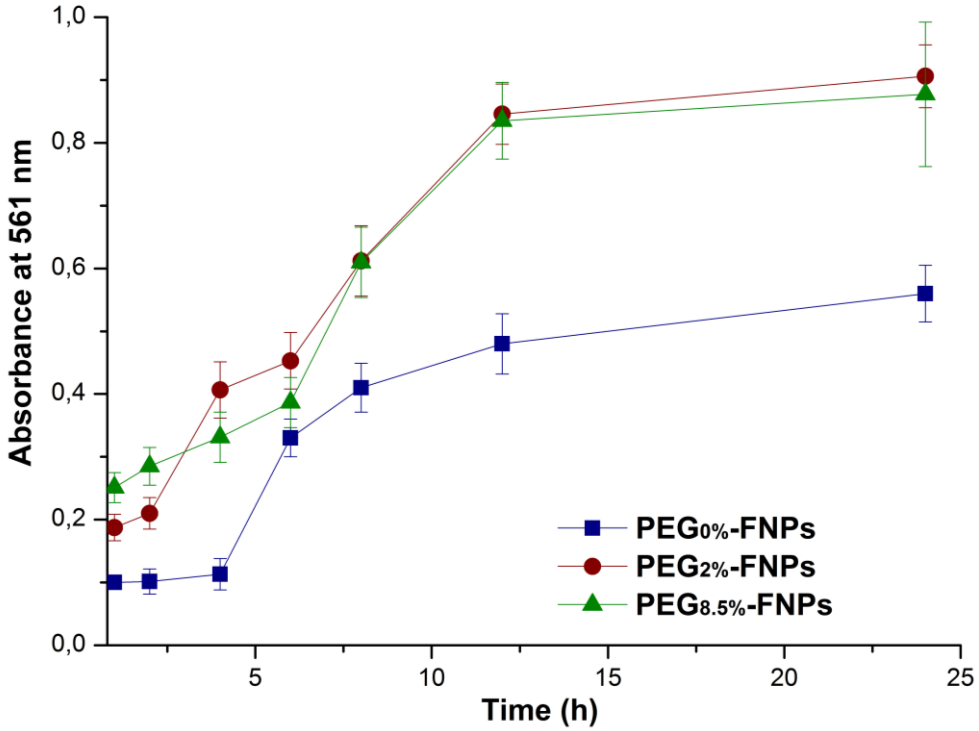

Fig.79: Absorbance at 561 nm of agarose gels recovered after incubation with $PEG_{0\%}$-FNPs, $PEG_{2\%}$-FNPs and $PEG_{8.5\%}$-FNPs as a function of time at 37°C.

Results demonstrated that all FNPs samples are able to penetrate through the mucus layer but the amount of FNPs that diffuse increases as a function of surface PEG density at the same incubation time. In fact, after 2 h incubation, the absorbance at 561 nm for $PEG_{8.5\%}$-FNPs is significantly higher to that obtained for $PEG_{2\%}$-FNPs (* $p < 0.05$) and for $PEG_{0\%}$-FNPs (** $p<0.01$), and the same value is significantly higher for $PEG_{2\%}$-FNPs (** $p < 0.01$) compared to that obtained with $PEG_{0\%}$-FNPs. Moreover, this value is still significantly higher for pegylated FNPs (** $p<0.01$) compared to that obtained for $PEG_{0\%}$-FNPs over 24 h incubation time, with the only exception at 6 h time point.

In particular, the percentage of FNPs reaching the agarose gel, expressed as percentage ratio between the absorbance at 561 nm detected in the agarose gel layer at each time point and that detectable if all the FNPs reached the gel, is equal to 7.1 and 7.9 % for $PEG_{0\%}$-FNPs, equal to

14.7 and 28.5 % for the $PEG_{2\%}$-FNPs, and equal to 20.0 and 26.2 % for $PEG_{8.5\%}$-FNPs, respectively after 2 and 4 hours incubation in mucus.

These results demonstrated that pegylated FNPs were more mucus-penetrating than unpegylated ones. This result is further confirmed by imaged acquired repeating the same experiment in presence of a larger volume of CF-AM between FNPs deposition zone (upperside) and the agarose gel (lower side), as reported in figure 80.

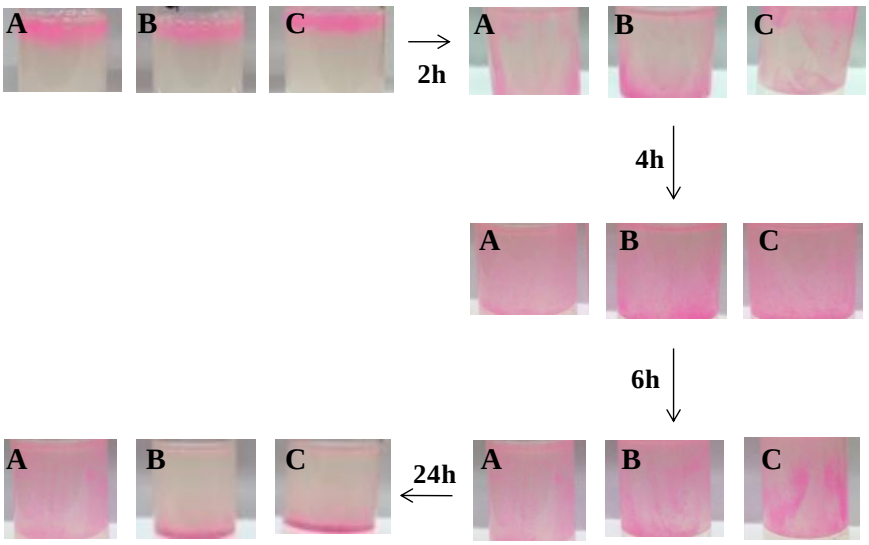

Fig.80: Visual inspection of $PEG_{0\%}$-FNPs (A), $PEG_{2\%}$-FNPs (B) and $PEG_{8.5\%}$-FNPs (C) penetration as a function of incubation time at 37°C.

As shown in the figure 80, $PEG_{2\%}$-FNPs and $PEG_{8.5\%}$-FNPs penetrated more quickly through the mucus layer since first hours, contrary to $PEG_{0\%}$-FNPs that remained mostly suspended within the mucus layer, confirming results previously showed.

Results obtained are in agreement with the other mucus-penetrating particle systems [88, 146], where a dense PEG brush configuration was found to allow NPs to rapidly penetrate through highly viscoelastic human mucus secretions by minimizing adhesive interactions between NPs and mucus components.

However, the obtained percentage of mucus-penetrated FNPs showed how the chemical nature of NPs matrix, based on copolymers synthesized in this work, allowed an higher penetration through mucus than other mucus-penetrating particle systems based on similar pegylated polyesters copolymers [65, 146].

Indeed, the percentage of mucus-penetrated FNPs deposed on the mucus layer for $PEG_{2\%}$-FNPs and $PEG_{8.5\%}$-FNPs is respectively the 28.5 and 26.2 % of FNPs after 4h incubation vs

the about 15 % for NPs based on poly(lactide-co-glycolide)–polyethylene glycol copolymers (PLGA–PEG) (with PEG 2 or 5 kDa) [146] obtained at the same incubation time or the about 10 % for tobramycin containing PLGA-PEG NPs [65] obtained after 24 h incubation.
Taken this consideration together to the ability of $PEG_{0\%}$-FNPs to allow a mucus-penetration even if at higher incubation time, we could hypothesize that the presence of PHEA, with its hydrophilic and neutral nature, in NPs matrix could further shield and protect the hydrophobic polyester NPs core, improving the mucus-penetration ability at long term.

3.4.3 Ibuprofen containing mucus-penetrating FNPs

Ibuprofen containing FNPs, prepared by following the same method used to prepare empty FNPs, were obtained starting from PHEA-RhB-$PLA_{(B)}$, PHEA-RhB-PLA-$PEG_{(D)}$ and PHEA-RhB-PLA-$PEG_{(E)}$ copolymers, and were named Ibu-$PEG_{0\%}$-FNPs, Ibu-$PEG_{2\%}$-FNPs and Ibu-$PEG_{8.5\%}$-FNPs, respectively.
All FNPs showed a good drug loading capacity, being 19.0, 13.6 and 12.8 wt% for $PEG_{0\%}$-FNPs, $PEG_{2\%}$-FNPs and $PEG_{8.5\%}$-FNPs respectively, which correspond to an entrapment efficacy respectively of 82.2, 59.1 and 55.7 wt%, as showed in table 16.

Table 16: Drug loading (DL,% wt), efficacy entrapment (EE % wt), mean size, polydispersity PDI and ζ potential of ibuprofen containing FNPs.

FNPs	DL% wt	EE% wt	Mean size (nm)	PDI	ζ Potential (mV)
Ibu-$PEG_{0\%}$-FNPs	18.9 ± 1.2	82.2 ± 5.2	126.3 ± 6.3	0.214 ± 0.043	-7.80 ± 0.21
Ibu-$PEG_{2\%}$-FNPs	13.6 ± 0.7	59.1 ± 3.1	156.7 ± 3.8	0.187 ± 0.025	-5.93 ± 0.16
Ibu-$PEG_{8.5\%}$-FNPs	12.8 ± 0.9	55.7 ± 3.9	186.8 ± 8.2	0.218 ± 0.032	-3.60 ± 0.44

In table 16, the characterization of freeze-dried ibuprofen containing FNPs also in terms of mean size, PDI and ζ potential in PBS is reported. As can be seen, main size values, PDI and ζ potential values of ibuprofen containing FNPs are quite similar to empty FNPs, showing how the purification process allowed us to successfully remove the amount of ibuprofen not entrapped into FNPs.
Once incorporated, ibuprofen release assays in presence of CF-AM were performed by using a vertical Franz-type diffusion cell [147], in order to know the ability of our FNPs to retain the incorporate drug in sink conditions and to ensure a sustained release at the site of action by firstly penetrating the CF-AM layer.

The percentage of ibuprofen released was reported in figure 81 as function of time.

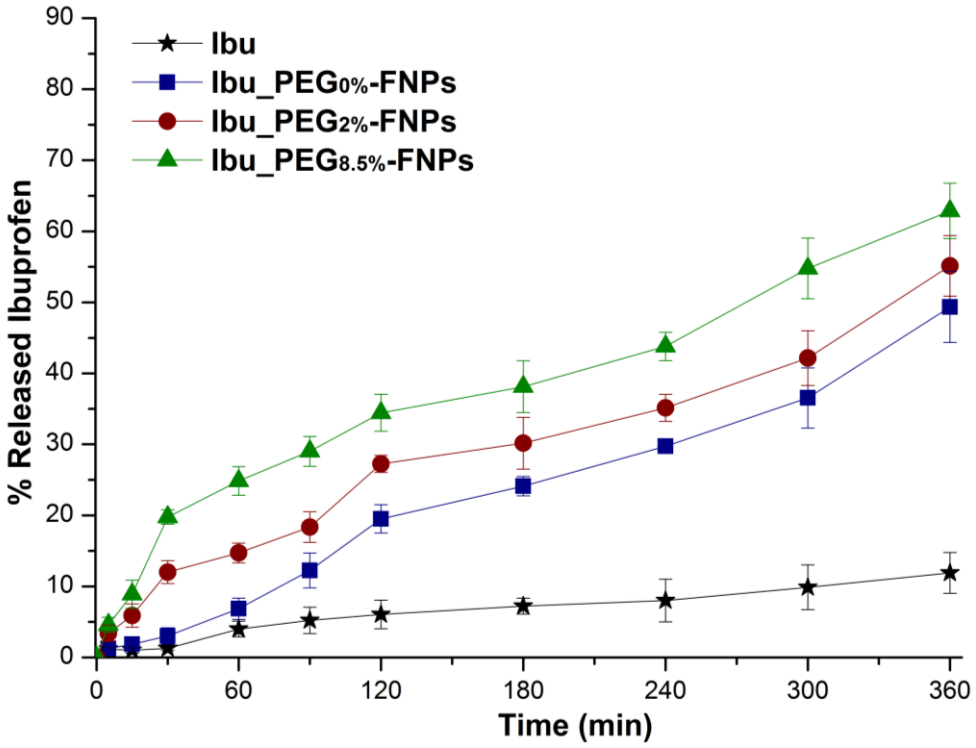

Fig.81: Release of ibuprofen from Ibu-PEG$_{0\%}$-FNPs, Ibu-PEG$_{2\%}$-FNPs and Ibu-PEG$_{8.5\%}$-FNPs through CF-AM layer in Franz-cells as a function of time at 37°C

Results showed that all FNPs samples are able to release an amount of ibuprofen significantly higher if compared to the diffusion of the drug. In fact, the amount of ibuprofen released from FNPs through the mucus layer resulted to be more than the 50% of the entrapped drug into FNPs placed in the donor chamber until 6 h, while the amount of ibuprofen diffused through the mucus layer resulted to be about the 9% of the drug placed in the donor chamber of Franz cell.

Furthermore the amount of ibuprofen released from FNPs increases as a function of surface PEG density of FNPs at the same time point. In fact, at 1, 2 and 4h, the amount of ibuprofen released from Ibu-PEG$_{8.5\%}$-FNPs is significantly higher than that obtained from Ibu-PEG$_{2\%}$-FNPs (**$p<0.01$) and for Ibu-PEG$_{0\%}$-FNPs (**$p<0.01$), and the same value is significantly higher for Ibu-PEG$_{2\%}$-FNPs (*$p<0.05$) compared to that obtained with Ibu-PEG$_{0\%}$-FNPs.

These results are perfectly in agreement with data obtained from the evaluation of FNPs penetration through CF-AM, showing how ibuprofen containing pegylated FNPs allowed the delivery of the drug by first rapidly penetrating the CF-AM layer and reaching the receptor chamber, offering a sustained delivery.

A UV detection of samples from the acceptor chamber was recorded at the λ of 561 nm (given by RhB linked to FNPs), in order to determine if the amount of ibuprofen quantified in the acceptor chamber was effectively the ibuprofen released from FNPs and not the ibuprofen encapsulated in FNPs.

No peak occurs at 561 nm, showing that FNPs are not able to permeate the membrane used, and confirming that the essay performed with the Franz-cell was really a release study.

3.4.4 In vitro essays on 16-HBE

In the light of the encouraging results so far obtained, the potential of ibuprofen containing mucus-penetrating FNPs as therapeutic tool for the treatment of inflammation in patients with CF was assessed *in vitro* on 16-HBE cells.

First, cytocompatibility of $PEG_{0\%}$-FNPs, $PEG_{2\%}$-FNPs and $PEG_{8.5\%}$-FNPs was evaluated by the MTS assay on 16HBE cells at different FNPs concentrations after 24 incubation. Moreover, cell viability was also evaluated in the presence of only trehalose used as cryoprotectant, at concentration equal to those used for FNPs. Results are reported in figure 82.

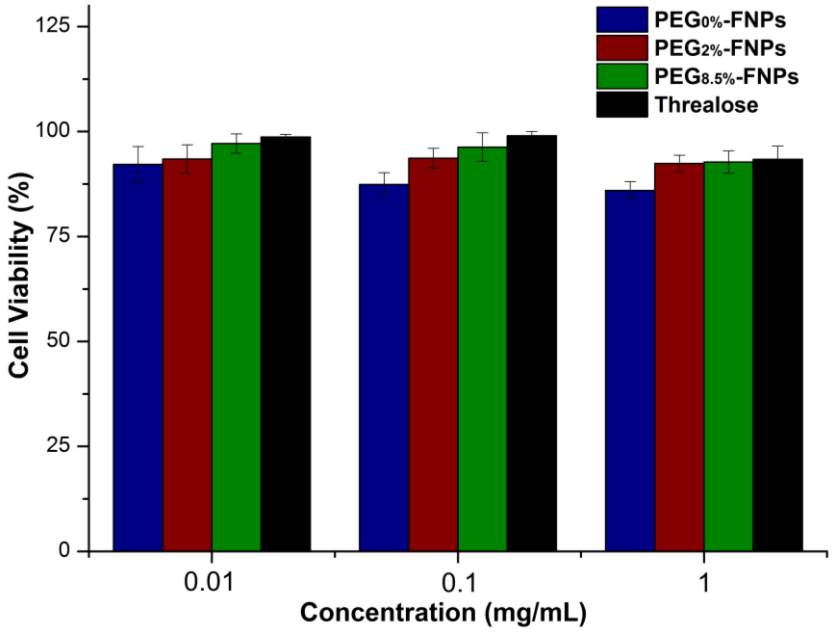

Fig.82: Cell viability % on 16-HBE cells after 24h incubation with $PEG_{0\%}$-FNPs, $PEG_{2\%}$-FNPs and $PEG_{8.5\%}$-FNPs, compared to the viability of to the viability of cells in trehalose-containing medium (Trehalose).

As can be seen, after 24h incubation, all FNPs showed an excellent cytocompatibility at all tested concentrations, showing a cell viability higher than 85% compared to the control consisting of cells alone in the DMEM medium.

Second, the ability of produced mucus-penetrating FNPs to enhance the intracellular uptake of ibuprofen in presence of CF-AM compared to only ibuprofen was determinated by detecting the amount of drug that penetrates into the 16-HBE cells.

To do this, 16-HBE cells were incubated with CF-AM and ibu-FNP dispersions in DMEM and compared to control experiments conducted by incubating 16-HBE cells with CF-AM and a DMEM solution of ibuprofen. After 2 and 4 h incubation the medium was removed.

The cells were washed twice to remove any remaining particles and lysed. The amount of ibuprofen presents in the cell lysate was quantified by HPLC analysis, and data are reported in table 18.

Table 18: Amount of Ibuprofen determined in cell lysate after 4h incubation in presence of CF-AM.

Sample	Ibuprofen amount % uptaked after 4 h incubation
Ibuprofen	4.7 ± 1.2
Ibu-PEG$_{0\%}$-FNPs	9.5 ± 0.9
Ibu-PEG$_{2\%}$-FNPs	11.6 ± 1.8
Ibu-PEG$_{8.5\%}$-FNPs	12.6 ± 1.5

A higher amount of drug was detected into the cells after 2 and 4 h incubation with Ibu-PEG$_{0\%}$-FNPs, Ibu-PEG$_{2\%}$-FNPs and Ibu-PEG$_{8.5\%}$-FNPs compared to the incubation with only ibuprofen.

In particular at 4h for FNPs, the internalized drug amount ranged from the 9.5 to the 12.6 wt % of the starting ibuprofen incubated with 16-HBE cells. This amount is significantly higher (*$p<0.05$) if compared to the internalized drug detected when an ibuprofen suspension was used, which is lower than the 5 wt% of the starting ibuprofen incubated with 16-HBE cells.

Even if the detection of ibuprofen by the HPLC method showed as mucus-penetrating FNPs were able to increase the cell uptake of ibuprofen, it couldn't allow to differentiate the uptake ability of FNPs at different PEG content. So, the same experiments were repeated in order to test cellular uptake of Ibu-FNPs by fluorescence imaging.

Cell nuclei were labelled with the 4′6-diamidino-2-phenylindole (DAPI) fluorescent dye, and images were acquired by using an inverted epifluorescence microscope.
As can be seen in figure 83, both Ibu-$PEG_{2\%}$-FNPs and above all Ibu-$PEG_{8.5\%}$-FNPs showed a higher amount of FNPs uptaked in 16-HBE cells compared to Ibu-$PEG_{0\%}$-FNPs.

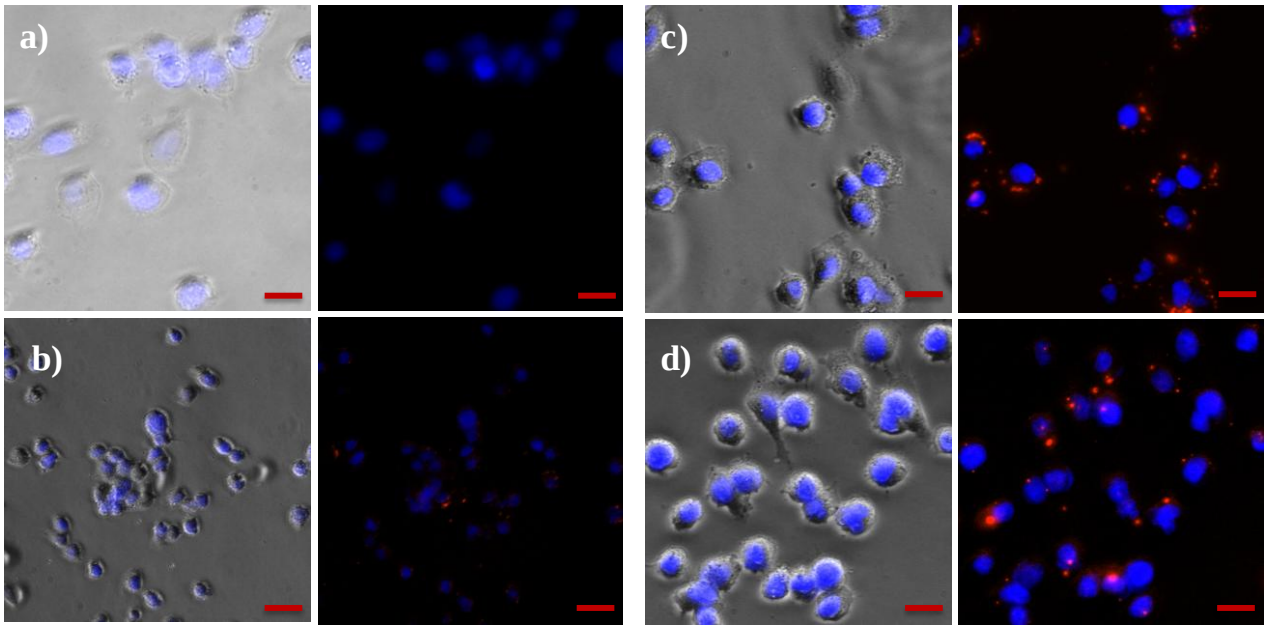

Fig.83: Fluorescence microscopy images of 16-HBE cells treated with a) Ibu, b) Ibu- $PEG_{0\%}$-FNPs, c) Ibu-$PEG_{2\%}$-FNPs and d) Ibu-$PEG_{8.5\%}$-FNPs after 4 h incubation in the presence of CF-AM (bar represents 20 µm).

These results suggest the hypothesis that these pegylated FNPs can be able to diffuse through the CF-AM mucus layer, interact with cell membrane and promote the uptake of encapsulated drug, upon FNPs endocytosis and drug diffusion.

3.4.5 Conclusions

In this paragraph, mucus-penetrating NPs for pulmonary administration of ibuprofen in patients with CF were described. FNPs, empty and loaded with ibuprofen, with mucus-penetrating ability were obtained starting from PHEA-RhB-PLA, PHEA-RhB-PLA-$PEG_{(D)}$ and PHEA-RhB-PLA-$PEG_{(E)}$ copolymers, each one containing 0, 2 and 8.5 mol% of PEG respectively.
All obtained FNPs showed proper sizes lower than 200 nm, slightly negative ζ potential and high biocompatibility on human bronchial epithelium cells.

The FNPs surface evaluation showed as the surface PEG density increases as the PEG derivatization degree (DD_{PEG}) of starting copolymers increases from 2 to 8.5 mol%.

Further investigation demonstrated as pegylated FNPs were coated by a dense brush-like PEG corona, conferring them a great potential to diffuse through a CF artificial mucus (CF-AM) layer. The mucus-penetrating ability of these systems was properly demonstrated and appears to grow as the PEG density increases on the FNP surface.

Ibuprofen release profile and cellular uptake in presence of CF-AM showed how the efficient transport of these NPs through the mucus layer could be a significant opportunity for the treatment of inflammation in patients with CF. In fact, ibuprofen loaded mucus-penetrating nanoparticles could rapidly diffuse through the mucus barrier reaching the mucosal surface, where they could offer a sustained delivery at the site of disease, resulting in superior efficacy, lower required dose and side effects.

3.5 Mucus-penetrating nanoparticles for enhanced intracellular delivery of ivacaftor for the treatment of the defective ion transport in broncho-epithelial cells in CF

In this paragraph, the preparation of mucus-penetrating NPs for pulmonary administration of ivacaftor in patients with CF is described.

In order to improve the drug accumulation in airway epithelial cells, carrier surface has been decorated with a cell-penetrating peptide (CPP) widely used for the enhancement of intracellular delivery of a broad variety of carriers and of their incorporated drugs. The chosen CPP is most intensively studied transactivating transcriptional activator peptide (Tat) derived from the protein transduction domain (PTD) of human immunodeficiency virus type 1 (HIV-1), extending from residues 47 to 57 (YGRKKRRQRRR), rich of positively charged amino acids arginine and lysine.

In order to decorate the surface of produced NPs with the Tat ligand, the CPP was covalently linked to PHEA-PLA backbone, obtaining PHEA-PLA-Tat. Then, FNPs were produced starting from a mixture between PHEA-PLA-Tat and PHEA-RhB-PLA-$PEG_{(F)}$ graft copolymer at the highest pegylation degree, whose synthesis and characterization is described in the 3.3.3 paragraph, by using the nanoprecipitation method. The mixture between PHEA-PLA and PHEA-RhB-PLA-$PEG_{(F)}$ was, instead, used to produce as control.

In order to evaluate the effective achievement of the best mucus-penetrating properties,

Prepared FNPs were analyzed in terms of suitable morphology, mean size, surface charge on the NPs surface. Moreover, their ability to elude steric interactions with mucin fibers and to diffuse through CF-AM was evaluated.

Then, ivacaftor was chosen as drug to be administrated by pulmonary delivery, by using mucus-penetrating NPs as tool to overcome the limitations caused by the poor penetration of drugs through the CF high dense and viscoelastic mucus barrier, potentially enhancing the drug concentration at the site of disease and reducing systemic side effects.

Ivacaftor is a CFTR potentiator that specifically targets the Class III mutations, increasing the open probability of CFTR channels by around 6 fold.

Thus, ivacaftor loaded mucus-penetrating NPs were prepared and characterized. After having determinated the ivacaftor content into NPs, drug release profile in absence or in presence of CF-AM was evaluated. Finally, their cytocompatibility on human bronchial epithelial cells tested after 4 and 24 h incubation.

3.5.1 Synthesis and characterization of PHEA-PLA-Tat

Derivatization of PHEA-PLA with HIV-1 Tat protein to obtain the PHEA- PLA-Tat graft copolymer was carried out by using CDI as coupling agent. In particular, the free carboxyl groups of Tat protein were activated for 4 h by using CDI, and left to react with hydroxyl side groups on PHEA-PLA for 48 h, in organic environment at 40°C.

The synthetic procedure and chemical structure of PHEA-PLA-Tat copolymer is reported in the Scheme 7.

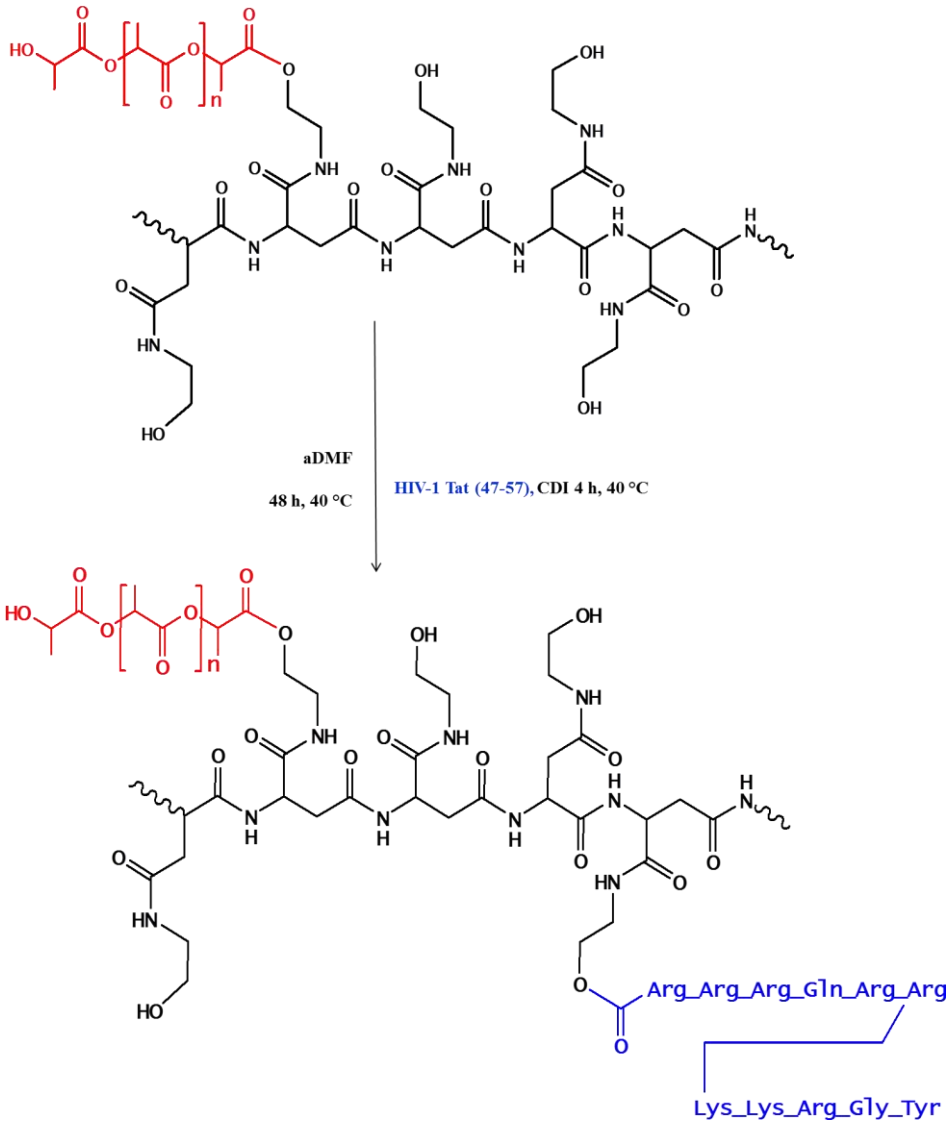

Scheme 7: Synthesis of PHEA-PLA-Tat graft copolymer (n = 194), (red: PLA chains, blue: Tat protein ligand).

The DD_{Tat} of PHEA-PLA-Tat was calculated by determining the amount of Tat molecules on PHEA-PLA-Tat by UV spectrometry. PHEA-PLA-Tat DMF solutions were analyzed at the λ

of 279 nm, by comparing the obtained absorbance, corresponding to the amount of Tat present on the copolymer backbone, to a calibration curve obtained by plotting areas versus standard solution concentrations of Tat in the same solvent. A negligible peak was observed when PHEA-PLA DMF solution was analyzed by UV spectrometry at the λ of 279 nm, which absorbance value was, however, subtracted to that obtained for PHEA-PLA-Tat.

The DD_{Tat} was expressed as mean values of three determinations and resulted to be 1.95 ± 0.05 mol% of repeating units.

SEC analysis confirmed the occurrence of derivatization, being $\overline{M}_w$ of PHEA-PLA-Tat increased if compared to the starting PHEA-PLA, being these one 191 and 184 kDa, respectively.

3.5.2 Preparation and characterization of FNPs

FNPs were produced by following a nanoprecipitation method [148–150]. PHEA-RhB-PLA-$PEG_{(F)}$ and PHEA-PLA-TAT or PHEA-PLA were mixed together at the weight ratio 1:1, dissolved in acetone, placed in a burette, added dropwise to twice-distilled water, and left under stirring for 3 h to form FNPs, without the use of surfactants or stabilizing agents. Residual acetone was removed under reduced pressure and FNP dispersion was, finally, freeze-dried.

FNPs obtained from PHEA-RhB-PLA-$PEG_{(F)}$ and PHEA-PLA were named PEG(FNPs), while FNPs obtained from PHEA-RhB-PLA-$PEG_{(F)}$ and PHEA-PLA-Tat were named Tat-PEG(FNPs). After preparation, PEG(FNPs) and Tat-PEG(FNPs) were characterized in terms of mean size, PDI, and ζ potential in PBS at pH 7.4 by PCS. Analytical data are reported in Table 19.

Table 19: Mean size, PDI and ζ potential in PBS at pH 7.4.

Before freeze-drying			
	Mean Size (nm)	**PDI**	**ζ Potential (mV)**
PEG(FNPs)	48.9 ± 6.0	0.164 ± 0.022	-12.2 ± 2.6
Tat-PEG(FNPs)	54.6 ± 8.7	0.196 ± 0.046	-11.4 ± 1.7
After freeze-drying			
PEG(FNPs)	63.9 ± 9.4	0.208 ± 0.018	-13.1 ± 1.1
Tat-PEG(FNPs)	74.1 ± 5.7	0.214 ± 0.031	-12.0 ± 2.3

As can be seen, main size values of obtained FNPs are quite similar, ranging between 48.9 and 54.6 nm. In order to evaluate how the freeze drying process could affect mean sizes, PCS analysis was repeated after the freeze-drying. Mean size and PDI values of PEG(FNPs) and Tat-PEG(FNPs) are slightly higher from those obtained before the freeze-drying process. Both PEG(FNPs) and Tat-PEG(FNPs) seem to be quite mono-dispersed being PDI around 0.2. In table 19, ζ potential values in a PBS aqueous solution, before and after freeze-drying, are reported. Both PEG(FNPs) and Tat-PEG(FNPs) showed a slightly negative ζ potential values and no significant differences are evidenced between ζ potential values before (-12.2, - and -11.4 mV, respectively) and after (-13.1 and -12.0 mV, respectively) the freeze-drying process. Images of PEG(FNPs) and Tat-PEG(FNPs), obtained by using an inverted epifluorescence microscope after the freeze drying process, are shown in figure 84.

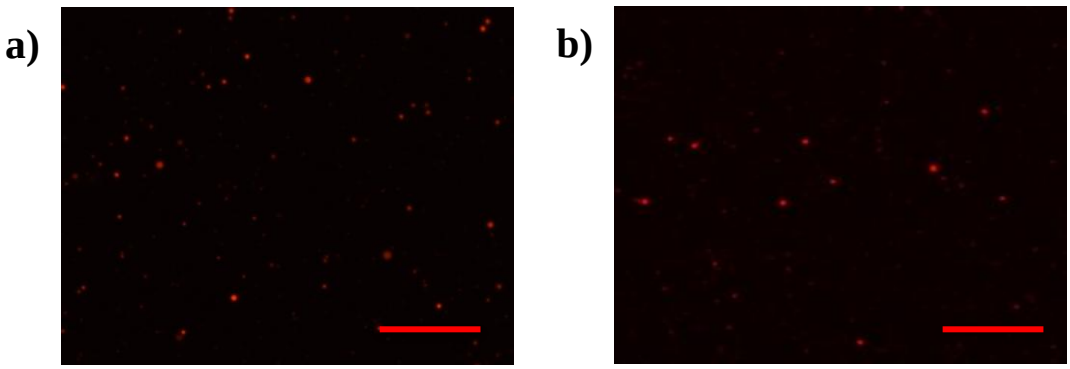

Fig.84: Fluorescence images of (a) PEG(FNPs) and (b) Tat-PEG(FNPs) aqueous dispersions (bar represents 10 µm).

As attended, samples possess high fluorescent properties, giving to these FNPs the necessary fluorescence for in vitro imaging application, allowing their tracking in further experiments useful to evaluate their mucus-penetrating properties.

AFM measurements obtained for Tat-PEG(FNPs) is shown in figure 85. AFM, used to study the detailed morphology of the NPs, gave clear 3D morphological images, highlighting a spherical nanoparticle shape and homogenous.

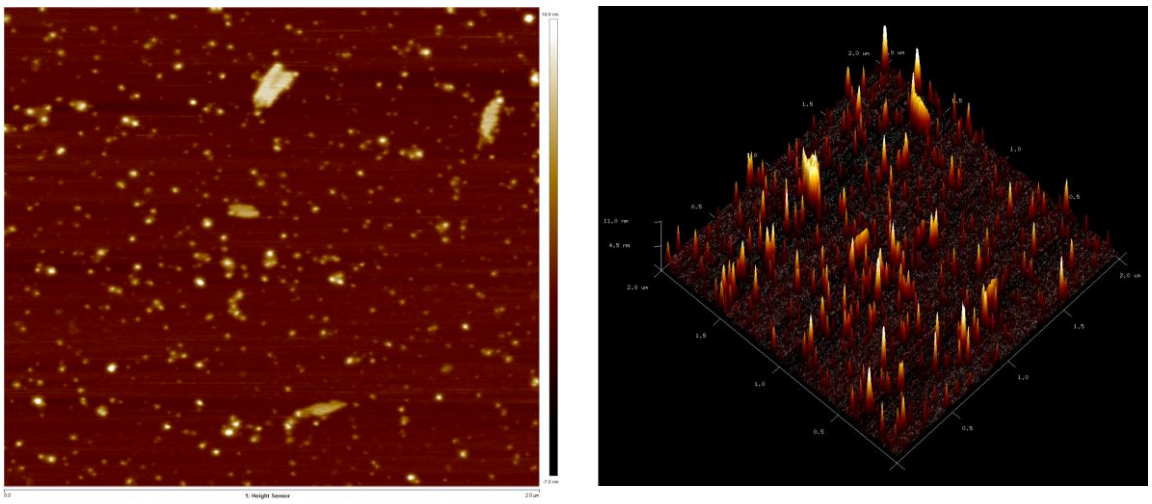

Fig. 85: AFM images of Tat-PEG(FNPs).

3.5.3 Evaluation of FNPs penetration through CF-AM

In order to investigate mucus-penetrating ability of PEG(FNPs) and Tat-PEG(FNPs), CF-AM was used. The interactions between FNPs and CF-AM were evaluated by turbidimetric and ζ potential measurements. In particular, CF-AM dispersions of PEG(FNPs) and Tat-PEG(FNPs) were prepared and the absorbance at the λ of 650 nm and ζ potential was measured during 6 h incubation at 37°C.

Obtained data are reported in figure 86 as function of incubation time.

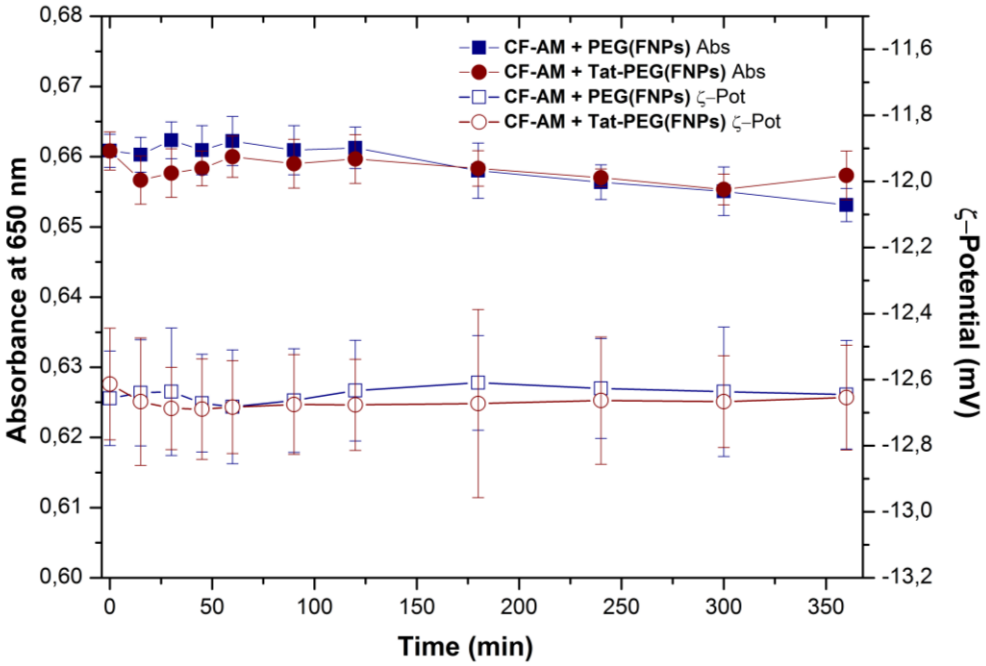

Fig.86: Turbidity and ζ potential values of PEG(FNPs) and Tat-PEG(FNPs) dispersions in CF-AM as function of incubation time at 37°C.

PEG(FNPs) and Tat-PEG(FNPs) show a similar behavior, being absorbance at 650 nm not significantly different between the two samples. The same value is also not significant different over the incubation time. These results, suggesting the not occurring of interactions between both FNPs and CF-AM components, indicate the potentiality of these FNPs to penetrate through the mucus layer.

ζ potential data confirmed the not occurring of interactions between FNPs and CF-AM components, being ζ potential values of the two different samples quite the same over all the incubation time.

These results showed how surface pegylation has allowed FNPs to avoid the mucoadhesive interactions within mucin fibers, conferring to both PEG(FNPs) and Tat-PEG(FNPs) an high potential of mucus penetration. Moreover the presence of Tat protein ligand into the polymer backbone does not exert an influence in the interacting behavior of FNPs with CF-AM components.

In the light of the encouraging results so far obtained, CF-AM was also used to study the mucus-penetrating ability of FNPs by using a penetration test, as reported in 3.4.2 paragraph and showed in the Scheme 8 of the experimental part of this thesis.

PEG(FNPs) and Tat-PEG(FNPs) CF-AM dispersions were placed each one in a vial over a CF-AM layer. Below the AM layer, an agarose gel was present with the function to capture FNPs which could diffuse through the CF-AM layer. Each vial was then incubated at 37°C and at regular time frames all the CF-AM were withdrawn.

Finally, agarose gels were rinsed with distilled water, melted at 60°C, placed in quarts cuvettes and analyzed by UV spectrophotometry.

The absorbance at the λ of 561 nm (given by RhB linked to FNPs) was recorded and reported in figure 87, as function of incubation time for each sample.

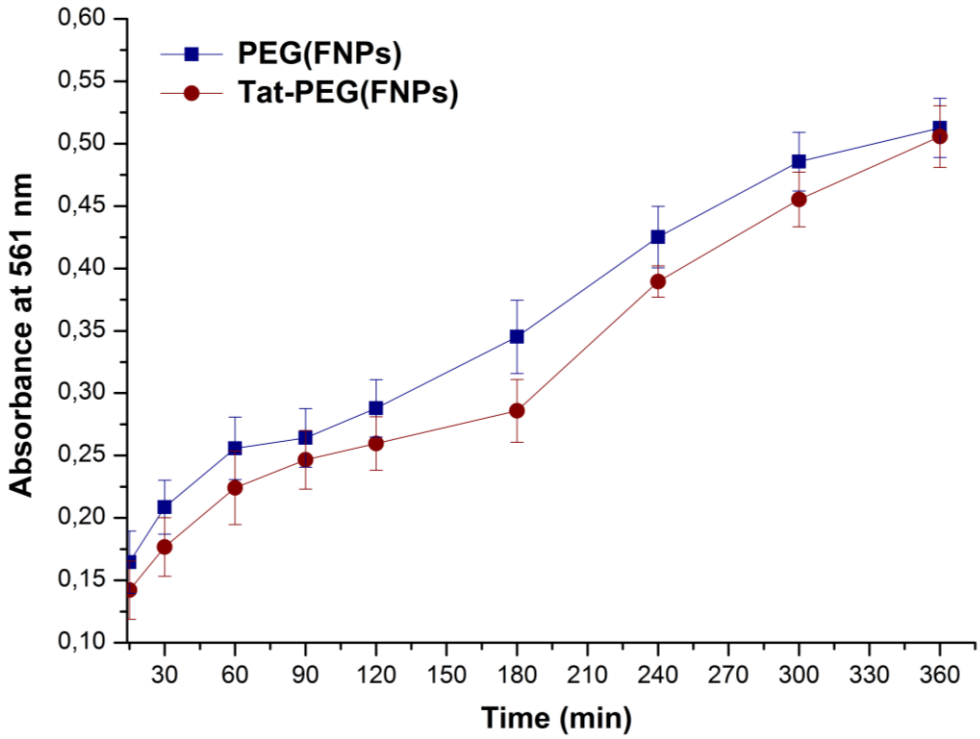

Fig.87: Absorbance at 561 nm of agarose gels recovered after incubation with PEG(FNPs) and Tat-PEG(FNPs) as a function of time at 37°C.

Results demonstrated that both FNPs samples are able to penetrate through the mucus layer but the amount of FNPs that diffuse increases as a function of incubation time.

In fact, the absorbance at 561 nm increased significantly until 6 h (** $p<0.01$), indicating that FNPs penetration progressively increases over time.

Moreover, no significant difference exists between the PEG(FNPs) and Tat-PEG(FNPs) penetration, as evidenced from the graphic in figure 87.

In particular, the percentage of FNPs reaching the agarose gel, expressed as percentage ratio between the absorbance at 561 nm detected in the agarose gel layer at each time point and that detectable if all the FNPs reached the gel, is equal to 35.8 and 35.2 after 6 hours incubation in mucus, respectively for PEG(FNPs) and Tat-PEG(FNPs).

This result is further confirmed by imaged acquired repeating the same experiment in presence of a larger volume of CF-AM between FNPs deposition zone (upperside) and the agarose gel (lower side), as reported in figure 88.

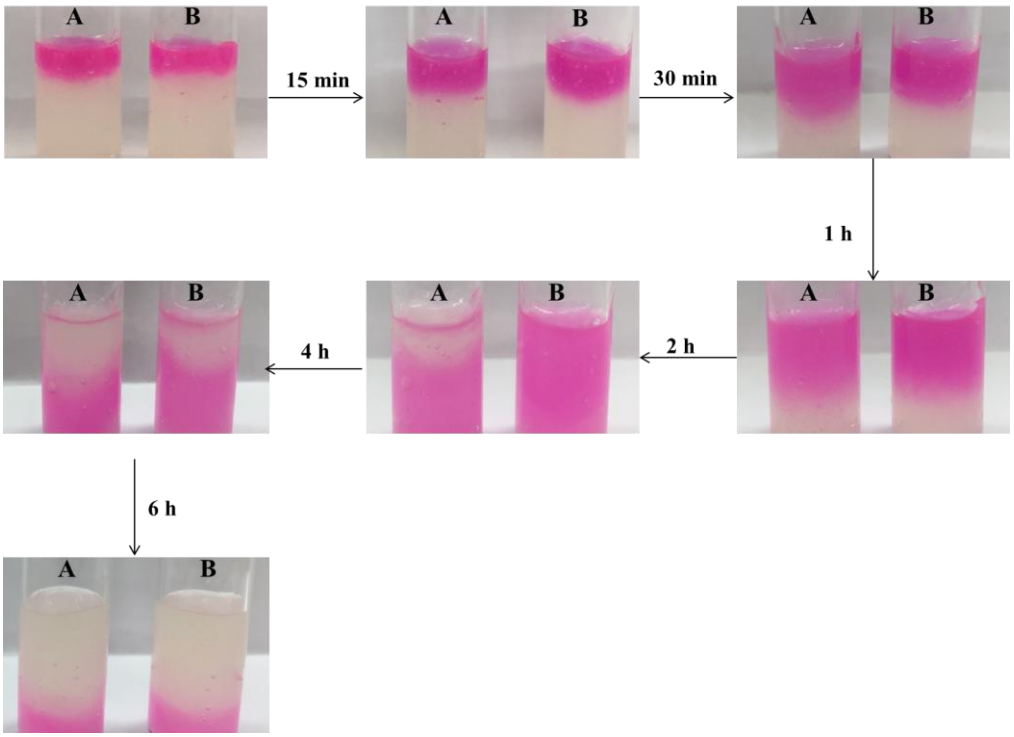

Fig.88: Visual inspection of PEG(FNPs) (A) and Tat-PEG(FNPs) (B) penetration as a function of incubation time at 37°C.

As shown in the figure 88, PEG(FNPs) and Tat-PEG(FNPs) penetrated quickly in CF-AM since first minutes, diffused through the mucus layer and starting from 4h incubation, both FNP samples deposited in the agarose gel layer.

3.4.3 Ivacaftor containing mucus-penetrating FNPs

Ivacaftor containing FNPs, prepared by following the same method used to prepare empty FNPs, were obtained starting from PHEA-RhB-PLA-$PEG_{(F)}$ and PHE-PLA or PHEA-PLA-Tat copolymers in a 1:1 mixture weight ratio, and were named Iva_PEG(FNPs) and Iva_Tat-PEG(FNPs), respectively. In addition to the method described for preparation of empty FNPs, a further step was added in order to remove the drug not entrapped into FNPs by centrifugation. The purified FNP dispersion was then freeze-dried

After freeze-drying, Iva_PEG(FNPs) and Iva_Tat-PEG(FNPs) were characterized in terms of mean size, PDI, ζ potential, DL and EE. Obtained data were reported in table 20.

Table 20: Drug loading (DL,% wt), efficacy entrapment (EE % wt), mean size, polydispersity PDI and ζ potential of ivacaftor loaded FNPs.

FNPs	DL% wt	EE% wt	Mean size (nm)	PDI	ζ Potential (mV)
Iva_PEG(FNPs)	15.2 ± 0.5	76.0 ± 2.5	74.9 ± 5.4	0.218 ± 0.051	-13.8 ± 1.4
Iva_Tat-PEG(FNPs)	15.5 ± 0.7	77.5 ± 3.5	78.6 ± 3.8	0.214 ± 0.037	-12.9 ± 2.1

Iva_PEG(FNPs) and Iva_Tat-PEG(FNPs) showed a good drug loading capacity being 15.2, and 15.5 wt% respectively, which correspond to an entrapment efficacy respectively of 74.9, and 78.6 wt%.

Main size values, PDI and ζ potential values of ivacaftor loaded FNPs are quite similar to empty FNPs, showing how the purification process allowed to successfully remove the amount of ivacaftor not entrapped into FNPs.

Once incorporated, ivacaftor release assays was in PBS at pH 7.4 by using the dialysis method and compared to free drug, in order to know the ability of produced FNPs to retain the incorporate drug in sink conditions and to ensure a sustained release.

Obtained data are reported in figure 89.

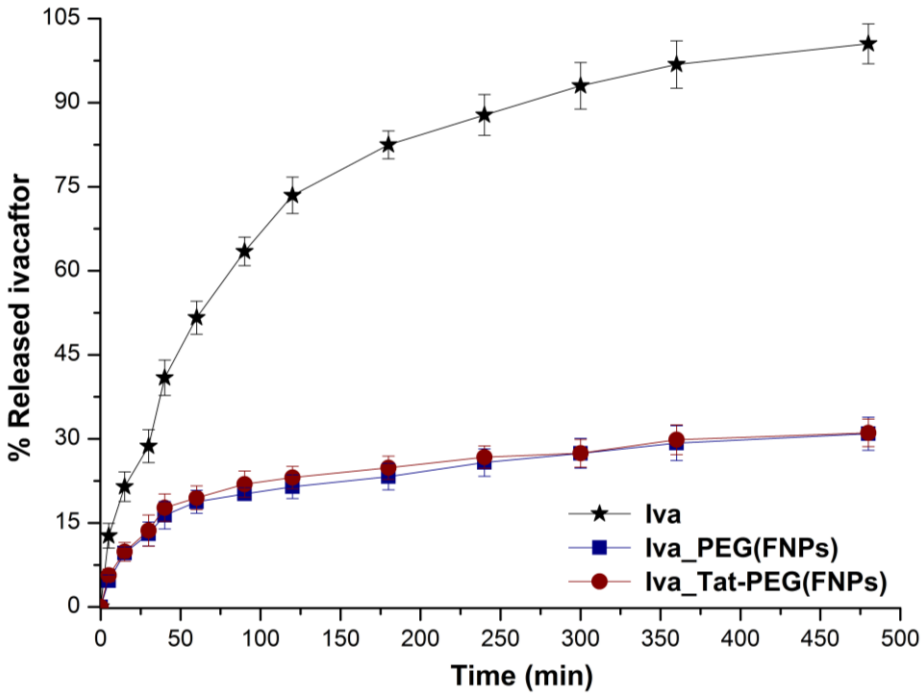

Fig. 89: Release profile of ivacaftor from Iva_PEG(FNPs) and Iva_Tat-PEG(FNPs) as a function of incubation time at 37 °C, compared to the diffusion of ivacaftor trough dialysis membrane in phosphate buffer medium at pH 7.4.

Results showed that when ivacaftor is incroporated in Iva_PEG(FNPs) and Iva_Tat-PEG(FNPs), it is slowly released in the aqueous medium. In fact, after 8 h incubation, the amount of ivacaftor released from both FNP samples reached the 30 wt% of the total amount, while at the same incubation time the free drug diffusion through dialysis membrane reached about the 100 wt%.

Moreover, no significant differences exist between the amount of ivacaftor released from Iva_PEG(FNPs) and Iva_Tat-PEG(FNPs).

Once assessed the ability of produced FNPs to achieve a sustained delivery of ivacaftor, the drug diffusion profile was evaluated in presence of CF-AM by using a vertical Franz-type diffusion cell [147].

The percentage of ivacaftor released from Iva_PEG(FNPs) and Iva_Tat-PEG(FNPs) in presence of CF-AM was reported in figure 90 as function of time.

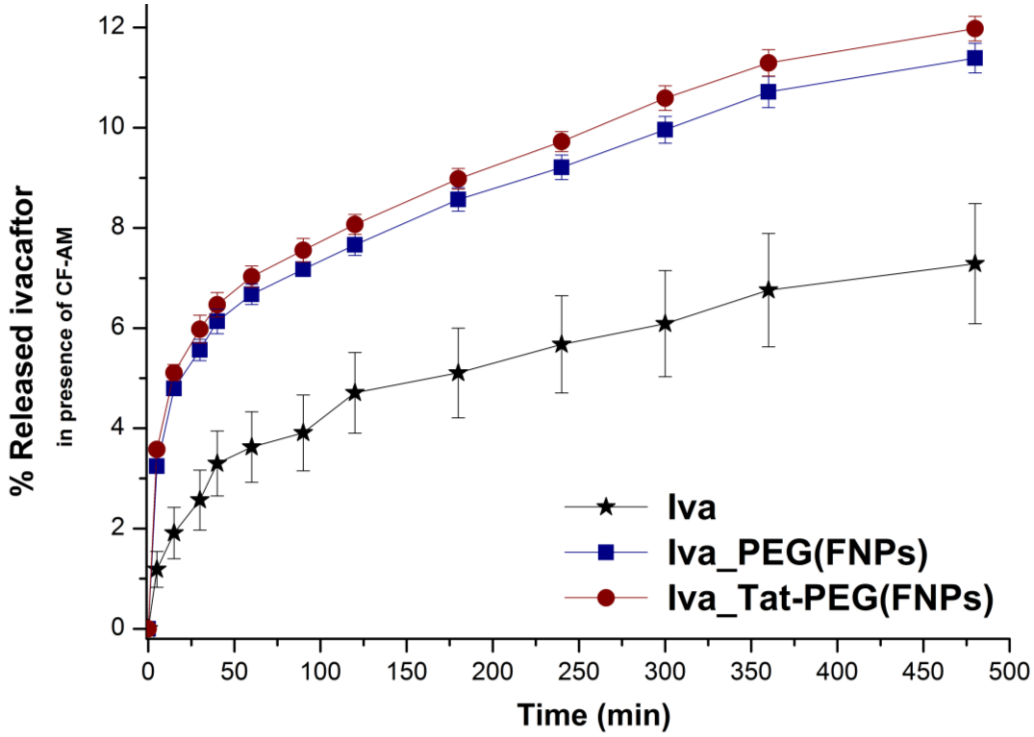

Fig.90: Release of ivacaftor from Iva_PEG(FNPs) and Iva_Tat-PEG(FNPs) in presence of CF-AM in Franz-cells as a function of time at 37°C

Results showed that both FNP samples are able to diffuse through CF-AM and release an amount of ivacaftor significantly higher if compared to the diffusion of the free drug.

In fact, the amount of ivacaftor released from FNPs through the mucus layer resulted to be more than the 12 wt% of the entrapped drug into FNPs placed in the donor chamber until 8 h,

while the amount of free ivacaftor diffused through the mucus layer resulted to be about the 6 wt% of the drug placed in the donor chamber of Franz cell.

Furthermore the amount of Iva_PEG(FNPs) and Iva_Tat-PEG(FNPs) diffused through the mucus layer is not statically different.

These results are perfectly in agreement with data obtained from the evaluation of FNPs penetration through CF-AM, showing how ivacaftor containing FNPs allowed the delivery of the drug by first rapidly penetrating the CF-AM layer and reaching the receptor chamber, offering a sustained delivery.

A UV detection of samples from the acceptor chamber was recorded at the λ of 561 nm (given by RhB linked to FNPs), in order to determine if the amount of ivacaftor quantified in the acceptor chamber was effectively the ivacaftor released from FNPs in presence of CF-AM and not the drug encapsulated in FNPs. Since no peak occurs at 561 nm, showing that FNPs are not able to permeate the membrane used, it is possible to confirm that the essay performed with the Franz-cell is a release study in presence of CF-AM.

3.5.4 In vitro essays on 16-HBE

In the light of the encouraging results so far obtained, the potential of mucus-penetrating Iva_PEG(FNPs) and Iva_Tat-PEG(FNPs), as therapeutic tool for the treatment of defective ion transport in epithelial cells of CF patients, was assessed *in vitro* on 16-HBE cells.

Cytocompatibility of Iva_PEG(FNPs) and Iva_Tat-PEG(FNPs) was evaluated by the MTS assay on 16HBE cells at different ivacaftor concentrations, and compared to free ivacaftor after 4 an 24 h incubation. Obtained data were reported in figure 91.

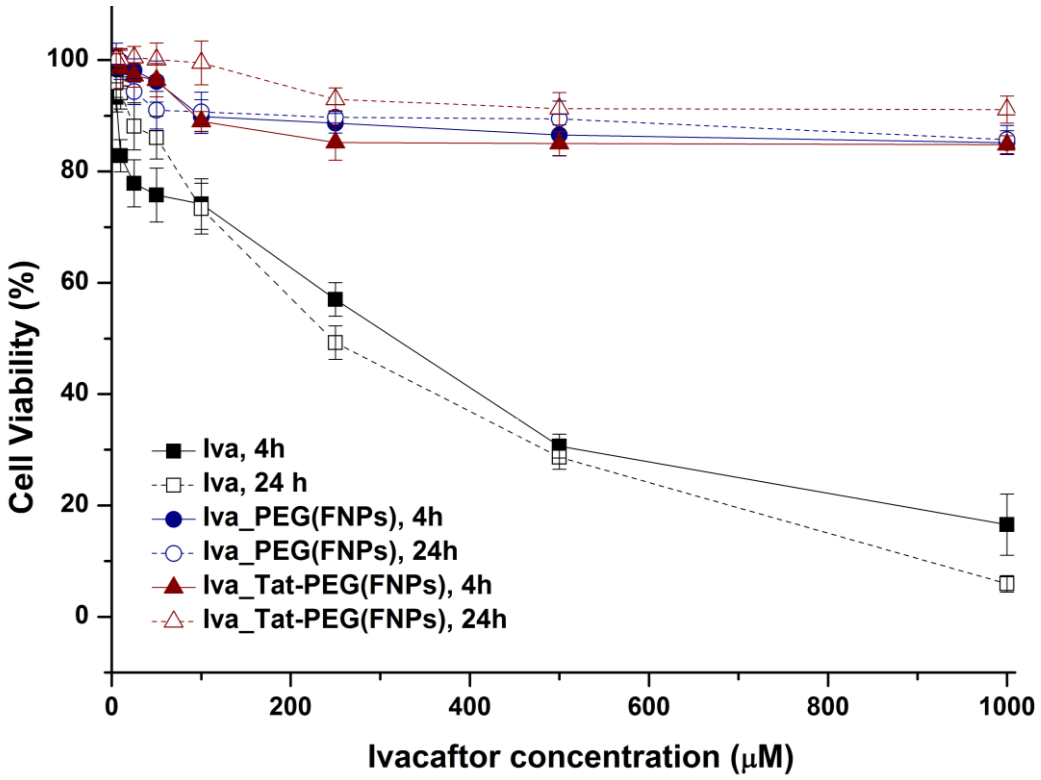

Fig.91: Cell viability % on 16-HBE cells after 4 and 24 h incubation with Iva_PEG(FNPs) and Iva_Tat-PEG(FNPs), compared to the viability of cells incubated with free ivacaftor.

As can be seen, after 4 and 24 h incubation, both ivacaftor loaded FNPs showed an excellent cytocompatibility, which is significantly higher than free drug at all tested corresponding concentrations.

3.5.5 Conclusions

In this paragraph, mucus-penetrating NPs for pulmonary administration of ivacaftor in patients with CF were described. FNPs, empty and loaded with ivacaftor, were prepared starting from an equal mixture between PHEA-PLA-Tat and PHEA-RhB-PLA-$PEG_{(F)}$ graft copolymer by using the nanoprecipitation method. The mixture between PHEA-PLA and PHEA-RhB-PLA-$PEG_{(F)}$ was instead used to produce as control.

All obtained FNPs showed nanometric proper sizes, slightly negative ζ potential and high cytocompatibility on human bronchial epithelium cells.

The mucus-penetrating ability of these systems was properly demonstrated and appears to be similar irrespective of FNP chemical composition.

Ivacaftor release profile in presence of CF-AM showed how the efficient transport of these NPs through the mucus layer could be a significant opportunity for the treatment of lung

defective ion transport in patients with CF. In fact, ivacaftor loaded mucus-penetrating NPs could rapidly diffuse through the mucus barrier reaching the mucosal surface, where they could offer a sustained delivery at the site of disease, resulting in superior efficacy, lower required dose and side effects.

Chapter 4

Conclusions

It is well consolidated that the efficacy of a therapeutic system could be significantly improved by using of new polymer-based pharmaceutical technologies, being, these ones, able to overcome the existing drawbacks encountered in clinical practice.

For this reason, micro- and nanotechnologies based on polymeric materials, were used to produce smart pulmonary drug delivery tools for the treatment of both pulmonary symptoms and the defective ion transport in lung epithelial cells of CF patients.

These drug delivery systems allowed a rapid permeation of the drug in the mucus layer and achieved a sustained delivery of the drugs at the site of disease, potentially reducing not only the administered dose, but also the dose frequency and consequently side effects, improving patient compliance.

Pulmonary symptoms, as consequence of infection and inflammation, or the defective ion transport in epithelial cells of CF patients were faced by using new micro and nanoparticle (MPs and NPs) based drug delivery systems loaded with the antibiotic tobramycin, the non-steroidal anti-inflammatory ibuprofen and the CFTR potentiator ivacaftor.

Firstly, a new "*nano into micro*" approach was realized as potential pulmonary delivery system for tobramycin in the treatment of *P. aeruginosa* infections in CF.

In particular, a polyelectrolyte complex was produced between the synthetic polyanion PHEA-EDA-GlucA and tobramycin positive charges, which shows nanometric dimensions and the ability to retain the drug via electrostatic interaction, slowing its release.

Once produced inhalable MPs based on mannitol, with adequate characteristics for pulmonary administration (spherical shape and micrometric size), were produced by spray drying and loaded with a tobramycin:PHEA-EDA-GlucA ion pair complex.

The mannitol micrometric matrix of this *nano into micro* formulation is able to modify the rheological properties of a CF artificial mucus model (CF-AM), facilitating the drug diffusion, but at the same time, thanks to the participation of tobramycin to the ion pair

complex with PHEA-EDA-GlucA, MPs are able to achieve a sustained tobramycin delivery at the site of disease.

At the same time, MPs loaded with the nanometric ion pair complex showed pronounced microbiological activity against *P.aeruginosa* pathogens and their biofilm, showing an interesting activity in inhibiting biofilm formation.

These results demonstrate the potential of obtained MPs as drug delivery systems for the treatment of pulmonary infections in CF patients and encouraged further investigations.

Since produced MPs containing the ion pair complex between the polyanion PHEA-EDA-GlucA and tobramycin (PTC) showed high potential, the therapeutic efficacy of obtained MPs was enhanced by adding helping materials with specific functions. Moreover, in order to evaluate if the mucoadhesive approach was a better strategy, in order to enhance the antibiotic activity of tobramycin, improving its residence time on mucus, polyvinilalchol (PVA) was used as polymeric MP matrix for the encapsulation of PTC

Materials used, as helping materials, together with mannitol or PVA, were N-acetylcysteine (NAC), L-Arginine (Arg) and cysteamine (Cyst).

The produced formulations were then compared with the only one commercially available dry powder inhalatory formulation based on MPs loaded with tobramycin, named Tobi® Podhaler®, by Novartis.

All produced MPs showed adequate characteristics for pulmonary administration, as spherical shape, micrometric size and high cytocompatibility towards human bronchial epithelial cells.

All produced MPs are able to modify rheological properties of CF-AM. In particular, PTC loaded mannitol-based MPs, and specifically those containing NAC and Cyst as helping material, are able to reduce the viscosity of mucus secretions. Contrariwise, PTC loaded PVA-based MPs seem to interact with CF-AM components via mucoadhesive interactions, which further increases over the incubation time.

Moreover, PTC mannitol-based MPs, and in particular those containing NAC and Cyst as helping material, are able to facilitate the drug diffusion, and at the same time to achieve a sustained tobramycin delivery, thanks to its participation to PTC, while PTC PVA-based MPs are not able to increase the drug diffusion, caused by the establishment of mucoadhesive interactions between MPs and mucus components, but are able to achieve a more sustained tobramycin release, thanks to the slower dissolution of PVA MP matrix.

Futher, as result of conducted studies in presence of CF-AM, it was possible to show how Tobi® Podhaler® MPs formulation interacted with CF-AM components via mucoadhesive interactions and consequently was not able to increase the drug diffusion, but was able to

achieve a more sustained tobramycin release, thanks to the slower dissolution of its water insoluble phospholipidic MP matrix.
Results obtained showed as produced MPs potentially could result in formulations of higher efficacy, for which it could be possible reducing the administered dose, the frequency of administrations, side effects and consequently antibiotic resistance problems.

The second aim of this thesis was the design of mucus-penetrating NPs. Mucus-penetrating NPs may deeply penetrate CF lung mucus secretions, achieving a sustained delivery of hydrophobic drug. So, polymeric NPs with mucus-penetrating properties was realized by firstly synthesis of an amphiphilic derivative of PHEA.
Firstly, PHEA was covalently linked with rhodamine B (RhB) moieties, polylactide (PLA) and poly(ethyleneglycol) (PEG) chains in order to produce the fluorescent PHEA-RhB-PLA-PEG graft copolymer. Then, starting from the PHEA-RhB-PLA-PEG derivative with different DD_{PLA} and DD_{PEG}, fluorescent nanoparticles (FNPs) were successfully prepared by or emulsion-high pressure homogenization (HPH)-solvent evaporation method, and showed nanometre size, slightly negative zeta potential and spherical shape.
Fluorescence and technological properties revealed that these particles possess a great potential for in vitro and in vivo imaging applications. In fact, chemical and enzymatic stability of the ester linkage between the fluorescent dye and copolymer, essential for imaging application, was demonstrated until 4 days of incubation.
Finally, the biodegradability of these particles was demonstrated by carrying out a chemical stability study until 21 days by incubating NPs based on a comparable non-rhodaminated similar copolymer, named PHEA-PLA-PEG, in two media mimicking physiological compartments.
The degradation seems to be dependent from the matrix chemical composition, involve mainly PLA and is more evident at pH 5.5 than at pH 7.4. Results demonstrate that obtained pegylated systems degrade faster than PLA NPs. So these systems can potentially be used as biodegradable carriers of drugs, avoiding critical bioaccumulation phenomena.
Once evaluated NP properties in terms of fluorescence, technological properties and biodegradability, mucus-penetrating NPs for pulmonary administration of ibuprofen in patients with CF were studied.
FNPs, empty and loaded with ibuprofen, with mucus-penetrating ability were obtained starting from PHEA-RhB-PLA, PHEA-RhB-PLA-$PEG_{(D)}$ and PHEA-RhB-PLA-$PEG_{(E)}$ copolymers, each one containing 0, 2 and 8.5 mol% of PEG respectively.

All obtained FNPs showed proper sizes lower than 200 nm, slightly negative ζ potential and high cytocompatibility on human bronchial epithelium cells.
The FNPs surface evaluation showed as the surface PEG density increases as the PEG derivatization degree (DD_{PEG}) of starting copolymers increases from 2 to 8.5 mol%.
Further investigation demonstrated as pegylated FNPs were coated by a dense brush-like PEG corona, conferring them a great potential to diffuse through a CF-AM.
The mucus-penetrating ability of these systems was properly demonstrated and appears to grow as the PEG density increases on the FNP surface.
Ibuprofen release profile and cellular uptake in presence of CF-AM showed how the efficient transport of these NPs through the mucus layer could be a significant opportunity for the treatment of inflammation in patients with CF. In fact, ibuprofen loaded mucus-penetrating NPs could rapidly diffuse through the mucus barrier reaching the mucosal surface, where they could offer a sustained delivery at the site of disease.

Finally, mucus-penetrating NPs for pulmonary administration of ivacaftor in patients with CF were obtained. Firstly, a new amphiphilic derivative of PHEA was produced in order to improve the drug accumulation in airway epithelial cells. For this reason, the transactivating transcriptional activator peptide (Tat) was covalently linked to PHEA-PLA backbone, in order to obtain PHEA-PLA-Tat.
Then, FNPs, empty and loaded with ivacaftor, were prepared starting from an equal mixture between PHEA-PLA-Tat and PHEA-RhB-PLA-PEG at the highest PEG content (12 mol %), by using the nanoprecipitation method.
All obtained FNPs possess proper sizes lower than 80 nm and slightly negative ζ potential, achieve an ivacaftor sustained delivery and show high cytocompatibility on 16-HBE cells.
The mucus-penetrating ability of these systems was properly demonstrated and appears to be similar for both NP formulation, decorated or not with Tat ligand.
Ivacaftor release profile in presence of CF-AM showed the efficient transport of these NPs through the mucus layer, being, these one, able to rapidly diffuse through the mucus barrier reaching the mucosal surface, where they could offer a sustained delivery at the site of disease.
As consequence of obtained results, the development of mucus-penetrating FNPs represents a promising strategy for overcoming the mucus-barrier, offering the prospect of sustained delivery of a variety of potentially important drugs to treat diseases at mucosal tissues.

4.1 Future perspectives

Since for NPs the direct pulmonary administration by nebulization is not feasible or convenient, the *nano into micro* strategy could be efficiently realized by spray-drying a dispersion of NPs in a in a solution containing sugars or polymers, to obtain a dry systems administered to the lungs by using dry powder inhalers (DPI) devices.

Nano embedded microparticles (NEMs) provide an excellent strategy for both stabilization of NPs and their delivery to the lungs. Materials composing the surrounding stabilizing matrix of NEMs could be inert, only acting as carrier for pulmonary administration or could possess a specific function.

For this reason, the *nano into micro* strategy could be used to produce NEMs based on mucus-penetrating NPs loaded with ivacaftor or ibuprofen.

Once produced NEMs, such as MPs based on mannitol and PVA loaded with the PTC, the aerodynamic properties and the aerosol performance of the formulations need to be tested.

Chapter 5

Experimental part

Materials

Anhydrous N,N'-dimethylformamide (a-DMF), bis(4-nitrophenyl) carbonate, sodium cyanoborohydride, phosphate buffer salts (PBS), ethylenediamine (EDA), D-(+)-glucuronic acid γ-lactone (GlucA), N,N'-dimethylacetamide (a-DMA) 1,1'-carbonyldiimidazole (CDI), Rhodamine B (RhB), D,L-poly(lactic acid) (PLA acid terminated, Mw =10-18kDa), N,N′-Disuccinimidyl carbonate (DSC), mannitol, polyvinyl alchol (PVA), N-acetylcysteine (NAC), L-arginine (Arg), cysteamine (Cyst), tobramycin, ibuprofen, agarose, esterase from porcine liver, lipase from porcine pancreas type II, diethylenetriaminepentaacetic acid (DTPA), RPMI amino acid solution, type II mucine from porcin stomach, egg yolk emulsion and deoxyrybonucleic acid (DNA) from calf thymus, 2,4,6-trinitrobenzene sulfonic Acid (TNBS), Trizma® buffer) and HIV-1 Tat Protein (47-57) were purchased from Sigma–Aldrich (Italy). O-(2-Aminoethyl)-O'-methyl poly(ethyleneglycol) (H_2N-PEG-OCH_3, Mw=2 KDa), trehalose, diethyl ether, acetone, ethanol and dichloromethane were obtained from Fluka (Italy).

Sodium chloride and potassium chloride were purchased from Merck (Italy).

All reagents were of analytic grade, unless otherwise stated.

Ivacaftor was purchased from Cayman Chemicals (Cabru, Italy). TOBI® Podhaler® (4 x 56 capsules and 5 inhalers) were purchased from a private pharmacy in Palermo (Italy).

α,β-poly(N-2-hydroxyethyl)-D,L-aspartamide (PHEA) was prepared and purified according to a procedure elsewhere reported [74]. Spectroscopic data are in agreement with attributed structures: ^{1}H-NMR (300 MHz, D_2O, 25 °C), δ: 2.82 (m, 2H, -CH-CH_2 -CO-NH-), 3.36 (t, 2H, -NH-CH_2-CH_2-OH), 3.66 (t, 2H,-CH_2-CH_2-OH), 4.72 (m, 1H, -NH-CH-CO-CH_2-).

The weight-average molecular weight of PHEA used in this study, determined by size exclusion chromatography (SEC) analysis, was 38.4 kDa , while its polydispersity index was 1.62.

Instruments

^{1}H-NMR spectra were obtained by a Bruker Avance II-300 spectrometer, working at 300 MHz. FT-IR spectra were obtained by a ALPHA FT-IR spectrometer (Bruker Instruments).

The SEC system (Waters, Mildford, MA) was equipped with a pump system, coloums and a 410 differential refractometer (DRI) as concentration detector (Waters, Mildford, USA).

The HPLC system was a Waters Breexe System Liquid Chromatograph, equipped with a Waters 717 plus Auto sampler (40 μL injection volume) and a Shimadzu UV-VIS HPLC detector on line with a computerized workstation.

Fluorescence properties were assessed by using an inverted epifluorescence microscope (Zeiss, Italy) equipped with a 40x/0.55 objective, and a AxioCam MRm camera (Zeiss, Italy).

Atomic Force Microscopy (AFM) measurements were performed in Tapping mode in air by a Bruker Dimension FastScan microscope equipped with closed-loop scanners. Triangular FastScan A probes (resonance frequency=1400 KHz, Tip radius=5 nm) were used.

Scanning Electron Microscopy (SEM) was performed by using a ESEM Philips XL30 microscope.

Mean size (nm) and polydispersity index (PDI) of ion pair complexes were determined by photon correlation spectroscopy (PCS) using a Zetasizer Nano ZS (Malvern Instrument, U.K.). Measurements were carried out at a fixed angle of 173° at a temperature of 25 °C by using filtered (0.2 μm) media. ζ-potential values were measured using principles of laser doppler velocimetry and phase analysis light scattering (M3-PALS technique) by dispersing samples in filtered filtered (0.2 μm) media.

Cell cultures

Human bronchial epithelial cells (16-HBE) were furnished by Istituto Zoo-profilattico of Lombardia and Emilia Romagna. 16-HBE cell line were grown in minimum essential medium (DMEM) supplemented with 10 vol% fetal bovine serum, 2 mM L-glutamine, 100 U/mL penicillin, 100 μg/mL streptomycin, and 2.5 μg/mL amphotericin B under standard conditions (95% relative humidity, 5% CO_2, 37°C). The cells were allowed to grow until confluence, trypsinized and seeded in plates for each experiment of cell viability or cell uptake.

Pseudomonas aeruginosa ATCC 15442, a reference strain in official tests for antibacterial evaluation in vitro (UNI EN European Standard), was used in this thesis.

CF artificial mucus

CF artificial mucus (CF-AM) was prepared as previously described [65, 136]. Briefly, 500 mg of deoxyribonucleic acid (DNA), 250 mg of mucin, 0.295 mg of diethylenetriaminepentaacetic acid (DTPA), 1 mL of RPMI 1640 amino acid solution, 250 µL of egg yolk emulsion, 250 mg of NaCl, and 110 mg of KCl were mixed together in a final volume of 50 mL of DNAse free water. This dispersion was allowed to equilibrate at 25°C for 2h. Sterile CF-AM was obtained by sterilizing DNA and mucin by exposure for 6 h to a germicidal lamp in a laminar flow hood, by mixing the sterile egg yolk emulsion and amino acid solution, autoclaved DTPA, NaCl, and KCl solution in sterile DNAse free water, under a laminar flow hood.

Statistical analysis

All the experiments were repeated at least three times. All data are expressed as means ± standard deviation. All data were analyzed by Student's t-test. A p-value <0.05 was considered as statistically significant, while a p-value <0.01 or 0.001 was considered as highly significant.

5.1 *Nano Into Micro* strategy: polyanion-tobramycin nanocomplexes into microparticles for the treatment of infection in cystic fibrosis (CF)

5.1.1 Synthesis and characterization of PHEA-EDA copolymer

A solution of PHEA (0.5 g, 3.2 mmol of repeating units) in 6 mL of anhydrous DMF was added dropwise to a solution of bis(4-nitrophenyl)carbonate (963 mg, 3.2 mmol) in 8 mL of anhydrous DMF under stirring and the mixture was kept for an activation time of 4h at 40° C. After activation times, EDA (1mL, 18.8 mmol) was added and each sample stirred for 3 h at room temperature. At this point, the reaction mixture was precipitated into acetone and obtained suspensions centrifuged at 12000 *g* for 10min at 4°C and washed several times with the same solvent. The obtained solid residues of sample was solubilized in distilled water and purified by exhaustive dialysis against distilled water (MWCO 12-14 kDa). After dialysis, solutions were freeze-dried.

The pure product was obtained in 90 wt% yield based on starting PHEA.

Obtained copolymer was characterized by ^{1}H-NMR and SEC analysis.

^{1}H-NMR (300 MHz, D_2O, 25°C, TMS) of PHEA-EDA reveals peaks at δ 2.84 (m, 2H, –CO–CH–**CH_2**–CO–NH–), 3.01 (m, 2H, –NH–CH_2–**CH_2**–NH_2), 3.38 (m, 2H, –NH–**CH_2**–CH_2–OH), 3.43 (m, 2H, –NH–**CH_2**–CH_2–NH_2), 3.68 (m, 2H, –NH–CH_2–**CH_2**–OH), 4.15 (m, 2 H, –NH–CH_2–**CH_2**–O(CO)NH– CH_2–CH_2–NH_2) 4.73 (m, 1H, –NH–**CH**(CO)CH_2).

The weight molecular weight of PHEA-EDA and its polydispersity index was determined by SEC analysis. Analyses was performed with phosphate buffer solution 0.1 M at pH 8 as eluent at 37°C, two TSK-GEL columns from Tosoh Bioscience (10^3Å and 10^4 Å pores size), with a flux of 0.8 mL/min and poly(ethylene oxide) standards (range 145–1.5 kDa) to obtain the calibration curve.

5.1.2 Synthesis and characterization of PHEA-EDA-GlucA copolymer

PHEA-EDA-GlucA copolymer was synthesized by a reductive amination of D-(+)-glucuronic acid γ-lactone (GlucA) with primary amine functions of PHEA-EDA in the presence of sodium cyanoborohydride in borate buffer at pH 9 (H_3BO_3 0.1 M). PHEA-EDA (500 mg, 1.24 mmol of NH_2 on PHEA-EDA) was dissolved in 30 mL of borate buffer at pH 9 and then GlucA(656.2 mg, 3.72 mmol), dissolved in 15 mL of the same medium, was added. Then, sodium cyanoborohydride (233.8 mg, 3.72 mmol), dissolved in 5 mL of the same medium, was added drop wise to the reaction mixture, which was left to react for 72 h at 40°C.

The product PHEA-EDA-GlucA was purified by exhaustive dialysis against distilled water (MWCO 12-14 kDa) and isolated by freeze-drying. The final product was obtained with a yield of 86 wt % based on the theoretical yield.

DD_{GlucA} of PHEA-EDA-GlucA was performed indirectly by the 2,4,6-Trinitrobenzene Sulfonic Acid (TNBS) colorimetric assay [78, 134]. Briefly, the TNBS reagent solution was prepared dissolving TNBS in borate buffer at pH 9.3 at the concentration of 0.03 M.

PHEA-EDA and PHEA-EDA-GlucA were dissolved in the same buffer at the concentration of 5 mg/mL, then 50 µL of obtained solutions were added to 900 µL of the same buffer and to 50 µL of TNBS reagent solution. This mixture was left to react for 100 min at 37 °C, placed in quartz cuvettes and analyzed by using UV spectrophotometry (Shimadzu, Italy), at the λ of 500 nm.

The obtained absorbance value, corresponding to the amount of free amino groups present in each polymer solution, was compared with a calibration curve, set up by using the H_2N-PEG-OCH_3 (Mw = 2 kDa), in concentrations ranging between 10^{-4}-10^{-1} mol of free amino groups/L ($y = 129.02x$, $R^2 = 0.9998$). DD_{GlucA} was expressed as percentage molar ratio between amino groups in PHEA-EDA-GlucA and in PHEA-EDA.

The reaction efficiency was determined using an acid-base titration, for which 27 mg of PHEA-EDA-GlucA was dissolved in 10 mL of twice distilled water. A known excess of NaOH 1M was added to the polymer solution, then this latter was back titrated with HCl 1 M and pH values were determined quantitatively using a pHmeter.

The weight molecular weight of PHEA-EDA-GlucA and its polydispersity index was determined by SEC analysis, as described for PHEA-EDA (5.1.1 paragraph).

5.1.3 Isothermal titration calorimetry

The interaction between PHEA-EDA-GlucA and tobramycin was investigated by using a NANO ITC Low Volume (TA Instruments, USA), with a reaction cell volume of 170 µL. All experiments were carried out at 25 °C in an aqueous medium at pH 6 (Trizma® buffer, 0.05 M). Prior to use, all solutions were degassed under vacuum to eliminate air bubbles. Three titration experiments were performed by successive 2 µL injections (25 total) of a freshly prepared tobramycin solution into a PHEA-EDA-GlucA solution. In particular, the concentration for each experiment was: A) 125 mg/mL for tobramycin, which correspond to 1337 mM of amino groups, and 80 mg/mL for PHEA-EDA-GlucA, which correspond to 141 mM of carboxylic groups; B) 30 mg/mL for tobramycin, which correspond to 321 mM of amino groups and 80 mg/mL for PHEA-EDA-GlucA, which correspond to 141 mM of

carboxylic groups; C) 30 mg/mL for tobramycin, which correspond to 321 mM of amino groups and 160 mg/mL for PHEA-EDA-GlucA, which correspond to 282 mM of carboxylic groups). The interval between injections was 600 s, and stirring at 310 rpm ensured a good mixing. Binding isotherms were corrected by subtracting the ligand dilution isotherms, determined by titrating drug solution into the same buffer. Data analysis was carried out using Nano Analyze Data Analysis TA® and MicroCal Origin 7.0 software.

5.1.4 Preparation of tobramycin: PHEA-EDA-GlucA ion pair complex, size and ζ-potential analysis

Tobramycin (125 mg/mL) and PHEA-EDA-GlucA (80 mg/mL) were dissolved in the Trizma® buffer at pH=6 at the weight ratios equal to 1:10 and 1:5, and left stirring for 12 h at room temperature, prior to use.

Mean size, PDI and of ion pair complexes were determined by dispersing sample in filtered (0.2 μm) PBS at pH of 7.4 and Trizma® buffer at pH=6.

5.1.5 Tobramycin quantification by HPLC analysis

The quantification of tobramycin was realized by HPLC. In particular, a modification of a pre-existing protocol of aminoglycoside detection based on o-phthaldialdehyde (OPA) and 2-mercaptoethanol, was followed [151]. The OPA reagent solution was prepared dissolving 40 mg of OPA dissolved in 1 mL of methanol and this solution was added to 7 mL of 1% w/v 2-mercaptoethanol in a borate buffer at pH 10.4 (H_3BO_3 0.4 M). 100 μL of each sample were added to 500 μL of a mixture of methanol and twice distilled water 85:15 v/v and to 100 μL of OPA reagent solution. This mixture was left to react for 35 min at room temperature and then injected into the column in isocratic mode. The column was a Eclipse Plus Zorbax C18 (C18- 100x4.6 mm, obtained from Agilent); the mobile phase was a mixture of methanol and twice distilled water 85:15 v/v with a flow rate of 0.6 mL/min, the column temperature was 25 °C, and the detection wavelength was 335 nm. The obtained peak area, corresponding to tobramycin released from the ion pair complex, was compared with a calibration curve obtained by plotting areas versus standard solution concentrations of tobramycin in twice-distilled water in a concentration range of 1-0.001 mg/mL ($y = 4*10^6x$, $R^2 = 0.999$).

5.1.6 Stability study of tobramycin:PHEA-EDA-GlucA ion pair complex

Tobramycin release profile from the ion pair complex was performed by using the dialysis method [152, 153]. To do this, the freshly prepared tobramycin:PHEA-EDA-GlucA ion pair complex (0.7 mL) at the weight ratio 1:10 or 1:5 (total tobramycin content equal to 5 mg) were placed into a dialysis tubing (MWCO 12-14 kDa), immersed into 15 mL of PBS isotonic solution at pH 7.4 and then incubated at 37°C under continuous stirring (100 rpm) in an orbital shaker. Aliquots of the external medium (1 mL) were withdrawn from the outside of the dialysis tubing at fixed time intervals (0, 15, 30, 45, 60, 120, 180, 240, 360 min) and replaced with equal amounts of fresh medium.

The profile of tobramycin diffusion trough dialysis membrane was evaluated by putting into the dialysis tubing a solution of drug (5 mg in 0.7 mL of Trizma® buffer at pH=6) and by following the same procedure described above.

Collected aliquots were treated with OPA reagent solution and analyzed by using the HPLC method described above.

5.1.7 Formulation and optimization of tobramycin:PHEA-EDA-GlucA ion pair complex-containing microparticles (MPs)

MPs were prepared by using a Nano Spray Dryer B-90 (Buchi, Italy). A fixed volume (100 mL) of mannitol solution, containing or not the tobramycin:PHEA-EDA-GlucA ion pair complex (table 20), was spray-dried for obtaining each formulation.

Table 20. Composition of MPs for 100 mL of spray dried solution.

Sample	Mannitol:PHEA-EDA-GlucA:tobramycin weight ratio (g)
MPs-A	2:0:0
MPs-B	1.5:0:0
MPs-C	**1:0:0**
MPs-D	1:0.8:0.16
MPs-E	**1:0.4:0.08**
MPs-F	1:0.3:0.06
MPs-G	1:0.4:0

In detail, to obtain empty MPs, aqueous mannitol solutions at different concentrations (2, 1.5 and 1 g/100 mL) were used to obtain MPs-A, MPs-B and MPs-C samples, respectively. To

obtain tobramycin-loaded MPs, freshly prepared tobramycin:PHEA-EDA-GlucA ion pair complex at the weight ratio of 1:5 dissolved into a 1% mannitol aqueous solutions (at a final ion pair complex of 0.96, 0.48, and 0.36 g/100 mL) were used to obtain MPs-D, MPs-E and MPs-F samples, respectively. Finally, PHEA-EDA-GlucA (0.4 g) was added to 100 mL of 1 wt/vol % aqueous mannitol solution to obtain MPs-G.

Once prepared, each solution was sorted through a 1.2 µm filter and then spray dried with a spray cap of 4.0 µm at the inlet temperature of 90°C. Filtered and dehumidified air was used as drying gas, the drying gas flow rate was of 133 L/min resulting an inside pressure of 44 mbar with a spray rate of 100%. The fraction of MPs produced was collected and appropriately stored at 4°C before analysis.

5.1.8 SEM and size distribution

Samples were dusted on a double sided adhesive tape previously applied on a stainless steel stub, stored under vacuum for 2 hours, sputter-coated with gold prior to microscopy examination and SEM images were then aquired.

The mean size distributions of MPs were disclosed from images obtained by using an optical microscope (Zeiss, Italy) equipped with a 40x/0.55 and the AxioCam MRm camera (Zeiss, Italy), by analyzing at least 500 individual MPs for each sample. Individual particle diameters were measured by using Zeiss software.

5.1.9 Determination of tobramycin content into MPs

The amount of tobramycin loaded into MPs was determined by HPLC method described in 5.1.5 paragraph. In particular, a exactly weighted amount of MPs was completely dissolved in twice-distilled water and 100 µL of the filtered (0.45 µm) obtained solution were treated as described above. Results were expressed as Drug Loading (DL wt%, that is the weight percent ratio between tobramycin found and the drug-loaded MPs) and Entrapment Efficacy (EE wt %, that is the weight percent ratio between the effective amount of tobramycin loaded into MPs and the theoretical value).

5.1.10 Rheological analysis of CF-AM

Rheological properties of CF-AM, alone or in the presence of MPs-E at three different concentrations (0.5, 2 and 3.5 mg/mL), were determined at the temperature of 20 °C by using a rheometer (TA Instruments) equipped with 8 mm parallel plate geometry and a controlled Peltier plate. Samples were incubated at 37°C for 1 h, then equilibrated to 20°C and a

preshear of 0.1 rad sec^{-1} for 120 s was applied, maintaining a gap of 150 μm. To prevent dehydration during rheological measurements, a solvent trap with water was placed on the top of the geometry.

A strain sweep (0.2-2 %) was performed on CF-AM at 0.1 Hz to determine the linear viscoelastic region, which was found to be in the range of 0.4-2 %. Then, a frequency sweep (0.01-1 Hz) was performed for all samples at 1.5% constant strain to determine storage moduli (G'), loss moduli (G''), and complex viscosity (η*).

5.1.11 Evaluation of tobramycin diffusion profile from MPs in CF-AM

Tobramycin diffusion profile from MPs was evaluated in CF-AM by using vertical Franz-type diffusion cells [137]. The system temperature was kept constant at 37 °C by recirculation of water from a thermostatically controlled bath. Continuous stirring at 180 rpm was provided by teflon-coated stirring bars placed in the acceptor chamber. The donor chamber was filled with 500 μL CF-AM and 50 mg of MPs-E (corresponding to 2.65 mg of tobramycin), the acceptor chamber with of 5 mL of PBS, and an hydrophilic polystyrene membrane (size pores: 0.45 μm), previously set in PBS overnight, was applied between the two compartments. Free tobramycin diffusion profile in CF-AM was evaluated by placing in the donor chamber 2.65 mg of tobramycin on a layer of 500 μL CF-AM.

At scheduled time intervals (0, 15, 30, 45, 60, 120, 180, 240, 360 min) aliquots (500 μL) were removed from the acceptor chamber replacing the same volume with fresh medium. The amount of tobramycin in each samples was quantified by the HPLC method described in 5.1.5 paragraph.

5.1.12 MTS cell viability essay on 16-HBE cells

Cell viability was assessed by a MTS assay on 16-HBE cells, using a commercially available kit (Cell Titer 96 Aqueous One Solution Cell Proliferation assay, Promega) containing 3-(4,5-dimethylthiazol-2-yl)-5-(3-carboxymethoxyphenyl)-2-(4-sulphophenyl)-2H-tetrazolium (MTS) and phenazine ethosulfate. 16HBE cells (2×10^5 cells/well) were seeded in microplates (tissue culture grade, 96 wells, flat bottom). Upon reaching confluence, 16-HBE cells were incubated with 200 μL per well of supplemented medium containing: MPs-E (at a final concentration per well of 2.5, 2, 1.5, 1 and 0.5 mg/mL); MPs-C (at concentrations corresponding to those of MPs-E), tobramycin and PHEA-EDA-GlucA at concentrations ranging between 6 and 0.01 mg/mL. After 4 h incubation, the growth medium was replaced

with 100 µL of fresh DMEM and 20 µL of a MTS/PMS solution was added to each well and plates were incubated for 1h at 37°C.

The absorbance at 492 nm was read using a microplate reader (Multiskan Ex, Thermo Labsystems, Finland). Relative cell viability (percentage) was expressed as (Abs_{492} treated cells/Abs_{492}control cells) × 100. Cells incubated with the medium were used as negative control.

5.1.13 Determination of Minimum Inhibitory Concentration (MIC) and Minimum Bactericidal Concentration (MBC)

MIC of tobramycin, tobramycin:PHEA-EDA-GlucA 1:5 w/w ion pair complex, MPs-C, MPs-E, MPs-G and PHEA-EDA-GlucA copolymer was evaluated against P. aeruginosa ATCC 15442, by using a two-fold broth dilution micro dilution method previously described [154] and Tryptic Soy Broth (TSB) was used as culture media. To determine MBC, the content of any well of a 96-well plate, with no visible growth at MIC evaluation, was inoculated in a tryptic soy agar (TSA) plate without inhibitors and incubated at 37°C for 24h. At the end of that time, the MBC was determined as the lowest concentration of inhibitor that yielded less than three colonies.

5.1.14 Antibacterial activity in *P. aeruginosa*-loaded CF-AM

A single colony of P. aeruginosa from an agar culture in TSA plate was collected, inoculated in 25 mL of TSB and incubated at 37°C, until that the optical density of the broth at 420 nm reached the value of 0.2. A small amount of the broth culture (10µL) was added to 1 mL of sterile CF-AM and incubated for 2h at 37°C before evaluating the antipseudomonal activity of samples. After the incubation, tobramycin, tobramycin:PHEA-EDA-GlucA 1:5 w/w ion pair complex and MPs-E, were added as dry powder to obtain a final concentration in CF-AM of 128 µg/mL and incubated for 90 min at 37°C. After the incubation time, 1mL of citrate buffer (citric acid 0.05 M) at pH 4.5 was added. Then, 100µL of each sample was firstly diluted with 900 µL of NaCl 0.9% and then a series of 10-fold dilutions were prepared. Aliquots of 100µL of each dilution were plated in TSA. Plates were then incubated at 37 °C, colony forming units (CFU)/mL were counted after 24 h and compared to CFU/mL formed on untreated CF-AM as control.

5.1.15 Inhibition of biofilm formation

Free tobramycin, tobramycin:PHEA-EDA-GlucA 1:5 w/w ion pair complex, and MPs-E, were screened for their activity to inhibit biofilm formation at a tobramycin sub-MIC concentration of 2 µg/mL for each sample. Bacteria were grown in TSB containing 2 % glucose overnight at 37°C in a shaking bath and then diluted 1:200 to a suspension with optical density (OD) of about 0.040 at 570 nm corresponding to ~10^6 CFU/mL. Polystyrene 24-well tissue culture plates were filled with 2 mL of diluted suspension and tobramycin sub-MIC concentrations of 2 µg/mL of each sample were directly added to bacterial suspension and incubated for 24 h at 37 °C [155]. After that time all the wells (growth control and samples) were washed at least three times with 1mL of sterile NaCl 0.9% w/v, the inocula scraped from the surface of each well were put in test tubes with 10 mL of NaCl (0.9% w/v solution) and sonicated for 2 min. A suitable number of 10-fold dilutions were prepared and 100 mL aliquots of each dilution were plated in TSA. Plates were then incubated at 37 °C, colony forming units (CFU)/mL were counted after 24 h and compared to CFU/mL formed on growth control wells. The activity is reported in terms of log reduction of viable plate counts [154].

5.1.16 Activity against pre-formed *P.aeruginosa* biofilm

Free tobramycin, tobramycin:PHEA-EDA-GlucA 1:5 w/w ion pair complex, and MPs-E, were screened at 32 µg/mL, a concentration equal to MBC (free tobramycin and tobramycin:PHEA-EDA-GlucA 1:5 w/w ion pair complex) or 2x MBC (MPs-E) for their antibiofilm activity against a pre-formed biofilm of 24 hours. P. aeruginosa strain was grown in TSB containing 2% w/vol glucose incubated and diluted as above described for inhibition of biofilm formation. The diluted suspension was added to the wells (2 mL per well) of a polystyrene microtiter 24-well plate and incubated for 24 h at 37°C. Following this incubation period the wells were washed three times as previously described and filled with 2mL of TSB containing 2% w/vol glucose and, except untreated growth control wells, supplemented with concentrations of 32µg/mL of each sample. Plates were then incubated for further 24 h at 37°C. After the incubation time the wells were washed and the inocula collected, diluted and counted as described in inhibition of biofilm formation method (5.1.15 paragraph).

5.2 Optimization of smart pulmonary drug delivery systems of tobramycin for the treatment of *P. aeruginosa* infections in CF

5.2.1 Optimization of tobramycin:PHEA-EDA-GlucA ion pair complex-containing MPs

MPs were prepared by using a Nano Spray Dryer B-90 (Buchi, Italy). A fixed volume (100 mL) of mannitol or PVA solution, containing or not helping material (NAC, Arg or Cyst) and the PHEA-EDA-GlucA:tobramycin 5:1 weight ratio ion pair complex (PTC), was spray-dried for obtaining each formulation. Detailed chemical composition of produced MPs is reported in table 21 and expressed as components weight ratio.

Table 21. Composition of MPs for 100 mL of spray dried solution.

Sample	**Chemical composition**
Empty MPs	**Mannitol or PVA: helping material weight ratio (g)**
Man	1:0
Man-NAC	1:0.1
Man-Arg	1:0.1
Man-Cyst	1:0.1
PVA	1:0
PVA-NAC	1:0.1
PVA-Arg	1:0.1
PVA-Cyst	1:0.1
PTC_MPs	**PTC:Mannitol or PVA: helping material weight ratio (g)**
PTC_Man	0.48:1:0
PTC_Man-NAC	0.48:1:0.1
PTC_Man-Arg	0.48:1:0.1
PTC_Man-Cyst	0.48:1:0.1
PTC_PVA	0.48:1:0
PTC_PVA-NAC	0.48:1:0.1
PTC_PVA-Arg	0.48:1:0.1
PTC_PVA-Cyst	0.48:1:0.1

In detail, to obtain empty MPs, aqueous mannitol or PVA solutions (1 g/100 mL) were used to obtain Man or PVA MPs. To each Man or PVA MP composition, NAC, Arg or Cys helping materials were added at the weight ratio of 1:0.1 mannitol or PVA: helping material,

to produce Man-NAC, Man-Arg, Man-Cys and PVA-NAC, PVA-Arg, PVA-Cys, respecitively.

To obtain PTC-loaded MPs, freshly prepared tobramycin:PHEA-EDA-GlucA ion pair complex at the weight ratio of 1:5 dissolved into a 1% mannitol or PVA aqueous solutions (at a final PTC concentration of 0.48 g/100 mL), containing or not helping materials, were used to obtain PTC_Man, PTC_Man-NAC, PTC_Man-Arg, PTC_Man-Cys and PTC_PVA, PTC_PVA-NAC, PTC_PVA-Arg, PTC_PVA-Cys, respecitively.

Once prepared, each solution was sorted through a 1.2 µm filter, degassed and then spray dried with a spray cap of 4.0 µm at the inlet temperature of 90°C. Filtered and dehumidified air was used as drying gas, the drying gas flow rate was of 133 L/min resulting an inside pressure of 44 mbar with a spray rate of 100%. The fraction of MPs produced was collected and appropriately stored at 4°C before analysis.

5.2.2 SEM images

Samples were dusted on a double sided adhesive tape previously applied on a stainless steel stub, stored under vacuum for 2 hours, sputter-coated with gold prior to microscopy examination and SEM images were then aquired.

5.2.3 Determination of tobramycin content into MPs

The amount of tobramycin loaded into MPs was determined by HPLC method described above. In particular, 5 mg of PTC_Man, PTC_Man-NAC, PTC_Man-Arg, PTC_Man-Cys, PTC_PVA, PTC_PVA-NAC, PTC_PVA-Arg, PTC_PVA-Cys were completely dissolved in 5 mL of twice-distilled water. Control experiments were conducted by dissolving 5 mg of Man-Arg and PVA-Arg MPs in 5 mL of twice-distilled water.

100 µL of the filtered (0.45 µm) obtained solutions were treated with OPA reagent solution and tobramycin amount was quantified by using the HPLC method described in 5.1.5 paragraph.

Arg amount obtained for Man-Arg and PVA-Arg MPs was subtracted to that obtained for PTC_Man-Arg and PTC_PVA-Arg MPs.Results were expressed as DL wt%, and EE wt %.

5.2.4 Evaluation of MPs properties in CF-AM

Measurement of interactions with CF-AM

Measurements of interactions between MPs and CF-AM was determined by turbidimetry [65]. Briefly, a dispersion of PTC_Man, PTC_Man-NAC, PTC_Man-Arg, PTC_Man-Cys,

PTC_PVA, PTC_PVA-NAC, PTC_PVA-Arg, PTC_PVA-Cys and TOBI® Podhaler® in CF-AM was prepared at the concentration of 2 mg/mL, and then left under magnetic stirring for 1 min. After incubation at 37°C, the turbidity of each dispersions were measured at time 0, 15, 30, 45, 60, 120, 180, 240, 360 min. The absorbance at the λ of 650 nm was recorded by UV spectrophotometer.

Rheological analysis of CF-AM

Rheological properties of CF-AM, alone or in the presence of PTC_Man, PTC_Man-NAC, PTC_Man-Arg, PTC_Man-Cys, PTC_PVA, PTC_PVA-NAC, PTC_PVA-Arg, PTC_PVA-Cys and TOBI® Podhaler® at the concentrations of 2 mg/mL, were determined at the temperature of 20 °C by using a rheometer (TA Instruments) as described in 5.1.10 paragraph.

5.2.5 Evaluation of tobramycin diffusion profile from MPs in CF-AM

Tobramycin diffusion profile from MPs was evaluated in CF-AM by using vertical Franz-type diffusion cells. The system temperature was kept constant at 37 °C by recirculation of water from a thermostatically controlled bath. Continuous stirring at 180 rpm was provided by teflon-coated stirring bars placed in the acceptor chamber. The donor chamber was filled with 500 µL CF-AM and 50 mg of PTC_Man, PTC_Man-NAC, PTC_Man-Arg, PTC_Man-Cys, PTC_PVA, PTC_PVA-NAC, PTC_PVA-Arg, PTC_PVA-Cys (corresponding to ~2.5 mg of tobramycin), the acceptor chamber with of 5 mL of PBS, and an hydrophilic polystyrene membrane (size pores: 0.45 µm), previously set in PBS overnight, was applied between the two compartments. Tobramycin diffusion profile from TOBI® Podhaler® in CF-AM was evaluated by placing in the donor chamber 4.5 mg of TOBI® Podhaler® (corresponding to ~2.5 mg of tobramycin) on a layer of 500 µL CF-AM.

At scheduled time intervals (0, 15, 30, 45, 60, 120, 180, 240, 360 min) aliquots (500 µL) were removed from the acceptor chamber replacing the same volume with fresh medium. The amount of tobramycin in each samples was quantified by the HPLC method described in 5.1.5 paragraph.

Control experiments were conducted by placing in the donor chamber empty Man-Arg and PVA-Arg MPs on 500 µL of CF-AM, 5 mL of PBS in the acceptor chamber and by placing an hydrophilic polystyrene membrane between the two compartments.

Arg diffusion profile was evaluated at 0, 15, 30, 45, 60, 120, 180, 240, 360 min by using the HPLC method described for tobramycin. Arg amount diffused at each time interval was

subtracted to that obtained by the diffusion of tobramycin from PTC_Man-Arg and PTC_PVA-Arg MPs.

5.2.6 MTS cell viability essay on 16-HBE cells

Cell viability was assessed by a MTS assay on 16-HBE cells, using a commercially available kit (Cell Titer 96 Aqueous One Solution Cell Proliferation assay, Promega) containing 3-(4,5-dimethylthiazol-2-yl)-5-(3-carboxymethoxyphenyl)-2-(4-sulphophenyl)-2H-tetrazolium (MTS) and phenazine ethosulfate. 16HBE cells (2×10^5 cells/well) were seeded in microplates (tissue culture grade, 96 wells, flat bottom). Upon reaching confluence, 16-HBE cells were incubated with 200 µL per well of supplemented medium containing: PTC_Man, PTC_Man-NAC, PTC_Man-Arg, PTC_Man-Cys, PTC_PVA, PTC_PVA-NAC, PTC_PVA-Arg, PTC_PVA-Cys and TOBI® Podhaler® (at a final concentration per well of 2.5, 2, 1.5, 1 and 0.5 mg/mL).

After 4 h and 24 h incubation, the growth medium was replaced with 100 µL of fresh DMEM and 20 µL of a MTS/PMS solution was added to each well and plates were incubated for 1h at 37°C. The absorbance at 492 nm was read using a microplate reader (Multiskan Ex, Thermo Labsystems, Finland). Relative cell viability (percentage) was expressed as (Abs_{492} treated cells/Abs_{492}control cells) × 100. Cells incubated with the medium were used as negative control.

5.3 Preparation and characterization of biodegradable fluorescent nanoparticles based on pegylated polyaspartamide–polylactide copolymers as delivery systems for hydrophobic drugs

5.3.1 Synthesis and characterization of PHEA-RhB copolymer

Derivatization of PHEA with RhB, to obtain PHEA-RhB copolymer, was carried out by using CDI as coupling agent. A calculated amount of CDI dissolved in a-DMF (26.0 mg/mL) under argon atmosphere, was added drop-wise to a RhB solution in a-DMF (8.7 mg/mL), according to $R_1 = 1.25$ being:

$$R_1 = \frac{\text{moles of CDI}}{\text{moles of RhB}}$$

The clear solution was stirred at 40°C for 4 h under argon atmosphere. Simultaneously, 33.3 mg/mL of PHEA were dissolved in a-DMF at 40°C under argon atmosphere and then DEA, as catalyst, was added. The amounts of PHEA and DEA were calculated according to $R_2 = 0.01$ and $R_3 = 5$, being:

$$R_2 = \frac{\text{moles of RhB}}{\text{moles of -OH groups on PHEA}}$$

$$R_3 = \frac{\text{moles of DEA}}{\text{moles of RhB}}$$

After activation time, the resulting polymeric solution was added drop-wise and slowly to CDI-activated RhB solution. The reaction mixture was left under argon atmosphere and continuous stirring at 40°C for 48 h, then was precipitated in diethyl ether and the suspension was centrifuged at 4°C for 15 min, at 9800 rpm by at 9800 rpm by using an Allegra X-22 R centrifuge (Beckman Coulter), equipped with a F0850 rotor and temperature control. The obtained solid product was recovered, washed four times with ethanol, separating the washing mixture by centrifugation at 4°C for 15 min, at 9800 rpm. Then, the product, dried under vacuum, was obtained with a yield of 85wt% based on the starting PHEA weight.

^{1}H-NMR (300 MHz, D_2O, 25°C, TMS): δ 1.15 (m, $12H_{RhB}$ **CH_3**-CH_2-); δ 2.71 (m, $2H_{PHEA}$ -CO-CH-**CH_2**-CO-NH-); δ 3.29 (t, $2H_{PHEA}$ -NH-**CH_2**-CH_2-O-); δ 3.58 (t, $2H_{PHEA}$ -NH-CH_2-**CH_2**-O-); δ 4.65 (m, $1H_{PHEA}$ -NH-**CH**(CO)CH_2-); δ 8.00-8.50 (m, $10H_{RhB}$ **H**-Ar).

$\overline{M}_w$ of PHEA-RhB graft copolymer was determined by SEC. Analyses were performed with 0.01 M LiBr DMF solution as eluent, two Phenogel columns from Phenomenex (5 μm particle size, 103 Å and 104 Å of pores size), with a flow of 0.8 mL/min and poly(ethylene oxide) standards (range 145−1.5 kDa) to obtain the calibration curve. The column temperature was set at 50°C (±0.1°C).

Molar Extinction Coefficient (ε) of RhB and PHEA-RhB were evaluated as reported elsewhere [156]. The absorption at maximum wavelength was measured and the ε was calculated from the curve obtained by plotting absorbance versus sample solution concentrations in concentration ranging between 10^{-7}-10^{-4} M, by recording UV spectra with a by a RF-5301PC spectrofluorometer (Shimadzu, Italy).

5.3.2 Synthesis and characterization of PHEA-RhB-PLA copolymers

Derivatization of PHEA-RhB with acid terminated PLA to obtain the PHEA-RhB-PLA graft copolymer was carried out by using CDI as coupling agent. In particular, a calculated amount of CDI dissolved in a-DMF (123 mg/mL) under argon atmosphere, was added drop-wise to acid terminated PLA solution in a-DMF (175 mg/mL), according to R_4= 2 being:

$$R_4 = \frac{\text{moles of CDI}}{\text{moles of PLA}}$$

The clear solution was stirred at 40°C for an activation time of 4 h under argon atmosphere. Simultaneously, 84 mg/mL of PHEA-RhB were dissolved in a-DMF at 40°C under argon atmosphere and then DEA, as catalyst, were added. The amounts of acid terminated PLA and DEA were calculated according to R_5 and R_6=8.5 being:

$$R_5 = \frac{\text{moles of PLA}}{\text{moles of -OH groups on PHEA-RhB}}$$

$$R_6 = \frac{\text{moles of DEA}}{\text{moles of PLA}}$$

In order to obtain three different hydrophobization degrees, molar ratios R_5 were chosen equal to 0.06, 0.08 and 0.1, and obtained derivatives were indicated as PHEA-RhB-$PLA_{(A)}$, PHEA-RhB-$PLA_{(B)}$ and PHEA-RhB-$PLA_{(C)}$.

After activation time, the resulting PHEA-RhB solution was added drop-wise and slowly to CDI-activated PLA solution. The reaction mixture was left under argon atmosphere and

continuous stirring at 40°C for 72 h, and then precipitated in diethyl ether:dichloromethane mixture (15:1 vol/vol). The obtained suspension was centrifuged at 4°C for 15 min, at 9800 rpm, and the obtained solid product was recovered, washed several times with the same mixture, separating the washing mixture by centrifugation. Then, the solid product, dried under vacuum, was obtained with a yield of 280wt% based on the starting PHEA-RhB weight.

^{1}H-NMR (300 MHz, d_7-DMF, 25°C, TMS): δ 1.15 (m,12H_{RhB} **CH_3**-CH_2-); δ 1.3 and δ 1.7 (2d, 582 H_{PLA} -O-CO-CH(**CH_3**)-O-); δ 2.8 (m, 2H_{PHEA} -CO-CH-**CH_2**-CO-NH-); δ 3.3 (t, 2H_{PHEA} -NH-**CH_2**-CH_2-O-); δ 3.59 (t, 2H_{PHEA} -NH-CH_2-**CH_2**-O-); δ 4.2-4.5 and δ 5.1-5.5 (m, 194 H_{PLA} -O-CO-**CH**(CH_3)-), and δ 4.8 (m, 1H_{PHEA} -NH-**CH**(CO)CH_2-); δ 7.0-8.0 (m, 10H_{RhB} **H**-Ar).

$\overline{M}_w$ of PHEA-RhB-PLA graft copolymers were determined by SEC analysis as described in 5.3.1 paragraph.

5.3.3 Synthesis and characterization of PHEA-RhB-PLA-PEG copolymers

Derivatization of PHEA-RhB-PLA with H_2N-PEG-OCH_3, to obtain PHEA-RhB-PLA-PEG copolymers with different derivatization degrees, named PHEA-RhB-PLA-$PEG_{(A)}$ and PHEA-RhB-PLA-$PEG_{(B)}$, PHEA-RhB-PLA-$PEG_{(C)}$, PHEA-RhB-PLA-$PEG_{(D)}$ and PHEA-RhB-PLA-$PEG_{(E)}$, was carried out by using DSC as coupling agent.

PHEA-RhB-PLA was dissolved in a-DMA (62.5 mg/mL) at 40°C under argon atmosphere and then a proper amount of triethylamine (TEA), as catalyst, and N,N'-disuccinimidyl carbonate (DSC) were added; subsequently, the reaction mixture was left at 40°C for 4 h.

The amounts of TEA and DSC were added according to the following ratios:

$$R_7 = \frac{\text{moles of DSC}}{\text{moles of -OH groups on PHEA-RhB-PLA}}$$

$$R_8 = \frac{\text{moles of TEA}}{\text{moles of DSC}}$$

After the activation time, the DSC-activated PHEA-RhB-PLA was added drop-wise to a solution of H_2N-PEG-OCH_3 in a-DMA following the R_9 ratio:

$$R_9 = \frac{\text{moles of } H_2N - PEG - OCH_3}{\text{moles of -OH groups on PHEA-RhB-PLA}}$$

For PHEA-RhB-PLA-PEG$_{(A)}$, PHEA-RhB-PLA-PEG$_{(B)}$ and PHEA-RhB-PLA-PEG$_{(C)}$ copolymers, R_7 equal to 0.075 was fixed, while the amount of DSC and TEA were defined according to R_8 equal to 0.1 and R_9 equal to 1.0, starting from PHEA-RhB-PLA$_{(A)}$, PHEA-RhB-PLA $_{(B)}$ and PHEA-RhB-PLA$_{(C)}$.

For PHEA-RhB-PLA-PEG$_{(D)}$, PHEA-RhB-PLA-PEG$_{(E)}$ and PHEA-RhB-PLA-PEG$_{(F)}$ copolymers, R_7 was equal to 0.04, 0.16 and 0.22, respectively; R_8 was fixed to 1.0, while R_8 was equal to 0.03, 0.12 and 0.18, starting from PHEA-RhB-PLA(B). A detailed description of molar ratios used for the derivatization reactions is reported in table 22.

The obtained mixture reactions were left at 25°C for 18 h under argon atmosphere and continuous stirring, then dialyzed against distilled water (MWCO 12-14 kDa) and lyophilized. ^{1}H-NMR (300 MHz, d$_7$-DMF, 25°C, TMS) of PHEA-RhB-PLA-PEG: δ 1.15 (m, 12H$_{RhB}$ **CH$_3$**-CH$_2$-); δ 1.48 and δ 1.96 (2d, 582 H$_{PLA}$ –O-CO-CH(**CH$_3$**)-O-); δ 3.0 (m, 2H$_{PHEA}$ -CO-CH-**CH$_2$**-CO-NH-); δ 3.48 (t, 2H$_{PHEA}$ -NH-**CH$_2$**-CH$_2$-O-); δ 3.71 (t, 2H$_{PHEA}$ -NH-CH$_2$-**CH$_2$**-O-); δ 3.78 (t, 176 H$_{PEG}$ **-CH$_2$-CH$_2$**-O-); δ 4.3-4.6 and δ 5.3-5.6 (m, 194 H$_{PLA}$ -O-CO-**CH**(CH$_3$)-), and δ 4.98 (m, 1H$_{PHEA}$ -NH-**CH**(CO)CH$_2$-); δ 7.0-8.0 (m, 10H$_{RhB}$ **H**-Ar).

$\overline{M}_w$ of PHEA-RhB-PLA-PEG graft copolymers were determined by SEC analysis as described in 5.3.1 paragraph.

Table 22. Detailed description of molar ratios used for the derivatization reactions.

Copolymers	Molar Ratios								
	R_1	R_1	R_3	R_4	R_5	R_6	R_7	R_8	R_9
PHEA-RhB	**1.25**	**0.01**	**5**	-	-	-	-	-	-
PHEA-RhB-PLA$_{(A)}$	1.25	0.01	5	**2**	**0.06**	**8.5**	-	-	-
PHEA-RhB-PLA$_{(B)}$	1.25	0.01	5	**2**	**0.08**	**8.5**	-	-	-
PHEA-RhB-PLA$_{(C)}$	1.25	0.01	5	**2**	**0.1**	**8.5**	-	-	-
PHEA-RhB-PLA-PEG$_{(A)}$	1.25	0.01	5	**2**	**0.06**	**8.5**	0.075	0.1	1.0
PHEA-RhB-PLA-PEG$_{(B)}$	1.25	0.01	5	**2**	**0.08**	**8.5**	0.075	0.1	1.0
PHEA-RhB-PLA-PEG$_{(C)}$	1.25	0.01	5	**2**	**0.1**	**8.5**	0.075	0.1	1.0

PHEA-RhB-PLA-PEG$_{(D)}$	1.25	0.01	5	**2**	**0.08**	**8.5**	**0.04**	**1.0**	**0.03**
PHEA-RhB-PLA-PEG$_{(E)}$	1.25	0.01	5	**2**	**0.08**	**8.5**	**0.016**	**1.0**	**0.012**
PHEA-RhB-PLA-PEG$_{(F)}$	1.25	0.01	5	**2**	**0.08**	**8.5**	**0.22**	**1.0**	**0.018**

5.3.4 Preparation of fluorescent nanoparticles starting from synthesized copolymers

PHEA-RhB-PLA-PEG$_{(A)}$, PHEA-RhB-PLA-PEG$_{(B)}$, PHEA-RhB-PLA-PEG$_{(C)}$, PHEA-RhB-PLA-PEG$_{(D)}$, PHEA-RhB-PLA-PEG$_{(E)}$ and PHEA-RhB-PLA-PEG$_{(F)}$ copolymers were used to realize FNPs by following the high pressure homogenization (HPH)-solvent evaporation method [157]. Briefly, each copolymer was dissolved in dichloromethane (17.7 mg/mL) and added drop wise to twice-distilled water (50 mL) and homogenized by using an ultraturrax (T 25, Janke&Kunkel Ika–Labortechnik) at 13500 rpm. The primary oil/water emulsion obtained was then diluted with twice-distilled water (25 mL) and broken down into nano-droplets by using an high pressure homogenizer at the pressure of 5000 ± 2500 psi (EmulsiFlex^{TM}-C5; Averting, Canada) for two cycle, equipped with Totem CCS 338 (FIAC, Italy) air compressor.

The organic solvent was extracted by evaporation under reduced pressure, by using a Buchi rotant evaporator, causing the precipitation of the FNPs.

Finally each FNP dipersion was freeze-dried (Modulyo freeze-dryer, Labconco Corporation, Missouri, U.S.A.) and stored in freezer (-20 °C) for further characterization.

FNPs prepared starting from PHEA-RhB-PLA-PEG$_{(A)}$, PHEA-RhB-PLA-PEG$_{(B)}$, PHEA-RhB-PLA-PEG$_{(C)}$, PHEA-RhB-PLA-PEG$_{(D)}$, PHEA-RhB-PLA-PEG$_{(E)}$ and PHEA-RhB-PLA-PEG$_{(F)}$ copolymers were respectively called FNPs $_{(A)}$, FNPs $_{(B)}$, FNPs $_{(C)}$, FNPs $_{(D)}$, FNPs $_{(E)}$ and FNPs $_{(F)}$.

5.3.4 Characterization of FNPs

Dimensional analysis and ζ-potential measurements

Mean size (nm), PDI and ζ potential values of FNPs were measured in filtered (0.2 µm) isotonic PBS solution at pH of 7.4 as dispersing medium after freeze-drying.

Particle morphology and fluorescence properties

FNPs were dusted on a double sided adhesive tape previously applied on a stainless steel stub, stored under vacuum for 2 hours, sputter-coated with gold prior to microscopy examination and SEM images were then aquired.

For fluorescence properties evaluation, a small drop of an aqueous dispersion of the freeze-dried FNPs was deposited between two microscope slides and images were acquired by using an inverted epifluorescence microscope (40x/0.55 objective).

5.3.5 FNP physical stability

Physical stability of FNP aqueous dispersions was studied in PBS by monitoring the mean size, PDI and ζ potential values as a function of incubation time until 24 h. Each sample was dispersed in PBS and incubated in a thermostatic compartment at 37°C.

5.3.6 FNP chemical and enzymatic stability

The chemical and enzymatic stability of ester linkage between RhB and copolymer was studied in different incubation media and in sink conditions by evaluating the release of RhB by a dialysis method.

To evaluate stability in physiological buffers, buffered saline (PBS, NaCl, Na_2HPO_4, KH_2PO_4) at pH 7.4 or at pH 5.5 were used as suspending media.

To evaluate enzymatic stability, PBS aqueous dispersions containing esterase from porcine liver or lipase from porcine pancreas type II (final theoretical ratio between the esterase activity of enzyme and ester groups between RhB and the polymeric backbone ∼100) were used as suspending media.

$FNPs_{(B)}$ was dispersed in the proper medium (2 mL), placed in a dialysis bag (MWCO 12-14 kDa) immersed in the same medium, and then incubated in a thermostatic orbital shaker (100 rpm, 37°C). At scheduled time-points, aliquots of the receiver medium was taken and replaced by fresh medium. A control experiment was also performed by carrying out the same experiments on an appropriate amount of PHEA-RhB. The released RhB amounts in the receiver medium were determined by the HPLC method described below.

RhB HPLC analysis

The amount of RhB released in the receiver medium was determined by an HPLC. Analyses were performed with a mobile phase constituded by a mixture of aqueous solution of $NaC_7H_{15}SO_3$ (5 mM):CH_3CN:MeOH 20:45:35 (v:v:v) and a flow rate of 0.8 mL/min. The column temperature was 25°C, and the detection wavelength was 550 nm.

The obtained peak area corresponding to free RhB was compared with a calibration curve obtained by plotting areas versus standard solution concentrations of RhB in twice-distilled

water in the range of 5-0.1 μg/mL (y = 9E+10^8x, R^2 = 0.9998). Results were expressed as the weight percent ratio between the released RhB and the total amount initially covalently linked to the incubated sample (FNPs or PHEA-RhB).

5.3.7 Evaluation of biodegradability of NPs

The biodegradability of pegylated polyaspartamide–polylactide copolymers based NPs was evaluated on NPs prepared starting from a non-rhodaminated polymer, with a chemical compostition and molecular weight similar to that of PHEA-RhB-PLA-$PEG_{(B)}$, and compared with NPs composed by only PLA.

Synthesis and characterization of PHEA–PLA

Derivatization of PHEA with acid terminated PLA to obtain the PHEA-PLA graft copolymer was carried out by using CDI as coupling agent. In particular, a calculated amount of CDI dissolved in a-DMF (123 mg/mL) under argon atmosphere, was added drop-wise to acid terminated PLA solution in a-DMF (175 mg/mL), according to R'_4= 2 being:

$$R'_4 = \frac{\text{moles of CDI}}{\text{moles of PLA}}$$

The clear solution was stirred at 40°C for an activation time of 4 h under argon atmosphere. Simultaneously, 84 mg/mL of PHEA were dissolved in a-DMF at 40°C under argon atmosphere and then DEA, as catalyst, were added. The amounts of acid terminated PLA and DEA were calculated according to R'_5=0.08 and R'_6=8.5 being:

$$R'_5 = \frac{\text{moles of PLA}}{\text{moles of -OH groups on PHEA}}$$

$$R'_6 = \frac{\text{moles of DEA}}{\text{moles of PLA}}$$

After activation time, the resulting PHEA-RhB solution was added drop-wise and slowly to CDI-activated PLA solution. The reaction mixture was left under argon atmosphere and continuous stirring at 40°C for 70 h, and then precipitated in diethyl ether:dichloromethane mixture (15:1 vol/vol). The obtained suspension was centrifuged at4°C for 15 min, at 9800 rpm, and the obtained solid product was recovered, washed several times with the same

mixture, separating the washing mixture by centrifugation. Then, the solid product, dried under vacuum, was obtained with a yield of 284 wt% based on the starting PHEA weight.

^{1}H-NMR (300 MHz, d_7-DMF, 25°C, TMS): δ 1.3 and δ 1.7 (2d, 582 H_{PLA} -O-CO-CH(**CH_3**)-O-); δ 2.8 (m, 2H_{PHEA} -CO-CH-**CH_2**-CO-NH-); δ 3.3 (t, 2H_{PHEA} -NH-**CH_2**-CH_2-O-); δ 3.59 (t, 2H_{PHEA} -NH-CH_2-**CH_2**-O-); δ 4.2-4.5 and δ 5.1-5.5 (m, 194 H_{PLA} -O-CO-**CH**(CH_3)-), and δ 4.8 (m, 1H_{PHEA} -NH-**CH**(CO)CH_2-).

$\overline{M}_w$ of PHEA-PLA graft copolymers were determined by SEC analysis as described before for PHEA-RhB-PLA derivatives (5.3.1 paragraph).

Synthesis and characterization of PHEA–PLA-PEG copolymer

Derivatization of PHEA-PLA with H_2N-PEG-OCH_3, to obtain PHEA-PLA-PEG copolymer was carried out by using DSC as coupling agent.

PHEA-PLA was dissolved in a-DMA (62.5 mg/mL) at 40°C under argon atmosphere and then a proper amount of TEA, as catalyst, and N,N'-disuccinimidyl carbonate (DSC) were added; subsequently, the reaction mixture was left at 40°C for 4 h.

The amounts of TEA and DSC were added according to following ratios (R'_7 = 0.075, R'_8 = 0.1):

$$R'_7 = \frac{\text{moles of DSC}}{\text{moles of -OH groups on PHEA-PLA}}$$

$$R'_8 = \frac{\text{moles of TEA}}{\text{moles of DSC}}$$

After the activation time, the DSC-activated PHEA-PLA was added dropwise to a solution of H_2N-PEG-OCH_3 in a-DMA following the R'_9 ratio equal to 1.0:

$$R'_9 = \frac{\text{moles of } H_2N - PEG - OCH_3}{\text{moles of -OH groups on PHEA-PLA}}$$

The obtained mixture reactions were left at 25°C for 18 h under argon atmosphere and continuous stirring, then dialyzed against distilled water (MWCO 12-14 kDa) and lyophilized.

^{1}H-NMR (300 MHz, d_7-DMF, 25°C, TMS) of PHEA-PLA-PEG: δ 1.48 and δ 1.96 (2d, 582 H_{PLA} –O-CO-CH(**CH_3**)-O-); δ 3.0 (m, 2H_{PHEA} -CO-CH-**CH_2**-CO-NH-); δ 3.48 (t, 2H_{PHEA} -NH-**CH_2**-CH_2-O-); δ 3.71 (t, 2H_{PHEA} -NH-CH_2-**CH_2**-O-); δ 3.78 (t, 176 H_{PEG} -**CH_2**-**CH_2**-O-); δ 4.3-4.6 and δ 5.3-5.6 (m, 194 H_{PLA} -O-CO-**CH**(CH_3)-), and δ 4.98 (m, 1H_{PHEA} -NH-**CH**(CO)CH_2-).

$\overline{M}_w$ of PHEA-PLA-PEG graft copolymers were determined by SEC analysis as described in 5.3.1 paragraph.

Preparation of NPs

NPs were prepared starting from PHEA-PLA-PEG graft copolymer or PLA by high pressure homogenization-solvent evaporation method, as described before for FNPs. Briefly, PHEA-PLA-PEG copolymer or PLA were dissolved in dichloromethane (17.7 mg/mL) and added drop wise to twice-distilled water (50 mL) and homogenized by using an ultraturrax (T 25, Janke&Kunkel Ika–Labortechnik) at 13500 rpm. The primary oil/water emulsion obtained was then diluted with twice-distilled water (25 mL) and broken down into nano-droplets by using an high pressure homogenizer at the pressure of 5000 ± 2500 psi (EmulsiFlex^{TM}-C5; Averting, Canada) for two cycle, equipped with Totem CCS 338 (FIAC, Italy) air compressor. The organic solvent was extracted by evaporation under reduced pressure, by using a Buchi rotant evaporator, causing the precipitation of the NPs. Finally each NP dipersion was freeze-dried (Modulyo freeze-dryer, Labconco Corporation, Missouri, U.S.A.) and stored in freezer (-20 °C) for further characterization.

Characterization of NPs

Mean size (nm), PDI, and ζ-potential values were measured in filtered (0.2 μm) isotonic PBS solution at pH of 7.4 as dispersing medium.

Moreover, NPs were dusted on a double sided adhesive tape previously applied on a stainless steel stub, stored under vacuum for 2 hours, sputter-coated with gold prior to microscopy examination and SEM images were then aquired.

Chemical hydrolysis

Aliquots (40 mg) of NPs based on PLA and PHEA-PLA-PEG copolymer were dispersed in PBS (4 mL) at pH 7.4 or 5.5 and the pH value was determined. Then, samples were incubated under continuous stirring (100 rpm) at 37.0 ± 0.1°C for 3, 7, 14 and 21 days.

After each time, the pH value was measured and then each dispersion was purified by exhaustive dialysis, in order to eliminate low molecular weight polymer fractions released upon eventual NP degradation. At the end of each time interval, the inner phase of the dialysis bag was freeze-dried for further 1H NMR, FT-IR, PCS and SEC analyses.

5.4 Ibuprofen containing pegylated polyaspartamide–polylactide mucus-penetrating based nanoparticles for the treatment of lung inflammation in CF

FNPs earlier obtained starting from PHEA-RhB-PLA-$PEG_{(D)}$ and PHEA-RhB-PLA-$PEG_{(E)}$ was chosen to study the mucus-penetrating ability in terms of surface PEG density and conformation of PEG chains on the NPs surface. For this reason PHEA-RhB-$PLA_{(B)}$, the starting polymer used for the further pegylation reaction that lead to PHEA-RhB-PLA-$PEG_{(D)}$ and PHEA-RhB-PLA-$PEG_{(E)}$, was used to produce unpegylated FNPs.

FNPs obtained from PHEA-RhB-$PLA_{(B)}$, PHEA-RhB-PLA-$PEG_{(D)}$ and PHEA-RhB-PLA-$PEG_{(E)}$ copolymers were named $PEG_{0\%}$-FNPs, $PEG_{2\%}$-FNPs and $PEG_{8.5\%}$-FNPs, respectively.

5.4.1 Determination of surface PEG density and PEG chains conformation on NP surface

The surface PEG density of pegylated FNPs ($PEG_{2\%}$-FNPs and $PEG_{8.5\%}$-FNPs sample) was determined by a ^{1}H NMR method, previously described by other authors [141–143].

A calibration curve was set up for the PEG signal at δ 3.6 ppm, by using PEG solutions in D_2O, in concentration ranging between 10^{-7}-10^{-5} M ($y = 378693x$, $R^2 = 0.9994$) and RhB (1mg/mL) as internal standard. Samples of pegylated FNPs were suspended in D_2O (12.5 mg/mL) and spectra were acquired, repeating each determination in triplicate. Control ^{1}H NMR experiments were also performed with non pegylated FNPs ($PEG_{0\%}$-FNPs).

By assuming all surface PEG chains were full length of 2 kDa PEG, the surface PEG density [Γ] was calculated as the number of PEG molecules per 100 nm^2 NP surface area.

PEG density can be calculated [88] by dividing the total PEG content (M PEG, mol) detected by ^{1}H NMR, by the total surface area of all nanoparticles as in the following equation:

$$[\Gamma] = \left[\frac{M_{PEG} \times 6.02 \times 10^{23}}{\frac{W_{NP}}{d_{NP}} / \frac{4}{3}\pi(D/2)^3} / 4\pi(D/2)^2 \right] \times 100$$

where W_{NP} is the total mass of NPs, d_{NP} is the density of NP (here it is assumed that the density of NPs is equal to the density of polymer, 1.21 g/mL for PLA), D is the particle diameter as measured by the dynamic light scattering.

The number of unconstrained PEG molecules that occupy 100 nm^2 of particle surface area [Γ*] could be calculated according to reference [158]. In order to determine [Γ*], the surface

area occupied by a single PEG chain could be calculated considering that a single PEG chain occupies an area at the interface given by a sphere of diameter ξ, as elsewhere reported [88]:

$$\xi\ (\mathrm{nm}) = 0.076\ \sqrt{m_{PEG}}$$

where m_{PEG} is the molecular weight of the PEG chain. The surface area occupied by one PEG molecule can be determined from $\pi(\xi/2)^2$. ξ for PEG 2 kDa was calculated and resulted to be 3.4 nm and occupies an area that is 9.07 nm^2. Then, the number of PEG molecules to fully cover 100 nm^2 surface area, [Γ*], is 11.025. [Γ/Γ*] is an index to measure the PEG density on the NP surface: values <1 indicates low PEG density where PEG molecules are in a mushroom-like conformation; whereas values >1 indicate high PEG density where PEG molecules are in a brush-like conformation.

5.4.2 Evaluation of FNPs penetration through CF-AM

Measurement of interactions with CF-AM

Measurements of interactions between FNPs and CF-AM was determined by turbidimetry and ζ potential measurements [65].

Briefly, a dispersion of $PEG_{0\%}$-FNPs, $PEG_{2\%}$-FNPs or $PEG_{8.5\%}$-FNPs in CF-AM was prepared at the concentration of 1.25 mg/mL, and then left under magnetic stirring for 1 min. After incubation at 37°C, the turbidity and the ζ potential of each dispersions were measured at time 0 and 2, 4, 6 and 24 h. The absorbance at the λ of 650 nm was recorded by UV spectrophotometer, while the ζ potential was measured by using a Zetasizer Nano ZS.

Penetration test in CF-AM

The mucus penetrating ability of FNPs was assessed by using a penetration test in CF-AM as described elsewhere [65, 136]. A 0.28% w/v agarose solution was prepared in hot distilled water. Two millilitres of agarose solution were placed in vials (Ø×A 24×52 mm), hardened at room temperature and stored at 4°C until use. 2 mL of CF-AM were placed on the hardened agarose gel. Then, 600 µL of a FNPs dispersion in CF-AM (8.33 mg/mL) were placed on the CF-AM layer and incubated at 37 °C. At regular time frames (2, 4, 6 and 24 h), FNPs-containing CF-AM was withdrawn, the remaining agarose gels were rinsed with 2 mL of distilled water three times, melted at 60°C and placed in quarts cuvettes and analysed by UV spectrophotometry, at the λ of 561 nm. All the experiments were run in triplicate. This procedure is schematised in Scheme 8.

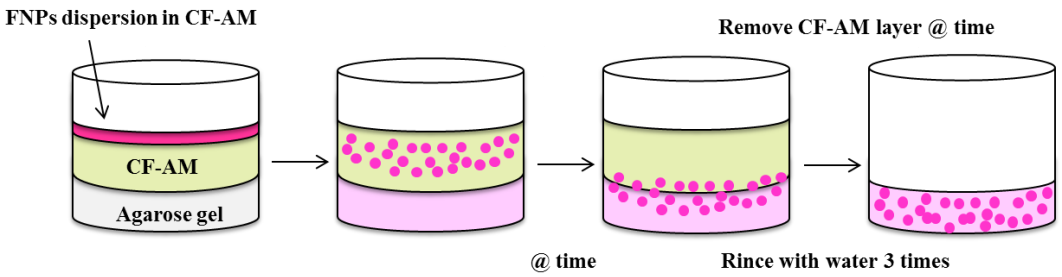

Scheme 8. Scheme for the determination of NP penetration through CF-AM.

The same experiments was repeated by using 5 mL of CF-AM in order to visually inspect the FNPs diffusive motion as function of time, by acquiring images by using a digital photo camera.

5.4.3 Cell viability essay of $PEG_{0\%}$-FNPs, $PEG_{2\%}$-FNPs and $PEG_{8.5\%}$-FNPs

Cell viability was assessed by a MTS assay on 16-HBE cells, using a commercially available kit (Cell Titer 96 Aqueous One Solution Cell Proliferation assay, Promega) containing 3-(4,5-dimethylthiazol-2-yl)-5-(3-carboxymethoxyphenyl)-2-(4-sulphophenyl)-2H-tetrazolium (MTS) and phenazine ethosulfate. 16HBE cells (2×10^5 cells/well) were seeded in microplates (tissue culture grade, 96 wells, flat bottom). Upon reaching confluence, 16-HBE cells were incubated with 10 µL per well of containing FNPs containing supplemented medium ($PEG_{0\%}$-FNPs, $PEG_{2\%}$-FNPs and $PEG_{8.5\%}$-FNPs) at a final concentration per well of 1, 0.1 and 0.01 mg/mL. Moreover, cell viability was also carried out by incubating cells in the presence of trehalose, at concentrations corresponding to those of FNPs dispersions. After 24 h incubation, the growth medium was replaced with 100 µL of fresh DMEM and 20 µL of a MTS/PMS solution was added to each well and plates were incubated for 2h at 37°C. The absorbance at 490 nm was read using a Microplate reader (Multiskan Ex, Thermo Labsystems, Finland). Relative cell viability (percentage) was expressed as (Abs_{490} treated cells/Abs_{490}control cells) × 100, on the basis of three experiments conducted in multiple of six. Cells incubated with the medium were used as negative control.

5.4.4 Preparation of ibuprofen loaded FNPs

Ibuprofen loaded FNPs were prepared by following the same procedure already used to produce empty FNPs. Briefly, each copolymer (17.7 mg/mL) and ibuprofen (5 mg/mL) was dissolved in the same volume of dichloromethane and added dropwise to twice-distilled water and homogenized by using the ultraturrax. The primary oil/water emulsion obtained was then

diluted and homogenized by using the high pressure homogenizer, as described in 5.3.4 paragraph. The organic solvent was extracted by evaporation under reduced pressure, causing the precipitation of the FNPs. Then, the dispersion of FNPs was purified by centrifugation at RT for 15 min, at 4000 rpm by using an Allegra X-22 R centrifuge (Beckman Coulter), equipped with a F0850 rotor and temperature control, in order to remove the amount of ibuprofen not loaded into FNPs. Trehalose was finally added and each FNP dispersion was freeze-dried.

FNPs obtained from PHEA-RhB-PLA$_{(B)}$, PHEA-RhB-PLA-PEG$_{(D)}$ and PHEA-RhB-PLA-PEG$_{(E)}$ copolymers were named Ibu-PEG$_{0\%}$-FNPs, Ibu-PEG$_{2\%}$-FNPs and Ibu-PEG$_{8.5\%}$-FNPs, respectively for Ibuprofen containing FNPs.

5.4.5 Characterization of ibuprofen loaded FNPs

Dimensional analysis and ζ-potential measurements

Mean size (nm), PDI and ζ potential values of ibuprofen containing FNPs were measured by dispersing samples in filtered isotonic PBS solution at pH 7.4.

Determination of ibuprofen content into FNPs

The amount of ibuprofen loaded into Ibu-PEG$_{0\%}$-FNPs, Ibu-PEG$_{2\%}$-FNPs and Ibu-PEG$_{8.5\%}$-FNPs (drug loading, DL%), was determined by an HPLC method. Ibuprofen was extracted by dissolving a known amount of FNPs in acetonitrile (1 mg/mL) for almost 30 minutes. The extracted sample was filtered (0.45 μm) and then injected into the column. The column was a Gemini C18 (C18-NX5U 110A 150x4.6 mm, obtained from Waters); the mobile phase was a mixture of acetonitrile and an aqueous solution of H_3PO_4 (0.4 %v/v) 50:50 v/v with a flow rate of 1 mL/min, the column temperature was 25 °C, and the detection wavelength was 264 nm. The obtained peak area corresponding to ibuprofen amount loaded into FNPs was compared with a calibration curve obtained by plotting areas versus standard solution concentrations of ibuprofen in acetonitrile in the range of 1-0.01 mg/mL ($y = 6698.8x$, $R^2 = 0.999$). Results were expressed as DL wt% and EE wt % of ibuprofen loaded FNPs.

5.4.6 Evaluation of ibuprofen release from FNPs in presence of CF-AM

Ibuprofen release assays in presence of CF-AM were performed by using vertical Franz-type diffusion cells [147]. The system temperature was kept constant at 37 °C by recirculation of water from a thermostatically controlled bath. Continuous stirring at 180 rpm was provided by teflon-coated stirring bars placed in the acceptor chamber. The acceptor chamber was filled

with 5 ml of PBS and a cellulose acetate membrane (size pores: 0.45 μm), previously set in PBS overnight, was applied between the two compartments.

Experiments were conducted by placing in the donor chamber a CF-AM layer (500μL), interposed between the membrane and 150 μL of a ibu-FNPs CF-AM dispersion at the concentration of 0.55, 0.76 and 0.96 mg/mL of Ibu-$PEG_{0\%}$-FNPs, Ibu-$PEG_{2\%}$-FNPs and Ibu-$PEG_{8.5\%}$-FNPs respectively, each one corresponding to an ibuprofen concentration of 0.16 mg/mL. Control experiment were conducted by placing in the donor compartment a CF-AM layer (500μL), interposed between the membrane and a 0.16 mg/mL ibuprofen CF-AM dispersion.

Aliquots of the external medium (500 μL) were were removed from the acceptor chamber at fixed time intervals (0, 15, 30, 45, 60, 120, 180, 240, 360 min) and replacing the same volume of PBS. Samples were freeze-dried and ibuprofen was extracted by dissolving the obtained powder in 500μL of a mixture of acetonitrile and an aqueous solution of H_3PO_4 (0.4 %v/v) 50:50 v/v, and left them stirring overnight. Obtained dispersions were purified by centrifugation at RT for 10 min, at 4000 rpm, filtered (0.45 μm) and injected by using the HPLC method described above.

5.4.7 Evaluation of ibuprofen loaded FNPs cellular uptake in presence of CF-AM

16-HBE (3.2×10^5/well) were seeded in microplates (tissue culture grade, 24 wells, flat bottom). Upon reaching confluence, 16-HBE cells were incubated with 400μL of supplemented DMEM, 50μL of CF-AM, and 50μL of ibu-FNP dispersion in DMEM corresponding to an amount of ibuprofen respectively of 1.04 mg/mL. Control experiments were conducted by incubating 16-HBE cells with 400μL of DMEM, 50μL of CF-AM, and 50μL of a DMEM solution of ibuprofen at 1.04 mg/mL. After 2 and 4 h incubation the medium was removed. The cell monolayer was washed twice with and then it was treated with an appropriate volume of twice-distilled water. After incubation on a shaker, cells were scraped and the cell-lysate collected and freeze-dried. The amount of ibuprofen presents in the cell lysate was quantified by HPLC analysis.

The same experiments were repeated in order to test cellular uptake of Ibu-FNPs by fluorescence imaging. Cell nuclei were labelled with the 4′6-diamidino-2-phenylindole (DAPI) fluorescent dye for 5 min, and images were aquired by using an inverted epifluorescence microscope.

5.5 Mucus-penetrating nanoparticles for enhanced intracellular delivery of ivacaftor for the treatment of the defective ion transport in broncho-epithelial cells in CF

5.5.1 Synthesis and characterization of PHEA-PLA-Tat

Derivatization of PHEA-PLA with HIV-1 Tat Protein (47-57) to obtain the PHEA- PLA-Tat graft copolymer was carried out by using CDI as coupling agent. In particular, a calculated amount of CDI dissolved in a-DMF (5.5 mg/mL) under argon atmosphere, was added drop-wise to a Tat solution in a-DMF (2.8 mg/mL), according to R_a= 2 being:

$$R_a = \frac{\text{moles of CDI}}{\text{moles of TAT}}$$

The solution was stirred at 40°C for an activation time of 4 h under argon atmosphere. Simultaneously, 28 mg/mL of PHEA-PLA were dissolved in a-DMF at 40°C under argon atmosphere. The amounts of HIV-1 Tat Protein was calculated according to R_b:

$$R_b = \frac{\text{moles of HIV-1 Tat Protein}}{\text{moles of -OH groups on PHEA-PLA}}$$

After activation time, the resulting PHEA-PLA solution was added drop-wise and slowly to CDI-activated Tat solution. The reaction mixture was left under argon atmosphere and continuous stirring at 40°C for 48 h, and then purified by exhaustive dialysis (MWCO 12-14 kDa) against distilled water and freeze-dried. The solid product was obtained with a yield of 78 wt% based on the starting PHEA-PLA weight.

The DD_{Tat} of PHEA-PLA-Tat was calculated by determining the amount of Tat molecules on PHEA-PLA-Tat by UV spectrometry. PHEA-PLA and PHEA-PLA-Tat DMF solutions were analyzed at the λ of 279 nm, by comparing the obtained absorbance, corresponding to the amount of Tat present on the copolymer backbone, to a calibration curve obtained by plotting areas versus standard solution concentrations of Tat in the same solvent (y=1014.6x R^2=0.99987).

$\overline{M}_w$ of PHEA-PLA-Tat was determined by SEC analysis, as described in 5.3.1 paragraph.

5.5.2 Preparation of empty and ivacaftor containing FNPs

Empty and ivacaftor containg FNPs were produced by following a nanoprecipitation method 50 mg of PHEA-RhB-PLA-$PEG_{(F)}$ and 50 mg of PHEA-PLA-TAT or PHEA-PLA were mixed (weight ratio 1:1 between the two copolymers) and dissolved in 10 mL of acetone.

The copolymers solution was placed in a burette and added dropwise to 100 mL of twice-distilled water. The mixture was left under stirring for 3 h to form FNPs. Acetone and part of the water were eliminated at 30° C under reduced pressure, by rotary evaporation.

FNP dispersion was then freeze-dried, collected and stored at -20°C for further characterization.

Ivacaftor loaded FNPs were prepared by following the same procedure already used to produce empty FNPs. Briefly, PHEA-RhB-PLA-$PEG_{(F)}$, PHEA-PLA-TAT or PHEA-PLA (weight ratio 1:1 between the two copolymers) and ivacaftor (2.5 mg/mL) was dissolved in the same volume of acetone, placed in a burette, added drop wise to twice-distilled water and left under stirring for 3 h. After acetone removal by rotary evaporation, the dispersion of FNPs was purified by centrifugation at RT for 15 min, at 4000 rpm by using an Allegra X-22 R centrifuge (Beckman Coulter), equipped with a F0850 rotor and temperature control, in order to remove the amount of ivacaftor not loaded into FNPs.

Empty FNPs obtained from PHEA-RhB-PLA-$PEG_{(F)}$ and PHEA-PLA were named PEG(FNPs), while empty FNPs obtained from PHEA-RhB-PLA-$PEG_{(F)}$ and PHEA-PLA-Tat were named Tat-PEG(FNPs). Finally, ivacaftor containing FNPs obtained from PHEA-RhB-PLA-$PEG_{(F)}$ and PHEA-PLA or starting from PHEA-RhB-PLA-$PEG_{(F)}$ and PHEA-PLA-Tat were named Iva_PEG(FNPs) or Iva_Tat-PEG(FNPs), respectively.

5.5.3 Characterization of empty and ivacaftor containing FNPs

Dimensional analysis and ζ-potential measurements

Mean size (nm). PDI and ζ potential values of empty and ivacaftor containing FNPs were determined by dispersing obtained FNPs in filtered isotonic PBS solution at pH of 7.4.

Atomic Force Microscopy

NPs morphology and polydispersity were determined by AFM. Samples were diluted at 1:100 with twice-distilled water. 10 μL of diluted sample was applied onto a freshly cleaved mica surface and fixed to metallic sample support and dried overnight in a vacuum dessicator before observation.

Determination of ivacaftor content into FNPs

The amount of ivacaftor loaded into Iva_PEG(FNPs) and Iva_Tat-PEG(FNPs), (drug loading, DL%), was determined by HPLC. Ivacaftor was extracted by dissolving a known amount of FNPs in acetonitrile (1 mg/mL) for almost 30 minutes. The extracted sample was filtered (0.45 µm) and then injected into the column. The column was a Gemini C18 (C18-NX5U 110A 150x4.6 mm, obtained from Waters); the mobile phase was a mixture of acetonitrile and an aqueous solution of H_3PO_4 (0.4 %v/v) 70:30 v/v with a flow rate of 1 mL/min, the column temperature was 25 °C, and the detection wavelength was 310 nm. The obtained peak area corresponding to ivacaftor amount loaded into FNPs was compared with a calibration curve obtained by plotting areas versus standard solution concentrations of ivacaftor in acetonitrile in the range of 1-0.001 mg/mL ($y = 1E+08x$, $R^2 = 0.9994$).

Results were expressed as DL wt% and EE wt % of ivacaftor loaded FNPs.

5.5.4 Evaluation of FNPs penetration through CF-AM

Measurement of interactions with CF-AM

Measurements of interactions between empty FNPs and CF-AM was determined by turbidimetry and ζ potential measurements [65]. Briefly, a dispersion of PEG(FNPs) or Tat-PEG(FNPs) in CF-AM was prepared at the concentration of 1.25 mg/mL, and then left under magnetic stirring for 1 min. After incubation at 37°C, the turbidity and the ζ potential of each dispersions were measured at time 0, 15, 30, 45, 60, 120, 180, 240, 360 and 480 min. The absorbance at the λ of 650 nm was recorded by UV spectrophotometer, while the ζ potential was measured by using a Zetasizer Nano ZS.

Penetration test in CF-AM

The mucus penetrating ability of PEG(FNPs) or Tat-PEG(FNPs) was assessed by using a penetration test in CF-AM as described in 5.4.2 paragraph and schematized in the Scheme 8. A 0.28% w/v agarose solution was prepared in hot distilled water. Two millilitres of agarose solution were placed in vials (Ø×A 24×52 mm), hardened at room temperature and stored at 4°C until use. 2 mL of CF-AM were placed on the hardened agarose gel. Then, 500 µL of a FNPs dispersion in CF-AM (10 mg/mL) were placed on the CF-AM layer and incubated at 37 °C. At regular time frames (0, 15, 30, 45, 60, 120, 180, 240, 360 min), FNPs-containing CF-AM was withdrawn, the remaining agarose gels were rinsed with 2 mL of distilled water three times, melted at 60°C and placed in quarts cuvettes and analysed by UV spectrophotometry, at the λ of 561 nm.

The same experiments was repeated by using an higher amount of CF-AM in order to visually inspect the FNPs diffusive motion as function of time, by acquiring images by using a digital photo camera.

5.5.5 Evaluation of ivacaftor release from FNPs

Ivacaftor release assays was realized by using the dialysis method in PBS at pH of 7.4 [152, 159]. A known amount of Iva_PEG(FNPs) or Iva_Tat-PEG(FNPs) (each one containing 0.12 mg of ivacaftor) was dispersed in PBS, placed into a dialysis tubing (MWCO 12-14 kDa), immersed into 50 mL of PBS at pH 7.4 and then incubated at 37°C under continuous stirring (100 rpm) in an orbital shaker. Control experiments were conducted by placing a 0.12 mg/mL. Ivacaftor PBS solution into a dialysis tubing (MWCO 12-14 kDa), immersed into 50 mL of PBS at pH 7.4 and then incubated at 37°C under continuous stirring (100 rpm) in an orbital shaker.

Aliquots of the external medium (1 mL) were withdrawn from the outside of the dialysis tubing at fixed time intervals (0, 15, 30, 45, 60, 120, 180, 240, 360 min) and replaced with equal amounts of fresh medium. Samples were freeze-dried and ivacaftor was extracted by dissolving the obtained powder in 500 µL of a mixture of acetonitrile and an aqueous solution of H_3PO_4 (0.4 %v/v) 70:30 v/v, and left them stirring overnight. Obtained dispersions were purified by centrifugation at RT for 10 min, at 4000 rpm, filtered (0.45 µm) and injected by using the HPLC method described in 5.5.3 paragraph.

5.5.6 Evaluation of ivacaftor release from FNPs in presence of CF-AM

Ivacaftor release assays in presence of CF-AM were performed by using vertical Franz-type diffusion cells [147]. The system temperature was kept constant at 37 °C by recirculation of water from a thermostatically controlled bath. Continuous stirring at 180 rpm was provided by teflon-coated stirring bars placed in the acceptor chamber. The acceptor chamber was filled with 5 ml of PBS and a hydrophilic polystyrene membrane (size pores: 0.45 µm), previously set in PBS overnight, was applied between the two compartments.

Experiments were conducted by placing in the donor chamber a CF-AM layer (500µL), interposed between the membrane and 150 µL of Iva_PEG(FNPs) or Iva_Tat-PEG(FNPs) CF-AM dispersion (each one containing 0.035 mg of ivacaftor). Control experiment were conducted by placing in the donor compartment a CF-AM layer (500µL), interposed between the membrane and a 0.12 mg/mL ivacaftor CF-AM dispersion.

Aliquots of the acceptorchamber (500 µL) were withdrawn at fixed time intervals (0, 15, 30, 45, 60, 120, 180, 240, 360 min) and replaced with equal amounts of fresh medium.
Samples were freeze-dried and ivacaftor was extracted by dissolving the obtained powder in 500µL of a mixture of acetonitrile and an aqueous solution of H_3PO_4 (0.4 %v/v) 70:30 v/v, and left them stirring overnight. Obtained dispersions were purified by centrifugation at RT for 10 min, at 4000 rpm, filtered (0.45 µm) and injected by using the HPLC method described in 5.5.3 paragraph.

5.4.7 Cell viability essay

Cell viability was assessed by a MTS assay on 16-HBE cells, using a commercially available kit (Cell Titer 96 Aqueous One Solution Cell Proliferation assay, Promega) containing 3-(4,5-dimethylthiazol-2-yl)-5-(3-carboxymethoxyphenyl)-2-(4-sulphophenyl)-2H-tetrazolium (MTS) and phenazine ethosulfate. 16HBE cells (2×10^5 cells/well) were seeded in microplates (tissue culture grade, 96 wells, flat bottom). Upon reaching confluence, 16-HBE cells were incubated with 10 µL per well with: empty FNPs, PEG(FNPs) or Tat-PEG(FNPs), at a final concentration per well ranging from 2.2 to 0.011; ivacaftor containing FNPs, Iva_PEG(FNPs) or Iva_Tat-PEG(FNPs), at a final concentration per well ranging from 2.6 to 0.013 mg/mL corresponding to ivacaftor final concentration per well ranging from 1000 to 5 µM. Control experiments were conducted by incubating free ivacaftor at a final concentration per well ranging from 1000 to 5 µM. After 4 and 24 h incubation, the growth medium was replaced with 100 µL of fresh DMEM and 20 µL of a MTS/PMS solution was added to each well and plates were incubated for 2h at 37°C. The absorbance at 490 nm was read using a Microplate reader (Multiskan Ex, Thermo Labsystems, Finland). Relative cell viability (percentage) was expressed as (Abs_{490} treated cells/Abs_{490}control cells) × 100, on the basis of three experiments conducted in multiple of six. Cells incubated with the medium were used as negative control.

References

1. Bilton D. Systemic and parenchymal lung diseases. Cystic fibrosis.
2. Rowe SM, Miller S, Sorscher EJ (2005) Cystic fibrosis. N Engl J Med 352:1992–2001.
3. O'Sullivan BP, Freedman SD (2009) Cystic fibrosis. Lancet 373:1891–1904.
4. Short DB, Trotter KW, Reczek D, et al. (1998) An apical PDZ protein anchors the cystic fibrosis transmembrane conductance regulator to the cytoskeleton. J Biol Chem 273:19797–801.
5. Garred P, Pressler T, Madsen HO, et al. (1999) Association of mannose-binding lectin gene heterogeneity with severity of lung disease and survival in cystic fibrosis. J Clin Invest 104:431–7. doi: 10.1172/JCI6861
6. Davies JC, Alton EWFW, Bush A (2007) Cystic fibrosis. BMJ 335:1255–9. doi: 10.1136/bmj.39391.713229.AD
7. Hindo H, Sigley C, Karlson K (2008) Cepacia Syndrome in an Adolescent With Cystic Fibrosis. Infect Dis Clin Pract 16:198–200. doi: 10.1097/IPC.0b013e318159d17d
8. Middleton PG, Chen SC-A, Meyer W (2013) Fungal infections and treatment in cystic fibrosis. Curr Opin Pulm Med 19:670–675. doi: 10.1097/MCP.0b013e328365ab74
9. Pihet M, Carrere J, Cimon B, et al. (2009) Occurrence and relevance of filamentous fungi in respiratory secretions of patients with cystic fibrosis--a review. Med Mycol 47:387–97. doi: 10.1080/13693780802609604
10. Kulczycki LL, Shwachman H (2010) Studies in Cystic Fibrosis of the Pancreas. http://dx.doi.org/10.1056/NEJM195808282590901
11. Cohn JA, Friedman KJ, Noone PG, et al. (1998) Relation between mutations of the cystic fibrosis gene and idiopathic pancreatitis. N Engl J Med 339:653–8.
12. Di Sant'Agnese PA, Vidaurreta AM, Fanconi G, et al. (1960) CYSTIC FIBROSIS OF THE PANCREAS. J Am Med Assoc 172:2065.
13. Wilschanski M, Durie PR (2007) Patterns of GI disease in adulthood associated with mutations in the CFTR gene. Gut 56:1153–63. doi: 10.1136/gut.2004.062786
14. Brand PL (2000) Bronchodilators in cystic fibrosis. J R Soc Med 37–9.
15. Reeves EP, Molloy K, Pohl K, McElvaney NG (2012) Hypertonic saline in treatment of pulmonary disease in cystic fibrosis. ScientificWorldJournal 2012:465230.
16. Enderby B, Doull I (2007) Hypertonic saline inhalation in cystic fibrosis--salt in the wound, or sweet success? Arch Dis Child 92:195–6. doi: 10.1136/adc.2006.094979

17. Sawicki GS, Chou W, Raimundo K, et al. (2015) Randomized trial of efficacy and safety of dornase alfa delivered by eRapid nebulizer in cystic fibrosis patients. J Cyst Fibros 14:777–783. doi: 10.1016/j.jcf.2015.04.003
18. Smyth A, Walters S (2001) Prophylactic antibiotics for cystic fibrosis. Cochrane database Syst Rev CD001912. doi: 10.1002/14651858.CD001912
19. Hewer SL (2012) Inhaled antibiotics in cystic fibrosis: what's new? J R Soc Med S19–24. doi: 10.1258/jrsm.2012.12s004
20. Konstan MW, Geller DE, Minić P, et al. (2011) Tobramycin inhalation powder for P. aeruginosa infection in cystic fibrosis: the EVOLVE trial. Pediatr Pulmonol 46:230–8. doi: 10.1002/ppul.21356
21. Chuchalin A, Amelina E, Bianco F (2009) Tobramycin for inhalation in cystic fibrosis: Beyond respiratory improvements. Pulm Pharmacol Ther 22:526–32.
22. Konstan MW, Vargo KM, Davis PB (1990) Ibuprofen attenuates the inflammatory response to Pseudomonas aeruginosa in a rat model of chronic pulmonary infection. Implications for antiinflammatory therapy in cystic fibrosis. Am Rev Respir Dis 141:186–92. doi: 10.1164/ajrccm/141.1.186
23. Konstan MW, Schluchter MD, Xue W, Davis PB (2007) Clinical use of Ibuprofen is associated with slower FEV1 decline in children with cystic fibrosis. Am J Respir Crit Care Med 176:1084–9. doi: 10.1164/rccm.200702-181OC
24. Lands LC, Dauletbaev N (2010) High-dose ibuprofen in cystic fibrosis. Pharmaceuticals 3:2213–2224. doi: 10.3390/ph3072213
25. Lands LC, Milner R, Cantin AM, et al. (2007) High-dose ibuprofen in cystic fibrosis: Canadian safety and effectiveness trial. J Pediatr 151:249–54. doi: 10.1016/j.jpeds.2007.04.009
26. Armstrong DS, Grimwood K, Carlin JB, et al. (1997) Lower airway inflammation in infants and young children with cystic fibrosis. Am J Respir Crit Care Med 156:1197–204. doi: 10.1164/ajrccm.156.4.96-11058
27. Carlile GW, Robert R, Goepp J, et al. (2014) Ibuprofen rescues mutant cystic fibrosis transmembrane conductance regulator trafficking. J Cyst Fibros 14:16–25.
28. Derichs N (2013) Targeting a genetic defect: cystic fibrosis transmembrane conductance regulator modulators in cystic fibrosis. Eur Respir Rev 22:58–65.
29. Quon BS, Rowe SM (2016) State of the Art Review: New and emerging targeted therapies for cystic fibrosis. BMJ. doi: 10.1136/bmj.i859

30. Hirawat S, Welch EM, Elfring GL, et al. (2007) Safety, Tolerability, and Pharmacokinetics of PTC124, a Nonaminoglycoside Nonsense Mutation Suppressor, Following Single- and Multiple-Dose Administration to Healthy Male and Female Adult Volunteers. J Clin Pharmacol 47:430–444. doi: 10.1177/0091270006297140
31. Van Goor F, Hadida S, Grootenhuis PDJ, et al. (2009) Rescue of CF airway epithelial cell function in vitro by a CFTR potentiator, VX-770. Proc Natl Acad Sci U S A 106:18825–30. doi: 10.1073/pnas.0904709106
32. Rogan MP, Stoltz DA, Hornick DB (2011) Cystic fibrosis transmembrane conductance regulator intracellular processing, trafficking, and opportunities for mutation-specific treatment. Chest 139:1480–90. doi: 10.1378/chest.10-2077
33. Jih K-Y, Hwang T-C (2013) Vx-770 potentiates CFTR function by promoting decoupling between the gating cycle and ATP hydrolysis cycle. Proc Natl Acad Sci U S A 110:4404–9. doi: 10.1073/pnas.1215982110
34. (2016) Lumacaftor/ivacaftor (Orkambi) for cystic fibrosis. Med Lett Drugs Ther 58:41–2.
35. Lane MA, Doe SJ (2014) A new era in the treatment of cystic fibrosis. Clin Med 14:76–8. doi: 10.7861/clinmedicine.14-1-76
36. Adler FR, Aurora P, Barker DH, et al. (2009) Lung transplantation for cystic fibrosis. Proc Am Thorac Soc 6:619–33. doi: 10.1513/pats.2009008-088TL
37. Sanders M (2007) Inhalation therapy: an historical review. Prim Care Respir J 16:71–81. doi: 10.3132/pcrj.2007.00017
38. Dessanges JF (2001) A history of nebulization. J Aerosol Med 14:65–71.
39. Tomashefski JF, Farver CF (2008) Anatomy and Histology of the Lung. In: Dail Hammar's Pulm. Pathol. Springer New York, New York, NY, pp 20–48
40. Loira-Pastoriza C, Todoroff J, Vanbever R (2014) Delivery strategies for sustained drug release in the lungs. Adv Drug Deliv Rev. doi: 10.1016/j.addr.2014.05.017
41. Fernández Tena A, Casan Clarà P (2012) Deposition of Inhaled Particles in the Lungs. Arch Bronconeumol (English Ed 48:240–246. doi: 10.1016/j.arbr.2012.02.006
42. Zhang J, Wu L, Chan H-K, Watanabe W (2011) Formation, characterization, and fate of inhaled drug nanoparticles. Adv Drug Deliv Rev 63:441–455.
43. Smola M, Vandamme T, Sokolowski A (2008) Nanocarriers as pulmonary drug delivery systems to treat and to diagnose respiratory and non respiratory diseases. Int J Nanomedicine 3:1–19.

44. Ibrahim M, Verma R, Garcia-Contreras L (2015) Inhalation drug delivery devices: technology update. Med Devices (Auckl) 8:131–9. doi: 10.2147/MDER.S48888
45. Anderson P (2006) Use of Respimat Soft Mist inhaler in COPD patients. Int J Chron Obstruct Pulmon Dis 1:251–9.
46. Islam N, Gladki E (2008) Dry powder inhalers (DPIs)—A review of device reliability and innovation. Int J Pharm 360:1–11. doi: 10.1016/j.ijpharm.2008.04.044
47. Komase Y, Asako A, Kobayashi A, Sharma R (2014) Ease-of-use preference for the ELLIPTA® dry powder inhaler over a commonly used single-dose capsule dry powder inhaler by inhalation device-naïve Japanese volunteers aged 40 years or older. Int J Chron Obstruct Pulmon Dis 9:1365–75. doi: 10.2147/COPD.S72762
48. Heijerman H, Westerman E, Conway S, Touw D (2009) Inhaled medication and inhalation devices for lung disease in patients with cystic fibrosis: A European consensus. J Cyst Fibros 8:295–315. doi: 10.1016/j.jcf.2009.04.005
49. Deterding R, Retsch-Bogart G, Milgram L, et al. (2005) Safety and tolerability of denufosol tetrasodium inhalation solution, a novel P2Y2 receptor agonist: results of a phase 1/phase 2 multicenter study in mild to moderate cystic fibrosis. Pediatr Pulmonol 39:339–48. doi: 10.1002/ppul.20192
50. www.ema.europe.com Bronchitol.
51. Smith S, Edwards CT (2016) Long-acting inhaled bronchodilators for cystic fibrosis. Cochrane Database Syst Rev. doi: 10.1002/14651858.CD012102
52. De Boeck K, De Baets F, Malfroot A, et al. (2007) Do inhaled corticosteroids impair long-term growth in prepubertal cystic fibrosis patients? Eur J Pediatr 166:23–8. doi: 10.1007/s00431-006-0198-9
53. D'Angelo I, Conte C, La Rotonda MI, et al. (2014) Improving the efficacy of inhaled drugs in cystic fibrosis: Challenges and emerging drug delivery strategies. Adv Drug Deliv Rev 75:92–111. doi: 10.1016/j.addr.2014.05.008
54. www.ema.europe.com TOBI Podhaler - Novartis.
55. Konstan MW, Flume PA, Kappler M, et al. (2011) Safety, efficacy and convenience of tobramycin inhalation powder in cystic fibrosis patients: The EAGER trial. J Cyst Fibros 10:54–61. doi: 10.1016/j.jcf.2010.10.003
56. Charrier C, Rodger C, Robertson J, et al. (2014) Cysteamine (Lynovex®), a novel mucoactive antimicrobial & antibiofilm agent for the treatment of cystic fibrosis. Orphanet J Rare Dis 9:189. doi: 10.1186/s13023-014-0189-2

57. Lai SK, Wang YY, Wirtz D, Hanes J (2009) Micro- and macrorheology of mucus. Adv Drug Deliv Rev 61:86–100. doi: 10.1016/j.addr.2008.09.012
58. Kim N, Duncan GA, Hanes J, Suk JS (2016) Barriers to inhaled gene therapy of obstructive lung diseases: A review. J Control Release. doi: 10.1016/j.jconrel.2016.05.031
59. Tarran R (2004) Regulation of airway surface liquid volume and mucus transport by active ion transport. Proc Am Thorac Soc 1:42–6. doi: 10.1513/pats.2306014
60. Tarran R, Button B, Picher M, et al. (2005) Normal and cystic fibrosis airway surface liquid homeostasis. The effects of phasic shear stress and viral infections. J Biol Chem 280:35751–9. doi: 10.1074/jbc.M505832200
61. Zhou QT, Leung SSY, Tang P, et al. (2015) Inhaled formulations and pulmonary drug delivery systems for respiratory infections. Adv Drug Deliv Rev 85:83–99. doi: 10.1016/j.addr.2014.10.022
62. Stern M, Ulrich K, Geddes DM, Alton EWFW (2003) Poly (D, L-lactide-co-glycolide)/DNA microspheres to facilitate prolonged transgene expression in airway epithelium in vitro, ex vivo and in vivo. Gene Ther 10:1282–1288. doi: 10.1038/sj.gt.3301994
63. Osman R, Al Jamal KT, Kan P-L, et al. (2013) Inhalable DNase I microparticles engineered with biologically active excipients. Pulm Pharmacol Ther 26:700–9. doi: 10.1016/j.pupt.2013.07.010
64. Vij N, Min T, Marasigan R, et al. (2010) Development of PEGylated PLGA nanoparticle for controlled and sustained drug delivery in cystic fibrosis. J Nanobiotechnology 8:22. doi: 10.1186/1477-3155-8-22
65. Ungaro F, D'Angelo I, Coletta C, et al. (2012) Dry powders based on PLGA nanoparticles for pulmonary delivery of antibiotics: Modulation of encapsulation efficiency, release rate and lung deposition pattern by hydrophilic polymers. J Control Release 157:149–159. doi: 10.1016/j.jconrel.2011.08.010
66. Truong-Le VL, Walsh SM, Schweibert E, et al. (1999) Gene transfer by DNA-gelatin nanospheres. Arch Biochem Biophys 361:47–56. doi: 10.1006/abbi.1998.0975
67. Ibrahim BM, Park S, Han B, Yeo Y (2011) A strategy to deliver genes to cystic fibrosis lungs: a battle with environment. J Control Release 155:289–95. doi: 10.1016/j.jconrel.2011.07.039

68. Davies LA, Hyde SC, Nunez-Alonso G, et al. (2012) The use of CpG-free plasmids to mediate persistent gene expression following repeated aerosol delivery of pDNA/PEI complexes. Biomaterials 33:5618–27. doi: 10.1016/j.biomaterials.2012.04.019
69. Boylan NJ, Suk JS, Lai SK, et al. (2012) Highly compacted DNA nanoparticles with low MW PEG coatings: in vitro, ex vivo and in vivo evaluation. J Control Release 157:72–9. doi: 10.1016/j.jconrel.2011.08.031
70. Singh R, Lillard JW Nanoparticle-based targeted drug delivery. doi: 10.1016/j.yexmp.2008.12.004
71. Beck-Broichsitter M, Merkel OM, Kissel T (2012) Controlled pulmonary drug and gene delivery using polymeric nano-carriers. J Control Release 161:214–24. doi: 10.1016/j.jconrel.2011.12.004
72. Harris JM, Chess RB (2003) Effect of pegylation on pharmaceuticals. Nat Rev Drug Discov 2:214–21. doi: 10.1038/nrd1033
73. Ishida T, Kiwada H (2008) Accelerated Blood Clearance (ABC) Phenomenon Induced by Administration of PEGylated Liposome. YAKUGAKU ZASSHI 128:233–243.
74. Giammona G, Carlisi B, Palazzo S (1987) Reaction of α,β-poly(N-hydroxyethyl)-DL-aspartamide with derivatives of carboxylic acids. J Polym Sci Part A Polym Chem 25:2813–2818. doi: 10.1002/pola.1987.080251016
75. Giammona G, Carlisi B, Pitarresi G, et al. (1992) Water-soluble copolymers of an antiviral agent: synthesis and their interaction with a biomembrane model. J Control Release 22:197–204. doi: 10.1016/0168-3659(92)90094-8
76. Craparo EF, Porsio B, Luisa M, et al. (2015) Evaluation of biodegradability on polyaspartamide-polylactic acid based nanoparticles by chemical hydrolysis studies. Polym Degrad Stab 119:56–67. doi: 10.1016/j.polymdegradstab.2015.05.003
77. Craparo EF, Porsio B, Mauro N, et al. (2015) Polyaspartamide-Polylactide Graft Copolymers with Tunable Properties for the Realization of Fluorescent Nanoparticles for Imaging. Macromol Rapid Commun. doi: 10.1002/marc.201500154
78. Craparo EF, Ognibene MC, Casaletto MP, et al. (2008) Biocompatible polymeric micelles with polysorbate 80 for use in brain targeting. Nanotechnology 19:485603. doi: 10.1088/0957-4484/19/48/485603
79. Craparo EF, Triolo D, Pitarresi G, et al. (2013) Galactosylated micelles for a ribavirin prodrug targeting to hepatocytes. Biomacromolecules 14:1838–49.

80. Craparo EF, Teresi G, Licciardi M, et al. (2013) Novel composed galactosylated nanodevices containing a ribavirin prodrug as hepatic cell-targeted carriers for HCV treatment. J Biomed Nanotechnol 9:1107–22.
81. Craparo EF, Teresi G, Bondi' ML, et al. (2011) Phospholipid-polyaspartamide micelles for pulmonary delivery of corticosteroids. Int J Pharm 406:135–44.
82. Craparo EF, Di Gioia S, Trapani A, et al. (2016) Realization of polyaspartamide-based nanoparticles and in vivo lung biodistribution evaluation of a loaded glucocorticoid after aerosolization in mice. Int J Pharm 510:263–70.
83. Ulery BD, Nair LS, Laurencin CT (2011) Biomedical Applications of Biodegradable Polymers. J Polym Sci B Polym Phys 49:832–864. doi: 10.1002/polb.22259
84. El-Sherbiny IM, El-Baz NM, Yacoub MH (2015) Inhaled nano- and microparticles for drug delivery. Glob Cardiol Sci Pract 2015:2. doi: 10.5339/gcsp.2015.2
85. Ungaro F, De Stefano D, Giovino C, et al. (2012) PEI-Engineered Respirable Particles Delivering a Decoy Oligonucleotide to NF-κB: Inhibiting MUC2 Expression in LPS-Stimulated Airway Epithelial Cells. PLoS One 7:e46457.
86. Vij N, Min T, Marasigan R, et al. (2010) Development of PEGylated PLGA nanoparticle for controlled and sustained drug delivery in cystic fibrosis. J Nanobiotechnology 8:22. doi: 10.1186/1477-3155-8-22
87. Ensign LM, Schneider C, Suk JS, et al. (2012) Mucus penetrating nanoparticles: biophysical tool and method of drug and gene delivery. Adv Mater 24:3887–94.
88. Xu Q, Boylan NJ, Cai S, et al. (2013) Scalable method to produce biodegradable nanoparticles that rapidly penetrate human mucus. J Control Release 170:279–286.
89. Yang M, Lai SK, Wang YY, et al. (2011) Biodegradable nanoparticles composed entirely of safe materials that rapidly penetrate human mucus. Angew Chemie - Int Ed 50:2597–2600.
90. Menon JU, Ravikumar P, Pise A, et al. (2014) Polymeric nanoparticles for pulmonary protein and DNA delivery. Acta Biomater 10:2643–2652. doi: 10.1016/j.actbio.2014.01.033
91. Lankalapalli S, Kolapalli VRM (2009) Polyelectrolyte Complexes: A Review of their Applicability in Drug Delivery Technology. Indian J Pharm Sci 71:481–7.
92. Deacon J, Abdelghany SM, Quinn DJ, et al. (2015) Antimicrobial efficacy of tobramycin polymeric nanoparticles for Pseudomonas aeruginosa infections in cystic fibrosis: Formulation, characterisation and functionalisation with dornase alfa (DNase). J Control Release 198:55–61.

93. Vivanti A, Yu L, Palmer M, et al. (2013) Short-term body weight fluctuations in older well-hydrated hospitalised patients. J Hum Nutr Diet 26:429–35.
94. Yu H, Teo J, Chew JW, Hadinoto K (2016) Dry powder inhaler formulation of high-payload antibiotic nanoparticle complex intended for bronchiectasis therapy: Spray drying versus spray freeze drying preparation. Int J Pharm 499:38–46.
95. Cheow WS, Hadinoto K (2012) Green preparation of antibiotic nanoparticle complex as potential anti-biofilm therapeutics via self-assembly amphiphile-polyelectrolyte complexation with dextran sulfate. Colloids Surf B Biointerfaces. doi: 10.1016/j.colsurfb.2011.11.024
96. Conti DS, Brewer D, Grashik J, et al. (2014) Poly(amidoamine) Dendrimer Nanocarriers and Their Aerosol Formulations for siRNA Delivery to the Lung Epithelium. Mol Pharm 11:1808–1822. doi: 10.1021/mp4006358
97. Yu H, Teo J, Chew JW, Hadinoto K (2016) Dry powder inhaler formulation of high-payload antibiotic nanoparticle complex intended for bronchiectasis therapy: Spray drying versus spray freeze drying preparation. Int J Pharm 499:38–46. doi: 10.1016/j.ijpharm.2015.12.072
98. Keck CM, Müller RH (2013) Nanotoxicological classification system (NCS) – A guide for the risk-benefit assessment of nanoparticulate drug delivery systems. Eur J Pharm Biopharm 84:445–448. doi: 10.1016/j.ejpb.2013.01.001
99. Lai SK, Wang YY, Hanes J (2009) Mucus-penetrating nanoparticles for drug and gene delivery to mucosal tissues. Adv Drug Deliv Rev 61:158–171. doi: 10.1016/j.addr.2008.11.002
100. Gref R, Lück M, Quellec P, et al. (2000) “Stealth” corona-core nanoparticles surface modified by polyethylene glycol (PEG): influences of the corona (PEG chain length and surface density) and of the core composition on phagocytic uptake and plasma protein adsorption. Colloids Surf B Biointerfaces 18:301–313.
101. Suk JS, Lai SK, Wang YY, et al. (2009) The penetration of fresh undiluted sputum expectorated by cystic fibrosis patients by non-adhesive polymer nanoparticles. Biomaterials 30:2591–2597. doi: 10.1016/j.biomaterials.2008.12.076
102. Yoncheva K, Gómez S, Campanero MA, et al. (2005) Bioadhesive properties of pegylated nanoparticles. Expert Opin Drug Deliv 2:205–18. doi: 10.1517/17425247.2.2.205
103. Shaikh R, Raj Singh TR, Garland MJ, et al. (2011) Mucoadhesive drug delivery systems. J Pharm Bioallied Sci 3:89–100. doi: 10.4103/0975-7406.76478

104. Carvalho FC, Bruschi ML, Evangelista RC, Gremião MPD (2010) Mucoadhesive drug delivery systems. Brazilian J Pharm Sci 46:1–17. doi: 10.1590/S1984-82502010000100002
105. Takeuchi H, Yamamoto H, Kawashima Y (2001) Mucoadhesive nanoparticulate systems for peptide drug delivery. Adv Drug Deliv Rev 47:39–54.
106. Sakagami M, Sakon K, Kinoshita W, Makino Y (2001) Enhanced pulmonary absorption following aerosol administration of mucoadhesive powder microspheres. J Control Release 77:117–29.
107. Kirch J, Guenther M, Doshi N, et al. (2012) Mucociliary clearance of micro- and nanoparticles is independent of size, shape and charge—an ex vivo and in silico approach. J Control Release 159:128–134. doi: 10.1016/j.jconrel.2011.12.015
108. Forier K, Raemdonck K, De Smedt SC, et al. (2014) Lipid and polymer nanoparticles for drug delivery to bacterial biofilms. J Control Release 190:607–623. doi: 10.1016/j.jconrel.2014.03.055
109. Venkatraman G, Ramya S, Shruthilaya A, et al. (2012) Nanomedicine: towards development of patient-friendly drug-delivery systems for oncological applications. Int J Nanomedicine 7:1043. doi: 10.2147/IJN.S25182
110. Grunwald J, Rejtar T, Sawant R, et al. (2009) TAT Peptide and Its Conjugates: Proteolytic Stability. Bioconjug Chem 20:1531–1537. doi: 10.1021/bc900081e
111. Shan W, Zhu X, Liu M, et al. (2015) Overcoming the Diffusion Barrier of Mucus and Absorption Barrier of Epithelium by Self-Assembled Nanoparticles for Oral Delivery of Insulin. ACS Nano 9:2345–2356. doi: 10.1021/acsnano.5b00028
112. Smola M, Vandamme T, Sokolowski A (2008) Nanocarriers as pulmonary drug delivery systems to treat and to diagnose respiratory and non respiratory diseases. Int J Nanomedicine 3:1–19.
113. Ong HX, Traini D, Cipolla D, et al. (2012) Liposomal Nanoparticles Control the Uptake of Ciprofloxacin Across Respiratory Epithelia. Pharm Res 29:3335–3346. doi: 10.1007/s11095-012-0827-0
114. Cohen TS, Prince A (2012) Cystic fibrosis: a mucosal immunodeficiency syndrome. Nat Med 18:509–19. doi: 10.1038/nm.2715
115. Guilbault C, Saeed Z, Downey GP, Radzioch D (2007) Cystic fibrosis mouse models. Am J Respir Cell Mol Biol 36:1–7. doi: 10.1165/rcmb.2006-0184TR
116. Grubb BR, Vick RN, Boucher RC (1994) Hyperabsorption of Na+ and raised Ca(2+)-mediated Cl- secretion in nasal epithelia of CF mice. Am J Physiol 266:C1478–83.

117. Clarke LL, Grubb BR, Yankaskas JR, et al. (1994) Relationship of a non-cystic fibrosis transmembrane conductance regulator-mediated chloride conductance to organ-level disease in Cftr(-/-) mice. Proc Natl Acad Sci U S A 91:479–83. doi: 10.1073/PNAS.91.2.479
118. Bragonzi A (2010) Murine models of acute and chronic lung infection with cystic fibrosis pathogens. Int J Med Microbiol 300:584–93. doi: 10.1016/j.ijmm.2010.08.012
119. Keiser NW, Engelhardt JF (2011) New animal models of cystic fibrosis: what are they teaching us? Curr Opin Pulm Med 17:478–83. doi: 10.1097/MCP.0b013e32834b14c9
120. Riordan JR, Rommens JM, Kerem B, et al. (1989) Identification of the cystic fibrosis gene: cloning and characterization of complementary DNA. Science 245:1066–73.
121. Boucher RC (2007) Evidence for airway surface dehydration as the initiating event in CF airway disease. J Intern Med 261:5–16. doi: 10.1111/j.1365-2796.2006.01744.x
122. Rogers DF (2007) Mucoactive agents for airway mucus hypersecretory diseases. Respir Care 52:1176–93; discussion 1193–7.
123. Sanders N, Rudolph C, Braeckmans K, et al. (2009) Extracellular barriers in respiratory gene therapy. Adv Drug Deliv Rev 61:115–27. doi: 10.1016/j.addr.2008.09.011
124. Di Gioia S, Trapani A, Castellani S, et al. (2015) Nanocomplexes for gene therapy of respiratory diseases: Targeting and overcoming the mucus barrier. Pulm Pharmacol Ther 34:8–24. doi: 10.1016/j.pupt.2015.07.003
125. Knowles MR, Boucher RC (2002) Mucus clearance as a primary innate defense mechanism for mammalian airways. J Clin Invest 109:571–7. doi: 10.1172/JCI15217
126. Conese M (2011) Cystic fibrosis and the innate immune system: therapeutic implications. Endocr Metab Immune Disord Drug Targets 11:8–22.
127. Ramsey DM, Wozniak DJ (2005) Understanding the control of Pseudomonas aeruginosa alginate synthesis and the prospects for management of chronic infections in cystic fibrosis. Mol Microbiol 56:309–22. doi: 10.1111/j.1365-2958.2005.04552.x
128. Tseng BS, Zhang W, Harrison JJ, et al. (2013) The extracellular matrix protects Pseudomonas aeruginosa biofilms by limiting the penetration of tobramycin. Environ Microbiol 15:n/a–n/a. doi: 10.1111/1462-2920.12155
129. Craparo EF, Di Gioia S, Trapani A, et al. (2016) Realization of polyaspartamide-based nanoparticles and in vivo lung biodistribution evaluation of a loaded glucocorticoid after aerosolization in mice. Int J Pharm 510:263–70.
130. Paradossi G, Cavalieri F, Chiessi E, et al. (2003) Poly(vinyl alcohol) as versatile biomaterial for potential biomedical applications. J Mater Sci Mater Med 14:687–91.

131. Karolewicz Boena (2016) A review of polymers as multifunctional excipients in drug dosage form technology - pharma excipients. Saudi Pharm J 24:525–536.
132. Craparo EF, Sardo C, Serio R, et al. (2014) Galactosylated polymeric carriers for liver targeting of sorafenib. Int J Pharm 466:172–80. doi: 10.1016/j.ijpharm.2014.02.047
133. Licciardi M, Campisi M, Cavallaro G, et al. (2006) Synthesis and characterization of polyaminoacidic polycations for gene delivery. Biomaterials 27:2066–2075. doi: 10.1016/j.biomaterials.2005.09.027
134. Craparo EF, Licciardi M, Conigliaro A, et al. (2015) Hepatocyte-targeted fl uorescent nanoparticles based on a polyaspartamide for potential theranostic applications. Polymer (Guildf) 70:257–270. doi: 10.1016/j.polymer.2015.06.009
135. Li X, Anton N, Arpagaus C, et al. (2010) Nanoparticles by spray drying using innovative new technology: The B??chi Nano Spray Dryer B-90. J Control Release 147:304–310. doi: 10.1016/j.jconrel.2010.07.113
136. Yang Y, Tsifansky MD, Shin S, et al. (2011) Mannitol-guided delivery of Ciprofloxacin in artificial cystic fibrosis mucus model. Biotechnol Bioeng 108:1441–9. doi: 10.1002/bit.23046
137. Craparo EF, Porsio B, Sardo C, et al. (2016) Pegylated polyaspartamide–polylactide based nanoparticles penetrating cystic fibrosis artificial mucus. Biomacromolecules acs.biomac.5b01480. doi: 10.1021/acs.biomac.5b01480
138. Hunt BE, Weber A, Berger A, et al. (1995) Macromolecular mechanisms of sputum inhibition of tobramycin activity. Antimicrob Agents Chemother 39:34–39. doi: 10.1128/AAC.39.1.34
139. Barraud N, Buson A, Jarolimek W, et al. (2013) Mannitol Enhances Antibiotic Sensitivity of Persister Bacteria in Pseudomonas aeruginosa Biofilms. PLoS One 8:e84220. doi: 10.1371/journal.pone.0084220
140. Beija M, Afonso CAM, Martinho JMG (2009) Synthesis and applications of Rhodamine derivatives as fluorescent probes. Chem Soc Rev 38:2410–33. doi: 10.1039/b901612k
141. Heald CR, Stolnik S, Kujawinski KS, et al. (2002) Poly(lactic acid)−Poly(ethylene oxide) (PLA−PEG) Nanoparticles: NMR Studies of the Central Solidlike PLA Core and the Liquid PEG Corona. Langmuir 18:3669–3675. doi: 10.1021/la011393y
142. Garcia-Fuentes M, Torres D, Martín-Pastor M, Alonso MJ (2004) Application of NMR spectroscopy to the characterization of PEG-stabilized lipid nanoparticles. Langmuir 20:8839–45. doi: 10.1021/la049505j

143. Vila A, Gill H, McCallion O, Alonso MJ (2004) Transport of PLA-PEG particles across the nasal mucosa: effect of particle size and PEG coating density. J Control Release 98:231–44. doi: 10.1016/j.jconrel.2004.04.026
144. De Gennes PG (1987) Polymers at an interface; a simplified view. Adv Colloid Interface Sci 27:189–209. doi: 10.1016/0001-8686(87)85003-0
145. Jokerst J V, Lobovkina T, Zare RN, Gambhir SS (2011) Nanoparticle PEGylation for imaging and therapy. Nanomedicine (Lond) 6:715–28. doi: 10.2217/nnm.11.19
146. Bourganis V, Karamanidou T, Samaridou E, et al. (2015) European Journal of Pharmaceutics and Biopharmaceutics On the synthesis of mucus permeating nanocarriers. 97:239–249.
147. Donnelly RF, McCarron PA, Cassidy CM, et al. (2007) Delivery of photosensitisers and light through mucus: investigations into the potential use of photodynamic therapy for treatment of Pseudomonas aeruginosa cystic fibrosis pulmonary infection. J Control Release 117:217–26. doi: 10.1016/j.jconrel.2006.11.010
148. Bilati U, Allémann E, Doelker E (2005) Development of a nanoprecipitation method intended for the entrapment of hydrophilic drugs into nanoparticles. Eur J Pharm Sci 24:67–75. doi: 10.1016/j.ejps.2004.09.011
149. Alshamsan A (2014) Nanoprecipitation is more efficient than emulsion solvent evaporation method to encapsulate cucurbitacin I in PLGA nanoparticles. Saudi Pharm J 22:219–222. doi: 10.1016/j.jsps.2013.12.002
150. Porsio B, Lemaire L, Habnouni S El, et al. (2015) MRI-visible nanoparticles from hydrophobic gadolinium poly(ε-caprolactone) conjugates. doi: 10.1016/j.polymer.2014.11.031
151. Stead DA (2000) Current methodologies for the analysis of aminoglycosides. J Chromatogr B Biomed Sci Appl 747:69–93. doi: 10.1016/S0378-4347(00)00133-X
152. Mauro N, Scialabba C, Cavallaro G, et al. (2015) Biotin-Containing Reduced Graphene Oxide-Based Nanosystem as a Multieffect Anticancer Agent: Combining Hyperthermia with Targeted Chemotherapy. Biomacromolecules 16:2766–75. doi: 10.1021/acs.biomac.5b00705
153. Licciardi M, Scialabba C, Sardo C, et al. (2014) Amphiphilic inulin graft co-polymers as self-assembling micelles for doxorubicin delivery. J Mater Chem B 2:4262. doi: 10.1039/c4tb00235k

154. Schillaci D, Petruso S, Raimondi MV, et al. (2010) Pyrrolomycins as potential anti-staphylococcal biofilms agents. Biofouling 26:433–8. doi: 10.1080/08927011003718673
155. Schillaci D, Maggio B, Raffa D, et al. (2008) 4-Diazopyrazole derivatives as potential new antibiofilm agents. Chemotherapy 54:456–62. doi: 10.1159/000159271
156. Craparo EF, Licciardi M, Conigliaro A, et al. (2015) Hepatocyte-targeted fluorescent nanoparticles based on a polyaspartamide for potential theranostic applications. Polymer (Guildf) 70:257–270. doi: 10.1016/j.polymer.2015.06.009
157. Craparo EF, Teresi G, Ognibene MC, et al. (2010) Nanoparticles based on novel amphiphilic polyaspartamide copolymers. J Nanoparticle Res 12:2629–2644. doi: 10.1007/s11051-009-9842-4
158. Auguste DT, Armes SP, Brzezinska KR, et al. (2006) PH triggered release of protective poly(ethylene glycol)-b-polycation copolymers from liposomes. Biomaterials 27:2599–2608. doi: 10.1016/j.biomaterials.2005.08.036
159. Di Meo C, Cilurzo F, Licciardi M, et al. (2014) Polyaspartamide-Doxorubicin Conjugate as Potential Prodrug for Anticancer Therapy. Pharm Res 32:1557–1569. doi: 10.1007/s11095-014-1557-2